Spine: 4.5 mm

Volume 74 • Issue 1 • January-March 2025

Journal of The Anatomical Society of India • Volume 74 • Issue 1 • January-March 2025 • Pages 1-88

ISSN : 0003-2778

Scopus Indexed

JASI

JOURNAL OF THE ANATOMICAL SOCIETY OF INDIA

An International Journal

An Official Publication of Anatomical Society of India

Full text online at **https://journals.lww.com/joai**
Submit articles online at **https://review.jow.medknow.com/jasi**

Editor-in-Chief
Dr. Vishram Singh

Wolters Kluwer

Medknow

Journal of the Anatomical Society of India

Print ISSN: 0003-2778

GENERAL INFORMATION

About the Journal

Journal of the Anatomical Society of India (ISSN: Print 0003-2778) is peer-reviewed journal. The journal is owned and run by Anatomical Society of India. The journal publishes research articles related to all aspects of Anatomy and allied medical/surgical sciences. Pre-Publication Peer Review and Post-Publication Peer Review Online Manuscript Submission System Selection of articles on the basis of MRS system Eminent academicians across the globe as the Editorial board members Electronic Table of Contents alerts Available in both online and print form. The journal is published quarterly in the months of January, April, July and October.

Scope of the Journal

The aim of the *Journal of the Anatomical Society of India* is to enhance and upgrade the research work in the field of anatomy and allied clinical subjects. It provides an integrative forum for anatomists across the globe to exchange their knowledge and views. It also helps to promote communication among fellow academicians and researchers worldwide. The Journal is devoted to publish recent original research work and recent advances in the field of Anatomical Sciences and allied clinical subjects. It provides an opportunity to academicians to disseminate their knowledge that is directly relevant to all domains of health sciences.

The Editorial Board comprises of academicians across the globe.

JASI is indexed in Scopus, available in Science Direct.

Abstracting and Indexing Information

The journal is registered with the following abstracting partners:

Baidu Scholar, CNKI (China National Knowledge Infrastructure), EBSCO Publishing's Electronic Databases, Ex Libris – Primo Central, Google Scholar, Hinari, Infotrieve, Netherlands ISSN center, ProQuest, TdNet, Wanfang Data

The journal is indexed with, or included in, the following:

SCOPUS, Science Citation Index Expanded, IndMed, MedInd, Scimago Journal Ranking, Emerging Sources Citation Index.

Impact Factor® as reported in the 2023 Journal Citation Reports® (Clarivate Analytics, 2024): 0.2

Information for Authors

Article processing and publication charges will be communicated by the editorial office. All manuscripts must be submitted online at https://review.jow.medknow.com/jasi.

Subscription Information

A subscription to JASI comprises 4 issues. Prices include postage. Annual Subscription Rate for non-members-		
Annual Subscription Rate for non-members		
	India	**Outside India**
Institutional	INR 15000	USD 1200
Individual	INR 7,500	USD 800
The Journal of Anatomical Society of India (ISSN: 0003-2778) is published quarterly **Subscriptions** are accepted on a prepaid basis only and are entered on a calendar year basis. Issues are sent by standard mail Priority rates are available upon request.		

Information to Members/Subscribers

All members and existing subscribers of the Anatomical Society of India are requested to send their membership/existing subscription fee for the current year to the Treasurer of the Society on the following address: Prof (Dr.) Punit Manik, Treasurer, ASI, Department of Anatomy, KGMU, Lucknow - 226003. Email: punitamanik@yahoo.co.in. All payments should be made through an account payee bank draft drawn in favor of the **Treasurer, Anatomical Society of India,** payable at **Lucknow** only, preferably for **Allahabad Bank, Medical College Branch, Lucknow.** Outstation cheques/drafts must include INR 70 extra as bank collection charges.

All complaints regarding non-receipt of journal issues should be addressed to the Editor-in-Chief, JASI at editorjasi@gmail.com. The new subscribers may, please contact wkhlrpmedknow_subscriptions@wolterskluwer.com.

Requests of any general information like travel concession forms, venue of next annual conference, etc. should be addressed to the General Secretary of the Anatomical Society of India.

For mode of payment and other details, please visit www.medknow.com/subscribe.asp

Claims for missing issues will be serviced at no charge if received within 60 days of the cover date for domestic subscribers, and 3 months for subscribers outside India. Duplicate copies cannot be sent to replace issues not delivered because of failure to notify publisher of change of address. The journal is published and distributed by Wolters Kluwer India Pvt. Ltd. Copies are sent to subscribers directly from the publisher's address. It is illegal to acquire copies from any other source. If a copy is received for personal use as a member of the association/society, one cannot resale or give-away the copy for commercial or library use.

The copies of the journal to the subscribers are sent by ordinary post. The editorial board, association or publisher will not be responsible for non receipt of copies. If any subscriber wishes to receive the copies by registered post or courier, kindly contact the publisher's office. If a copy returns due to incomplete, incorrect or changed address of a subscriber on two consecutive occasions, the names of such subscribers will be deleted from the mailing list of the journal. Providing complete, correct and up-to-date address is the responsibility of the subscriber.

Nonmembers: Please send change of address information to subscriptions@medknow.com.

Advertising Policies

The journal accepts display and classified advertising. Frequency discounts and special positions are available. Inquiries about advertising should be sent to Wolters Kluwer India Pvt. Ltd, advertise@medknow. com.

The journal reserves the right to reject any advertisement considered unsuitable according to the set policies of the journal.

The appearance of advertising or product information in the various sections in the journal does not constitute an endorsement or approval by the journal and/or its publisher of the quality or value of the said product or of claims made for it by its manufacturer.

Addresses

Editorial Office

Dr. Vishram Singh, Editor-in-Chief, JASI
B5/3 Hahnemann Enclave, Plot No. 40, Sector 6, Dwarka Phase – 2,
New Delhi - 110 075, India.
Email: editorjasi@gmail.com

Published by

Wolters Kluwer India Pvt. Ltd.,
Fourth Floor, East Wing, Marisoft III, Marisoft Premises,
Part of Software Technology Park, S. No. 15, Vadgaon Sheri,
Kalyani Nagar, Pune – 411 014, Maharashtra, India.
Website: www.medknow.com

Printed at

Nikeda Art Printers Pvt. Ltd.,
Building No. C/3 - 14,15,16, Shree Balaji Complex, Vehele Road,
Village Bhatale, Taluka Bhiwandi, District Thane - 421302, India.

Journal of the Anatomical Society of India

Print ISSN: 0003-2778

EDITORIAL BOARD

Journal of the Anatomical Society of India

Volume 74 | Issue 1 | January-March 2025

CONTENTS

Journal of the Anatomical Society of India on Web

https://review.jow.medknow.com/jasi

The Journal of the Anatomical Society of India now accepts articles electronically. It is easy, convenient and fast. Check following steps:

1 Registration

- Register from https://review.jow.medknow.com/jasi as a new author (Signup as author)
- Two-step self-explanatory process

2 New article submission

- Read instructions on the journal website or download the same from manuscript management site
- Prepare your files (Article file, First page file and Images, Copyright form & Other forms, if any)
- Login as an author
- Click on 'Submit new article' under 'Submissions'
- Follow the steps (guidelines provided while submitting the article)
- On successful submission you will receive an acknowledgement quoting the manuscript ID

3 Tracking the progress

- Login as an author
- The report on the main page gives status of the articles and its due date to move to next phase
- More details can be obtained by clicking on the ManuscriptID
- Comments sent by the editor and reviewer will be available from these pages

4 Submitting a revised article

- Login as an author
- On the main page click on 'Articles for Revision'
- Click on the link "Click here to revise your article" against the required manuscript ID
- Follow the steps (guidelines provided while revising the article)
- Include the reviewers' comments along with the point to point clarifications at the beginning of the revised article file.
- Do not include authors' name in the article file.
- Upload the revised article file against New Article File - Browse, choose your file and then click "Upload" OR Click "Finish"
- On completion of revision process you will be able to check the latest file uploaded from Article Cycle (In Review Articles-> Click on manuscript id -> Latest file will have a number with 'R', for example XXXX_100_15R3.docx)

Facilities

- Submission of new articles with images
- Submission of revised articles
- Checking of proofs
- Track the progress of article until published

Advantages

- Any-time, any-where access
- Faster review
- Cost saving on postage
- No need for hard-copy submission
- Ability to track the progress
- Ease of contacting the journal

Requirements for usage

- Computer and internet connection
- Web-browser (Latest versions - IE, Chrome, Safari, FireFox, Opera)
- Cookies and javascript to be enabled in web-browser

Online submission checklist

- First Page File (rtf/doc/docx file) with title page, covering letter, acknowledgement, etc.
- Article File (rtf/doc/docx file) - text of the article, beginning from Title, Abstract till References (including tables). File size limit 4 MB. Do not include images in this file.
- Images (jpg/jpeg/png/gif/tif/tiff): Submit good quality colour images. Each image should be less than 10 MB) in size
- Upload copyright form in .doc / .docx / .pdf / .jpg / .png / .gif format, duly signed by all authors, during the time mentioned in the instructions.

Help

- Check Frequently Asked Questions (FAQs) on the site
- In case of any difficulty contact the editor

Journal of the Anatomical Society of India

Print ISSN: 0003-2778

EDITORIAL BOARD

Journal of the Anatomical Society of India

Volume 74 | Issue 1 | January-March 2025

CONTENTS

Journal of the Anatomical Society of India on Web

https://review.jow.medknow.com/jasi

The Journal of the Anatomical Society of India now accepts articles electronically. It is easy, convenient and fast. Check following steps:

1 Registration

- Register from https://review.jow.medknow.com/jasi as a new author (Signup as author)
- Two-step self-explanatory process

2 New article submission

- Read instructions on the journal website or download the same from manuscript management site
- Prepare your files (Article file, First page file and Images, Copyright form & Other forms, if any)
- Login as an author
- Click on 'Submit new article' under 'Submissions'
- Follow the steps (guidelines provided while submitting the article)
- On successful submission you will receive an acknowledgement quoting the manuscript ID

3 Tracking the progress

- Login as an author
- The report on the main page gives status of the articles and its due date to move to next phase
- More details can be obtained by clicking on the ManuscriptID
- Comments sent by the editor and reviewer will be available from these pages

4 Submitting a revised article

- Login as an author
- On the main page click on 'Articles for Revision'
- Click on the link "Click here to revise your article" against the required manuscript ID
- Follow the steps (guidelines provided while revising the article)
- Include the reviewers' comments along with the point to point clarifications at the beginning of the revised article file.
- Do not include authors' name in the article file.
- Upload the revised article file against New Article File - Browse, choose your file and then click "Upload" OR Click "Finish"
- On completion of revision process you will be able to check the latest file uploaded from Article Cycle (In Review Articles-> Click on manuscript id -> Latest file will have a number with 'R', for example XXXX_100_15R3.docx)

Facilities

- Submission of new articles with images
- Submission of revised articles
- Checking of proofs
- Track the progress of article until published

Advantages

- Any-time, any-where access
- Faster review
- Cost saving on postage
- No need for hard-copy submission
- Ability to track the progress
- Ease of contacting the journal

Requirements for usage

- Computer and internet connection
- Web-browser (Latest versions - IE, Chrome, Safari, FireFox, Opera)
- Cookies and javascript to be enabled in web-browser

Online submission checklist

- First Page File (rtf/doc/docx file) with title page, covering letter, acknowledgement, etc.
- Article File (rtf/doc/docx file) - text of the article, beginning from Title, Abstract till References (including tables). File size limit 4 MB. Do not include images in this file.
- Images (jpg/jpeg/png/gif/tif/tiff): Submit good quality colour images. Each image should be less than 10 MB) in size
- Upload copyright form in .doc / .docx / .pdf / .jpg / .png / .gif format, duly signed by all authors, during the time mentioned in the instructions.

Help

- Check Frequently Asked Questions (FAQs) on the site
- In case of any difficulty contact the editor

Neuroanatomical Basis of Epilepsy and a Brief Insight into Related Imaging Modalities

Epilepsy is a chronic neurological disorder characterized by recurrent, unprovoked seizures. These seizures are the result of abnormal electrical discharges in the brain, which can disrupt normal brain function and consciousness. The main signs and symptoms of epilepsy include head-and-eye deviation, jerking automatic movements, involuntary chewing, uncontrolled shaking, body stiffening, and loss of consciousness. The disorder affects approximately 1% of the global population, with about 30%–40% of patients experiencing seizures that are resistant to antiepileptic drugs.[1-3] This resistance to treatment warrants a deeper understanding of its neuroanatomical basis and the role of advanced imaging modalities such as functional magnetic resonance imaging (fMRI) and single-photon emission computed tomography (SPECT) in its diagnosis.

The Neuroanatomical Basis of Epilepsy

Epilepsy is often associated with specific structural and functional abnormalities in the brain. These abnormalities can be either localized or generalized, based on the epilepsy type. The most common forms are as follows:

Temporal lobe epilepsy

- The temporal lobe epilepsy (TLE) is the most common form of focal epilepsy. It originates in temporal lobe, which is responsible for memory, emotions, and interpreting sound. It is often associated with mesial temporal sclerosis, a condition characterized by hippocampal atrophy and neuronal loss.[2,4] The hippocampus is crucial for memory and spatial navigation, and its dysfunction is linked to cognitive impairments in TLE patients. Functional and structural connectivity studies have shown that TLE is associated with widespread network alterations, including reduced functional connectivity in the default mode network (DMN) and sensory-motor networks.[4,5]

Extratemporal lobe epilepsy

- Extratemporal lobe epilepsy (ELTE) is a type of epilepsy that originates outside the temporal lobe. It can affect the frontal, parietal, or occipital lobes. The ELTE is often associated with malformations of cortical development, such as focal cortical dysplasia, which are congenital abnormalities in brain development.[2,3] These malformations can lead to abnormal neuronal connectivity and hyperexcitability, making them highly epileptogenic.[3]

Idiopathic generalized epilepsy

- Idiopathic generalized epilepsy (IGE) involves generalized seizures affecting both brain hemispheres simultaneously. It is often associated with genetic mutations that affect ion channel function and neuronal excitability.[6] Functional imaging studies have shown that IGE is associated with altered functional connectivity in large-scale brain networks, including the DMN and attention networks.[6,7]

Insights into the Imaging Modalities in Epilepsy

Functional magnetic resonance imaging

It is a noninvasive imaging modality that measures changes in blood oxygen level-dependent (BOLD) signals, providing insights into brain activity and connectivity. In the context of epilepsy, fMRI has been instrumental in mapping the epileptogenic zone and understanding the underlying neural networks.

- Mapping the epileptogenic zone: The epileptogenic zone is the region of the brain that generates seizures. fMRI can identify this zone by detecting abnormal BOLD signal changes associated with epileptic discharges.[8,9] Resting-state fMRI (rs-fMRI) has been particularly useful in identifying alterations in functional connectivity within and between brain networks, which are often disrupted in epilepsy[5,9]
- Functional connectivity and network analysis: rs-fMRI studies have shown that epilepsy is associated with reduced functional connectivity within the DMN and between the DMN and other networks, such as the sensory-motor and attention networks.[5,8] These connectivity alterations are thought to contribute to the cognitive and behavioral impairments observed in epilepsy patients.[5,10]

fMRI is increasingly being used in presurgical evaluation to map the epileptogenic zone and to plan surgical resections.[8,11]

Single-photon Emission Computed Tomography

It is a nuclear imaging modality that measures regional cerebral blood flow. It has been widely used in the presurgical evaluation of epilepsy to localize the epileptogenic zone.

- Ictal and interictal single-photon emission computed tomography: Ictal SPECT, performed during a seizure, shows hyperperfusion in the epileptogenic zone due to increased blood flow.[1,9] Interictal SPECT, performed between seizures, often shows hypoperfusion in the epileptogenic zone.[1,9] The subtraction ictal SPECT co-registered to MRI (SISCOM) technique enhances the localization of the epileptogenic zone by subtracting interictal from ictal SPECT images and co-registering the result with MRI.[1,9]

SPECT is particularly useful in patients with MRI-negative epilepsy, where structural abnormalities are not evident on MRI.

Both fMRI and SPECT provide complementary information in the evaluation of epilepsy. The integration of these modalities with other imaging techniques, such as MRI and PET, has revolutionized the presurgical evaluation of epilepsy, enabling more accurate localization of the epileptogenic zone and improved surgical planning.[3,6]

Conclusion

The neuroanatomical basis of epilepsy involves an intricate interplay of structural, functional, and cellular mechanisms that contribute to the generation and propagation of seizures. Advanced imaging modalities such as fMRI and SPECT have significantly enhanced our understanding of the epileptogenic zone and the underlying neural networks. These techniques are invaluable in the presurgical evaluation of epilepsy, offering insights that guide surgical resections and improve patient outcomes. Furthermore, they contribute to the development of personalized treatment strategies, such as neuromodulation therapies (e.g., vagus nerve stimulation or deep brain stimulation), which target specific nodes within the epileptic network[12] to further refine the management of epilepsy.

Financial support and sponsorship

Nil.

Conflicts of interest

There are no conflicts of interest.

Vishram Singh, Krishna Chaitanya Reddy[1], Rashi Singh[2], Gaurav Singh[3]

Department of Anatomy, Kasturba Medical College, Manipal Academy of Higher Education, Mangalore, Karnataka, [2]Department of Pediatric and Preventive Dentistry, Santosh Dental College and Hospital, NCR Delhi, Ghaziabad, [3]Clinical Editor, British Medical Journal, NCR Delhi, Noida, Uttar Pradesh, India, [1]Department of Anatomy, Faculty of Medicine, MAHSA University, Selangor, Malaysia

Address for correspondence: *Prof. Vishram Singh, B5/3 Hahnemann Enclave, Plot No. 40, Sector 6, Dwarka Phase - 2, New Delhi - 110 075, India.*
E-mail: drvishramsingh@gmail.com

References

1. Sukprakun C, Tepmongkol S. Nuclear imaging for localization and surgical outcome prediction in epilepsy: A review of latest discoveries and future perspectives. Frontiers in neurology, 2022;13:1083775.
2. Tavakol S, Royer J, Lowe AJ, Bonilha L, Tracy JI, Jackson GD, *et al.* Neuroimaging and connectomics of drug-resistant epilepsy at multiple scales: From focal lesions to macroscale networks. Epilepsia 2019;60:593-604.
3. Yao L, Cheng N, Chen AQ, Wang X, Gao M, Kong QX, *et al.* Advances in neuroimaging and multiple post-processing techniques for epileptogenic zone detection of drug-resistant epilepsy. J Magn Reson Imaging 2024;60:2309-31.
4. Xie K, Royer J, Larivière S, Rodriguez-Cruces R, Frässle S, Cabalo DG, *et al*. Atypical connectome topography and signal flow in temporal lobe epilepsy. Progress in neurobiology, 2024;236:102604.
5. Courtiol J, Guye M, Bartolomei F, Petkoski S, Jirsa VK. Dynamical mechanisms of interictal resting-state functional connectivity in epilepsy. J Neurosci 2020;40:5572-88.
6. Hsu YC, Lim SN, Chao Y.P. Brain Functional Network Topology and Seed-based Connectivity Alterations in Idiopathic Generalized Epilepsy Patients: An fMRI Study. In Proceedings of the 2023 7th International Conference on Medical and Health Informatics 2023:39-43.
7. Centeno M, Carmichael DW. Network connectivity in epilepsy: Resting state fMRI and EEG-fMRI contributions. Front Neurol 2014;5:93.
8. Ikemoto S, von Ellenrieder N, Gotman J. Electroencephalography-functional magnetic resonance imaging of epileptiform discharges: Noninvasive investigation of the whole brain. Epilepsia 2022;63:2725-44.
9. Wirsich J, Iannotti GR, Ridley B, Shamshiri EA, Sheybani L, Grouiller F, *et al*. Altered correlation of concurrently recorded EEG-fMRI connectomes in temporal lobe epilepsy. Network Neuroscience, 2024;8:466-485..
10. Maesawa S, Bagarinao E, Nakatsubo D, Ishizaki T, Takai S, Torii J, *et al.* Multitier network analysis using resting-state functional MRI for epilepsy surgery. Neurol Med Chir (Tokyo) 2022;62:45-55.
11. Cankurtaran CZ, Templer J, Bandt SK, Avery R, Hijaz T, McComb EN, *et al.* Multimodal presurgical evaluation of medically refractory focal epilepsy in adults: An update for radiologists. Am J Roentgenol 2022;219:488-500.
12. Englot DJ, Chang EF, Auguste KI. Vagus nerve stimulation for epilepsy: A meta-analysis of efficacy and predictors of response. J Neurosurg 2011;115:1248-55.

Article Info

Received: 15 February 2025
Accepted: 01 March 2025
Available online: 31 March 2025

Access this article online	
Quick Response Code:	**Website:** https://journals.lww.com/joai
	DOI: 10.4103/jasi.jasi_40_25

How to cite this article: Singh V, Reddy KC, Singh R, Singh G. Neuroanatomical basis of Epilepsy and a brief insight into related imaging modalities. J Anat Soc India 2025;74:1-2.

Original Article

Exploring *Ceratonia siliqua* Seeds Oil and Metformin for PCOS Treatment: Mechanistic Insights into PI3K/AKT Pathway, Inflammation, and Oxidative Stress

Xu Zhang, Anyu Tang[1], Juan Zhang[2], Xiaofei Wang[3]

Department of Gynecology, The First Hospital of Shanxi Medical University, Taiyuan Shanxi, [1]Department of Ophthalmology, Affiliated Hospital of Xiangnan University, Chenzhou Hunan, [2]Department of Obstetrical, The Affiliated Jiangning Hospital of Nanjing Medical University, Nanjing Jiangsu, [3]Department of Gynecology, The Obstetrics and Gynecology Hospital of Fudan University (Shanghai Red House Obstetrics and Gynecology Hospital), Shanghai, China

Abstract

Introduction: Polycystic ovary syndrome (PCOS) is a leading cause of infertility, irregular menstrual cycles, and anovulation in women. This study aimed to investigate the therapeutic effects of *Ceratonia siliqua* L. seed oil (CSSO) on PCOS in rats. **Subjects and Methods:** In this experimental study, 70 rats were divided into seven groups (n = 10/group) and studied over 50 days: The healthy control, patient (PCOS), metformin (MET + PCOS), 100 and 200 mg/kg CSSO treatment (100 and 200 CSSO + PCOS), and synergistic (MET + 100 and 200CSSO + PCOS) groups. Levels of luteinizing hormone, follicle-stimulating hormone, progesterone, and testosterone were measured. Serum levels of inflammatory cytokines and antioxidant parameters were assessed. Total antioxidant capacity and lipid peroxidation levels in ovarian tissue were analyzed. Gene expression of GLUT-4, AKT, PI3K, and PTEN was evaluated using real-time polymerase chain reaction, and their protein expression was assessed by western blotting. The expression of Ki-67 protein and apoptosis were evaluated using immunohistochemistry. **Results:** CSSO, especially in combination with MET, significantly improved hormonal, inflammatory, and antioxidant parameters compared to the PCOS and MET groups. In the synergistic groups, CSSO enhanced apoptosis of granulosa cells by activating the PI3K/AKT pathway, leading to an increase in Ki-67-positive cells. CSSO extract, particularly when used in combination with MET, can enhance the hypothalamic–pituitary–ovary axis function through its anti-inflammatory and antioxidant effects. **Conclusion:** CSSO can promote apoptosis in cystic granulosa cells, making it a potential therapeutic agent for PCOS.

Keywords: *Ceratonia silique L, estradiol, inflammation, oxidative stress, polycystic ovarian syndrome*

Introduction

Polycystic ovary syndrome (PCOS) is a prevalent cause of female infertility, accounting for 12%–15% of cases and nearly 45% in couples.[1] This multifactorial disorder is characterized by symptoms such as hyperandrogenism, irregular ovulation, and menstrual disturbances, and poses increased risks for cardiovascular disease, type 2 diabetes, and psychological issues.[2,3] PCOS disrupts the hypothalamic–pituitary–ovarian (HPO) axis, leading to hormonal imbalances that impair ovarian function and increase T levels. Oxidative stress exacerbates insulin resistance, contributing to cyst formation and reproductive health issues.[4] Metformin (MET) is commonly prescribed to improve insulin sensitivity in PCOS patients, aiding in ovulation restoration and enhancing IVF outcomes.[5]

Ceratonia siliqua L. (carob) is a Mediterranean tree known for its health benefits. Its seeds, rich in bioactive compounds such as polyphenols and fibers, possess antioxidant, anti-inflammatory, and antidiabetic properties.[6,7] *Ceratonia siliqua* L. seed oil (CSSO) may help reduce oxidative stress affecting ovarian function and regulate blood sugar levels, benefiting women with PCOS.[8] In addition, its anti-inflammatory properties can mitigate chronic inflammation impacting reproductive health, while compounds such as isoflavonoids and flavonoids enhance pathways relevant to fertility, supporting hormonal balance and overall reproductive health. Furthermore, CSSO's anti-inflammatory compounds (modulate pro-inflammatory cytokines IL-1 β, CRP, TNF-α, and IL-6) may reduce chronic inflammation that impacts reproductive health, and its role in regulating metabolic

How to cite this article: Zhang X, Tang A, Zhang J, Wang X. Exploring *Ceratonia siliqua* seeds oil and metformin for PCOS treatment: Mechanistic insights into PI3K/AKT pathway, inflammation, and oxidative stress. J Anat Soc India 2025;74:3-11.

Article Info

Received: 08 October 2024
Revised: 01 February 2025
Accepted: 15 February 2025
Available online: 31 March 2025

Address for correspondence:
Dr. Xiaofei Wang, Department of Gynecology, The Obstetrics and Gynecology Hospital of Fudan University (Shanghai Red House Obstetrics and Gynecology Hospital), Shanghai 200090, China.
E-mail: wangxiaofei2024@outlook.com

Access this article online

Website: https://journals.lww.com/joai

DOI: 10.4103/jasi.jasi_164_24

Quick Response Code:

and cardiovascular health could promote hormonal balance.[9] Isoflavonoids and flavonoids in CSSO, such as daidzein, luteolin, and quercetin, are known to modulate pro-inflammatory cytokines and enhance the PI3K/AKT pathway, which is relevant for fertility.[10]

This study examined the impact of CSSO on endocrine and biochemical markers, focusing on its anti-inflammatory and antioxidant properties, as well as its influence on folliculogenesis and granulosa cell apoptosis pathways, including the PI3K/AKT/GLUT-4 axis, in a rat model of PCOS induced by estradiol.

Subjects and Methods

Ceratonia siliqua L. seed oilpreparation

To produce the CSSO, 4400 g of dried *Ceratonia siliqua* L. seeds were finely ground using a soil grinder (Humboldt Company, US, Catalog Number: H-4199.5F). The resulting powder was combined with a solvent mixture of hexane and ethanol (20:80 v/v) and incubated at 40°C in darkness for 72 h. After the incubation period, the solution was filtered through filter paper (Millipore, US, Catalog Number: 1442-125; No. 40) and concentrated with a rotary evaporator (Buchi Rotavapor, Switzerland, model 9230). The extraction yielded 320 g of CSSO, with an efficiency rate of 7.2%, and was stored at −4°C.[11]

Animal care procedures, group assignments, treatment protocols, experimental design, and research timeline

Animal care

A total of 110 adult Wistar rats, aged 3 months and weighing 180 ± 40 g, were housed in propylene cages under controlled conditions. The environment was maintained at a temperature of 24 ± 4°C, with a relative humidity of 35 ± 5%, and a 12-h dark/light cycle. The rats were given 72 h to acclimate to the laboratory setting before initiating the PCOS model. They had continuous access to tap water and standard laboratory rat pellets. The study adhered to international guidelines, protocols, and ethical standards, as approved by the Ethics Committee of the Hospital of Fudan University.[12]

Polycystic ovary syndrome induction and animal grouping

A total of 100 rats received intramuscular injections of estradiol valerate at a dose of 2 mg/kg, dissolved in 0.5 ml of olive oil, administered twice with a 1-week interval. Sixty days later, 60 rats were selected based on clinical signs. Indicators such as permanent vaginal cornification in the vaginal epithelium, vaginal smear assessments, and the presence of vaginal plaques were used to monitor and evaluate PCOS induction in the rats. These markers are useful for tracking hormonal changes and reproductive abnormalities linked to PCOS. Rats showing permanent vaginal cornification in the vaginal epithelium, epithelial keratinocytes in vaginal smears, and vaginal plaques were chosen as the PCOS model. The study groups were organized as follows:

- Healthy control group: Non-PCOS rats were given 1 ml of normal saline daily via gavage for 50 days
- PCOS-induced group (PCOS): Rats with induced PCOS were given 1 ml of normal saline daily via gavage for 50 days
- MET + PCOS group: Rats with induced PCOS were administered 300 mg/kg of MET, dissolved in 1 ml of normal saline, daily via gavage for 50 days
- 100 and 200 CSSO + PCOS groups: Rats with induced PCOS were administered 100 or 200 mg/kg of CSSO daily via gavage for 50 days
- MET + 100 and 200 CSSO + PCOS groups: Rats with induced PCOS were given 100 or 200 mg/kg of CSSO along with 300 mg/kg of MET, dissolved in 1 ml of normal saline, daily via gavage for 50 days.

During the 50-day study period, CSSO was administered daily at 9:00 am and MET at 3:00 pm.[12,13]

Assay of serum progesterone (P), follicle-stimulating hormone, luteinizing hormone, testosterone (T), and hormones

On the 51st day, at the culmination of the study, the rats were euthanized using a preanesthetic protocol with 100 mg/kg xylazine 2% (Sigma, St. Louis, MO, US), followed by anesthesia with 15 mg/kg ketamine 10% (Sigma, St. Louis, MO, US). Following euthanasia, blood samples were collected via cardiac puncture. The serum was then separated by centrifuging the blood at 12,000 g for 10 min. Hormone levels were measured using commercial ELISA kits from Novus Biologicals (Centennial, Colorado, US) according to the manufacturer's instructions: T (Catalog Number: NBP2-42044), P (Catalog Number: NBP2-60127-1), follicle-stimulating hormone (FSH) (Catalog Number: KA2330), and luteinizing hormone (LH) (Catalog Number: NBP2-68054). All procedures adhered strictly to the recommended protocols provided by the manufacturer.[14]

Ovarian tissue antioxidant assay

Ovarian tissue total antioxidant capacity

To assess the total antioxidant capacity (TAC) of ovarian tissue, we employed ferric-reducing ability of plasma (FRAP) assays. First, ovarian tissue was carefully separated from surrounding peri-ovarian fat and prepared into homogenized samples. Specifically, 100 µl of the homogenized tissue was washed with 200 µl of cold phosphate-buffered saline and transferred into a 2 ml polyethylene tube. Subsequently, 10 µl of FRAP solution (Catalog Number: EIAFECL2; Thermo Fisher Scientific Inc., Lonsee, Germany) was added to the tube. The mixture was incubated for 15 min at 25°C, followed by centrifugation at 12,000 g for 10 min. The absorbance of the resulting supernatant was then measured using a UV-visible spectrophotometer.[15]

Ovarian tissue lipid peroxidation levels

To assess ovarian lipid peroxidation levels, a thiobarbituric acid reactive substance (TBARS) assay was employed. Initially, 100 µl of homogenized ovarian tissue was added to a 2 ml polyethylene tube. Subsequently, 100 µl of TBARS solution (Catalog Number: EEA021, Invitrogen Inc, Lonsee, Germany) was added to the tube. The resulting mixture was then incubated at 37°C for 30 min. Following incubation, the absorbance was measured using a UV-visible spectrophotometer, as previously described.[16]

Real-time polymerase chain reaction assay

Total RNA extraction, cDNA synthesis, and quantitative real-time polymerase chain reaction assay

To extract total RNA from 60 mg of ovarian tissue, 1 ml of TRIzol reagent (Catalog Number: 12183555, Invitrogen Inc, Lonsee, Germany) was added and incubated for 2 min at 25°C. Subsequently, a commercial cDNA synthesis kit (Catalog Number: RTK0104, Takara Bio., Tokyo, Japan) was employed to synthesize cDNA from the extracted RNA, following the manufacturer's guidelines. The cDNA synthesis reaction mixture consisted of 1000 ng of total RNA, 1 µl of oligo and random primers, 10 µl of Takara Bio Mastermix, and 8 µl of deionized water. This mixture was then transferred to a thermal cycler (Thermo Fisher Scientific Inc, Lonsee, Germany) and subjected to a temperature protocol consisting of 10 min at 25°C, 45 min at 60°C, and 5 min at 60°C. For real-time polymerase chain reaction (PCR), a mixture was prepared containing 1000 nanograms of cDNA, 1 µl of reverse and forward primers, and 8 µl of Takara Bio Mastermix. The expression levels of GLUT-4, PI3K, AKT, PTEN, and AKT genes were measured using this mixture in an Applied Biosystems thermocycler (Quantstudio 1, Chicago, US). The annealing temperature was set to 60°C for 1 min per cycle, and a melting curve was generated by increasing the temperature from 60°C to 95°C at a rate of 1°C per second. The threshold cycle (CT) values for the genes, including the control (C), sample (S), and β-actin, were recorded and used to calculate the fold change using the formula $2^{-\Delta\Delta CT}$.

$\Delta\Delta CT = [(CT_S - Ct_{\beta\text{-actin}}) - (CT_S - CT_C)]$, Fold change of genes = $2^{-\Delta\Delta CT}$

The internal reference gene used was β-actin, which was chosen due to its stability and consistency. The primers used in the study were designed using Primer-3 and validated through NCBI's blast search. The primer sequences used were as follows: β-actin forward, 5′-AGGCATCCTCACCCTGAAGTA-3′; β-actin reverse, 5′-CACACGCAGCTCATTGTAGA-3′; PI3K forward, 5′-AACACAGAAGACCAATACTC-3′; PI3K reverse, 5′-TTCGCCATCTACCACTAC-3′; PTEN forward, 5′-AATTCCCAGAGGCGCTATGT-3′; PTEN reverse, 5′-GATTGCAAGTTCCGCCACTGAACA-3′; GLUT-4 forward, 5′-ACCCACCGGCAGCCTCTGATT-3′; GLUT-4 reverse, 5′-GGTGGCGTAGGCTGGCTGTT-3′; and AKT forward, 5′-GTGGCAAGATGTGTATGAG-3′; AKT reverse, 5′-CTGGCTGAGTAGGAGAAC-3′.[17]

Western blotting assay

The expression of PI3K/AKT pathway proteins was evaluated using Western blotting. To begin, 200 µl of phosphate-buffered saline was used to wash the ovarian tissue. Subsequently, 50 mg of the homogenized ovarian tissue was lysed with radio-immunoprecipitation assay (RIPA) buffer (Sigma, St. Louis, MO, US), which contained 50 mmol/l Tris-HCl, 150 mmol/l NaCl, and 0.1% w/v nonyl phenoxypolyethoxylethanol. After centrifugation at −4°C for 10 min at 12,000 g, 50 µg of the supernatant was mixed with 10 µl of loading buffer. The loading buffer (Sigma, St. Louis, MO, USA) comprised 62.5 mmol/l Tris-HCl, 1 µl β-mercaptoethanol, 5 µl of 10% glycerol, and 5 µl of 0.5% w/v sodium deoxycholate. This mixture was incubated for 10 min and then loaded onto a 10% SDS polyacrylamide gel (Catalog Number: WBKLS0100; Millipore Bio Inc., Feltham, UK). Following electrophoresis, the proteins were transferred to a polyvinylidene fluoride (PVDF) membrane. The membrane was incubated overnight at 4°C with primary antibodies: GeneTex AKT (Catalog Number: GTX121937; 1:500), GLUT-4 (Catalog Number: GTX60674; 1:200), PTEN (Catalog Number: GTX101025; 1:1000), and PI3K (Catalog Number: GTX100462; 1:100), all sourced from GeneTex Bio (Chicago, US). Afterward, an HRP-conjugated secondary antibody was applied and incubated for 1 h at 37°C. Excess antibodies were removed by washing with tris-buffered saline containing 0.05% Tween-20. Protein bands were visualized using enhanced chemiluminescence reagent (e-BLOT Company, Beijing, China) and recorded with Bio-Rad software (Bio-Rad Laboratories, Inc., California, US). Image J software was used for further analysis.[18]

Immunohistochemistry assay

The presence of Ki-67-positive cells was used as a marker to identify apoptotic differentiation in ovarian follicular and parenchymal cells. The ovarian tissues were first washed with phosphate-buffered saline, followed by routine processing, and then embedded in paraffin wax. Thin sections (5 µm) were cut from these blocks and mounted on slides. The slides were then deparaffinized in xylene for 5–10 min, followed by rehydration in ethanol/distilled water solutions at 100%, 95%, 70%, and 50% (v/v) for 2–5 min each, and then rinsed in distilled water for 5 min. This process was performed in Coplin jars. Next, the slides were incubated overnight at 95°C in a dry bath. The slides were then treated with 0.3% hydrogen peroxide in methanol for 20 min at room temperature, followed by incubation with primary Ki-67 antibodies (1:1000; Catalog Number: AF7649) from RandD Systems, Inc.(Centennial, Colorado, US) for 1 h at 25°C. Tween-20 was used as a washing buffer, and 5% w/v bovine serum albumin was

used to block residual antibodies. A biotinylated secondary antibody was applied, followed by streptavidin-HRP for 60 min at room temperature. The sections were then rinsed with PBS and treated with 3,3'-diaminobenzidine. All slides were counterstained with hematoxylin. The tissue sections were evaluated under a BX61TRF light microscope (Olympus, Tokyo, Japan) connected to ImageJ software at × 100 magnification, and the percentage of Ki-67-positive cells relative to all cells was reported in 10 random fields of view in each experimental group.[17]

Ovarian tissue histopathology

Ovarian tissue was processed and 5 µm sections were cut from paraffin wax blocks. These sections were stained with hematoxylin and eosin. The sections were then evaluated using a BX61TRF light microscope (Olympus, Tokyo, Japan) connected to ImageJ software to assess follicle differentiation and histopathological features, including cystic follicles, inner and outer theca layers, and granulosa/corona radiata cells. In addition, the mean number of cystic (CF), primordial follicle (PrF), primary follicle (PF), and antral follicles (AF) was determined by counting them in 10 random fields of view for each experimental group. Histological examination revealed CFs, characterized by enlarged size, a thinned granulosa layer, changes in the theca layer, and the absence or degeneration of the oocyte. In contrast, AFs, a normal stage of follicular development, featured multiple layers of proliferative granulosa cells, a well-defined antrum filled with follicular fluid, and distinct theca layers. AFs typically exhibited healthy oocyte and organized granulosa cells with normal theca interna.[12]

Statistical analysis

To compare the quantitative results between the experimental groups, we employed a one-way analysis of variance (ANOVA) followed by the Newman–Keuls *post hoc* test. A $P < 0.05$ was considered statistically significant. The normality of the data was assessed using the Kolmogorov–Smirnov test, and a $P > 0.05$ was considered statistically significant for normally distributed and homogeneous data. All results were presented as means ± standard deviation (SD). For data analysis, we utilized SPSS software version 16 [IBM Inc., Endicott, New York, US].

Results

Weights of body and femur in rats

The PCOS group exhibited a significant increase in both body weight and ovarian weight compared to the healthy control group ($P < 0.05$). In the MET + PCOS group, while both weight parameters were lower than in the PCOS group, the reduction was statistically significant only for body weight ($P < 0.05$). Treatment with CSSO extract significantly reduced both body and ovarian weights in the MET + 100 CSSO + PCOS and MET + 200 CSSO + PCOS groups compared to the PCOS group ($P < 0.05$). Although CSSO extract alone (in the 100 CSSO + PCOS and 200 CSSO + PCOS groups) also resulted in a reduction in body and ovarian weights relative to the PCOS group, these decreases were not statistically significant ($P > 0.05$) [Figure 1].

Serum follicle-stimulating hormone, luteinizing hormone, progesterone, and testosterone levels

The PCOS group demonstrated significantly elevated serum levels of LH and T compared to the healthy control group ($P < 0.05$), while serum levels of FSH and progesterone (P) were significantly reduced in the PCOS group ($P < 0.05$). In comparison, the MET + PCOS group showed a significant reduction in LH levels ($P < 0.05$). Although MET treatment in the MET + PCOS group resulted in higher serum FSH and P levels compared to the PCOS group, these increases were not statistically significant ($P > 0.05$). Treatment with CSSO extract significantly raised serum P levels in the MET + 100 CSSO + PCOS group relative to the PCOS group ($P < 0.05$). In the groups receiving CSSO extract, serum LH and T levels in the MET + 100 and MET + 200 CSSO + PCOS groups were significantly reduced ($P < 0.05$) compared to the PCOS group, while FSH and P levels significantly increased ($P < 0.05$). These improvements were most pronounced in the MET + 200 CSSO + PCOS co-treatment group [Figure 2].

Ovarian tissue thiobarbituric acid reactive substance and ferric-reducing ability of plasma levels

The analysis of oxidative stress markers in tissues revealed a significant decrease in FRAP and TBARS

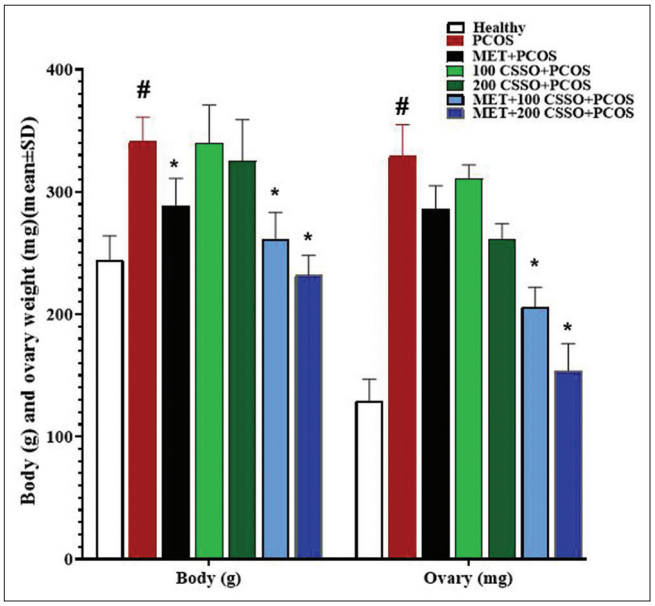

Figure 1: Body and ovarian weights across various experimental groups. Data are presented as mean ± standard deviation, $n = 10$ per group. $^{\#}P < 0.05$: Polycystic ovary syndrome (PCOS) group vs. healthy control. $^{*}P < 0.05$: Treated groups versus PCOS group

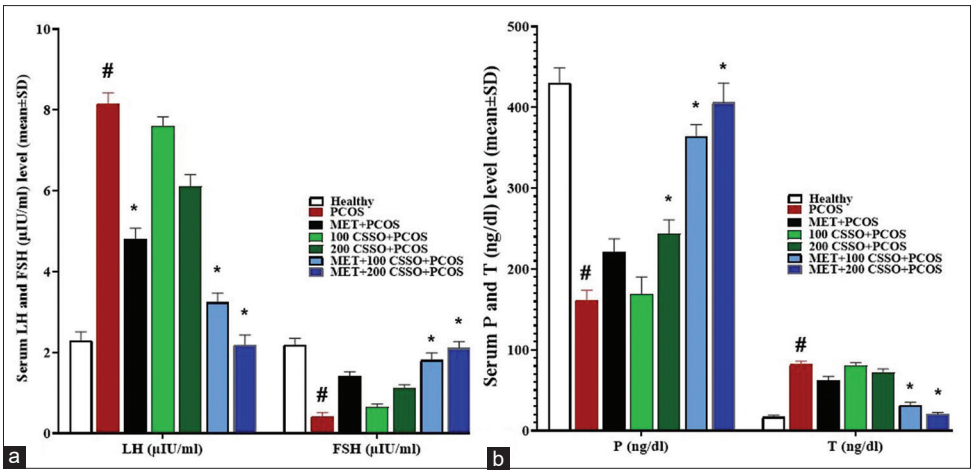

Figure 2: (a) The mean serum levels of follicle-stimulating hormone and luteinizing hormone (µIU/ml) and (b) The mean levels of P (ng/dl) and T (ng/dl) in the different experimental groups. Data are presented as mean ± standard deviation, *n* = 10 per group. #*P* < 0.05: Polycystic ovary syndrome (PCOS) group vs. healthy control. **P* < 0.05: Treated groups versus PCOS group. FSH: follicle-stimulating hormone, LH: luteinizing hormone

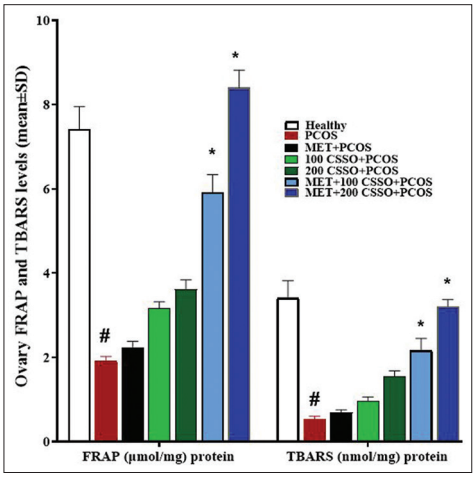

Figure 3: Mean ovary tissue levels of thiobarbituric acid reactive substance (nmol/mg) and ferric-reducing ability of plasma (µmol/mg) in the different experimental groups. Data are presented as mean ± standard deviation, *n* = 10 per group. #*P* < 0.05: Polycystic ovary syndrome (PCOS) group vs. healthy control. **P* < 0.05: Treated groups versus PCOS group. TBARS: Thiobarbituric acid reactive substance, FRAP: Ferric-reducing ability of plasma

levels in the PCOS group compared to the healthy control group ($P < 0.05$). While the MET + PCOS group exhibited an increase in both oxidative stress parameters compared to the PCOS group, this rise was not statistically significant ($P > 0.05$). However, in the MET + 100 and MET + 200 CSSO + PCOS groups, there was a significant increase in the tissue levels of both oxidative stress markers compared to the PCOS group ($P < 0.05$) [Figure 3].

Expression of ovarian GLUT-4, AKT, PI3K, and PTEN genes

Evaluation of PI3K/AKT pathway gene expression revealed that the pathway was notably suppressed in the PCOS group, with all four genes (PTEN, GLUT-4, AKT, and PI3K) showing significantly reduced expression compared to the healthy control group. Although the MET + PCOS group demonstrated an increase in the expression of these genes compared to the PCOS group, the improvement was not statistically significant ($P > 0.05$). In contrast, the CSSO treatment led to a significant upregulation ($P < 0.05$) of the PI3K and PTEN genes in the MET + 100 CSSO + PCOS group compared to the PCOS group. The most pronounced activation of the PI3K/AKT pathway was seen in the MET + 200 CSSO + PCOS group, where all four genes exhibited a significant increase in expression ($P < 0.05$) relative to the PCOS group [Figure 4].

Expression of ovarian GLUT-4, AKT, PI3K, and PTEN proteins

In line with the gene expression findings, the protein levels of PTEN, GLUT-4, AKT, and PI3K in the PI3K/AKT pathway were significantly reduced ($P < 0.05$) in the PCOS group compared to the healthy control group. In the MET + 100 CSSO + PCOS co-treatment group, the expression of PTEN and PI3K proteins was significantly elevated ($P < 0.05$) compared to the PCOS group, while the levels of GLUT-4 and AKT also increased, although not statistically significant ($P > 0.05$). The most notable enhancement of PI3K/AKT pathway protein expression was observed in the MET + 200 CSSO + PCOS group, where all four proteins demonstrated a significant increase ($P < 0.05$) compared to the PCOS group [Figure 5].

Immunohistochemistry assay for expression of Ki-67 and p53 proteins in ovarian tissue

The Ki-67 protein expression was significantly elevated ($P < 0.05$) in the PCOS group compared to the healthy control group. In the MET + PCOS group, Ki-67 expression decreased compared to the PCOS group, though this reduction was not statistically significant ($P > 0.05$). Conversely, CSSO treatment led to a dose-dependent decrease in Ki-67 protein levels compared to the PCOS groups, with the most notable reductions observed in

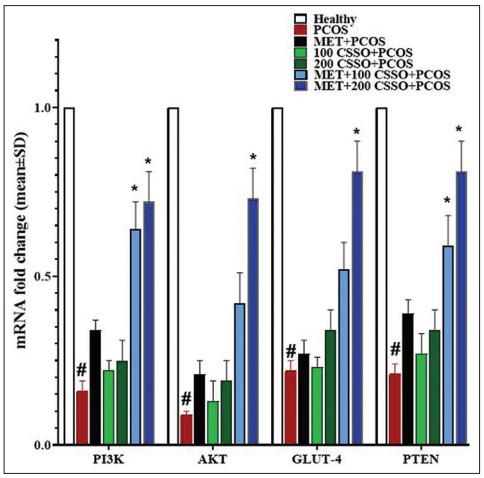

Figure 4: Mean PTEN, PI3K, AKT, and GLUT-4 gene expression in the different experimental groups. Data are presented as mean ± standard deviation, *n* = 10 per group. #*P* < 0.05: Polycystic ovary syndrome (PCOS) group versus healthy control. **P* < 0.05: Treated groups versus PCOS group

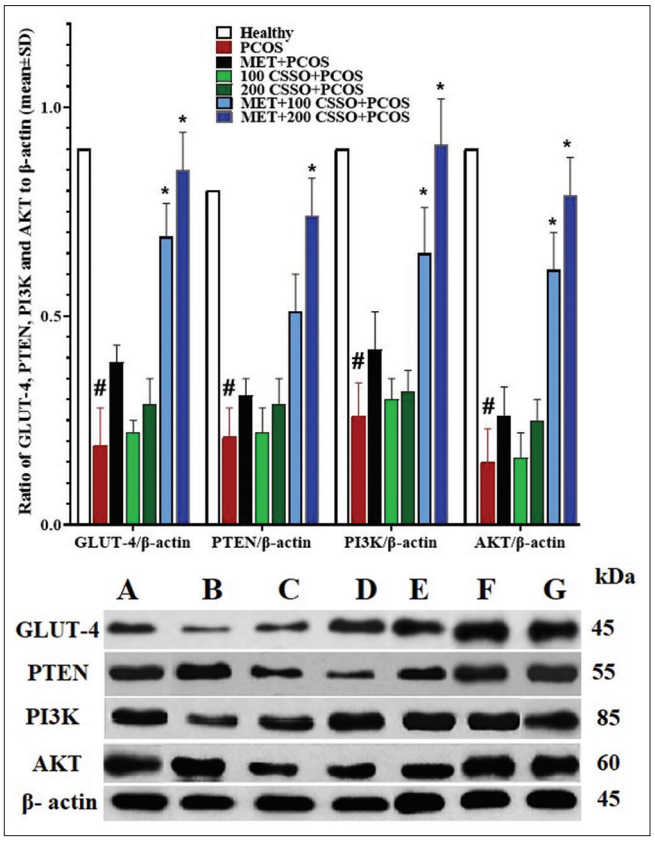

Figure 5: Upper charts: The mean ratio of PTEN, PI3K, AKT, and GLUT-4 protein expressions to β-actin protein expression in ovary tissue. Healthy (A), Polycystic ovary syndrome (PCOS) (B), metformin (MET) + PCOS (C), 100 *Ceratonia siliqua* L. seed oil (CSSO) + PCOS (D), 200 CSSO + PCOS (E), MET + 100 CSSO + PCOS (F), MET + 200 CSSO + PCOS (G). Data given as means ± standard deviation. *n* = 10/group. Lower chart: Western blot-related bands. **P* < 0.05: Treated groups versus PCOS group

the co-treatment groups. Specifically, in the MET + 100 and 200 CSSO + PCOS groups, there was a significant decrease ($P < 0.05$) in Ki-67 protein expression compared to the PCOS group [Figure 6].

Ovarian tissue histopathological evaluations

The histopathological evaluation of ovarian tissues across the different groups revealed that PCOS led to an increase in collagen fibers (CFs) and a reduction in differentiated follicles, including PF, SF, and AFs, compared to the healthy control group. However, treatment with MET, CSSO, and their combination resulted in a decrease in CFs and an increase in differentiating follicles, particularly AF, compared to the PCOS group. These changes were most pronounced in the MET + 200 CSSO + PCOS co-treatment group. In this group, the ovarian germinal parenchyma displayed normal tissue structure without lymphocytic infiltration. A high density of PrFs was also observed in the ovarian cortex, whereas in the PCOS group, these follicles were degenerated and replaced by collagen fibers [Figure 7].

Discussion

This study demonstrated that CSSO regulated the LH/FSH ratio by modulating the HPO axis, resulting in reduced T levels. In addition, CSSO was shown to increase tissue levels of TAC and reduce lipid peroxidation. It also promoted dominant follicle differentiation by activating the AKT/PI3K pathway and inducing mitochondrial apoptosis. Together, these effects helped preserve ovarian function and structure, protecting the tissue from oxidative damage.

During PCOS, the LH/FSH ratio increases, disrupting steroidogenesis in the ovarian theca and granulosa cells. This leads to reduced estrone synthesis and elevated androgen metabolites, such as T and dehydroepiandrosterone.[1] Dysregulation of the HPO axis in PCOS causes higher serum levels of T and LH, while P and FSH levels are lower than normal. Research suggests that isoflavonoids like genistein and formononetin act as estrogen mimics, regulating the HPO axis by modulating gonadotropin-releasing hormone (GnRH), reducing the LH/FSH ratio, and promoting apoptosis in granulosa cells of CFs through activation of the AKT/PI3K, Nrf2, and Foxo1 pathways.[3] This accelerates dominant follicle differentiation. Plants rich in isoflavonoids, such as *Glycyrrhiza* spp., *Paeonia lactiflora* L., *Calendula officinalis* L., and *Ecklonia cava* L., either alone or combined with MET, can also reduce the LH/FSH ratio, T, and pro-inflammatory cytokines such as IL-6, CRP, and TNF-α in PCOS models induced by estradiol valerate, letrozole, and androgen.[19,20] In this study, CSSO, rich in isoflavonoids like daidzein, genistein, biochanin-A, and formononetin, demonstrated estrogen-like activity. Combined with MET, particularly in the MET + 200 CSSO + PCOS group, CSSO significantly reduced the LH/FSH ratio and inhibited androgen (T) synthesis in a dose-dependent manner, showing synergistic effects. Furthermore, treatment with CSSO and MET elevated serum P levels compared to the PCOS group, aligning with

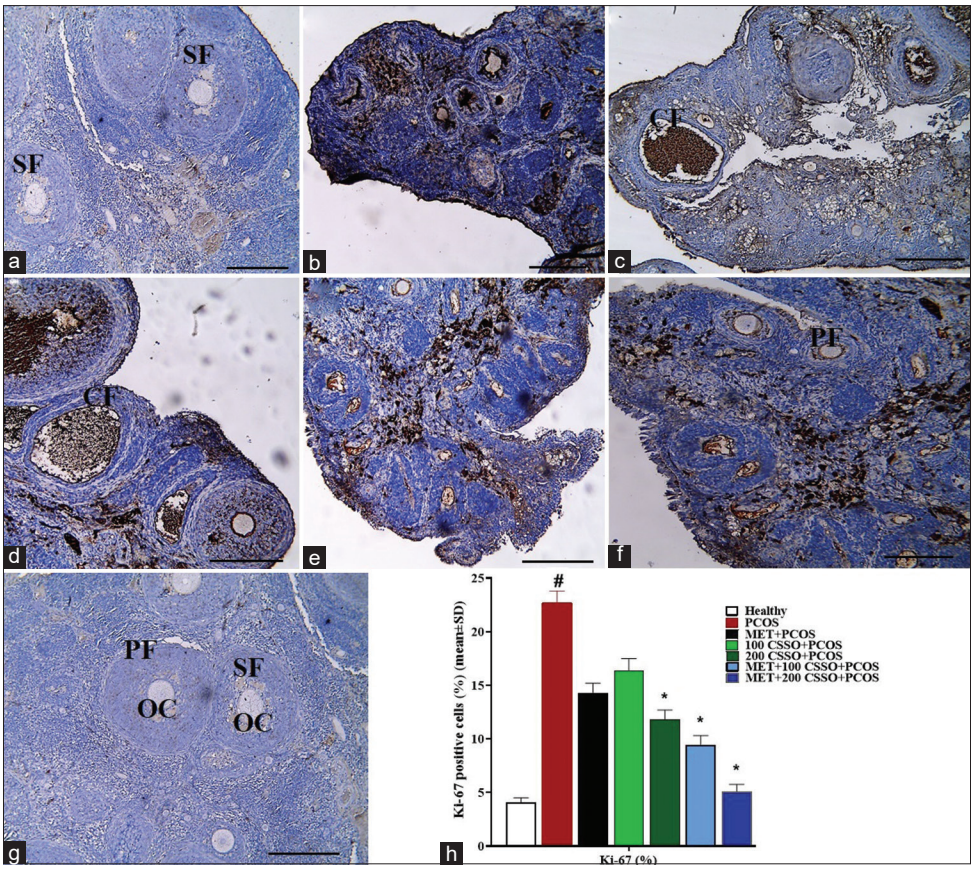

Figure 6: (a-g) Micrographs illustrating the immunohistochemical staining of Ki-67-positive cells in the various experimental groups. The sequence of images is the same as the sequence in the chart alongside. Cystic follicles, oocyte cell, AFs. DAB staining, ×100. Scale bar: 100 μm. Alongside: a chart plotting mean Ki-67-positive cells in ovary tissue, detected by immunohistochemistry, against Ki-67 protein. Data given as means ± standard deviation. *n* = 10/group. #*P* < 0.05: Polycystic ovary syndrome (PCOS) group vs. healthy control. **P* < 0.05: Treated groups vs. PCOS group. Healthy (a), PCOS (b), MET + PCOS (c), 100 CSSO + PCOS (e), 200 CSSO + PCOS (f) MET + 100 CSSO + PCOS (g), MET + 200 CSSO + PCOS (h)

findings from previous studies. These effects were achieved by enhancing the HPO axis and regulating GnRH secretion.

In PCOS, the P450-oxidoreductase enzyme and the P450c17 system, influenced by ROS and RONs, inhibit key enzymes involved in androgen conversion (17, 20-lyase, 17-hydroxylase, and 5α-reductase) within ovarian theca and granulosa cells. This disruption reduces androgen synthesis but paradoxically leads to elevated levels of dehydroepiandrosterone and T, rather than estrogen and other estrones.[4] This hormonal imbalance causes hypothalamic insensitivity and a persistent elevation of LH levels. The resulting increase in LH, coupled with higher androgen levels and estrogen suppression, disrupts both folliculogenesis and steroidogenesis, impeding dominant follicle differentiation and promoting the formation of polycystic follicles in the ovarian cortex.[7] Studies indicate that elevated RONs in PCOS suppress the ovarian antioxidant defense system, reducing TAC and impairing the balance between free radical production and scavenging. This oxidative stress increases the oxidation of unsaturated fatty acids in ovarian cell membranes, as evidenced by increased nitric oxide (NO) levels and decreased TBARS, leading to disrupted follicular integrity.[21] In the present study, PCOS induction was associated with decreased ovarian TBARS and FRAP levels. RONs have also been shown to inhibit the PI3K/AKT pathway, an insulin-dependent pathway, thereby exacerbating CF formation. Estrone-like compounds found in CSSO can enhance the activity of androgen-estrone convertases, reducing androgen synthesis. In addition, these compounds lower the LH/FSH ratio, stimulate steroidogenesis, and promote folliculogenesis by enhancing hypothalamic sensitivity to steroids and regulating gonadotropin-releasing hormone (GnRH) secretion. Flavonoids such as kaempferol, coumaric acid, catechin, quercetin, and apigenin, present in CSSO, contribute to increased TAC by reacting with ROS and RONs within ovarian cells, further supporting antioxidant defenses.[11]

The PI3K/AKT pathway is critical for regulating steroidogenesis and insulin synthesis, and its suppression promotes androgen production and the development of PCOS in the ovaries.[21] In this study, it was observed that PCOS inhibited this pathway. Research has shown that the PI3K/AKT pathway, through the mitogen-activated protein kinase (MAPK) and AKT/IRS-1 signaling cascades, plays a key role in the progression of PFs into secondary

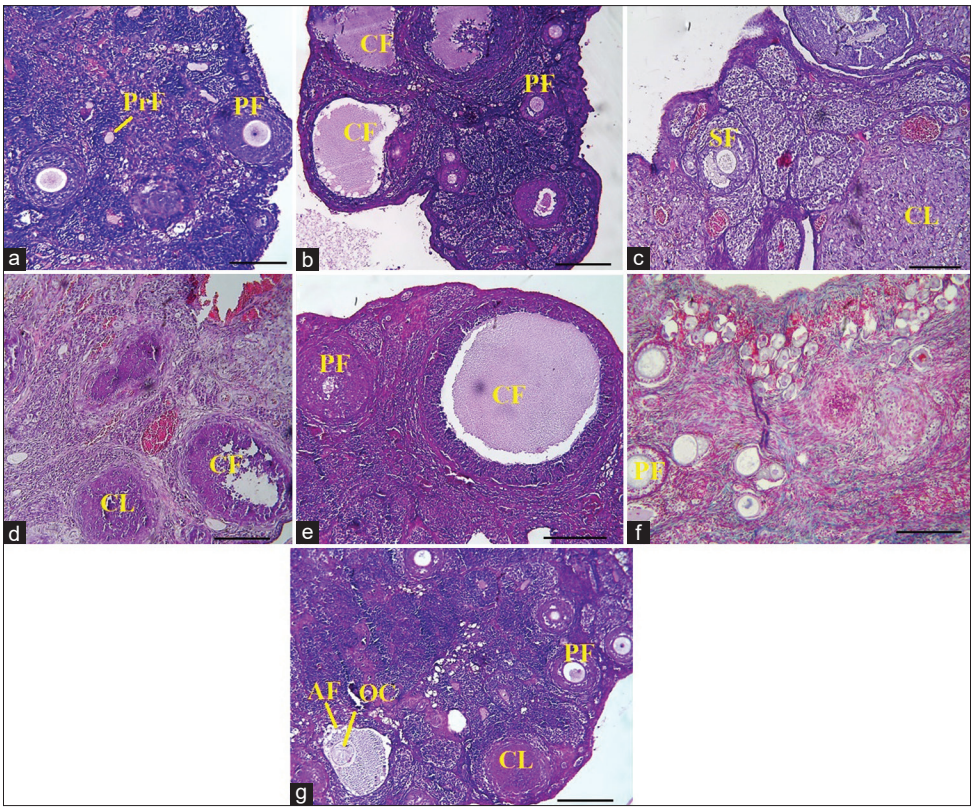

Figure 7: (a-g) Representative micrographs illustrating cystic, corpus luteum, primary, primordial, secondary, AFs, and oocyte cell in ovary tissues in the different experimental groups. H and E staining, ×100. Scale bar: 100 µm. Alongside: a chart plotting numbers of cystic and AFs. (a) *P* < 0.05: PCOS versus normal group. (b) *P* < 0.05: All treated groups versus Healthy (a), PCOS (b), MET + PCOS (c), 100 CSSO + PCOS (d), 200 CSSO + PCOS (e), MET + 100 CSSO + PCOS (f), MET + 200 CSSO + PCOS (g)

and Graafian follicles.[22] In addition, studies suggest that isoflavonoid-rich plants, such as CSSO, containing compounds such as formononetin, genistein, daidzein, luteolin, and quercetin, can enhance the PI3K/AKT pathway via the NF-κB/p53/Cas-3 and WNT/β-catenin signaling pathways.[23] These bioactive compounds also upregulate the expression of hepatocyte nuclear factors 1 alpha (HNF1A) and 4-alpha (HNF-4α), both of which are implicated in PCOS. This activation stimulates the PI3K/AKT/Bax/p53 pathway, promoting apoptosis in granulosa cells of cystic follicles and facilitating the differentiation of dominant follicles into Graafian follicles.[24] In the current study, CSSO exhibited dose-dependent effects, particularly in the MET + 200 CSSO + PCOS group, by strengthening the PI3K/AKT pathway and improving apoptotic markers (as indicated by reduced Ki-67-positive cells) in granulosa cells. These alterations led to the differentiation of PFs into AFs and a reduction in the number of CFs in the MET + 100 and 200 CSSO + PCOS groups.

Conclusion

The results of this study suggest that CSSO enhances steroidogenesis and promotes follicular differentiation by modulating the hormonal regulation of the HPO axis. The isoflavonoid and flavonoid content in CSSO provides potent anti-inflammatory and antioxidant effects, protecting follicular germ cells and ovarian tissue from damage caused by RONs. In addition, CSSO activates the PI3K/AKT signaling pathway and the apoptotic/differentiation pathways involving Ki-67, inducing apoptosis in granulosa cells of CFs. To further explore the clinical potential of CSSO, more *in vivo* and *in vitro* studies are needed to investigate other related pathways. These findings could pave the way for clinical trials in women with PCOS, where CSSO or its active compounds might be used as complementary treatments alongside conventional therapies. CSSO shows promising potential as a natural therapeutic option for managing PCOS.

Ethical approval

The experimental protocols of this study were approved by the Hospital of Fudan University ethics committee.

Author contributions

Xu Zhang and Anyu Tang are co-first authors, they contributed equally to this work.

Financial support and sponsorship

Nil.

Conflicts of interest

There are no conflicts of interest.

References

1. Yu O, Christ JP, Schulze-Rath R, Covey J, Kelley A, Grafton J, *et al.* Incidence, prevalence, and trends in polycystic ovary syndrome diagnosis: A United States population-based study from 2006 to 2019. Am J Obstet Gynecol 2023;229:39. e1- 39.e12.
2. Zuchelo LT, Alves MS, Baracat EC, Sorpreso IC, Soares JM Jr. Menstrual pattern in polycystic ovary syndrome and hypothalamic-pituitary-ovarian axis immaturity in adolescents: A systematic review and meta-analysis. Gynecol Endocrinol 2024;40:2360077.
3. Liang J, Gao Y, Feng Z, Zhang B, Na Z, Li D. Reactive oxygen species and ovarian diseases: Antioxidant strategies. Redox Biol 2023;62:102659.
4. Xie F, Zhang J, Zhai M, Liu Y, Hu H, Yu Z, *et al.* Melatonin ameliorates ovarian dysfunction by regulating autophagy in PCOS via the PI3K-Akt pathway. Reproduction 2021;162:73-82.
5. Attia GM, Almouteri MM, Alnakhli FT. Role of metformin in polycystic ovary syndrome (PCOS)-related infertility. Cureus 2023;15:e44493.
6. Sadeghzadeh F, Sadeghzadeh A, Changizi-Ashtiyani S, Bakhshi S, Mashayekhi FJ, Mashayekhi M, *et al.* The effect of hydro-alcoholic extract of *Ceratonia silique* L. on spermatogenesis index in rats treated with cyclophosphamide: An experimental study. Int J Reprod Biomed 2020;18:295-306.
7. Zhang J, Zhang H, Xin X, Zhu Y, Ye Y, Li D. Efficacy of flavonoids on animal models of polycystic ovary syndrome: A systematic review and meta-analysis. Nutrients 2022;14:4128.
8. Abdulkareem RS. Yaseen Al-Hayali WR, Ibrahim II. Antimicrobial activity of *Ceratonia silique* L. extract against diarrheagenic *E-coli*. Sys Rev Pharm 2020;11:2020.
9. Marks H, Grześkowiak Ł, Martinez-Vallespin B, Dietz H, Zentek J. Porcine and chicken intestinal epithelial cell models for screening phytogenic feed additives-chances and limitations in use as alternatives to feeding trials. Microorganisms 2022;10:629.
10. Al-Ameri MT, Nasser AK. *In vitro* antioxidant properties of gum extract from the carob (*Ceratonia silique* L.) plant. Basrah J Agric Sci 2021;34:83-92.
11. Kavvoura DA, Stefanakis MK, Kletsas D, Katerinopoulos HE, Pratsinis H. Biological Activities of *Ceratonia siliqua* Pod and seed extracts: A comparative analysis of two Cretan cultivars. Int J Mol Sci 2023;24:2104.
12. Naseri L, Khazaei MR, Khazaei M. Synergic effect of bee pollen and metformin on proliferation and apoptosis of Granulosa cells: Rat model of polycystic ovary syndrome. J Food Biochem 2022;46:e13635.
13. Alqudah A, Qnais EY, Wedyan MA, Oqal M, Alqudah M, AbuDalo R, *et al. Ceratonia siliqua* leaves ethanol extracts exert anti-nociceptive and anti-inflammatory effects. Heliyon 2022;8:e10400.
14. Antari NW, Damayanti IA, Wulansari NT. The effectiveness testing of l-carnitine on the quality of spermatozoa and testosterone hormone in white rats (*Rattus norvegicus*) feeding with high fat. Int J Health Sci 2021;4:102-9.
15. Billur D, Aktay I, Bayram P, Bitirim CV, Turan B. Morphological and functional analysis of cardiac ameliorations in elderly rats supplemented with a magnolol extract complex. Int J Morphol 2023;41:915-925.
16. Peng F, Hu Y, Peng S, Zeng N, Shi L. Apigenin exerts protective effect and restores ovarian function in dehydroepiandrosterone induced polycystic ovary syndrome rats: A biochemical and histological analysis. Ann Med 2022;54:578-87.
17. Akbaribazm M, Khazaei MR, Khazaei M. *Trifolium pratense* L. (red clover) extract and doxorubicin synergistically inhibits proliferation of 4T1 breast cancer in tumor-bearing BALB/c mice through modulation of apoptosis and increase antioxidant and anti-inflammatory related pathways. Food Sci Nutr 2020;8:4276-90.
18. Gao Y, Chen J, Ji R, Ding J, Zhang Y, Yang J. USP25 regulates the proliferation and apoptosis of ovarian granulosa cells in polycystic ovary syndrome by modulating the PI3K/AKT pathway via deubiquitinating PTEN. Front Cell Dev Biol 2021;9:779718.
19. Park MJ, Han SE, Kim HJ, Heo JD, Choi HJ, Ha KT, *et al. Paeonia lactiflora* improves ovarian function and oocyte quality in aged female mice. Anim Reprod 2020;17:e20200013.
20. Gharanjik F, Shojaeifard MB, Karbalaei N, Nemati M. The effect of hydroalcoholic calendula officinalis extract on androgen-induced polycystic ovary syndrome Model in Female Rat. Biomed Res Int 2022;1:7402598.
21. Gong Y, Luo S, Fan P, Zhu H, Li Y, Huang W. Growth hormone activates PI3K/Akt signaling and inhibits ROS accumulation and apoptosis in granulosa cells of patients with polycystic ovary syndrome. Reprod Biol Endocrinol 2020;18:121.
22. Rahman MS, Hossain KS, Das S, Kundu S, Adegoke EO, Rahman MA, *et al.* Role of insulin in health and disease: An update. Int J Mol Sci 2021;22:6403.
23. Yi G, Sang X, Zhu Y, Zhou D, Yang S, Huo Y, *et al.* The SWGEDWGEIW from soybean peptides reduces insulin resistance in 3T3-L1 adipocytes by activating p-Akt/GLUT4 signaling pathway. Molecules 2023;28:3001.
24. Banday MZ, Sameer AS, Nissar S. Pathophysiology of diabetes: An overview. Avicenna J Med 2020;10:174-88.

Original Article

Histopathology of Placenta in Stillbirth

B. Madhupriya, Varun Byrappa[1], Pranup Roshan Quadras[2], Amit Massand[3]

Departments of Pathology and [1]Emergency Medicine, Kempegowda Institute of Medical Science, Bengaluru, Karnataka, [2]Department of Anatomy, A. J. Institute of Medical Sciences, [3]Department of Anatomy, Smt. B K Shah Medical Institute and Research Center, Sumandeep Vidyapeeth, Vadodara, Gujarat, India

Abstract

Purpose: For the development and survival of the fetus, the placenta plays an important role before birth. Examination of the placenta can aid/tell us the sequence of events prebirth, which will aid in identifying the etiology of unfavorable outcomes such as stillbirth, preterm delivery, intrauterine growth retardation, and neurodevelopmental impairment. We attempt to study the histopathological features of the placenta in stillbirths and categorize the various factors of placental pathology contributing to the same. **Materials and Methods:** From 60 stillbirths, placentae with umbilical cord and membranes were studied for 18 months at Kempegowda Institute of Medical Sciences. Detailed histomorphology with clinical details was recorded. TULIP classification of stillbirth was used to categorize the placental pathology. **Results:** Women from 19 to 38 years (38 multigravida, 22 primigravidae) with the majority in the gestational age of 20–28 weeks formed the study group. Maternal comorbidities were associated in 80% of cases, the most common being hypertensive disorders of pregnancy. The major cause of stillbirth in our cohort was placental bed pathology (maternal vascular underperfusion – 41%) followed by parenchymal pathology (fetal thrombotic vasculopathy – 17%, massive perivillous fibrin deposition – 12%). Placental pathology was seen in 86% of mothers with recurrent fetal loss. **Conclusion:** Histomorphology of the placenta is an essential step in determining the cause of stillbirth, especially in recurrent conditions. This will aid in planning future pregnancies and tailoring appropriate treatment plans.

Keywords: *Placental pathology, recurrent fetal loss, stillbirth*

Introduction

Stillbirth is considered death of the fetus by 20 weeks or higher.[1] Stillbirths cause psychological effect and affect the social well-being of both mother and father. Unfortunately, the cause of fetal death is reported as unexplained in up to 2/3rd of stillbirths.[2]

Placenta, a very complex organ with a life span of 9 months, serves as a channel between fetus and mother. The study of Placenta is the most accurate record of the foetal prenatal studies[3] which can provide invaluable information to understand the cause of foetal deaths. The placental examination can be helpful in identifying the etiology of stillbirth, preterm delivery, intrauterine growth restriction (IUGR), and neurodevelopmental impairment. Examination of the placenta can identify the preventable or treatable conditions and those with implications for the immediate prognosis or long-term growth and development of the infant, improving outcome in subsequent pregnancies,[4] resulting in adequate treatment, and preventive measures during subsequent pregnancies.

The India Newborn Action Plan goals for <10 stillbirths from thousand births by year 2030. For that, we need to understand the risk factors for stillbirths and compared with live birth, which can be helpful in the reduction of stillbirth.

Studies describing placental findings in stillbirth are scant. Thus, there is a need to emphasize placental examination in cases of stillbirth, to identify the cause. Hence, we have formulated this study to observe the morphology of placentae of stillbirth to identify the cause of stillbirth.

Materials and Methods

The sample of placenta was collected after obtaining the ethical clearance from Kempegowda Institute of Medical Sciences (KIMS), Bengaluru.

Placentae collection

A total of 60 placentae were collected from women with stillbirths. The study

How to cite this article: Madhupriya B, Byrappa V, Quadras PR, Massand A. Histopathology of placenta in stillbirth. J Anat Soc India 2025;74:12-8.

Article Info

Received: 03 February 2024
Revised: 23 November 2024
Accepted: 19 February 2025
Available online: 31 March 2025

Address for correspondence:
Dr. Amit Massand, Department of Anatomy, Smt. B K Shah medical Institute and Research center, Sumandeep Vidyapeeth, Vadodara- 391 760, Gujarat, India.
E-mail: amitmassand86@gmail.com

Access this article online

Website: https://journals.lww.com/joai
DOI: 10.4103/jasi.jasi_18_24
Quick Response Code:

was conducted in the department of pathology, KIMS, Bengaluru, from December 2015 to June 2017. The women of different ages and parity with stillbirth were included in the study. The comorbidities such as diabetes mellitus, hypertension, and thyroid disorders were recorded. The stillbirth gestational age ranged from 20 to 39 weeks and hence gestational age matched. Placentae of live birth could not be obtained for a control group.

Placental examination

Placentae were examined in the fresh state for the presence of retroplacental clot and attachment of the membrane. Length of the umbilical cord (UC) and weight were recorded. Placentae were then fixed in the neutral buffer of 10% formalin for a minimum of 3 days, and details were recorded according to the worksheet [Table 1].

Three transverse sections were taken from the UC-near the placental attachment, fetal attachment, and one in the middle. Membranes were rolled in a Jelly Roll fashion, and one section was taken. One section each from the maternal and fetal surfaces was taken. Additional sections from infarcted, hemorrhagic areas were included wherever necessary. Tissues were processed routinely. Histosections of 3–5 μ thickness were obtained from paraffin-embedded blocks and routinely stained with H and E. The sections of UC were investigated for the number of vessels and vascular ectasia and sections of Membranes were investigated for presence of chorioamnionitis (CA). Placenta to grade the maturity of the placenta, type of villi, presence of syncytial knots, calcification, inflammatory cells, inter and intravillous hemorrhage, villous edema, nucleated red blood cell (RBC), and fibrin deposition around villi. Sections from the maternal surface were specially examined for muscularization of vessels, atherosis, etc., and the fetal surface for thrombi and endothelial cushions.

Statistical analysis

The findings were tabulated and correlated with the maternal comorbidity if present to arrive at a particular diagnosis. The results were depicted in percentages and graphs using Microsoft excel office 2019 1808, Microsoft Windows, Trailware, Redmond, Washington, USA.

Results

The youngest patient in our cohort was 19 years old, and the oldest was 38 years old. The majority of the cases were in the age group of 23–30 years (38 cases); the study group comprised 38 multigravida and 22 primigravidae. Stillbirth was higher in multigravida than in primi (63% versus 37%, respectively). We had one case with high parity (≥parity 5) with para 5 and previous history of fetal loss, and the cause of the present stillbirth was due to aberrant implantation. The majority of the stillbirth were in the gestational age of 20–28 weeks followed by 29–36 weeks. Pregnancy-induced hypertension, preeclampsia, and eclampsia were the most common comorbidities. The others were gestational diabetes mellitus (GDM), anemia, fever, hypothyroidism, thrombotic disorders, and placenta previa. In around 20%, no comorbidities were observed.

Gross examination of umbilical cord

Hypocoiling was seen in 7%, whereas hypercoiling in 2%, whereas the rest (91%) seemed unremarkable. Central insertion of UC was seen in the majority (97%), whereas one (3%) showed velamentous insertion [Figure 1a]. Single umbilical artery (SUA) with thinning of the cord was observed in 3 (5%) cases [Figure 1b].

Gross examination of membranes

Membranes were clear looking in 50 (83%) placentae, with membranes of 10 (17%) having an opaque and slight yellowish discoloration [Figure 2a].

Table 1: Placental gross examination worksheet

Placental worksheet
Cord insertion _____ cm from margin
Cord length _____ cm
Cord color _____ (white, green, yellow, brown)
Number of vessels _____
Number of cord twists per 6 cm _____
Other cord findings _____ (knots, nodules, masses, etc.)
Membranes inserted _____% (marginally, circummarginate, circumvallate)
Membrane color _____
Other membrane findings _____ (nodules, hemorrhage, membranous vessels, etc.)
Placental weight_____ (fresh)
Placental disc measurement _____ cm in greatest diameter, _____ cm thick
Fetal surface _____ (nodules, masses, chronic vascular thrombosis, etc.)
Maternal surface _____ (disrupted, masses, calcification, fibrin, hematomas, indentations, etc.)
Parenchyma _____ (normal, beefy, spongy; lesions - number, size, % of mass involved, location)

Membranes of all 60 (100%) placentae were marginally attached [Figure 2b].

Gross examination of placenta

Morphometry of placenta

Appropriate size for the gross appearance (GA) was seen in 50 (83%) placentae [Figure 3a], whereas 7 (12%) placentae were small for GA [Figure 3b]. Of these 7 cases of small placentae, three were with SUA, and 4 of them had associated hypertensive disorders of pregnancy. There were 3 (5%) placentae large for GA, where in 2 of them had associated anemia and one had GDM.

The majority of the placentae, i.e. 49 (82%) of them were of normal weight for the appropriate GA, eight (14%) placentae had <10th percentile weight for GA, which included 3 cases of SUA, and 4 cases associated hypertensive disorder of pregnancy and 1 case with hypothyroidism. There were 3 (5%) placentae with more than 10% weight for GA. Among these placentae, 2 had associated anemia and one had GDM.

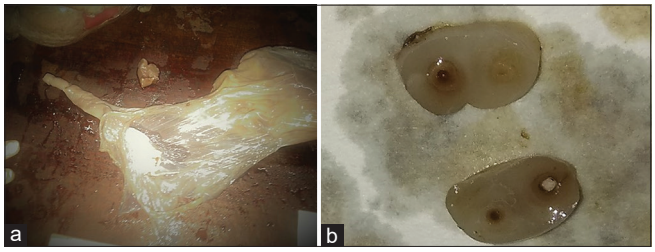

Figure 1: Umbilical cord (UC). (a) Velamentous attachment of UC – UC attached to the membranes. (b) C/S of UC showing one artery and one vein – A case of single umbilical artery

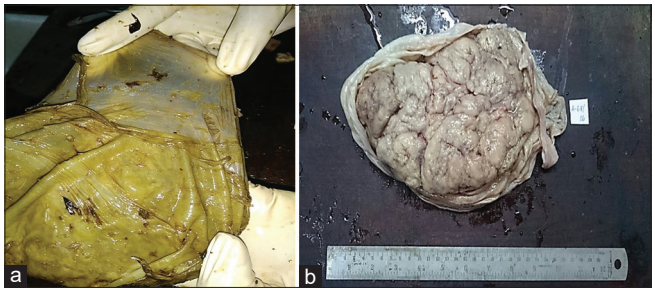

Figure 2: Placental membrane. (a) Opaque appearance of membranes – A case of chorioamnionitis. (b) Gross appearance of placental membrane – Maternal surface with cotyledons and marginal attachment of membrane

In the cohort, 58 (97%) of placentae had normal parenchymal texture except for 2 (3%) having spongy, friable parenchyma [Figure 3c]. Among these 2 cases, one had associated hypothyroidism and one had GDM.

Gross findings of placenta

The normal placenta was found in twelve patients, in three patients there was in district maternal and fetal surface in placenta, in five patients placenta was with clot, intraparenchymal placental hemorrhage was seen in twelve patients which was more than 50% whereas in nine patients it was less than 50%, Placental infarction with more than 50% was observed in twelve patients whereas in six patients was less than 50%, in one patient myometrial fibers were attached with placenta [Table 2].

Microscopic examination

Microscopic examination of umbilical cord

In our study, Group 3 (2%) cases had SUA with vein, three cases with ectatic vessels, two of these were associated with hypertensive disorders of pregnancy, and one with the thrombotic disorder. These were associated with fetal vascular obstruction (FVO).

Microscopic examination of membranes

In most of the cases in the cohort, 53 (88%) placentae had normal membranes. Seven (12%) placental membranes showed evidence of CA consisting of chronic inflammatory cell infiltrate, lymphocytes with few plasma cells, extending up to the amnion layer. Two cases also showed few acute inflammatory cells admixed with these chronic cells. These cases on gross had opaque-looking membranes. Among these seven cases, only 3, i.e. 43%, had associated fever during the antenatal period.

Microscopic examination of placenta

The histopathological findings of both maternal and fetal surface were recorded. In about 11 placentae, no pathology was detected.

Figure 3: Gross appearance (GA) of the placenta. (a) GA of normal placenta – Fetal surface with centrally attached umbilical cord (UC). (b) Thinned out UC with caked up and small for GA placenta along with intrauterine growth restriction of the fetus. (c) Spongy pale looking placenta, with friable parenchyma – In a case associated with anemia

Maternal surface

Thirty placentae showed hypermature villi (prematurely small terminal villi) resulting from increased branching to increase the effective surface area of diffusion. Among these 30 placentae with hypermature villi, 18 cases showed atherosis, lesion of the arteries in the maternal surface characterized by accumulation of macrophages in the vessel wall, perivascular mononuclear inflammatory infiltrate, and associated fibrinoid necrosis of the vessel wall. Twelve cases showed muscularization of basal plate vessels where the absence of remodeling leads to persistence of the mural layer of the vessels (smooth muscle layer >50% of the diameter of the vessel or <50% of vessel lumen), which affects the perfusion [Figure 4].

Tenny–Parker change (increased syncytial knots more than 30%) was seen in 21 of these cases, suggesting morphological evidence of ischemia [Figure 4].

Calcification can occur with or without placental pathology. Calcification of basal plate and parenchyma are common in late and postterm placentae normally. Calcification is commented on, if dense and in early weeks of gestation. Dense focal calcification was seen in 18 cases [Figure 4]. This is usually seen in the placentae of patients with preeclampsia.

Among the cases with the above changes, 25 cases were categorized as maternal vascular underperfusion (MVU). MVU comprised vascular and villous lesions. Vascular lesions included (1) atherosis (2) persistent muscularization of the basal plate vessels. Villous changes include (1) hypermature villi and (2) infarcted villi (expressed in the percentage of placental surface affected).

Four placentae showed edematous villi, with less number of tertiary villi for corresponding gestational age. This was observed in two cases associated with GDM and two cases of anemia.

Seventeen cases showed areas of infarction, with increased villous crowding, pink acellular villi (ghost villi), increased surrounding fibrin, and old infarcts with calcification [Figure 4]. Eight cases showed intervillous hemorrhage [Figure 4]. Thirteen cases showed lace-like fibrin deposition encasing the villi [Figure 4]. Among these 13 cases, 7 cases showed extensive fibrin deposition and were labeled as massive perivillous fibrin deposition (MPVFD). MPVFD was diagnosed by the presence of increased lace-like perivillous fibrin amounting to minimum of 30%–50% of intervillous space.

We have observed increased (>10/villi) nucleated RBC in the villi in five cases. This finding is not specific for etiology but indicative of fetal hypoxia [Figure 4]).

One case showed intravillous chronic inflammatory cells infiltrate comprising lymphocytes and histiocytes. The causes of infection were ruled out, and this was diagnosed as chronic villitis of unknown etiology (CVUE). This was based on lack of evidence of infection along with chronic inflammatory cell infiltrate comprising of lymphocytes and histiocytes [Figure 4]. This patient had past history of recurrent (2) fetal loss.

Fetal surface

Thirty placentae showed hypermature villi, 8 cases showed thrombi in the vessels and intervillous hemorrhage. Thirteen cases showed perivillous fibrin deposition. One case showed intravillous chronic inflammatory cell infiltration. These were similar to those seen in maternal suface.

Ten cases showed avascular fibrotic villi and two of these cases had ectatic vessels in the UC and seven cases among these showed increased nucleated RBC's. Four of these cases showed mural intimal fibrin thrombi. These cases were labeled as fetal thrombotic vasculopathy (FTV) [Figure 4]. This was diagnosed based on the presence of avascular villi along with endothelial cushions (mural intimal fibrin thrombi) or the presence of nucleated RBC's or ectatic vessels.

Observations recorded in both the surfaces were analyzed and put together to arrive at a diagnosis. Among the 60 patients, the final diagnosis was as follows. Eight (13%)

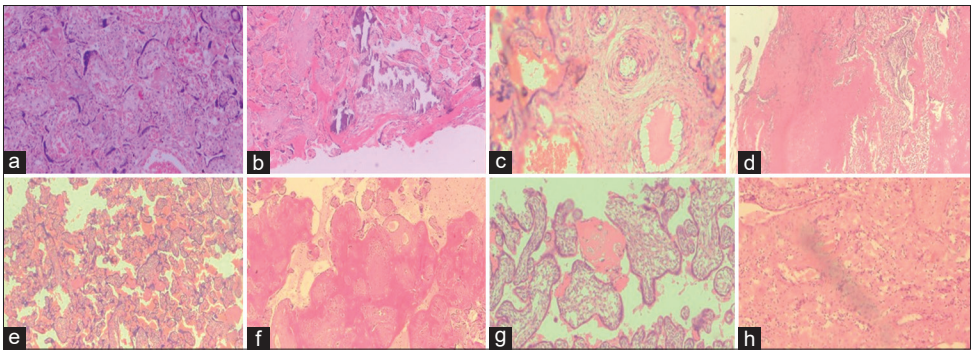

Figure 4: Histopathology of placenta with H and E stained (×100). (a) Tenny Parker's change. (b) Diffuse dense calcification along with few hyalinized villi – A case of maternal vascular underperfusion (MVU). (c) Muscularization of bassel plate vessles – A case of MVU. (d) Placental infarction (areas of hyalinized villi) – A case of MVU. (e) Increased terminal villi with intraparenchymal hemorrhage – A case of MVU. (f) Lace-like fibrin encasing villi – A case of massive perivillous fibrin deposition. (g) Increased nucleated red blood cells along with hyalinized villi fetal Hypoxia – A case of fetal thrombotic vasculopathy. (h) Lymphohistiocytic infiltration of villi – A case of villitis of unknown etiology

patients had unremarkable UC, membranes, and placenta. Three (5%) cases of stillbirth were due to SUA. Five cases (8%) of stillbirth due to retroplacental hemorrhage, 25 (41%) due to MVU, 10 (17%) due to FTV, 7 (12%) due to MPVFD, and 1 (2%) each of CVUE and aberrant implantation.

Isolated CA was not seen in any of the 60 placentae, however, among the 49 cases with evident placental pathology, 7 showed associated CA (4 cases were associated with MVU, 2 cases with MPVFD, and 1 case with FVO), thereby indicating a combined pathology of infection and circulatory disturbances [Figure 5].

Among the 60 cases, 8 cases had no associated pathology in the placenta, membranes, and cord. The majority of the cases, 37/60, i.e.,62%, had pathology due to maternal circulatory disturbances, including MVU, MPVFD, and retroplacental hemorrhage. Fetal circulatory disturbances, including FVO, were seen in 10/60, i.e.,17% of cases. Inflammatory causes, including CVUE in 1/60, i.e. 2% and developmental anomalies, including SUA 3/60, i.e. 5% of cases were documented. However, MPVFD and CVUE have recently received immunological basis supported by their high recurrence rate.

Although not a part of this study, parents of 55 cases of stillbirth consented to fetal autopsy. Among these, none of them showed any morphologically identifiable developmental anomaly. Among these, 20 fetuses showed evidence of IUGR wherein 17 of them had associated placental pathology and 3 had SUA.

Recurrence

There were 26 cases with a previous history of fetal loss, among which 23/26 (86%) placentae showed evident pathology, and no diagnosis was made in 3/26 (14%) of the cases. Among 34 cases with no history of fetal loss, placental pathology was evident in 26/34 (76%) cases and no evident placental pathology in 8/34 (24%) cases [Figure 6].

Pathology was slightly higher in cases of recurrent fetal loss. In patients with previous history of fetal loss, 16 cases were diagnosed as MVU, 4 cases as MPVFD, 2 cases as FVO, and 1 case as CVUE.

Discussion

The placenta is very important to get examined after stillbirth as it is highly responsible for fetal mortality in the uterus. According to reports, higher than 60% of mortality of fetus is due to abnormality in the placenta.[5] There has been very less percentage of unexplained stillbirth recorded after concentrating on placental findings by following TULIP as well as ReCoDe classification on perinatal death.[6] We used the TULIP classification system in our study to sub classify placental pathology. TULIP (in 2006) classification to identify the underlying cause and mechanism of death (maternal fetal and placental pathology). TULIP classification has been accepted worldwide. It was designed by a multidisciplinary panel, in anticipation of current needs.[7]

TULIP subclassified the placental causes into,
1. Placental bed pathology
2. Placental pathology
3. UC complications
4. Not otherwise specified.

TULIP was shown to have the best agreement and a low proportion of unexplained stillbirths.[5] However, most of the studies in literature to date have recorded individual findings in placentae, unlike us, where we have grouped the findings into specific pathologic entities such as MVU and MPVFD hence, specific correlation for our study was difficult. The variation in placental disorders cited in different classification systems makes it difficult to draw conclusions on the comparision of the incidence of different placental pathologies by various authors. Few of them provide descriptions of placental abnormalities without definitive

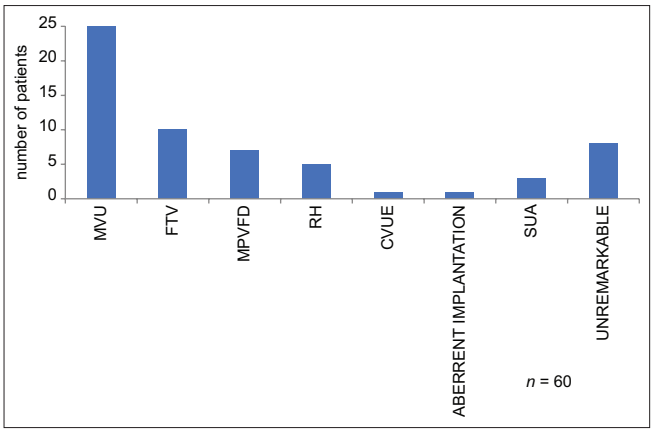

Figure 5: Distribution of patients according to the final diagnosis. MVU: Maternal vascular underperfusion, FTV: Fetal thrombotic vasculopathy, MPVFD: Massive perivillous fibrin deposition, CVUE: Chronic villitis of unknown aetiology, SUA: Single umbilical artery, RH: Retroplacental haemorrhage

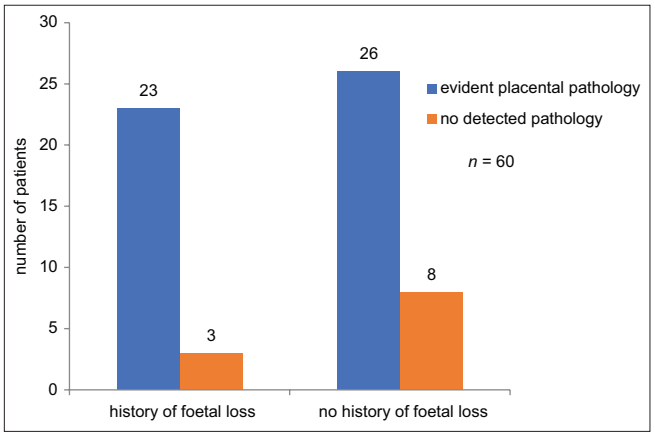

Figure 6: Distribution of patients according to history of fetal loss and evident placental pathology

diagnosis and few have classified based on defined diagnosis. We have correlated the cord abnormalities, vascular lesions, and inflammatory and infectious lesions categorized in the other studies to the best possible extent.

In our study, in 82% (49) of cases, underlying placental pathology was observed, in 18% of cases, we could not attribute any cause of stillbirth. The placental examination helps in reducing the number of undetermined causes of stillbirth, hence proving the need for placental examination for aiding in future pregnancy. The following studies had similar conclusion with minor variations in the percentages [Table 3].

In the multicentric study (at Massachusetts, Georgia, Texas, and Utah) conducted by Pinar *et al*. during 2006–2008 examined placentae of 518 stillbirths and 1200 live births, placentas from singleton pregnancies were examined using a standard protocol. He classified stillbirth according to TULIP classification and he observed, SUA in 7.7%, velamentous cord insertion in 5%, diffuse terminal villous immaturity in 10.3%, inflammation (e.g. acute CA of placental membranes) in 30.4%, vascular degenerative changes in chorionic plate in 55.7%, retroplacental hematoma in 23.8%, intraparenchymal thrombi in 19.7%, parenchymal infarction in 10.9%, fibrin deposition in 9.2%, fetal vascular thrombi in 23%, avascular villi in 7.6%, and hydrops in 6.4% of stillbirths.[1]

Rayburn *et al*.[10] conducted a study during 1979–1983 (a period of 4.5 years) at Michigans Women's Hospital with 89 stillbirth placentas. He categorized based on placental abnormalities which he observed without putting them into defined diagnosis. In 98% (87/89) cases, he could identify the cause of stillbirth, which included 26% (23/89) had vascular insufficiency, 25% (22/89) had hydrops, 18% (16/89) each of hemorrhagic endovasculitis and hematoma, 8% (7/89) each of CA and UC abnormalities, 4% (4/89) each of acute villitis, chronic villitis and chromosomal abnormalities along with other causes contributing to 5%. The study concluded that histological examination of the placenta after a recent fetal death provides useful information in counseling the parents and in planning any future childbearing.[10] The variation in placental disorders cited in different classification systems makes it difficult to draw conclusion on the comparison of the incidence of different placental pathologies by various authors. Few of them provide descriptions of placental abnormalities without definitive diagnosis and few have classified based on defined diagnosis. We have correlated the cord abnormalities, vascular lesions, and inflammatory and infectious lesions categorized in the other studies to the best possible extent.

Korteweg MD *et al*.[8] conducted two studies and classified stillbirths using TULIP classification. First study was done in the Netherlands with 750 stillbirths in 2002–2006. The majority of the cases were under placental pathology (64.9%), comprising UC complications in 2%, MVU 26.6%, abruption 7%, villous immaturity 17.6%, and placental parenchymal pathology (MPVFD, CVUE, FTV) in 31%. Congenital anomalies were seen in 5.3%, infections in 1.9%, others in 5.3%, and 23% remained unexplained. Most of the women (16%) with hypertensive disorders of pregnancy presented with MVU/abruption.

A second study was conducted by the same above said authors in Dutch hospitals during 2002–2008 with 1025 stillbiths. The major cause of stillbirth was placental pathology (65.2%), comprising 25% of MVU, 6% abruption, villous immaturity in 18.8%, placental parenchymal pathology (MPVFD, CVUE, and FTV) in 28%. Congenital anomalies were seen in 4.8%, infections in 1.8%, others in 5%, and 23.2% remained unexplained.[9]

Most of the results of these studies were consistent with the results of our study. The major cause in our study and those studies was MVU with minor difference in the percentage, which could be attributed to the difference in the race, ethnicity, and associated comorbidities. In

Table 2: Gross findings of placenta (*n*=60)

Gross findings	Number of patients	Percentage of cases
No gross abnormalities	12	20
Indistinct maternal and fetal surface	3	05
Attached clot	5	08
Intraparenchymal hemorrhage (<50% of placenta)	12	20
Intraparenchymal hemorrhage (>50% of placenta)	9	15
Infarction (<50% of placenta)	12	20
Infarction (>50% of placenta)	6	10
Attached myometrial fibres	1	02
Total	60	100

Table 3: Authors used TULIP classification for stillbirths

Studies	stillbirths	Method used	Maternal comorbidity (%)	No comorbidity (%)	Placental Pathology
Pinar *et al*.[1]	518	TULIP	100	0	Vascular insufficiency - 56%
Korteweg *et al*., 2009[8]	750	TULIP	77	23	MVU - 27%
Korteweg *et al*., 2012[9]	1025	TULIP	77	23	MVU - 27%
Present study	60	TULIP	82	18	MVU - 41%

MVU: Maternal vascular underperfusion

the above studies, the major comorbidity was Pregnancy induced hypertension (PIH) and majority of them presented with maternal vascular underperfusion (MVU). We have documented Similar findings in our study.

The limitations of our study are that we could not have age-matched control group to compare the placental changes. In cases of CA, the causative organism could not be established by microbiological examination. In cases where we could not find any pathological lesion, chromosomal analysis could have yielded information that we could not perform due to the unavailability of the same facility.

To date, we could not find any similar study on placental pathology and stillbirth from the Indian subcontinent. This highlights the need for similar studies in different geographical zones of India to further strengthen the need for placental examination in case of stillbirth. There is a need for awareness among obstetricians regarding the importance of placental examination in stillbirths.

Conclusion

Histomorphology of the placenta is an underused tool, a goldmine of information that helps in determining the probable cause of fetal loss, undetectable by other modalities. This study confirms the relationship between abnormal placental morphology and adverse perinatal outcome, more so in cases of recurrent fetal loss. Conditions like MPVFD and VUE are recurrent, early diagnosis of the same in future pregnancies by placental biopsies can allow the obstetrician to initiate the appropriate treatment to ensure fetal well-being. This study also highlights the need to create awareness about the importance of placental examination to document various pathologies leading to stillbirth among different geographic zones and ethnicity.

Financial support and sponsorship

Nil.

Conflicts of interest

There are no conflicts of interest.

References

1. Pinar H, Goldenberg RL, Koch MA, Heim-Hall J, Hawkins HK, Shehata B, *et al*. Placental findings in singleton stillbirths. Obstet Gynecol 2014;123:325-36.
2. Downe S, Kingdon C, Kennedy R, Norwell H, McLaughlin MJ, Heazell AE. Post-mortem examination after stillbirth: Views of UK-based practitioners. Eur J Obstet Gynecol Reprod Biol 2012;162:33-7.
3. Benirschke K, Driscoll SG. The Pathology of the Human Placenta. Germany: Springer Berlin Heidelberg; 1967. p. 97-571.
4. Fretts RC. Etiology and prevention of stillbirth. Am J Obstet Gynecol 2005;193:1923-35.
5. Flenady V, Frøen JF, Pinar H, Torabi R, Saastad E, Guyon G, *et al*. An evaluation of classification systems for stillbirth. BMC Pregnancy Childbirth 2009;9:24.
6. Vergani P, Cozzolino S, Pozzi E, Cuttin MS, Greco M, Ornaghi S, *et al*. Identifying the causes of stillbirth: A comparison of four classification systems. Am J Obstet Gynecol 2008;199:319.e1-4.
7. Gude NM, Roberts CT, Kalionis B, King RG. Growth and function of the normal human placenta. Thromb Res 2004;114:397-407.
8. Korteweg FJ, Erwich JJ, Holm JP, Ravisé JM, van der Meer J, Veeger NJ, *et al.* Diverse placental pathologies as the main causes of fetal death. Obstet Gynecol 2009;114:809-17.
9. Korteweg FJ, Erwich JJ, Timmer A, van der Meer J, Ravisé JM, Veeger NJ, *et al.* Evaluation of 1025 fetal deaths: Proposed diagnostic workup. Am J Obstet Gynecol 2012;206:53.e1-12.
10. Rayburn W, Sander C, Barr M Jr., Rygiel R. The stillborn fetus: Placental histologic examination in determining a cause. Obstet Gynecol 1985;65:637-41.

Original Article

Interconnected Dimensions: A Three-dimensional Computed Tomography Study of Scaphoid Size Relative to Adjacent Carpal Bones

Navbir Pasricha, Mahapatra Swagat[1], Sthapak Eti, Narayan Shamrendra[2], Singh Arvind[3]

Departments of Anatomy, [1]Orthopaedics, [2]Radiodiagnosis and [3]Community Medicine, Dr RML Institute of Medical Sciences, Lucknow, Uttar Pradesh, India

Abstract

Introduction: The accurate assessment of scaphoid bone morphometry is a prerequisite before internal fixation treatment for fractures. We intended to arrive at a method for exact quantification of the scaphoid length by measuring intact adjacent bones and the contralateral scaphoid in the normal population, which can then be translated into use for planning surgical repair in case of fracture or nonunion. **Methodology:** A prospective, descriptive study was conducted where three-dimensional reconstruction of the wrist with computed tomography scan was done to document lengths of the scaphoid (bilaterally), capitate, radius width, and lateral intra scaphoid angle and dorsal cortical angle of scaphoid were measured. **Results:** The mean scaphoid length, capitate length, and width of radius were significantly more in males as compared to females. The capitate length and contralateral scaphoid length were most significantly related to scaphoid length. The mean scaphoidcapitate ratio (SCR) was found to be 1.08. **Conclusion:** Using the liner regression model, scaphoid length can be predicted from variables such as capitate length and SCR with 99.99% accuracy, aiding surgeons in scaphoid fixation in cases of fractured scaphoid, malunion, and nonunion.

Keywords: *Carpal alignment measurements, fracture fixation, imaging, scaphoid bone, three dimensional*

Introduction

Carpal fractures account for 8% out of all hand fractures, of which scaphoid fractures are the most common.[1] In surgeries conducted for correcting humpback deformity seen with scaphoid nonunions, restoration of the normal scaphoid length is often recommended. Scaphoid length is restored using trapezoidal iliac crest bone graft, or fixated with headless screws, as around 80% of the surface of the bone is covered with articular cartilage.[2] Despite the fact that screw fixation is being exceedingly used to repair scaphoid fractures, literature is quite sparse and debatable over its morphological variations.[3] To be able to define the precise length that would yield optimal clinical results, a precise method for investigating the original scaphoid length is required. Screws required for scaphoid fixation are mainly designed on the results of literature based on Western studies. Clinicians also find it difficult to detect the true displacement pattern because of the substantial overlapping of carpal shadows apart from the complexity of the three-dimensional (3D) structure of the scaphoid. Only a few studies in the past have tried to find out reliable carpal alignment indices but could comment only on the validity of the radiolunate angle.[4] The scaphoid bone not only plays an important role in wrist mechanics by acting as a link between two rows of carpals, but it is also the most frequently fractured carpal bone, with an incidence of about 82%–89% among all carpal fractures.[5,6] These fractures are usually through the waist and, although not displaced often, can be complicated by a "humpback deformity" with or without union because of extension, supination, and anterior translation of the proximal fragment relative to the distal fragment.[7-10] Humpback deformities are of special concern because they disrupt carpal kinematics of the entire wrist and very often cause instability of the dorsal intercalated segment that may decrease the range of motion of the wrist, and lead to chronic pain and osteoarthritis.[11] The specific problem with scaphoid anatomy can be attributed to its unique bean shape with constriction at the waist and no clear-cut

How to cite this article: Pasricha N, Swagat M, Eti S, Shamrendra N, Arvind S. Interconnected dimensions: A three-dimensional computed tomography study of scaphoid size relative to adjacent carpal bones. J Anat Soc India 2025;74:19-25.

Article Info

Received: 14 December 2024
Revised: 25 January 2025
Accepted: 15 February 2025
Available online: 31 March 2025

Address for correspondence:
Dr. Navbir Pasricha, Department of Anatomy, Dr RML Institute of Medical Sciences, Lucknow, Uttar Pradesh, India.
E-mail: nivibedi@gmail.com

Access this article online

Website: https://journals.lww.com/joai

DOI: 10.4103/jasi.jasi_193_24

Quick Response Code:

demarcation of its bony center required for morphometric clarity before screw placement.[12] Although research has been taken up in the past to understand the morphometric variations of the scaphoid, most of these studies have used dried cadaveric bone specimens of unknown age and pathology, in which case the specimens used in those studies might have undergone major deformation since the time of their preservation, which may be the reason why marked differences are seen in measurements of dry and wet scaphoid specimens.

Only a few studies have been done to quantitate geometric parameters of the wrist taking measurements such as carpal angles and carpal ratios. Radiographic measurements of capitate length and distal radioulnar joint distance have been made in normal wrists by Schuind *et al*.[13] Other studies have been done using measurements created on two-dimensional (2D) x-ray films, like the one by Metz *et al*., which calculated scapholunate joint distance[14] and by McMurtry *et al*., which have calculated the 2D carpal height ratio by standard posteroanterior x-ray films.[15] Very few 3D measurements have been made, which are vital to detect and appreciate the true pattern of displacement of the scaphoid because of the overlapping of carpal shadows and the complexity of the 3D scaphoid structure. A study done by Megerle *et al*.[16] investigated the correlation of carpal alignment indices on plain radiographs and intrascaphoid angles on computed tomography (CT) scans with the clinical outcome and concluded that scaphoid reconstructions correlated with the radio-lunate angle. They also suggested that carpal alignment indices of known reliability and validity should be created to determine the treatment option or the surgical outcome of scaphoid fractures. A recent study tried to investigate the scaphoid morphometry by trying to analyze the curvature and waist diameters for safe screw placement.[17] Surgeons have often used the opposite healthy bone as a guideline for surgical correction of complex traumatic injuries, mal- or nonunions[9] but still the left-right variability is rarely evaluated, and the exact knowledge about 3D differences is still limited[3] and to the best of our knowledge not documented in the Indian diasporas. A 3D reconstruction template study done to quantify potential left-right differences found that regions of the scaphoid contra laterally may differ up to 1.9 mm, a fact which must be taken into account if the contralateral scaphoid is to be used in surgical planning.[18] Surgeons dealing with the treatment of mal-union or nonunion of the scaphoid may use various indices such as lateral intrascaphoid angle (LISA) or dorsal cortical angle (DCA) for predicting the outcome such as restoration of movement and function,[4] but their normal ranges have not been determined for major population groups and to the best of our knowledge never in the Indian population. The purpose of this study is to investigate the precision of estimating normal scaphoid lengths based on intact adjacent bone dimensions, also compared with the contralateral scaphoid length in the normal adult population by creating a reference database of normal carpal anatomy which will provide valuable reference information to facilitate diagnosis and treatment in planning for injuries and diseases in the wrist.

Methodology

This was a prospective, descriptive, cross-sectional study that was conducted in the department of anatomy and radiology, where 55 subjects of both sexes were recruited, and CT scan with the 3D reconstruction of the wrist was done, for12 months. The sampling technique used was random purposive sampling, and the recruitment of patients was done from the department of orthopedics and radiology of a tertiary care institute. The subjects were healthy adults recruited for the study, or alternately, patients with fractures at other sites or soft-tissue injuries where CT is mandatory for treatment. Patients with a previous history of any bony pathology, a history of degenerative or metabolic diseases, recurrent wrist pain, or any inflammatory arthropathy were excluded from the study. Furthermote, patients with a known history of prolonged intake of glucocorticoids, proton pump inhibitors, selective serotonin receptor inhibitors, thiazolidinediones, anticonvulsants, medroxyprogesterone acetate, aromatase inhibitors, androgen deprivation therapy, heparin, calcineurin inhibitors, and chemotherapies were excluded from the study. The subjects were duly explained the minimal radiation exposure associated with CT scan. The sample size was calculated using study (Morphometric Variations of Scaphoid and Safety of Screw Fixation for Its Waist Zone Fractures in Indian Population: A Preliminary Report. Trikha V *et al*. Journal of Hand Surgery Global Online, Volume 1, Issue 3, 166 – 173) and it came out to be 55. Since the carpus is not a weight-bearing joint when not in use or under gravitational force, age vise changes are less frequently seen, so the sample size was not stratified according to age.

CT examinations were performed on a 64-MDCT scanner (Extended Brilliance Workspace, Version 6.4, Philips Medical System), which works at 64 mm × 1 mm collimation, with a minimum slice thickness of 0.625 mm. CT scan images were retrieved from the PACS, processed, and analyzed with multiplanar reformation at the available workstation. The wrists were imaged in the standard neutral position[5,6] with the participant's shoulder abducted at 90°, the elbow flexed at 90° and the forearm in neutral rotation with the palm resting on the tray. The distal radius and capitate measurements were taken as they are most important in understanding wrist biomechanics, particularly due to their close morphological relationship with the scaphoid.[18] The length of the scaphoid was taken from its most proximal to distal aspect using a line drawn along the anterior facet [Figure 1]. The radial width at the waist region was measured as the maximal anteroposterior extent,

directed perpendicular to the horizontal plane. The capitate length was measured as the length of the capitate axis. All measurements were taken independently by two observers, a muskuloskeletal radiologist and an orthopedic surgeon, trained in using the software application, and the mean of their observations was taken as the final reading. The LISA was documented by measuring the angle between to perpendicular lines drawn on proximal and distal articular surfaces [Figure 2]. The DCA of the scaphoid was measured as the angle between two tangential lines drawn over the flattest part of the cortex of the dorsal surface [Figure 3].

Since the study involved the recruitment of healthy volunteers and those who had to undergo CT scan hand for any other reason, only those who consented for the study were recruited. The study was undertaken only after due Ethics committee approvals vide IEC No. 174/22, Ref no. 626 RMLIMS/2023. The cost of CT was borne from the intramural funding obtained from the institution. Statistical analysis was performed using R-4.3.2 Statistical Software (R Core Team (2021) R: A Language and Environment for Statistical Computing. R Foundation for Statistical Computing, Vienna. https://www.R-project.org) and independent *t*-test to compare related parameters and regression analysis and model prediction using liner regression model were undertaken.

Results

The total number of participants was 55, out of which 18 (32.73%) subjects were female, and male participants were 37 (67.27%). The mean age of the participants was 33.45 ± 9.77 years. The mean scaphoid length was found to be 24.32 ± 1.32 (mm), capitate length 24.44 ± 1.25 (mm), contralateral scaphoid length was 24.33 ± 1.32 (mm), LISA was 27.47 (in degree), radius width: 26.31 ± 1.33 (mm), and DCA of scaphoid was 127.73 (in degree). Table 1 presents the study variables as a categorical form of data in frequency and percentage and quantitative data measures as mean and standard deviation (SD).

Table 1: The demographic table presented frequency, percent, and mean and standard deviation

Variable	*n* (%)/mean±SD
Sex	
Female	18 (32.73)
Male	37 (67.27)
Age	33.45±9.77
Scaphoid length (mm)	24.32±1.32
Capitate length (mm)	24.44±1.25
Contralateral scaphoid length (mm)	24.33±1.32
LISA (in degree)	27.47±0.69
Radius width (mm)	26.31±1.33
DCA of scaphoid (in degree)	127.73±1.04
Ratio (scaphoid/capitate)	1.08±0.01

LISA: Lateral intra scaphoid angle, SD: Standard deviation, DCA: Dorsal cortical angle

As shown in Table 2, gender variations of the study variables were compared using independent *t*-test. These study variables satisfied the normality criteria using the

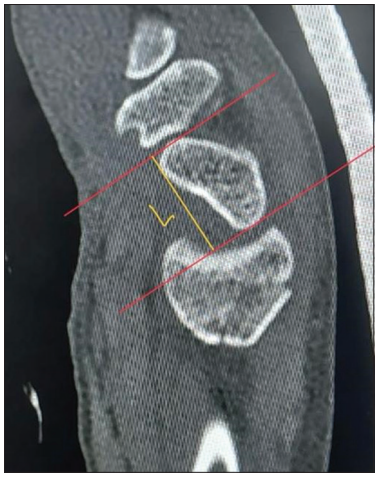

Figure 1: Scaphoid Length taken in sagittal plane

Figure 2: Lateral intrascaphoid angle taken in sagittal plane. LISA: Lateral intrascaphoid angle

Figure 3: Dorsal cortical angle of scaphoid taken in sagittal plane. DCA: Dorsal cortical angle

Shapiro–Wilk test as well. It was observed that males have a higher mean value of scaphoid length than the females, and $P < 0.001$. The capitate length (mm) in males has a higher mean value than the females, and $P < 0.001$. The contralateral scaphoid length (mm) in males had a higher mean value as compared to females, and $P < 0.001$. The radius width (mm) had a significant difference in females and males, as males have a higher mean value of radius width (mm) than the females, and $P < 0.001$. Scaphoid-capitate ratio (SCR) was taken as the ratio between scaphoid length and ipsilateral capitate length[17] and was found to be 1.08 ± 0.01 and if seen separately gender vise, 1.08 ± 0.02 in females and 1.08 ± 0.01 in males.

In Figure 4, we observed the correlation coefficient between age and scaphoid length $r = 0.09$ and $P = 0.503$, which was not significant: no significant relation of length increase with age.

For the regression analysis and model prediction using the liner regression model for variables, scaphoid length was found dependent on capitate length, contralateral scaphoid length, LISA (in degree), radius width (mm), and DCA of the scaphoid (in degree). It was observed that the regression model and residual followed the normality condition, as seen in Figures 2 and 3.

Model 1 to determine scaphoid length:

Y(Scaphoid Length (mm))

$=\beta_0+\beta_1$ (Capitate Length (mm)) + β_2 (Contralateral Scaphoid Length)

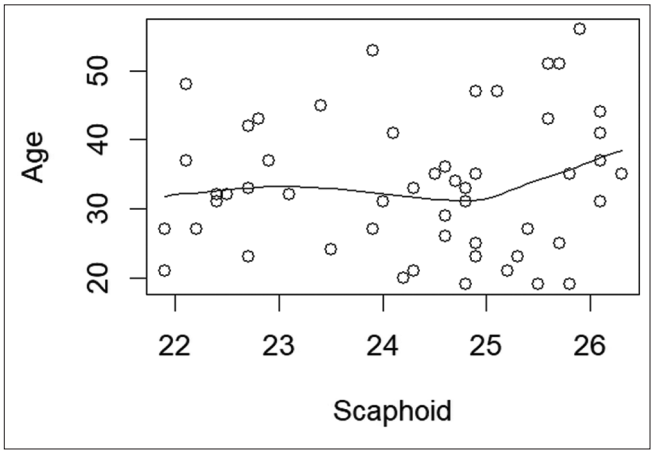

Figure 4: Correlation between age and scaphoid length (mm)

Table 2: Gender wise comparison of study variables using independent *t*-test

Study variables	Sex	Frequency (*n*)	Mean±SD	Independent *t*-test (*P*)
Age	Female	18	34.389±8.9188	0.625
	Male	37	33.000±10.244	
Scaphoid length (mm)	Female	18	22.683±0.5639	<0.001***
	Male	37	25.122±0.6676	
Capitate length (mm)	Female	18	20.961±0.6545	<0.001***
	Male	37	23.159±0.7085	
Contralateral scaphoid length (mm)	Female	18	22.694±0.5724	<0.001***
	Male	37	25.127±0.6760	
LISA (°)	Female	18	27.244±0.7648	0.088
	Male	37	27.584±0.6357	
Radius width (mm)	Female	18	24.689±0.5346	<0.001***
	Male	37	27.097±0.7507	
DCA of scaphoid (°)	Female	18	127.500±1.3394	0.264
	Male	37	127.838±0.8665	
Ratio (scaphoid/capitate)	Female	18	1.08±0.02	0.553
	Male	37	1.08±0.01	

Significant codes: ***0.001. LISA: Lateral intrascaphoid angle, SD: Standard deviation, DCA: Dorsal cortical angle

Table 3: Parameter estimates and *P* value of study variables

Coefficients	Estimate (*B*)	SE	*t*	*P*
β_0 (intercept)	1.715	1.27777	1.343	0.1856
β_1 capitate length (mm)	0.106	0.04214	2.520	0.0150
β_2 (contralateral scaphoid length)	0.877	0.05280	16.607	<0.001***
β_3 (LISA)	0.0180	0.01551	1.160	0.2518
β_4 (radius width [mm])	0.022	0.03489	0.630	0.5319
β_5 (DCA of scaphoid)	−0.017	0.01005	−1.700	0.0954
β_6 (scaphoid - capitate ratio)	21.062	0.7969	26.429	<0.001***

Significant codes: ***0.001. SE: Standard error, LISA: Lateral intrascaphoid angle, DCA: Dorsal cortical angle

$+\beta_3$ (LISA) + β_4 (Radius width (mm)) + β_5 (DCA of scaphoid) + β_6 (Ratio) +ϵ

As seen in Table 3 and Figures 5 and 6, t statistic, and P value of the coefficient of parameters of study variable presented in the model are shown here. We observed the capitate length (mm) and intercept are significant with respect to scaphoid length (mm), and the $P < 0.05$. It showed that the scaphoid length increased with the capitate length and intercept (constant) increase. Furthermore, for the model, we observed the residual standard error was 0.01925 on 48 degrees of freedom. Multiple r^2 was the coefficient of determination for the model is 0.9998, and the adjusted $r^2 = 0.9998$. The model perfectly explained the scaphoid length relation and determination. Furthermore, the *F*-statistic was 4.2×10^4 on 6 and 48 degree of freedom, and the $P < 2.2 \times 10^{-16}$.

In Table 4, using the abovementioned regression model and the coefficient of parameters with the respective study variable arbitrary values we could predict the scaphoid length.

Second model for scaphoid length prediction

Y(Scaphoid Length (mm))

$=\beta_0+\beta_1$ (Capitate Length (mm)) $+\beta_2$ (Scaphoid capitate Ratio) + ϵ

In Table 5, estimates, *t*-statistic, and *P* value of the coefficient of parameters of study variable presented in the model are shown here. We observed that capitate length and intercept (constant) were most significant with respect to scaphoid length, and the $P < 0.05$. For the model, we observed the residual standard error was 0.01909 on 52 degrees of freedom. Multiple r^2 is the coefficient of determination for the model is 0.9998, and the adjusted $r^2 = 0.9998$. This model perfectly explained the study variables' relation and determination. Furthermore, the *F*-statistic was 1.28×10^5 on 2 and 52 degree of freedom, and the $P < 2.2 \times 10^{-16}$.

In Table 6, using the abovementioned regression model and the coefficient of parameters with the respective study variables arbitrary values, we can predict the scaphoid length.

Since the $r = 0.9998$, it means in 99.98% of cases it can predict the length of the scaphoid correctly.

Table 4: Prediction of scaphoid length using estimates of carpal dimensions

Study variables	Estimate (*B*)	Estimate (*B*)		
		Set 1	Set 2	Set 3
Independent variable				
Intercept	−23.2284			
Capitate length	1.0559	22	24.44	27
Contralateral scaphoid length	0.0219	45	24.33	20
LISA	0.0044	24	27.47	30
Radius width	0.0033	45	26.31	21
DCA of scaphoid	0.0021	110	127.73	135
Ratio	21.062	1.0	1.08	1.15
Dependent variable				
Scaphoid length (predicted)		23.1004	26.944	31.075

LISA: Lateral intra scaphoid angle, DCA: Dorsal cortical angle

Table 5: Parameter estimates and *P* value of most significant study variables

Coefficients	Estimate (*B*)	SE	*t*	*P*
β_0 (intercept)	−23.4168	0.2652	−88.28	<0.001***
β_1 capitate length (mm)	1.0842	0.0021	505.64	<0.001***
β_2 (scaphoid capitate ratio)	21.5938	0.2304	93.71	<0.001***

Significant codes: ***0.001. SE: Standard error

Table 6: Prediction of scaphoid length using capitate length and scaphoid capitate ratio

Study variables	Estimate (*B*)	Values (arbitrary)		
		Set 1	Set 2	Set 3
Independent variable				
Intercept	−23.4168			
Capitate length	1.0842	22	24.44	27
Scaphoid/capitate ratio	21.5938	1.0	1.08	1.15
Dependent variable				
Scaphoid length (predicted)		22.029	26.403	30.689

Discussion

Scaphoid fractures have a reported nonunion incidence of 5%–50%,[11] and for these patients, open surgical procedures with grafting are often indicated. Restoration of the scaphoid length is the primary endeavor of the orthopedic surgeon as it is crucial for maintaining the structural integrity of the radial column in the wrist.[19] By re-establishing this length, proper tension in the palmar radiocarpal ligaments is ensured, which plays a key role in wrist stability and function. This restoration helps to prevent complications such as arthritis and loss of motion, supporting overall wrist biomechanics. Proper alignment and length are essential for optimal force transmission during activities involving the hand and wrist. Thus, an accurate estimation of scaphoid length is essential.

In the present study, the mean length of scaphoid was found to be 24.32 ± 1.32 and 22.68 ± 0.56 mm in females and 25.12 ± 0.67 mm in males (significant difference, $P < 0.001$) which is comparable to a magnetic resonance image study done in American population in which the mean scaphoid length was 24.5 ± 2.4 mm, the scaphoid length in males was 26 ± 1.9 mm, whereas in females it was 22.5 ± 1.4 mm.[20] The scaphoid length in our study is also comparable to a CT study[21] done in Canadian and European population, which documented scaphoid length as 22.5 ± 2.9 mm, with mean scaphoid DCA as 139° ± 25°, whereas in our study this was seen

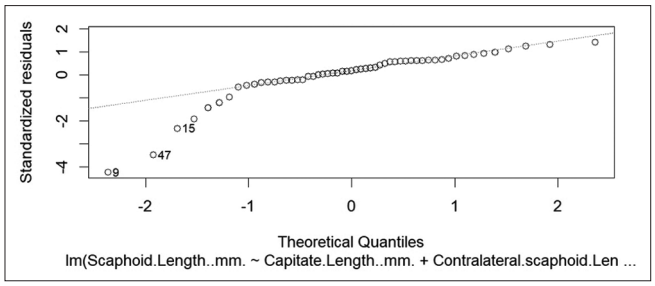

Figure 5: Residuals Q-Q plot for the model which lies on the diagonal line

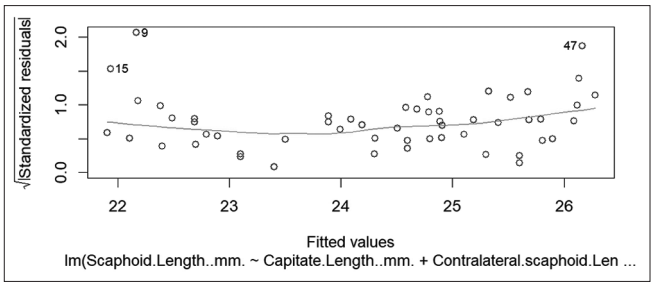

Figure 6: Standard residuals of scale location plot for the model which lies on one

to be 127.73° ± 1.04°. However, in Western, European, and Chinese populations, some studies document the scaphoid length to be close to 26 mm, with some CT studies also claiming the average length close to 31 mm in Western males and the Kenyan population,[17,20,22,23] which underlines the importance of more studies in our population to have specific population-based data for screw manufacturers, which usually follow the western norms.

The mean capitate length in our study was 24.44 ± 1.25 mm, with mean length in males 23.16 ± 0.71 and females 20.96 ± 0.65. This is comparable to a study by Schuind *et al*., which reported mean capitate lengths in females as 20.03 ± 1.6 mm and males as 23.0 ± 1.7 mm.[13] These measurements are more in a study on the American population, with mean Capitate length being 28.3 ± 3.8 mm and in females 25.8 ± 2.6 and male subjects 29.5 ± 3.7 mm.[24]

Orthopedic surgeons do try to estimate the original normal scaphoid dimensions using the contralateral healthy scaphoid as a reference as there is a general bilateral symmetry[25] but there are still differences in left to right bones in individual cases.[17] Computer-assisted surgical planning techniques often use the contralateral scaphoid as a 3D reconstruction template which prompted us to quantitatively assess left-right differences in scaphoid anatomy precisely. Previous studies document surface-to-surface differences of up to 1.9 mm in certain regions of the scaphoid,[17] highlighting the need for caution when using the contralateral scaphoid in surgical planning. In the present study, a strong correlation was found between the length of the left and right scaphoid, underscoring the overall symmetry in scaphoid morphology despite the noted differences. Furthermore, using regression analysis, we could document that it is a very good predictor of scaphoid length.

We hypothesized that estimating the length of the scaphoid using the dimensions of adjacent intact bones could serve as a reliable alternative. This method might yield alternate estimations than those just derived from measurements of just the contralateral scaphoid, which can be affected by variability and injury. In our study, the mean SCR and ratio in males was found to be 1.08 ± 0.01 and 1.08 ± 0.02 in females, which is quite similar to a study in the Kuwaiti population, which documented mean SCR as 1.01 with SD 0.084.[17] The SCR offers several advantages in clinical practice as it provides a reliable method to estimate scaphoid length in conditions associated with a shortened scaphoid and also to calculate the appropriate size of bone grafts needed for scaphoid reconstruction and in conditions with size discrepancies, which can be congenital or due to obstetric brachial plexus palsy. The author could not find any Indian study which had calculated SCR.

A CT study on the Dutch population documented normal ranges for LISA and DCA as 27 and 128 degrees, respectively.[26] These findings are quite similar to our study, which recorded mean LISA as 27.47 ± 0.69 degrees and DCA as 127.73 ± 1.04 degrees. Only a few studies in the past have documented these angles, and these studies had limitations of small sample size,[27] including cases with scaphoid pathologies[21] and thus the values of LISA (31 degrees[27]) and DCA (139 degrees[21,27]) do not correspond with our study. Since these angles are predictors of outcome and influence clinical decision-making when assessing malunion, the present study provides normative data that can help surgeons before planning for intervention. LISA and DCA also help in evaluation of humpback deformity[21] and thus are very relevant clinically. To the best of our knowledge, there is no Indian study that gives a normative data of these angles. The mean radial width in the present study was found to be 26.31 ± 1.33 mm, and 24.69 mm in females. The radial width, although not significant in relation to the length of the scaphoid, is an important index. It has been documented that smaller radial width increases the risk for fracture irrespective of bone mineral density, as a smaller width means a smaller cross-sectional area and a higher pressure per cm^2.[28] Earlier studies have either mentioned contralateral scaphoid length or SCR, to aid in scaphoid length determination preoperatively. The present study provides with a very precise method of scaphoid length assessment, tailored for each individual to provide accurate size of either bone graft or screw for fixation, reducing the chances of overexpanding, which can cause restricted wrist flexion.[25]

By focusing on the surrounding anatomy, our aim was to enhance the precision of scaphoid length assessments,

ultimately improving surgical outcomes and rehabilitation strategies.

Conclusion

Internal fixation required for scaphoid fractures requires precise assessment of the screw length tailored for a particular population. It is imperative to restore scaphoid length, which can be obtained with 99.9% accuracy with the formula using capitate length and SCR hypothesized in our study.

Financial support and sponsorship

This project was funded by the Research Committee of RML Institute of Medical Sciences, Lucknow.

Conflicts of interest

There are no conflicts of interest.

References

1. van Onselen EB, Karim RB, Hage JJ, Ritt MJ. Prevalence and distribution of hand fractures. J Hand Surg Br 2003;28:491-5.
2. Kawamura K, Chung KC. Treatment of scaphoid fractures and nonunions. J Hand Surg Am 2008;33:988-97.
3. Ceri N, Korman E, Gunal I, Tetik S. The morphological and morphometric features of the scaphoid. J Hand Surg Br 2004;29:393-8.
4. Roh YH, Noh JH, Lee BK, Baek JR, Oh JH, Gong HS, *et al.* Reliability and validity of carpal alignment measurements in evaluating deformities of scaphoid fractures. Arch Orthop Trauma Surg 2014;134:887-93.
5. Hardy DC, Totty WG, Reinus WR, Gilula LA. Posteroanterior wrist radiography: Importance of arm positioning. J Hand Surg Am 1987;12:504-8.
6. Mann FA, Wilson AJ, Gilula LA. Radiographic evaluation of the wrist: What does the hand surgeon want to know? Radiology 1992;184:15-24.
7. Brauer RB, Dierking M, Werber KD. Use of the Herbert screw with the freehand method for osteosynthesis of acute scaphoid fracture. Unfallchirurg 1997;100:776-81.
8. Kozin SH. Incidence, mechanism, and natural history of scaphoid fractures. Hand Clin 2001;17:515-24.
9. Schaefer M, Siebert HR. Fracture of the semilunar bone. Unfallchirurg 2002;105:540-52.
10. Schwarcz Y, Schwarcz Y, Peleg E, Joskowicz L, Wollstein R, Luria S. Three-dimensional analysis of acute scaphoid fracture displacement: Proximal extension deformity of the scaphoid. J Bone Joint Surg Am 2017;99:141-9.
11. Schweizer A, Fürnstahl P, Nagy L. Three-dimensional computed tomographic analysis of 11 scaphoid waist nonunions. J Hand Surg Am 2012;37:1151-8.
12. Nakamura P, Imaeda T, Miura T. Scaphoid malunion. J Bone Joint Surg Br 1991;73:134-7.
13. Schuind FA, Linscheid RL, An KN, Chao EY. A normal data base of posteroanterior roentgenographic measurements of the wrist. J Bone Joint Surg Am 1992;74:1418-29.
14. Metz VM, Schimmerl SM, Gilula LA, Viegas SF, Saffar P. Wide scapholunate joint space in lunotriquetral coalition: A normal variant? Radiology 1993;188:557-9.
15. McMurtry RY, Youm Y, Flatt AE, Gillespie TE. Kinematics of the wrist. II. Clinical applications. J Bone Joint Surg Am 1978;60:955-61.
16. Megerle K, Harenberg PS, Germann G, Hellmich S. Scaphoid morphology and clinical outcomes in scaphoid reconstructions. Injury 2012;43:306-10.
17. Letta C, Schweizer A, Fürnstahl P. Quantification of contralateral differences of the scaphoid: A comparison of bone geometry in three dimensions. Anat Res Int 2014;2014:904275.
18. Buijze GA, Lozano-Calderon SA, Strackee SD, Blankevoort L, Jupiter JB. Osseous and ligamentous scaphoid anatomy: Part I. A systematic literature review highlighting controversies. J Hand Surg Am 2011;36:1926-35.
19. Guo Y, Tian GL. The length and position of the long axis of the scaphoid measured by analysis of three-dimensional reconstructions of computed tomography images. J Hand Surg Eur Vol 2011;36:98-101.
20. Smith DK. Anatomic features of the carpal scaphoid: Validation of biometric measurements and symmetry with three-dimensional MR imaging. Radiology 1993;187:187-91.
21. Bain GI, Bennett JD, MacDermid JC, Slethaug GP, Richards RS, Roth JH. Measurement of the scaphoid humpback deformity using longitudinal computed tomography: Intra- and interobserver variability using various measurement techniques. J Hand Surg Am 1998;23:76-81.
22. Heaton DJ, Trumble T, Rhodes D. Determination of the central axis of the scaphoid. J Wrist Surg 2015;4:214-20.
23. Kigera JW, Owira P, Saidi H. Scaphoid dimensions and appropriate screw sizes in a Kenyan population. East Afr Orthop J 2017;11:3e5.
24. Patterson RM, Elder KW, Viegas SF, Buford WL. Carpal bone anatomy measured by computer analysis of three-dimensional reconstructions of computed tomography images. J Hand Surg Am 1995;20:923-9.
25. Eggli S, Fernandez DL, Beck T. Unstable scaphoid fracture nonunion: A medium-term study of anterior wedge grafting procedures. J Hand Surg Br 2002;27:36-41.
26. Guldbrandsen CW, Radev DI, Gvozdenovic R. Normal ranges for measurements of the scaphoid bone from sagittal computed tomography images. J Hand Surg Eur Vol 2021;46:594-9.
27. Afshar A, Mohammadi A, Zohrabi K, Navaeifar N, Sami SH, Taleb H. Correlation of reconstructed scaphoid morphology with clinical outcomes. Arch Bone Jt Surg 2015;3:244-9.
28. Kiebzak G, Sassard WR. Smaller radius width in women with distal radius fractures compared to women without fractures. Cureus 2017;9:e1950.

Original Article

Analysis of Proximal Femoral Morphologic Parameters in Turkish Adult Population by Computed Tomography

Büsra Nur Özcan Erisgin, Ahmet Uzun

Department of Anatomy, Faculty of Medicine, Ondokuz Mayıs University, Samsun, Türkiye

Abstract

Aim: The study was performed to understand the differences in the morphometric properties of the proximal femur between age, sex and right-left side in the Turkish population. **Materials and Methods:** Morphometric measurements were made on CT images of 404 people (210 men, 194 women). People were four grouped into 10 year age ranges. We measured femoral head diameter, femoral neck diameter, femoral head length, femoral neck length, inter trochanteric length, hip axis length, femoral axis length, acetabular depth, inclination angle, lateral central edge angle, Alsberg Angle, anterior central edge angle, posterior central edge angle, acetabular anteversion angle, Sharp Angle, acetabular abduction angle. We calculated femoral head coverage ratio and acetabular depth width index. **Results:** All length, depth, diameter measurements, inclination angle and acetabular abduction angle were found greater in males than in females. Posterior center edge angle, acetabular anteversion angle and Sharp angle were found greater in women than in men. Femoral head diameter was measured smaller in the 20-29 age group compared to other age groups. It was determined the femoral head coverage ratio increased with age. Sharp angle decreased significantly between the ages of 20-29 and 50-59. depth width index were found larger on the left side. **Conclusion:** Knowing the morphometric values of the proximal femur revealed in this study may contribute to the procedures to be applied to the proximal femur and hip region and may also increase the reliability of operative situations.

Keywords: *Computer tomography, measurement, proximal femur*

Introduction

The femur is the heaviest, longest and strongest bone of the skeletal system, joining the hip joint. Many studies have been conducted on the morphometric properties of the femur.[1-3] Normal ranges of morphometric values may differ between age and sex.[4] Morphometric measurements can be used to regional differences within the same race. Morphometric studies can be used to standardize individuals in the societies in which they are performed.[5] Knowing the morphometric properties of skeletal components can be clinically guiding in many matters. Revealing normal morphometric parameters is the key to distinguishing deformities from anatomical variations. In addition, morphometric measurements are also used for early diagnosis and classification of patients.[6]

Proximal femur and acetabulum may show various morphological variations depending on age and sex. These variations sometimes can be pathological. Abnormal morphometry is defined as a biomechanical risk factor for osteoarthritis due to disproportionate load distribution in the joint.[7] The relationship between abnormal morphometry and degenerative arthritis of the hip was first demonstrated by Stulberg *et al.*[8] Femoroacetabular impingement is a pathological condition between the femoral head and acetabular rim that is thought to develop coxaarthrosis.[9] It is characterized by morphological changes such as abnormalities of the head and neck contour of the femur and excessive covering of the femoral head. It is one of the leading causes of acetabular labrum rupture and degenerative arthritis.[10] One of the most common conditions that causes arthritis is hip dysplasia.[11] Developmental hip dysplasia in children occurs with proximal femur deformations as well as acetabular malformation and hypoplasia. If left untreated, this condition results in rapidly progressive osteoarthritis in adulthood.[12] The most common

How to cite this article: Erisgin BN, Uzun A. Analysis of proximal femoral morphologic parameters in Turkish adult population by computed tomography. J Anat Soc India 2025;74:26-35.

Article Info

Received: 14 May 2024
Revised: 18 November 2024
Accepted: 24 January 2025
Available online: 31 March 2025

Address for correspondence:
Prof. Ahmet Uzun,
Department of Anatomy, Faculty of Medicine, Ondokuz Mayıs University, Samsun, Türkiye.
E-mail: auzun@omu.edu.tr

Access this article online

Website: https://journals.lww.com/joai

DOI: 10.4103/jasi.jasi_63_24

Quick Response Code:

reason for hip arthroplasty in young adulthood untreated developmental dysplasia of the hip.[13] The smooth movements of the hip joint depend on the harmony of the femoral head and acetabulum. One of the factors this harmony is the inclination angle (IA). Any deviation of the IA beyond normal values can cause a number of disorders such as developmental hip dysplasia.[14] To detect such abnormalities and follow their progression, normal ranges of morphometric parameters of the proximal femur must be defined. Morphometry of the proximal femur has been used as an important marker for hip fracture risk in recent years. As the hip axis length (HAL) increases, the load increases as the lever arm between the center of the hip joint and the femur lengthens. When low body mass index is added to this situation, the risk of fracture increases significantly.[15] Another study suggested that the morphometry of the proximal femur is related to bone strength.[16] One of the important factors for the success of hip prosthesis is the geometry of the prosthesis. Incompatible prosthesis may cause negative consequences such as dislocation, osteolysis, and limitation of range of motion. For the success of hip replacement, the morphometry of the person's proximal femur must be well known.[17] Although personalized prosthesis design is possible, it is very costly and time consuming. For this reason, standard prostheses are preferred. In order to eliminate the compatibility problem of standard prostheses, morphometric studies based on race, age, and gender are required.[18]

In the present study, it was aimed to determine the normal range of the proximal femur according to age and sex in the Turkish population by making various morphometric measurements on computed tomography (CT) images and to compare age, sex and side.

Materials and Methods

In this study, CT archive images of people aged 20–59 years (mean age 40.33 ± 11.35 years men, 38.80 ± 11.69 years women) who applied to Ondokuz Mayıs University Health Practice and Research Center were examined. Cases with fractures in the hip joint and thigh region, previous surgery and prosthesis were not included in the study. This study was done with due permission of Ondokuz Mayıs University Clinical Research Ethics Committee (Protocol number: 220/557, Date: October 08, 2020).

The present study group consists of 210 men and 194 women between the ages of 20 and 59 years. The people in the study were aged 20–29 (46 men, 54 women), 30–39 (52 men, 50 women), 40–49 years old (53 men, 45 women), 50–59 (59 men, 45 women) divided into four groups. Length, diameter, depth, and angle were measured from the transaxial, coronal, and sagittal images. The indexes were calculated.

The femoral head diameter (FHD) was measured at the distance at which the convexity of the head was widest vertically. Femoral head length (FHL) was measured as the distance between two points where the upper width of the femoral neck and the upper border of the femoral head intersect on the femoral neck axis. The femoral neck diameter (FND) was measured by the length of the vertical line taken from the midpoint of the line connecting the epiphyseal line and intertrochanteric line. Femoral neck length (FNL) was measured as the distance between the midpoint of the epiphyseal line and the midpoint of the intertrochanteric line. Intertrochanteric length (ITL) was measured between the peaks of the greater and lesser trochanters. Femoral axis length (FAL), the length of the line connecting the top of the femoral head and the outer point of the greater trochanter was measured. HAL, the line starting from the outer point of the greater trochanter and extending to the inner pelvic lip, was measured. Acetabular depth (AD) is the vertical distance between the horizontal line between the edges of the acetabulum and the deepest point of the acetabular cavity was measured in the coronal plane. IA, between the anatomical axis of the femur and the axis of the femoral neck was measured on the frontal plane. Alsberg angle (AA), between the axis of the femoral shaft and the epiphyseal line was measured. Lateral center edge angle (LCEA) is also known as Wiberg angle. This angle between the line drawn from the center of the femoral head to the lateral acetabular edge and the vertical axis of the pelvis was measured on the frontal plane. Anterior center edge angle (ACEA), between the vertical line passing through the middle of the femoral head and the line connecting the femoral head to the anterior point of the acetabular edge was measured on the sagittal plane. Posterior center edge angle (PCEA), between the vertical line passing through the midpoint of the femoral head and the line connecting the femoral head to the posterior point of the acetabular edge was measured on the sagittal plane. Sharp angle (SA) between the line connecting the lower ends of both pelvic teardrops and the line drawn from the outer edge of the acetabulum bone roof to the lower end of the pelvic teardrop was measured on the coronal plane. The acetabular anteversion angle (AAA) between the line connecting the anterior and posterior edges of the acetabulum and the sagittal line drawn from the posterior end of the acetabulum was measured on the transaxial plane. The acetabular abduction angle (AABDA) between the line between the upper and lower ends of the acetabulum and the line drawn downwards from the upper edge of the acetabulum was measured on the coronal plane. The femoral head coverage ratio (CR) was calculated as the ratio of the distance between the innermost point of the femoral head metaphysis and the outer edge of the acetabulum to the distance between the outermost point of the superior femoral epiphysis and the inner point of the femoral metaphysis. The AD width index (ADWI) was calculated as the ratio of the length of the line created

between the upper-outer corner of the acetabulum and the lower border of the teardrop figure and the length of the perpendicular line drawn from the deepest point of the acetabulum to this line. Taken measurements are shown in Figures 1 and 2. These measurements and indices were analyzed by four age groups, sex and side.

The measurements were measured three times by BNOE in millimeters and angle degree using the OsiriX program, and the mean values were calculated. The data were obtained with the IBM SPSS Statistics for Windows, (Version 20.0. Armonk, NY: IBM Corp.) program at the 95% confidence interval; it was evaluated at the $P < 0.05$ level. The normal distribution of the variables was analyzed using the Shapiro–Wilk test. Student's *T*-test, one of the parametric tests, Mann–Whitney *U*-test, one of the nonparametric tests, was used to evaluate the difference between the sexes. One-Way ANOVA was used for parametric data and Kruskal–Wallis test was used for nonparametric data to examine the differences between age groups with more than two groups. Bonferroni correction was made to control Type I error in

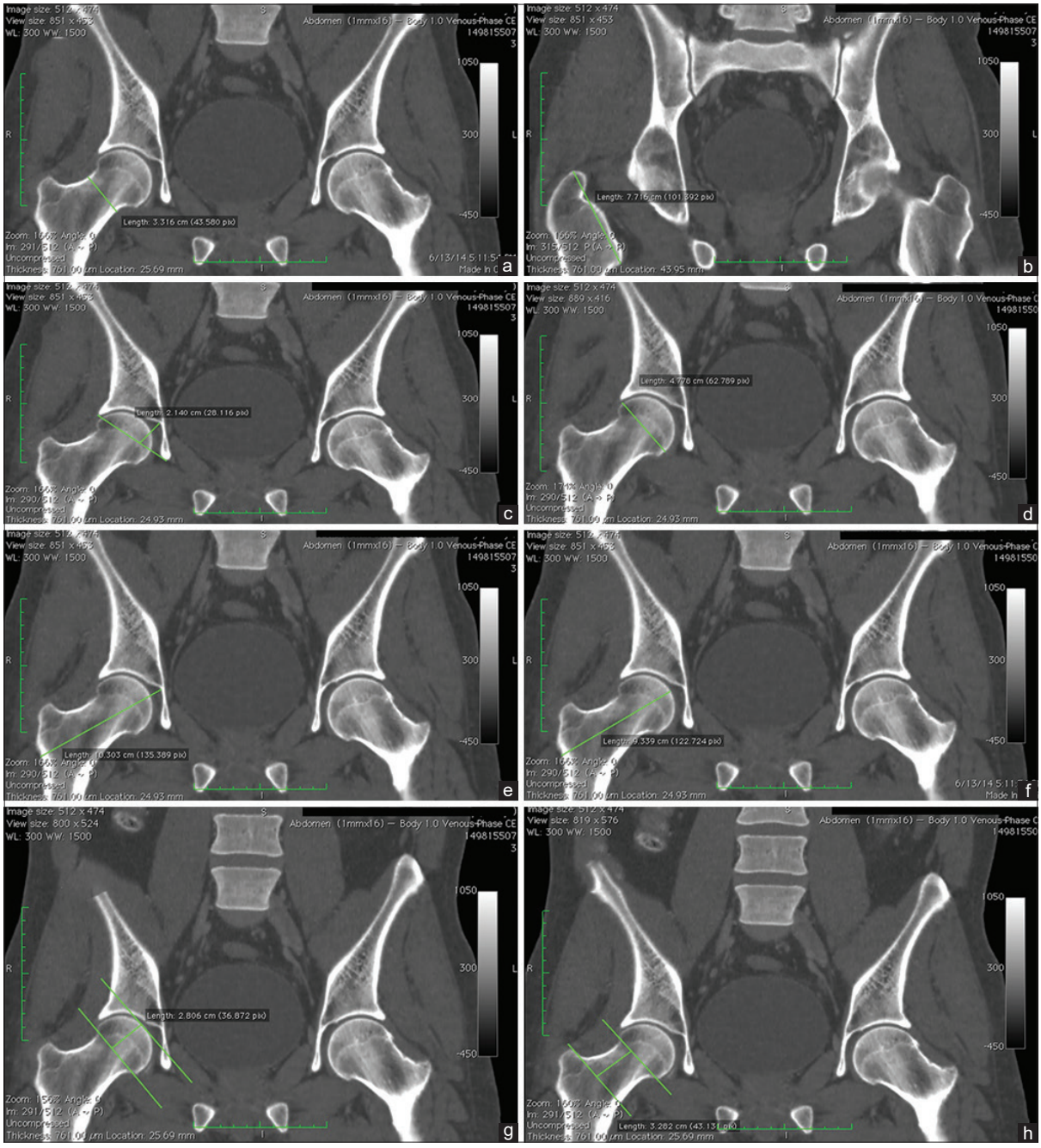

Figure 1: (a) Femoral neck diameter, (b) Intertrochanteric length, (c) Acetabular depth, (d) Femoral head diameter, (e) Hip axis length, (f) Femoral axis length, (g) Femoral head length, (h) Femoral neck length

multiple comparisons. In order to examine the difference between age groups, the results for $P < 0.0083$ according to Bonferroni correction were considered statistically significant. Analysis results were given as mean, standard deviation, minimum, and maximum values.

Results

In this study, we found length, depth and diameter measurements larger in males than females on both sides ($P < 0,001$) [Table 1].

IA and AABDA were found greater on both sides in males. PCEA, SA, and AAA were greater on both sides in females. LCEA was found larger on the right side in males. AA was found greater on the left side in females ($P < 0,001$) [Table 2].

When length, depth, and diameter measurements were compared between age groups, FHD increased on the both sides between 20–29 and 50–59 age groups. FND increased on the both sides between the 20–29 and 30–39, 50–59 age groups. CR increased between the 20–29 age group and the 40–49 and 50–59 age groups ($P \leq 0.001$). The mean value of FHD, FND, ITL, and CR increased with increasing age [Tables 3 and 4].

When angle measurements were compared according to age groups, SA decreased on the both sides between 20–29 and 50–59 ages ($P < 0.001$). AABDA increased on the both sides

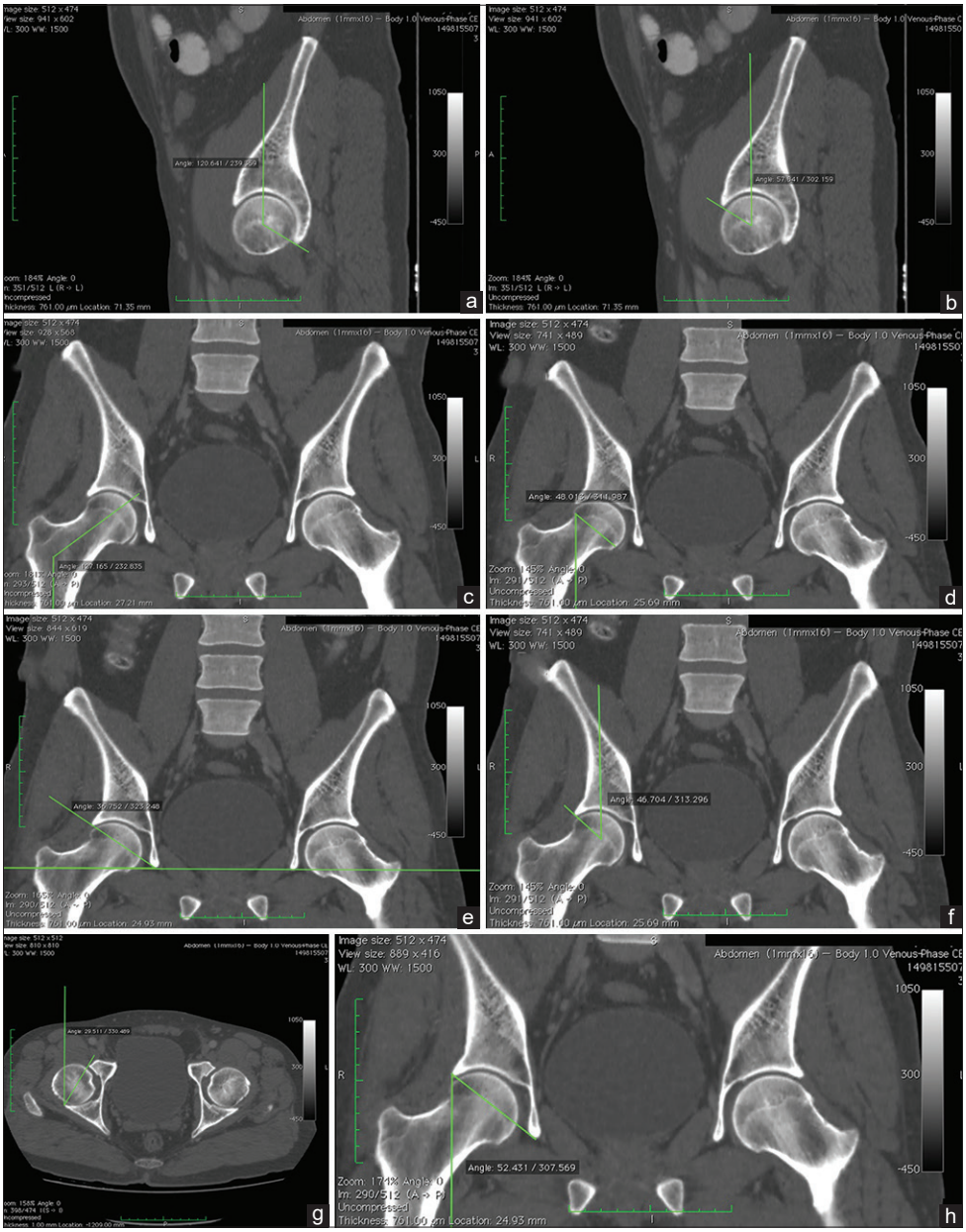

Figure 2: (a) Posterior center edge angle (PCEA), (b) Anterior center edge angle (ACEA), (c) Inclination angle, (d) Alsberg angle, (e) Sharp angle, (f) Lateral center edge angle (LCEA), (g) Acetabular anteversion angle, (h) Acetabular abduction angle (AABDA)

between 20–29 and 50–59 ages. The mean value of LCEA, AABDA increased with increasing age [Tables 5 and 6].

When the right and left sides of the people included in the study were compared, regardless of sex, there was

Table 1: Comparison of average values of length, depth and diameter measurements according to sex

Measurement	Male		Female		*P*
	Mean±SD (mm)	Minimum–maximum	Mean±SD (mm)	Minimum–maximum	
Right					
FHD	46.90±3.04	37.84–53.60	43.04±2.68	34.88–52.26	<0.001*
FHL	30.33±3.98	21.04–49.46	28.63±3.07	20.64–37.73	<0.001*
FND	30.20±3.54	18.61–48.20	27.72±2.59	21.13–36.38	<0.001*
FNL	28.30±4.80	10.42–43.30	25.89±4.15	15.78–39.64	<0.001*
ITL	78.89±5.89	57.47–98.56	68.67±5.26	53.58–85.77	<0.001*
FAL	88.48±9.03	65.30–114.82	83.12±6.57	55.10–99.27	<0.001*
HAL	95.96±9.50	71.72–120.51	90.13±6.95	61.27–108.99	<0.001*
AD	25.14±3.96	16.80–37.49	23.28±3.15	15.79–32.48	<0.001*
CR	91.99±7.96	71.04–119.97	91.53±8.10	72.13–124.31	0.629
ADWI	2.68±0.41	1.86–3.77	2.62±0.38	2.01–3.90	0.203
Left					
FHD	46.82±3.48	28.95–53.49	42.78±3.05	30.21–52.40	<0.001*
FHL	30.83±3.79	22.17–41.47	29.19±3.34	20.08–39.79	<0.001*
FND	30.92±3.46	21.11–48.97	28.55±3.21	20.99–45.33	<0.001*
FNL	27.98±4.62	16.91–44.13	25.35±4.16	12.59–34.62	<0.001*
ITL	78.41±5.56	59.81–92.60	68.68±4.84	58.08–85.02	<0.001*
FAL	88.02±9.27	63.78–109.45	82.57±6.82	60.13–102.32	<0.001*
HAL	95.16±9.74	68.28–118.75	89.34±7.25	62.95–111.10	<0.001*
AD	24.61±3.83	14.76–35.05	22.83±3.26	14.31–34.59	<0.001*
CR	91.66±8.33	69.05–121.92	91.27±8.28	70.49–121.27	0.787
ADWI	2.74±0.44	1.03–4.37	2.68±0.41	1.84–4.29	0.146

*Significant difference. SD: Standard deviation, FAL: Femoral axis length, HAL: Hip axis length, ITL: Intertrochanteric length, FNL: Femoral neck length, FND: Femoral neck diameter, FHL: Femoral head length, FHD: Femoral head diameter, ADWI: Acetabular depth width index, CR: Coverage ratio, AD: Acetabular depth

Table 2: Comparison of average values of angle measurements by sex

Measurement	Male		Female		*P*
	Mean±SD (°)	Minimum–maximum	Mean±SD (°)	Minimum–maximum	
Right					
IA	133.74±5.22	121.46–152.75	131.86±5.22	119.31–146.63	<0.001*
AA	53.87±7.32	33.77–73.69	54.90±7.77	31.24–70.0	0.069
LCEA	45.24±7.34	25.88–67.87	43.47±7.63	20.40–65.79	0.012*
ACEA	62.09±7.17	40.21–82.32	61.96±7.10	42.08–82.14	0.928
PCEA	115.06±17.90	11.74–157.21	119.00±15.17	83.76–148.76	0.014*
SA	36.99±4.24	24.58–50.17	39.01±4.41	24.92–50.40	<0.001*
AAA	26.45±9.11	8.61–49.65	28.58±8.08	10.71–47.68	0.01*
AABDA	51.69±4.25	37.52–65.00	49.76±4.20	39.13–64.09	<0.001*
Left					
IA	132.09±4.74	120.14–146.19	130.54±4.84	116.85–146.85	0.001*
AA	54.06±7.34	36.28–73.49	55.89±8.06	25.41–83.32	0.004*
LCEA	41.35±8.44	22.69–97.81	39.86±8.20	23.33–63.20	0.072
ACEA	63.25±7.28	47.84–85.41	62.32±6.83	48.32–93.48	0.171
PCEA	113.15±15.31	81.25–151.0	117.14±15.98	67.22–156.03	0.003*
SA	38.58±3.88	22.45–51.19	40.44±4.11	29.04–52.02	<0.001*
AAA	24.96±8.50	7.11–46.39	27.82±8.71	5.52–53.64	<0.001*
AABDA	50.84±4.05	38.87–68.18	49.22±4.20	37.95–60.79	<0.001*

*Significant difference. SD: Standard deviation, IA: Inclination angle, AAA: Acetabular anteversion angle, AABDA: Acetabular abduction angle, LCEA: Lateral center edge angle, ACEA: Anterior center edge angle, PCEA: Posterior center edge angle, SA: Sharp angle, AA: Alsberg angle

no significant difference in other measurements except AA, FHD, ITL, femoral axis line, femoral head CR while there was a difference between the sides in other measurements [Table 7].

Discussion

Knowing the morphometric properties of the bones that make up the skeleton is important for many fields such as anatomy, orthopedics, forensic medicine, anthropology, ergonomics, and bioengineering. Studies were conducted on healthy subjects in order to obtain standard data in different races.[17,19] Direct radiography, CT, and dual energy X-ray absorptiometry (DEXA) imaging methods were used in the studies.[3,20,21]

Chantarapanich *et al*.[18] made morphometric measurements of the proximal femur on CT images of 40 Thai men, 80 Thai women. The mean age of the people 47.85 ± 11.2 years. They measured FHD 46.84 ± 2.21 mm in men, 41.27 ± 2.24 mm in women; FND 30.87 ± 2.18 mm in men, 26.38 ± 1.93 in women. FHD and FND are similar to our study. In addition, FNL was measured 47.31 ± 3.81 mm in men, 43.71 ± 3.43 mm in women. FNL is greater than our study. We think that this difference is due to the difference in measurement points. Because they measured from the center of femoral head to the femoral neck isthmus. Lee *et al*.[22] measured the FHD by removing it during hip arthroplasty surgery. The mean age of the people in the study is 75.2 ± 9.4 and they are Malay, Chinese, Indian. FHD was measured 48.0 ± 2.7 mm in Chinese men, 44.0 ± 2.4 mm in Chinese women; 47.4 ± 3.1 mm in Malay men, 43.0 ± 2.0 in Malay women; 47.0 ± 2.7 in Indian men, 42.8 ± 2.6 in Indian women. The mean values are similar to our study. Karasik *et al*.[23] in their study in the USA defined the FNL as the distance between the center of the caput femoris and the anatomical axis of the femur. They measured on the DEXA images the FNL 54 ± 8 mm in men, 46 ± 7 mm in women. Their average values are greater than our values. This is because the measurement starts from the femoral head. In the same study, ITL was measured 59 ± 5 mm in men, 52 ± 4 mm in women. This value is smaller than our study. FND was measured 33 ± 3 mm in men, 30 ± 2 mm in women. This value is greater than our study.

Theobald *et al*.[24] in their study with 21 Nigerian women, 21 Afro-American women, and 21 Caucasian women, the FAL was 99.3 ± 4.7 mm in Nigerians, 110.8 ± 6.3 mm in African Americans, and 111 mm in Caucasians. The average values of

Table 3: Average, minimum and maximum values of length, depth and diameter measurements

Measurement	20–29 age		30–39 age		40–49 age		50–59 age	
	Mean±SD (mm)	Minimum–maximum	Mean±SD (mm)	Minimum–maximum	Mean±SD (mm)	Minimum–maximum	Mean±SD (mm)	Minimum–maximum
Right								
FHD	43.83±3.65	34.88–51.33	45.17±3.16	37.74–52.72	45.35±3.43	38.08–52.68	45.75±3.36	38.05–53.6
FHL	29.24±3.21	21.40–38.86	30.16±3.48	22.60–49.46	29.48±4.41	20.64–47.47	29.12±3.37	21.04–38.85
FND	27.84±3.63	21.63–48.2	29.3±2.79	18.61–36.85	29.3±3.40	21.13–37.47	29.55±3.41	21.13–37.18
FNL	27.2±4.48	16.25–37.28	27.09±5.07	15.78–43.3	26.62±4.46	16.91–37.68	27.72±4.51	10.42–41.56
ITL	71.86±7.29	58.02–87.23	74.13±6.91	58.39–91.87	74.79±7.27	53.58–91.58	75.09±8.39	56.88–98.56
FAL	85.26±7.85	67.59–114.82	86.43±7.94	66.60–108.38	85.33±9.008	55.10–105.91	86.68±8.52	65.30–107.27
HAL	92.22±8.38	72.45–120.51	93.95±8.13	75.62–114.98	92.39±9.64	61.27–114.8	94.19±9.14	71.72–118.02
AD	23.8±3.25	16.80–30.75	24.09±3.20	17.64–31.71	24.11±3.90	55.79–34.67	24.99±4.26	15.95–37.49
CR	89.02±6.84	74.35–109.4	92.05±8.10	75.03–116.18	92.27±7.77	71.04–119.97	93.57±8.53	72.13–124.31
ADWI	2.61±0.38	2.04–3.71	2.66±0.37	2.03–3.67	2.68±0.39	1.86–3.9	2.65±0.45	1.87–3.77
Left								
FHD	43.83±3.70	32.88–51.93	44.73±3.35	28.95–52.1	44.98±4.38	30.21–52.53	45.9±3.68	39.30–53.49
FHL	30.03±3.82	21.10–40.54	30.62±2.91	23.40–37.43	29.94±4.19	21.03–41.47	29.58±3.58	20.08–37.99
FND	28.67±3.49	20.99–44.14	29.83±2.71	21.11–37.48	29.98±3.85	22.45–45.33	30.54±3.83	22.91–48.97
FNL	26.16±4.61	13.82–37.17	26.98±4.87	12.59–40.16	26.15±4.05	17.21–37.57	27.58±4.61	15.15–44.13
ITL	71.71±6.66	59.37–90.42	73.48±6.33	58.20–86.19	74.9±6.99	58.08–88.9	74.82±8.04	58.91–92.6
FAL	84.39±8.33	60.13–106	86.26±8.01	67.39–109.45	84.46±9.08	61.35–105.17	86.57±9.0	65.14–108.55
HAL	91.01±8.86	62.95–112.11	93.41±8.40	72.76–113.8	91.32±9.44	67.67–114.31	93.76±9.56	71.58–118.75
AD	23.62±3.61	14.76–32.44	23.52±3.45	15.9–35.86	23.3±3.76	14.31–34.59	24.52±3.75	16.60–35.05
CR	88.73±6.92	69.05–109.08	91.5±8.62	71.83–116.3	91.87±8.11	75.28–121.92	93.6±8.62	69.89–121.27
ADWI	2.67±0.48	1.99–4.37	2.75±0.39	1.84–3.69	2.8±0.43	2.06–4.29	2.65±0.40	1.03–3.5

SD: Standard deviation, FAL: Femoral axis length, HAL: Hip axis length, ITL: Intertrochanteric length, FNL: Femoral neck length, FND: Femoral neck diameter, FHL: Femoral head length, FHD: Femoral head diameter, ADWI: Acetabular depth width index, CR: Coverage ratio, AD: Acetabular depth

Table 4: Comparison of length, diameter and depth measurements between age groups

Measurement	20–29; 30–39	20–29; 40–49	20–29; 50–59	30–39; 40–49	30–39; 50–59	40–49; 50–59
Right						
FHD	0.013	0.008*	0.001*	0.777	0.245	0.405
FHL	0.054	0.945	0.731	0.094	0.026	0.875
FND	<0.001*	0.002*	0.001*	0.543	0.514	0.309
FNL	1	1	1	1	1	0.545
ITL	0.193	0.037	0.014	1	1	1
FAL	0.285	0.898	0.242	0.397	0.829	0296
HAL	0.14	0.912	0.127	0.225	0.962	0.196
AD	1	1	0.136	1	0.498	0.545
CR	0.012	0.001*	<0.001*	0.395	0.064	0.238
ADWI	0.225	0.163	0.61	0.747	0.546	0.471
Left						
FHD	0.07	0.032	<0.001*	0.513	0.045	0.226
FHL	0.094	0.996	0.64	0.165	0.028	0.624
FND	0.002*	0.016	<0.001*	0.887	0.328	0.302
FNL	1	1	0.164	1	1	0.163
ITL	0.036	0.001*	0.005*	0.172	0.299	0.837
FAL	0.74	1	0.427	0.845	1	0.497
HAL	0.115	0.882	0.062	0.08	0.751	0.058
AD	1	1	0.469	1	0.294	0.107
CR	0.012	0.007*	<0.001*	0.813	0.074	0.108
ADWI	0.054	0.018	0.688	0.543	0.102	0.133

*Significant difference. FAL: Femoral axis length, HAL: Hip axis length, ITL: Intertrochanteric length, FNL: Femoral neck length, FND: Femoral neck diameter, FHL: Femoral head length, FHD: Femoral head diameter, ADWI: Acetabular depth width index, CR: Coverage ratio, AD: Acetabular depth

all three races are greater than ours. In the same study, HAL was measured as 113.3 ± 5.0 mm in Nigerians, 127.2 ± 8.2 mm in African Americans, and 129.3 ± 10.4 mm in Caucasians. The average values of all three races are greater than ours.

Paul *et al*.[25] calculated the same index as the distance of a vertical line drawn from the center of the acetabulum to the line connecting the lateral edge of the acetabulum multiplied by 1000. ADWI was calculated 341.03 ± 29.6 on the right side and 341.9 ± 25.1 on the left side. This may be due to the calculation method and average age. CR is classically used to evaluate femoral head coverage.[25] Lavy *et al*.[20] in their study based on direct radiographs of 58 men and 41 women, CR was calculated as 85.5 ± 5.1 for men and 84.8 ± 5.0 for women. There was no statistically significant difference between the two sexes. Ma *et al*.[17] calculated CR 87.1 ± 5.4 on the right side and 87.5 ± 4.8 on the left side for men, while it was 86.6 ± 5.2 on the right side and 88.0 ± 7.3 on the left side for women. There was no significant difference between sexes. The mean data in both studies is smaller than the mean data in our study. In our study and other studies, there is no statistically significant difference between sexes in terms of CR.

Ma *et al*.[17] made a study in China on CT images. The mean age of the female was 61.6 years and male was 51.7 years in this study. They measured IA, AAA, AABDA, LCEA, ACEA, PCEA. Their mean values of IA, AAA, LCEA, ACEA, and PCEA are smaller than our

Table 5: Average, minimum and maximum values of angle measurements

Measurement	20–29 age		30–39 age		40–49 age		50–59 age	
	Mean±SD (mm)	Minimum–maximum	Mean±SD (mm)	Minimum–maximum	Mean±SD (mm)	Minimum–maximum	Mean±SD (mm)	Minimum–maximum
Right								
IA	133.77±5.21	120.83–147.21	132.49±4.61	120.63–143.50	133.06±5.25	119.31–147.75	132.24±5.98	121.23–152.75
AA	56.32±6.93	41.43–73.69	53.30±7.41	31.24–69.28	53.87±6.71	33.77–67.78	53.78±8.75	31.98–71.99
LCEA	42.74±6.56	27.16–60.21	44.62±7.29	26.49–67.87	44.22±7.28	25.88–64.63	45.85±8.47	20.4–67.04
ACEA	63.21±7.24	41.12–82.32	61.18±6.39	42.08–76.43	61.65±7.55	46.94–80.8	61.84±7.36	40.21–79.64
PCEA	118.75±18.82	11.74–144.54	116.94±14.96	83.76–145.97	117.14±15.44	85.18–152.35	115.08±17.50	75.34–157.21
SA	39.53±4.00	29.20–47.94	38.19±4.12	26.31–50.17	37.74±4.02	29.48–49.10	36.43±4.91	24.58–50.40
AAA	28.44±8.22	8.61–46.96	27.86±7.90	10.71–47.68	27.41±8.62	10.60–46.46	26.27±9.83	10.31–49.65
AABDA	49.41±3.85	40.64–58.57	50.38±4.06	37.52–61.02	51.04±4.19	40.95–59.18	52.13±4.68	39.13–65.00
Left								
IA	131.64±4.60	119.48–141.97	131.42±4.83	119.55–146.85	131.78±4.19	124.07–145.69	130.65±5.69	116.82–146.19
AA	56.52±6.63	36.28–71.93	54.27±7.76	35.61–73.64	55.67±7.48	43.19–83.32	53.34±8.59	25.41–72.91
LCEA	38.84±7.21	25.64–56.05	40.67±9.18	23.33–97.81	40.68±8.32	24.35–62.93	42.27±8.22	22.69–63.35
ACEA	63.57±7.11	47.84–85.41	62.35±7.42	49.09–93.48	61.84±6.90	48.32–79.88	63.29±6.80	49.11–80.77
PCEA	119.26±16.26	82.67–146.21	114.49±15.58	84.30–156.03	113.30±15.46	81.28–151.33	112.83±15.50	67.22–151.0
SA	40.94±3.66	31.35–49.39	39.91±3.68	28.62–48.10	39.63±3.78	28.94–47.84	37.52±4.40	22.45–52.02
AAA	28.19±8.52	9.52–44.41	26.21±9.09	7.11–53.64	26.07±8.66	5.52–51.51	24.77±8.46	9.45–46.39
AABDA	48.68±3.66	40.73–58.92	49.44±3.89	38.87–62.44	49.96±3.88	41.70–61.20	52.10±4.50	37.95–68.18

SD: Standard deviation, IA: Inclination angle, AAA: Acetabular anteversion angle, AABDA: Acetabular abduction angle, LCEA: Lateral center edge angle, ACEA: Anterior center edge angle, PCEA: Posterior center edge angle, SA: Sharp angle, AA: Alsberg angle

Table 6: Comparison of angle measurements between age groups

Measurement	20–29; 30–39	20–29; 40–49	20–29; 50–59	30–39; 40–49	30–39; 50–59	40–49; 50–59
Right						
IA	0.521	1	0.233	1	1	1
AA	0.004*	0.012	0.027	0.482	0.793	0.603
LCEA	0.044	0.108	0.01	0.658	0.593	0.276
ACEA	0.264	0.758	1	1	1	1
PCEA	0.162	0.184	0.054	0.965	0.296	0.316
SA	0.016	0.003*	<0.001*	0.536	0.017	0.054
AAA	0.458	0.331	0.055	0.694	0.132	0.32
AABDA	0.588	0.04	<0.001*	1	0.02	0.412
Left						
IA	1	1	0.891	1	0.603	0.603
AA	0.016	0.188	0.015	0.276	0.798	0.249
LCEA	0.204	0.135	0.004*	0.69	0.096	0.234
ACEA	0.189	0.077	0.818	0.622	0.235	0.099
PCEA	0.03	0.001*	0.005*	0.681	0.508	0.756
SA	0.039	0.011	<0.001*	0.627	<0.001*	<0.001*
AAA	0.095	0.069	0.003*	0.904	0.195	0.272
AABDA	0.144	0.012	<0.001*	0.299	<0.001*	<0.001*

*Significant difference. IA: Inclination angle, AAA: Acetabular anteversion angle, AABDA: Acetabular abduction angle, LCEA: Lateral center edge angle, ACEA: Anterior center edge angle, PCEA: Posterior center edge angle, SA: Sharp angle, AA: Alsberg angle

Table 7: Comparison of right and left side of data

Measurement	Right	Left	Paired two sample *t*-test	*P*
IA	132.88±5.30	131.37±4.87	5.773	<0.001*
AA	54.31±7.58	54.92±7.74	−1.692	0.091
LCEA	44.37±7.50	40.63±8.33	9.996	<0.001*
ACEA	61.97±7.16	62.77±7.07	−2.493	0.013*
PCEA	116.96±16.75	114.96±15.85	2.759	0.006*
SA	37.96±4.41	39.48±4.08	−6.693	<0.001*
AAA	27.48±8.69	26.30±8.74	3.105	0.002*
AABDA	50.75±4.32	50.06±4.19	2.922	0.004*
FHD	45.03±3.47	44.87±3.85	1.435	0.152
FHL	29.50±3.65	30.04±3.65	−3.929	<0.001*
FND	28.99±3.37	29.76±3.55	−5.250	<0.001*
FNL	27.16±4.64	26.73±4.57	2.592	0.010*
ITL	73.98±7.57	73.73±7.13	1.599	0.111
FAL	85.94±8.35	85.44±8.64	1.821	0.069
HAL	93.20±8.85	92.40±9.12	2.923	0.004*
AD	24.26±3.70	23.75±3.66	2.955	0.003*
CR	91.74±7.99	91.45±8.26	0.954	0.341
ADWI	2.65±0.40	2.71±0.43	−3.191	0.002*

*Significant difference. IA: Inclination angle, AAA: Acetabular anteversion angle, AABDA: Acetabular abduction angle, LCEA: Lateral center edge angle, ACEA: Anterior center edge angle, PCEA: Posterior center edge angle, SA: Sharp angle, AA: Alsberg angle, CR: Coverage ratio, AD: Acetabular depth, FAL: Femoral axis length, HAL: Hip axis length, ITL: Intertrochanteric length, FNL: Femoral neck length, FND: Femoral neck diameter, FHL: Femoral head length, FHD: Femoral head diameter, ADWI: Acetabular depth width index

values. The mean values of AABDA are similar to ours. Ma *et al*. measured ACEA and PCEA on transaxial plane but we measured on coronal plane. Fischer *et al*.[26] made a study in Germany, using magnetic resonance imaging images. The mean age of the male was 53 years and female was 52 years in this study. Their mean values are smaller than ours. In Ahmad *et al*.[27] study in Egyptian people on CT; the mean age of 40.9 ± 12.55 years. Their mean value of IA is smaller than our mean values [Table 8].

The lateral center edge angle is a frequently used parameter in the evaluation of acetabular dysplasia.[25] The mean age of 63.8 ± 17.2 years in this study. They measured LCEA, AAA was measured regardless of right or left side. Their LCEA and AAA mean values are smaller than in our study. In a study by Aydin *et al*.,[28] the mean age was 39.6 years. They measured LCEA on direct radiography images on Turkish people. LCEA the average values reported are smaller than our values. Lavy *et al*.[20] measured the LCEA and SA on direct radiographs of 58 men and 41 women. The LCEA mean values measured by Lavy *et al*.[20] are smaller than our mean values and their SA mean values are similar to ours. Aydin *et al*.[28] defined the SA defined by Sharp[29] as the acetabular index. The mean values measured by Aydin *et al*.[28] are similar to our mean values. Imai *et al*.[21] in their study on 84 Japanese women mean aged 35.0 ± 9.2 years. They measured ACEA and PCEA. Their mean values are smaller than our mean values. Miyasaka *et al*.[30] conducted on CT images of 57 male and 63 female, they measured ACEA and PCEA. Their mean values of ACEA similar to our study but their mean values of PCEA smaller than our study [Table 8].

Conclusion

In the present study, we determined the normal range of the values of the various measurements of the proximal femur. In all length, depth and diameter measurements, the average values were measured to be statistically significantly higher in men than in women. While the mean values of IA and AABDA were measured to be significantly higher in men than in women on both sides; PCEA, SA, and AAA were measured to be significantly larger in women than in men on both sides. When the right and left sides of all people are compared, IA, LCEA, ACEA, PCEA, SA, AAA, AABDA, FHL, FND, FNL, hip significant differences were found between sides in axis length and AD measurements. When comparison was made between age groups, it was found that the FHD, FND and CR increased significantly as age increased on both sides. The detailed knowledge of the morphometric data of the proximal femur will help the especially ortopedics during reconstructive surgery and provide necessary information for the prosthesis designer for designing the prosthesis more appropriately suited for Turkish

Table 8: Comparison of the angle measurements in different studies

Studies	Side	IA		SA		AAA		AABDA		LCEA		ACEA		PCEA	
		Male	Female	Male	Female	Male	Female	Male	Female	Male	Female	Male	Female	Male	Female
Lavy *et al.*, 2003[20]				36.9±4.0	38.6±4.9					34.0±7.5	34.3±7.5				
Ma *et al.*, 2014[17]	Right	126.0±63.8	126.2±63.8			20.36±5.8	21.16±6.0	52.16±4.8	51.36±3.8	38.06±8.9	35.16±6.1	30.36±8.3	30.06±8.5	11.76±6.7	10.66±7.1
	Left	127.6±63.8	126.7±63.6			20.46±5.5	21.66±5.6	51.363±0.7	50.46±3.9	37.06±5.7	34.66±6.6	30.16±7.1	31.26±8.5	11.56±6.3	11.76±5.9
Aydin *et al.*, 2016[28]	Right			36.46±5.20	39.23±5.02					36.65±6.90	32.83±7.54				
	Left			36.84±4.66	39.22±4.70					36.16±6.44	34.21±7.06				
Miyasaka *et al.*, 2017[29]												58.2±8.2	56.0±10.1	97.1±16.2	102.9±13.5
Imai *et al.*, 2019[21]												40.6±9.5°		99.8±18.4	
Fischer *et al.*, 2020[26]	Right	127.7±7.1	127.9±7.1												
	Left	125.3±7.7	126.8±7.1												
Paul *et al.*, 2020[25]						17.2±2.7	17.7±2.6			33.6±4.07	33.3±5.5				
Ahmad *et al.*, 2023[27]		129.65±4.13°	129.28±3.71												
Present study, 2024	Right	133.74±5.22	131.86±5.22	36.99±4.24	39.01±4.41	26.45±9.11	28.58±8.08	51.69±4.25	49.76±4.20	45.24±7.34	43.47±7.63	62.09±7.17	61.96±7.10	115.06±17.90	119.00±15.17
	Left	132.09±4.74	130.54±4.84	38.58±3.88	40.44±4.11	24.96±8.50	27.82±8.71	50.84±4.05	49.22±4.20	41.35±8.44	39.86±8.20	63.25±7.28	62.32±6.83	113.15±15.31	117.14±15.98

IA: Inclination angle, AAA: Acetabular anteversion angle, AABDA: Acetabular abduction angle, LCEA: Lateral center edge angle, ACEA: Anterior center edge angle, PCEA: Posterior center edge angle, SA: Sharp angle

population. In addition, we think that it will contribute to national and international studies in areas such as anatomy, biomechanics, and ergonomics.

Financial support and sponsorship

Nil.

Conflicts of interest

There are no conflicts of interest.

References

1. Steyn M, Işcan MY. Sex determination from the femur and tibia in South African whites. Forensic Sci Int 1997;90:111-9.
2. Bergot C, Bousson V, Meunier A, Laval-Jeantet M, Laredo JD. Hip fracture risk and proximal femur geometry from DXA scans. Osteoporos Int 2002;13:542-50.
3. Travison TG, Beck TJ, Esche GR, Araujo AB, McKinlay JB. Age trends in proximal femur geometry in men: Variation by race and ethnicity. Osteoporos Int 2008;19:277-87.
4. Nicholls AS, Kiran A, Pollard TC, Hart DJ, Arden CP, Spector T, *et al.* The association between hip morphology parameters and nineteen-year risk of end-stage osteoarthritis of the hip: A nested case-control study. Arthritis Rheum 2011;63:3392-400.
5. Noble PC, Alexander JW, Lindahl LJ, Yew DT, Granberry WM, Tullos HS. The anatomic basis of femoral component design. Clin Orthop Relat Res 1988;235:148-65.
6. Chiron P, Espié A, Reina N, Cavaignac E, Molinier F, Laffosse JM. Surgery for femoroacetabular impingement using a minimally invasive anterolateral approach: Analysis of 118 cases at 2.2-year follow-up. Orthop Traumatol Surg Res 2012;98:30-8.
7. Beck M, Kalhor M, Leunig M, Ganz R. Hip morphology influences the pattern of damage to the acetabular cartilage: Femoroacetabular impingement as a cause of early osteoarthritis of the hip. J Bone Joint Surg Br 2005;87:1012-8.
8. Stulberg S, Cordell L, Harris W. Unrecognized childhood hip disease: A major cause of idiopathic osteoarthritis of the hip. In: Proceedings of the Third Open Scientific Meeting of the Hip Society. St. Louis: Cv Mosby; 1975. p. 212-28.
9. Derin Cicek E, Cevik H. Analysis of morphological parameters in pelvic radiography and hip MRI: A practical reporting recommendation. Acta Orthop Belg 2021;87:275-83.
10. Hack K, Di Primio G, Rakhra K, Beaulé PE. Prevalence of cam-type femoroacetabular impingement morphology in asymptomatic volunteers. J Bone Joint Surg Am 2010;92:2436-44.
11. Murphy SB, Ganz R, Müller ME. The prognosis in untreated dysplasia of the hip. A study of radiographic factors that predict the outcome. J Bone Joint Surg Am 1995;77:985-9.
12. Reijman M, Hazes JM, Pols HA, Koes BW, Bierma-Zeinstra SM. Acetabular dysplasia predicts incident osteoarthritis of the hip: The Rotterdam study. Arthritis Rheum 2005;52:787-93.
13. Murphy SB, Kijewski PK, Millis MB, Harless A. Acetabular dysplasia in the adolescent and young adult. Clin Orthop Relat Res 1990;261:214-23.
14. Makdoomi MA, Khan JA, Mohammad BG, Bhat SA, Hamid S. Study of neck-shaft angle in plain radiographs of adult Kashmiri population. J Anat Soc India 2023;72:343-8.
15. Dinçel VE, Sengelen M, Sepici V, Cavuşoğlu T, Sepici B. The association of proximal femur geometry with hip fracture risk. Clin Anat 2008;21:575-80.
16. Mikhail MB, Vaswani AN, Aloia JF. Racial differences in femoral dimensions and their relation to hip fracture. Osteoporos Int 1996;6:22-4.
17. Ma H, Han Y, Yang Q, Gong Y, Hao S, Li Y, *et al.* Three-dimensional computed tomography reconstruction measurements of acetabulum in Chinese adults. Anat Rec (Hoboken) 2014;297:643-9.
18. Chantarapanich N, Rojanasthien S, Chernchujit B, Mahaisavariya B, Karunratanakul K, Chalermkarnnon P, *et al.* 3D CAD/reverse engineering technique for assessment of Thai morphology: Proximal femur and acetabulum. J Orthop Sci 2017;22:703-9.
19. Mall G, Graw M, Gehring K, Hubig M. Determination of sex from femora. Forensic Sci Int 2000;113:315-21.
20. Lavy CB, Msamati BC, Igbigbi PS. Racial and gender variations in adult hip morphology. Int Orthop 2003;27:331-3.
21. Imai N, Suzuki H, Nozaki A, Hirano Y, Endo N. Correlation of tilt of the anterior pelvic plane angle with anatomical pelvic tilt and morphological configuration of the acetabulum in patients with developmental dysplasia of the hip: A cross-sectional study. J Orthop Surg Res 2019;14:323.
22. Lee CK, Kwan MK, Merican AM, Ng WM, Saw LB, Teh KK, *et al.* Femoral head diameter in the Malaysian population. Singapore Med J 2014;55:436-8.
23. Karasik D, Dupuis J, Cupples LA, Beck TJ, Mahaney MC, Havill LM, *et al.* Bivariate linkage study of proximal hip geometry and body size indices: The Framingham study. Calcif Tissue Int 2007;81:162-73.
24. Theobald TM, Cauley JA, Gluer CC, Bunker CH, Ukoli FA, Genant HK. Black-white differences in hip geometry. Study of Osteoporotic Fractures Research Group. Osteoporos Int 1998;8:61-7.
25. Paul S, Singh S, Raja BS, Mishra D, Kalia RB. CT based analysis of acetabular morphology in Northern Indian population: A retrospective study. Indian J Orthop 2020;55:606-13.
26. Fischer CS, Kühn JP, Völzke H, Ittermann T, Gümbel D, Kasch R, *et al.* The neck-shaft angle: An update on reference values and associated factors. Acta Orthop 2020;91:53-7.
27. Ahmad MI, Bushra MT, Galal AT, Ouies SM. Computed tomography reference values estimation for femoral neck shaft angle in Egyptian healthy adults of both sexes. Egypt J Radiol Nuc M 2023;54:96.
28. Aydin M, Kircil C, Polat O, Arikan M, Erdemli B. Adult acetabulo – Pelvic parameters in Turkish society: A descriptive radiological study. Acta Orthop Traumatol Turc 2016;50:623-7.
29. Sharp IK. Acetabular dysplasia: The acetabular angle. J Bone Joint Surg Br 1961;43:268-72.
30. Miyasaka D, Sakai Y, Ibuchi S, Suzuki H, Imai N, Endo N. Sex- and age-specific differences in femoral head coverage and acetabular morphology among healthy subjects-derivation of normal ranges and thresholds for abnormality. Skeletal Radiol 2017;46:523-31.

Original Article

Morphology of the Lunate Fossa on the Left Atrial Surface of the Interatrial Septum and its Clinical Significance

Subhash Joshi, Sharda Joshi, Harsh Chawre, Nilesh V. Joshi[1]

Department of Anatomy, Sri Aurobindo Medical College and Post Graduate Institute, Indore, Madhya Pradesh, [1]Department of Periodontology, Bharati Vidyapeeth (Deemed to be) University Dental College and Hospital, Navi Mumbai, Maharashtra, India

Abstract

Introduction: During the routine dissection of the hearts, in some hearts, the left surface of the interatrial septum showed the presence of strands traversing the lunate fossa extending from the semilunar fold and dividing the space of the lunate fossa. **Aims:** The presence of strands in the lunate fossa prompted us to undertake a detailed study of this region. This knowledge being significant in imaging of atrial septal defects (ASDs) and the transseptal catheterization procedures. **Materials and Methods:** Fifty adult hearts were utilized for the present study. After opening of the atrial chambers, the left surface of the interatrial septum was examined in details. The Common symbols used to mark various features on left atrial surface of interatrial septum are, Blue Star indicates- Fossa Ovalis, Red Star indicates: Lunate Fossa. Yellow Arrows indicates: Semi Lunar Fold, Black Arrows Indicates: Openings of Venae Cordis Minimi, Double Headed Red Arrow Indicates: Overlap by Septum Secundum. **Results:** The strands were seen in 12 hearts; the average vertical height of the lunate fossa was 7.87 mm and transverse diameter was 7.38 mm. The shape of the semilunar fold was seen to be semilunar and U, V, W, or J shaped. Probe patency of the foramen ovale was found in 16% of hearts. **Conclusion:** The detailed morphology of the lunate fossa and the semilunar fold assumes great significance considering the newer imaging technologies of visualization of ASDs and also the methods of transseptal catheterization in the repair of these defects.

Keywords: *Interatrial septum, lunate fossa, ostium secundum, semilunar fold, septum primum, septum secundum*

Introduction

During the development of the interatrial septum, the formation of the ostium secundum has been vividly described by the process of coalescence of the perforations, which are produced by apoptosis in the cranial part of the septum primum, to allow for the flow of blood from the right to the left atrium. The septum secundum, which is placed to the right of the septum primum, grows caudally to overlap the lower edge of the ostium secundum, thereby producing an oblique cleft of communication between the two atria known as foramen ovale. The right surface of the interatrial septum shows the fossa ovalis and limbus fossa ovalis. The left surface of the interatrial septum has the presence of semilunar fold and above that the lunate fossa. These features of the left surface of the interatrial septum are distinctly seen as a normal finding. The number of cardiac patients who undergo interventional transseptal approach has increased over the past few years, hence the importance of the detailed study of the lunate fossa.

In few hearts, we had observed that this lunate fossa was traversed by strands of the septum primum extending from the semilunar fold cranially to the roof of the atrial wall. This is a feature which has not been shown or described in the literature reviewed, and this prompted us to undertake a detailed study of the lunate fossa.

Materials and Methods

The institutional ethical committee's clearance was obtained before undertaking the present study.

This study was carried out on 50 adult hearts available in the department. The cavities of the right and left atria were opened to visualize the two surfaces of the interatrial septum. The main emphasis was on its left atrial surface. The lunate fossa

How to cite this article: Joshi S, Joshi S, Chawre H, Joshi NV. Morphology of the lunate fossa on the left atrial surface of the interatrial septum and its clinical significance. J Anat Soc India 2025;74:36-40.

Article Info

Received: 28 December 2024
Accepted: 15 February 2025
Available online: 31 March 2025

Address for correspondence:
Dr. Nilesh V. Joshi, Department of Periodontology, Bharati Vidyapeeth (Deemed to be) University Dental College and Hospital, Navi Mumbai - 400 614, Maharashtra, India.
E-mail: nileshjoe@gmail.com

Access this article online

Website: https://journals.lww.com/joai

DOI: 10.4103/jasi.jasi_204_24

Quick Response Code:

and semilunar fold were recognized, and various features like the shape, size, presence of strands, and openings of venae cordis minimi were noted and photographed. The presence of probe patency of the foramen ovale, where present, was confirmed by introducing a probe between the two atria through the oblique passage. The size of the lunate fossa and overlapping of the caudal margin of the septum secundum beyond the ostium secundum was also measured with the help of a digital Vernier caliper. Various features were noted and photographed.

Results

The observations and findings of the present study were as follows:

1. The average vertical height of the lunate fossa was 7.87 mm (maximum: 13.88 mm and minimum: 3.68 mm); and the average transverse diameter was 7.38 mm (maximum: 16.85 mm and minimum: 1.85 mm) [Figure 1]
2. When the interatrial septum was viewed from the left against the light, it clearly showed the difference in the thickness of the two septa. The septum primum in the region of the fossa ovalis was thin and translucent [Figure 2]
3. The region of overlap of the caudal margin of the septum secundum over the caudal margin of the ostium secundum was seen [Figure 3a and b], which was varying from minimum 1.64 mm to maximum 12.74 mm (average = 4.25 mm)
4. It was observed that in 12 hearts, there were strands of the septum primum, varying in number and dimensions, extending from the semilunar fold and dividing the region of the ostium secundum into a number of foramina of variable sizes and shapes [Figures 3b, 4, and 5a]
5. Some of these strands were wide and were seen to be branching [Figure 5b]
6. The shape of the semilunar fold was found to be U shaped [Figure 2] in 6 (12%) hearts; V shaped [Figure 3a] in 6 (12%) hearts; semilunar [Figure 6b] in 20 (40%) hearts; W shaped [Figure 6a] in 8 (16%) hearts; and J shaped [Figure 7] in 10 (20%) hearts
7. Varying number of openings of the venae cordis minimi were seen in the septum secundum [Figure 6a] and cranial part of attachment of the septum secundum to the left atrial wall [Figure 6b] opening into the left atrial chamber in 7 (14%) hearts
8. In 8 (16%) hearts, a probe patency of the foramen ovale could be distinctly observed and a probe could be inserted between the two atria [Figure 8a and b]
9. In one heart, multiple perforations were observed in the septum secundum above the lunate fold [Figure 9].

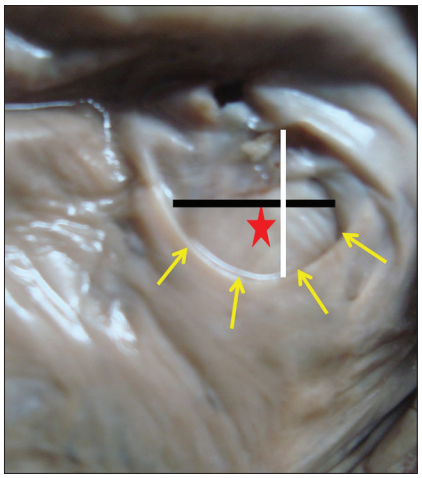

Figure 1: Semilunar fold is semilunar in shape

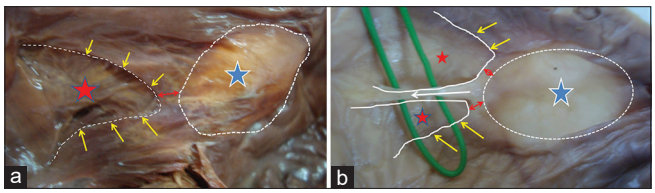

Figure 3: (a) Semilunar fold is V shaped. (b) Semilunar fold is W shaped and Single strand (white arrow) traversing lunate fossa and dividing it in two parts of left atrium

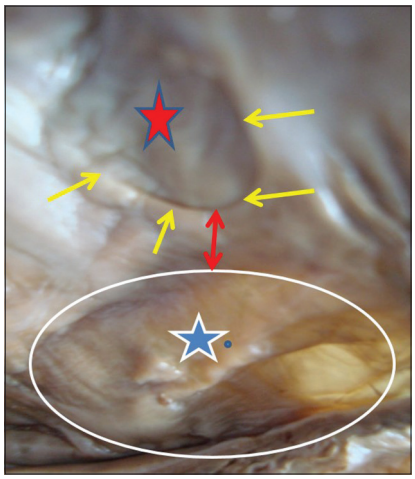

Figure 2: Semilunar fold is U shaped and Overlap by Septum Secundum is indicated by double headed red arrow

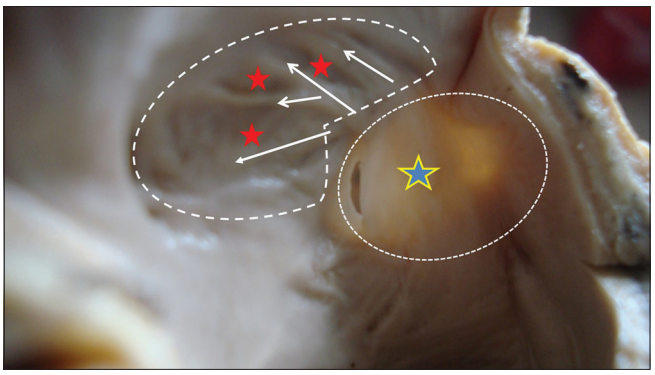

Figure 4: Multiple strands (white arrows) dividing lunate fossa into small areas

Discussion

Sadler[1] stated that the anomalies of the heart constitute approximately 1% of cases in liveborn infants. Singh[2] stated that the atrial septal defect (ASD) accounts for an incidence of 6.4/10,000 births with a 2: 1 prevalence in female-to-male infants and that one of the most significant defects is the ostium secundum defect. Shizukuda[3] described that the number of cardiac patients who underwent interventional transseptal approach has risen substantially over the past few years. This further emphasizes the importance of understanding the anatomy and anomalies of the lunate fossa in the left atrium.

Septum primum begins to develop at 28 days. It is thin, crescentric fold of the endocardium.[4] The ostium primum is sealed around 5th week of gestation.[5] Before the foramen primum disappears, perforations, produced by apoptosis, appear in the superior part of the septum primum. As the septum fuses with the fused endocardial cushions, these perforations coalesce to form another opening in the septum primum, the foramen secundum. Ostium secundum is formed before the end of the 5th week of development. This structure replaces the ostium primum as the conduit for the right-to-left shunting of oxygenated blood from the umbilical vein.[6-8]

The thick septum secundum grows to the right of the septum primum during the 5th and the 6th weeks, and it gradually overlaps the foramen secundum in the septum primum.[9] Datta stated that the septum secundum grows in the later part of the 7th week on the right side of the septum primum from the roof of the right atrium in the region of interseptovalvular space. After birth, the caudal edge of the septum secundum persists as the limbus fossa ovalis. The cephalic free edge of the septum primum forms a semilunar fold on the left side of the interatrial septum.[10]

Holes can occur at various locations within the flap valve itself. The degree of fenestration can vary greatly, and if widespread, the floor of the fossa can have fishnet like appearance. The flap valve can take the appearance of windsock blowing into the left atrium. Such extensive flap valve has the potential to become aneurismal.[11] In the present study, in one heart, multiple perforations were found in the septum secundum above the semilunar fold [Figure 9]; this may have resulted from the similar process that leads to the formation of perforations in septum primum to form the ostium secundum.

The left surface of the septal wall of the atrium presents a semilunar fold, which is concave upward and represents the upper margin of the septum primum. A lunate impression is situated above this fold; the floor of this impression is formed by the septum secundum [Figure 2]. Foramina venarum minimarum are found in the septal wall.[12] We have also found these in this study [Figure 6a].

In our study, we have found variations in the shapes of semilunar fold, namely U (12%), V (12%), W (16%), J (20%), and semilunar (40%). Regarding the size of the lunate

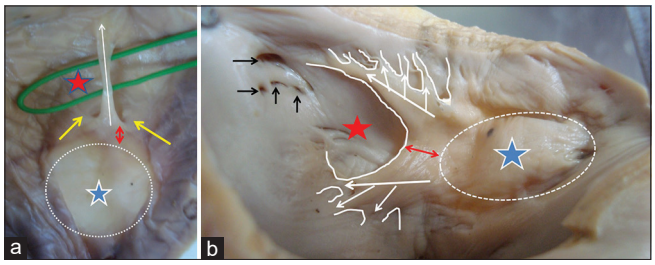

Figure 5: (a) Single strand (white arrow) traversing lunate fossa. (b) Branching strands (white arrows) traversing lunate fossa

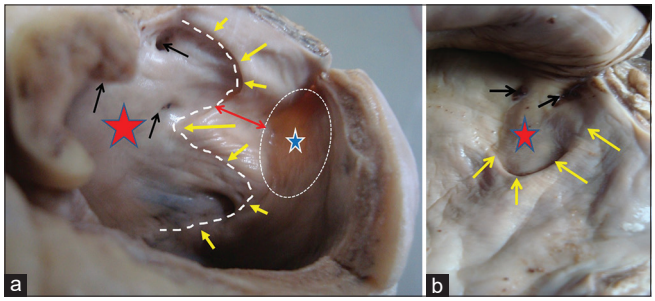

Figure 7: (a) Venae cordis minimi opening into the Septum Secundum, Semilunar fold is W shaped. (b) Venae cordis minimi opening near the attachment of Septum Secundum to the roof of left atrium. Fold is semilunar shaped

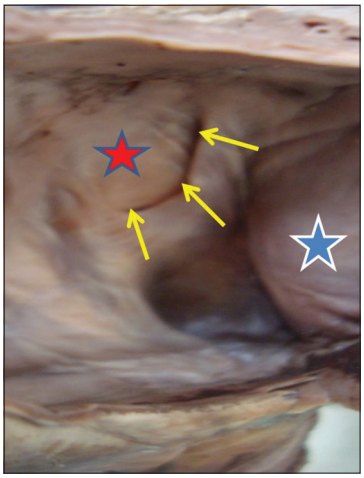

Figure 6: Semilunar fold is J shaped

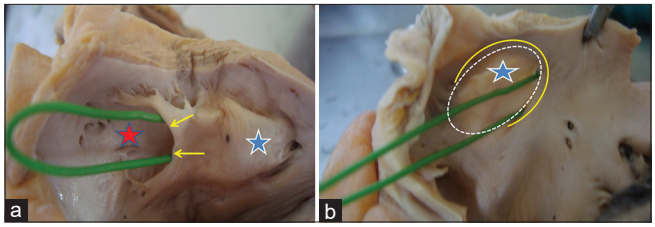

Figure 8: (a) U shaped green probe passing through patent foramen ovale deep to semilunar fold. (b) Shows the right surface of interatrial septum. Limbus fossa ovalis marked by yellow curved line. Green probe is seen emerging through the foramen ovale

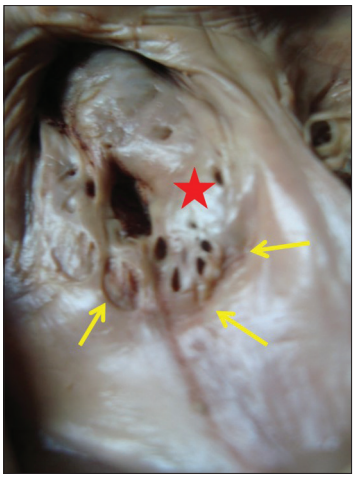

Figure 9: Showing fenestrated septum secundum

fossa, the average vertical height of the lunate fossa was 7.87 mm (maximum: 13.88 mm and minimum: 3.68 mm); and the average transverse diameter was 7.38 mm (maximum: 16.85 mm and minimum 1.85 mm). These values have not been described in the literature reviewed.

Near the cranial part of attachment of the septum secundum to the atrial wall varying number of openings of venae cordis minimi perforating the septum secundum has been described by Datta,[12] and in the present study, these were seen opening in the left atrial chamber [Figure 6b].

The region of overlap of the caudal margin of the septum secundum over the caudal margin of the ostium secundum was seen [Figure 2], which was varying from minimum 1.64 mm to maximum 12.74 mm (average = 4.25 mm). Although the overlap of the caudal margin of the septum secundum to the cranial margin of the septum primum at the ostium secundum is described, its extent has not been mentioned in the literature reviewed.

In the present study, we found a probe patency of the foramen ovale in 16% of hearts and a probe could be inserted between the two atria [Figure 8a and b]. Moore and Persaud described it in 25% of people,[9] and an incidence of 20% was described by Sadler[1] and Datta.[10]

Small ASDs can remain completely asymptomatic and hemodynamically insignificant throughout life.[11]

There are four clinically significant types of ASD: (i) ostium secundum defect, (ii) endocardial cushion defect with ostium primum defect, (iii) sinus venosus defect, and (iv) common atrium. The first two types are common. Large ostium secundum ASD may also occur because of a combination of excessive resorption of the septum primum and a large oval foramen.[9,13] ASDs constitute 8%–13% of all congenital heart defects.[13] The most common form of ASD is patent foramen ovale. A small isolated patent oval foramen is of no hemodynamic significance. A probe patent oval foramen is present in up to 25% of people.[9] Ninety percent of the ASDs comprise ostium secundum defects, with the female preponderance, female:male = 2:1.[8]

A secundum ASD can result from (i) inadequate formation of the septum secundum, so that it does not completely cover the ostium secundum and (ii) more often, the ostium secundum is excessively large because of increased resorption, so that the septum secundum cannot cover it. Isolated secundum ASDs account for approximately 7% of congenital cardiac defects.[9,14] Thus, when the septum secundum fails to overlap the septum primum, it permits shunting of the blood between the right and left atria. Cyanosis develops when the blood shunts from the right to left.[10]

In the present study, 12 (24%) hearts showed strands of the septum primum, varying in number and dimensions, extending from the semilunar fold and dividing the region of the ostium secundum into a number of foramina of variable sizes and shapes. Strands were seen traversing the lunate fossa and their number varied from 1 to 3 [Figures 3b and 4]. Some of these strands were wide and were seen to be branching [Figure 5b]. These features have not been described in the available literature, except by Sweeney and Rosenquist who have described a network of muscular trabeculations that can be seen in the left surface of the atrial septum. Some of these may be seen along the anterior border of the oval fossa representing the remnants of the ostium secundum and have been named the crescentric muscular arch. Further, it has been emphasized that this variation could interfere with navigating guiding wires and catheters in the left atrium through transseptal approach.[3,15]

Several imaging techniques are used to image ASDs and its size. These include cross-sectional echocardiography, intracardiac ultrasound, magnetic resonance imaging, and balloon sizing during cardiac catheterization.[11] Three-dimensional (3D) imaging echocardiography provides an accurate assessment of the exact shape of the defect as this can be important in device closure of ASDs.[14] This technique provides more accurate descriptions of the varying dynamic morphology, dimensions, and spatial relationship of interatrial communications. The use of this technique in centers today permits the detection of more than 90% of interatrial communications, using transthoracic and transesophageal echocardiography (TEE) to view the defects in various planes.[11]

The 3D-TEE revealed a ridge-like structure on the left atrial side of the atrial septum protruding into the left atrial lumen: (a) the ridge (semilunar fold) was formed along the superior edge of the oval fossa in the left atrium and extended to the left atrial free wall medially and superiorly and (b) this ridge-like structure overhung posteriorly creating a hollow-like structure (lunate fossa). This ridge-like structure on the left atrial side has not been well described in the literature. We have found this ridge to be variable in shape.

The number of cardiac patients who undergo interventional transseptal approach has risen substantially over the past few years, further underlying the importance of understanding the left atrial anatomy and anomalies.[3] In the treatment of ASDs, nowadays, various techniques are used for closure of holes between the atria. These include minimal access surgery and percutaneous closure using a device inserted on a catheter.[11]

For transcatheter closer, a large number of devices have been developed (i) Bard clamshell septal occluder and buttoned device and other devices (Das Angel-Wing, ASDOS, Amplatzer, Cardioseal, HELEX and others) have been introduced.[13] The results of the repair continue to improve because of the better understanding of the morphology of the lesion, refinement in surgical technique, improvement in preoperative and operative care including better myocardial protection.[16]

Conclusion

The findings of the present study show that the coalescence of the foramina in the cranial part of the septum primum does not completely fuse to form a single ostium secundum in all the developing hearts, and that some remnants of the septum primum persist as strands traversing the lunate fossa. The number of cardiac patients who undergo interventional transseptal approach has risen substantially over the past few years, emphasizing the importance of understanding the anatomy and anomalies of the lunate fossa in the left atrium. One of the most significant defects is the ostium secundum defect. The significance of the present study lies in the fact that the morphology of the semilunar fold and lunate fossa on left atrial surface of the interatrial septum is not described in detail in the literature reviewed.

The present study shows that there are variations in the size of the lunate fossa and the ridge formed by the semilunar fold which is also variable in shape. The presence of variable number and size of strands traversing the lunate fossa has also been observed. Thus, these variations could interfere with navigating the guiding wires and catheters in the left atrium through transseptal approach. Therefore, this knowledge can be of great importance for an accurate assessment by imaging techniques of the exact shape of the ostium secundum defect, which can be of help to the cardiac surgeon and the interventionists for the choice of the device for closure of ASDs.

Financial support and sponsorship

Nil.

Conflicts of interest

There are no conflicts of interest.

References

1. Sadler TW. Langman's Medical Embryology. l3th ed. New Delhi: Wolters Kluwer; 2015. p. 187, 191.
2. Singh V. Text Book of Clinical Embryology. New Delhi: Elsevier- A division of Reed Elsevier India Pvt. Ltd.; 2012. p. 200, 203, 204.
3. Shizukuda Y, Muth J, Chaney C, Attari M. Anomalous ridge on the left atrial side of the atrial septum. Ann Card Anaesth 2012;15:161-2.
4. Cuschieri A. Development of the Heart and Cardiovascular System. Available from: https://um.edu.mt/acus1/Heart-a.htm. [Last accessed on 2024 oct 2].
5. Rivenes SM, Rao PS. Ostium Primum Atrial Septal Defects; 2015. Available from: https://emedicine.medscape.com/article/890880-overview. [Last accessed on 2025 October 5].
6. Standring S. Gray's Anatomy. The Anatomical Basis of Clinical Practice. 40th ed. Amsterdam: Churchill Livingstone, Elsevier; 2008. p. 1023, 1030.
7. Calvert PA, Rana BS, Kydd AC, Shapiro LM. Patent foramen ovale: anatomy, outcomes, and closure. Nature Reviews Cardiology 2011;8:148-60.
8. Rajeshwari MS, Fasila P. Ostium secundum atrial septal defect: A case report. Int J Curr Res Rev 2013;5:23-5.
9. Moore KL, Persaud TV. The Developing Human –Clinically Oriented Embryology. 8th ed. Philadelphia: Saunders; 2008. p. 295, 310, 312.
10. Datta AK. Essentials of Human Embryology. 6th ed. Kolkata: Current Books International; 2010. p. 162-3, 165-66, 172.
11. McCarthy K, Ho S, Anderson R. Defining the morphologic phenotypes of atrial septal defects and interatrial communications. Images Paediatr Cardiol 2003;5:1-24.
12. Datta AK. Essentials of Human Anatomy- Thorax and Abdomen. 9th ed. Calcutta: Current Books International; 2018. p. 71.
13. Rao PS. Atrial Septal Defect- A Review, Atrial Septal Defect, Ed, in Tech; 2012. Available from: https://www.ilntechopen.com/books/atrial-septal-defect/atrial-septal-defects-a-review. [Last accessed on 2024 Oct 09]
14. Gessner IH, Neish SR. Ostium Secundum Atrial Septal Defects. Available from: https://emedicine.medscape.com/article/890991-overview. [Last accessed on 2024 October 11].
15. Sweeney LJ, Rosenquist GC. The normal anatomy of the atrial septum in the human heart. Am Heart J 1979;98:194-9.
16. Najm HK, Williams WG, Chuaratanaphong S, Watzka SB, Coles JG, Freedom RM. Primum atrial septal defect in children: Early results, risk factors, and freedom from reoperation. Ann Thorac Surg 1998;66:829-35.

Original Article

Variations of the Superior Cerebellar Artery on Magnetic Resonance Angiography

Svjetlana Mujagić, Davor Ivanić, Mirza Haličević, Renata Hodžić[1], Zlatan Mehmedović[2], Nihad Mešanović[3], Duško Kozić[4,5]

Clinic for Radiology and Nuclear Medicine, University Clinical Center Tuzla, [1]Clinic for Neurology, University Clinical Center Tuzla, [2]Clinic for General Surgery, University Clinical Center Tuzla, [3]Department for Information Technology, University Clinical Center Tuzla, Tuzla, Bosnia and Herzegovina, [4]Faculty of Medicine, University of Novi Sad, Novi Sad, [5]Center for Imaging Diagnostics, Oncology Institute of Vojvodina, Sremska Kamenica, Serbia

Abstract

Introduction: The superior cerebellar artery (SCA) is the most consistent branch of the basilar artery. Its most frequent variations include duplication, hypoplasia, a common trunk of the SCA with the P1 segment of the posterior cerebral artery (PCA), early branching, triplication, and fenestration. **Aim:** To determine the frequency and characteristics of individual variations of the SCA on magnetic resonance angiography (MRA). **Subjects and Methods:** This retrospective study included 1000 subjects older than 18 years, who underwent native MRA, which was performed using 1.5 Tesla machines. Patients with cerebrovascular disease, vascular malformations, or brain tumors in the immediate vicinity of the analyzed arteries were excluded from the study. **Results:** The average internal diameter of the SCA was 1.24 mm. The SCA was symmetrical in 63.4% of cases, and the most common anatomical variation was duplication of the SCA, with 19.8% of cases, where bilateral duplication was more common in men than in women (P = 0.03). Hypoplasia and fenestration were both present in 0.2% of cases. The frequency of a common SCA and PCA trunk was 14.2%. **Conclusion:** SCA exhibits a wide range of anatomical variations that may have profound clinical implications, influencing surgical approaches, endovascular interventions, and overall patient management strategies. MRA offers noninvasive, high-resolution visualization of the SCA, making it a superior method for comprehensive assessment of SCA anatomy and possible variations.

Keywords: *Anatomical variations, magnetic resonance angiography, superior cerebellar artery*

Introduction

The superior cerebellar artery (SCA) is the most consistent branch artery of the posterior cerebral circulation in terms of origin and location[1] and usually emerges from the distal segment basilar artery (BA) immediately before its bifurcation in the form of a single tree, which is then divided into rostral and caudal branches.[2] The BA bifurcation represents an important orientation point when visualizing the exit of the SCA. The most frequently described anatomical variations of SCA are duplication, triplication, a common trunk of the SCA with the P1 segment of the posterior cerebral artery (PCA), hypoplasia, early branching of the SCA, and fenestration.[3] Most anatomical variations of SCA have no major clinical significance, but several studies have been conducted in which their significance is shown in various compressive syndromes: trigeminal neuralgia,[4] oculomotor compressive syndromes,[5] and hemifacial spasm,[6] as well as thromboembolic occlusions of the distal segment of the BA.[7]

There is a difference between cadaveric and radiological studies, and some authors show the limitations of radiological studies, in which the analysis is based on hemodynamically efficient arteries, which may explain the greater number of aplasias in radiological studies compared to cadaveric ones.[1]

The aim of this study was to determine the frequency and characteristics of individual variations of the SCA on magnetic resonance angiography (MRA).

Subjects and Methods

Examinees

This retrospective study, performed in the period from July 2008 to May 2013 at our Clinic of Radiology and Nuclear Medicine, included 376 men and 624 women, older than 18 years, who consecutively underwent native MRA of the cerebral arteries. Patients with cerebrovascular disease, vascular malformations, or brain

How to cite this article: Mujagić S, Ivanić D, Haličević M, Hodžić R, Mehmedović Z, Mešanović N, *et al.* Variations of the superior cerebellar artery on magnetic resonance angiography. J Anat Soc India 2025;74:41-5.

Article Info

Received: 06 May 2024
Revised: 04 December 2024
Accepted: 15 February 2025
Available online: 31 March 2025

Address for correspondence:
Dr. Davor Ivanić,
Clinic for Radiology and Nuclear Medicine, University Clinical Center Tuzla, Tuzla, Bosnia and Herzegovina.
E-mail: ivanic.davor@yahoo.com

Access this article online

Website: https://journals.lww.com/joai
DOI: 10.4103/jasi.jasi_57_24
Quick Response Code:

tumors in the immediate vicinity of the analyzed arteries on MR imaging (MRI) were excluded from the study.

Methods

MRA was performed using one of two 1.5 Tesla machines (Siemens, model Avanto, Germany, or Philips, model Achieva, The Netherlands). The MRA protocol consisted of noncontrast three-dimensional time of flight (3D-TOF) angiograms with axial slice thickness at 0.9 mm, covering the area of the first cervical vertebra to the upper contour of the corpus callosum by MRA. On the Siemens 1.5T machine, the following imaging parameters were set as follows: time of repetition (TR), 25 ms; time of echo (TE), 7 ms; flip angle, 20°; matrix size, 256 × 256; and field of view (FOV), 220 mm. The imaging parameters on the Phillips machine were as follows: TR, 23 ms; TE, 6.91 ms, flip angle, 20°; matrix, 328 × 208; and FOV, 180 mm. In this study, the axial 3D-TOF angiograms, maximum intensity projection images, and volume rendering of the 3D-MR angiograms were analyzed by the Voxar system.

All images were analyzed by a single radiologist with 5 years' experience in MRI, and all unclear cases were further analyzed by a neuroradiologist with many years of experience. The inner diameter of the SCA was measured at the distance of 0.5 mm from its branching point.

To adequately compare our results with individual studies that did not use the vascular asymmetry coefficient when determining symmetry/asymmetry/hypoplasia, but used the concept of the dominance of one SCA compared to the other (if one SCA had a larger diameter by 0.5 mm or more in comparison to the contralateral one), the dominance of the artery was determined in the research.[8]

Statistical analysis

The collected data were entered into the Microsoft Access database (Microsoft Corporation, Redmond, Washington, United States), while statistical analysis was performed using MedCalc statistical software (MedCalc Software Ltd, Ostend, Belgium). The standard methods of descriptive statistics were used for statistical data processing (mean and standard deviation). Since the inner diameter differences of the SCAs between males and females were approximately normally distributed variables, they were tested with the parametric *t*-test for independent samples. The frequency differences of each variation by gender were evaluated using the Chi-square test. Differences on the level of $P < 0.05$ were considered statistically significant.

Results

The average internal diameter of the SCA was 1.24 mm (minimum 0.5 mm; maximum 2.2 mm). Men had a significantly larger average internal diameter of the SCA artery compared to women, at the significance level of $P < 0.0001$ [Table 1].

Table 1: Internal diameter of the superior cerebellar artery

	Diameter		*t*-test (*P*)
	n	AM±SD (mm)	
Male	751	1.27±0.21	<0.0001
Female	1247	1.21±0.19	
Total	1998	1.24±0.2	

n: Size of the sample (right + left), AM: Arithmetic mean, SD: Standard deviation

Table 2: Prevalence of anatomical variations of the superior cerebellar artery

Variation	Male, *n* (%)	Female, *n* (%)	Total, *n* (%)	Chi-square test (*P*)
Symmetry	222 (59)	412 (66)	634 (63.4)	0.031
Asymmetry				
Right SCA <	38 (10.1)	51 (8.2)	89 (8.9)	0.15
Left SCA <	32 (8.5)	43 (6.9)	75 (7.5)	0.19
Total	70 (18.6)	94 (15.1)	164 (16.4)	0.07
Hypoplasia				
Right	1 (0.3)	-	1 (0.1)	-
Left	-	1 (0.2)	1 (0.1)	-
Total	1 (0.3)	1 (0.2)	2 (0.2)	0.66
Duplication				
Right	33 (8.9)	56 (9)	89 (8.9)	0.70
Left	35 (9.3)	49 (7.8)	84 (8.4)	0.23
Bilateral	14 (3.7)	11 (1.8)	25 (2.5)	0.03
Total	82 (21.8)	116 (18.6)	198 (19.8)	0.10
Fenestration				
Right	-	-	-	-
Left	1 (0.3)	1 (0.2)	2 (0.2)	0.66
Total	1 (0.3)	1 (0.2)	2 (0.2)	0.66

SCA: Superior cerebellar artery

Table 2 shows the prevalence of anatomical variations of the SCA, from which it can be seen that the right and left SCAs were symmetrical in most cases (63.4%) and that the most common anatomical variation was duplication of the SCA, which was found in 198 (19.8%) subjects. One hundred and seventy-three (17.3%) subjects had unilateral duplication of the SCA, and 25 (2.5%) subjects had bilateral duplication, which means that 223 duplicate SCAs were found in 198 subjects. Bilateral SCA duplication was significantly more common in men than in women ($P = 0.03$). There was no statistically significant difference in the frequency of other individual variations of the SCA between genders [Table 2].

Figure 1 shows the anatomical variations of the SCA on MR angiograms from Table 1, except for hypoplasia (due to the small diameter, the hypoplastic artery could not be adequately shown on angiograms).

When calculating the dominance of one SCA in relation to the other, subjects with duplication and fenestration of the SCA were excluded from the sample, and the dominance of

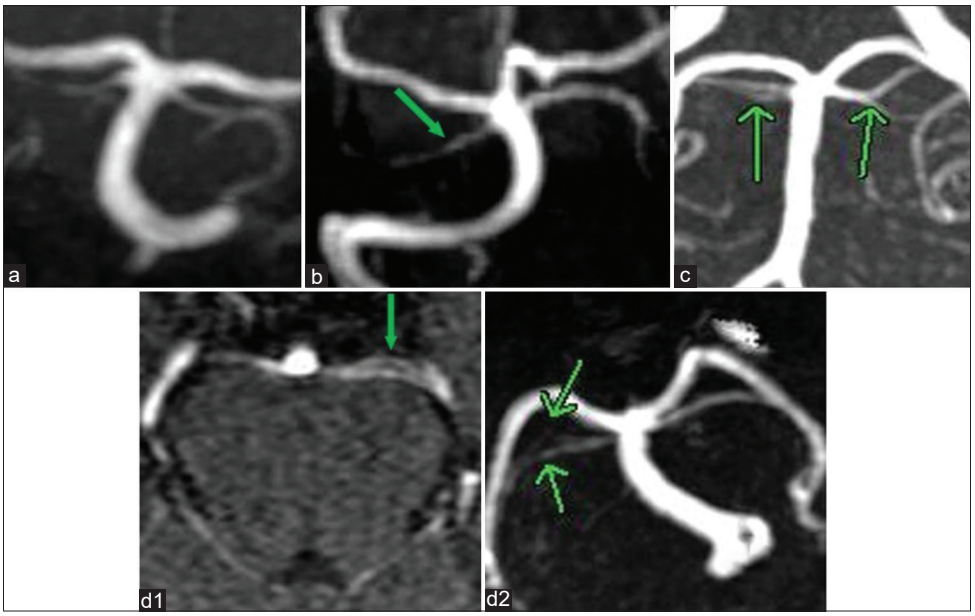

Figure 1: Anatomical variations of the superior cerebellar artery (SCA) highlighted by green arrows: (a) Symmetry, (b) asymmetry, and (c) duplication of the right SCA, early branching of the left SCA; (d1 and 2) fenestration ([d1] axial Three-dimensional time of flight tomogram, [d2] maximum intensity projection reconstruction)

the SCA was determined on the basis of the diameter of the arteries in 800 subjects. Table 3 shows the dominance of one SCA in relation to another, which shows that it existed only in 1.6% of subjects.

Table 4 shows the frequency of a common trunk of the SCA and the PCA. In 142 (14.2%) subjects, the common trunk of the SCA and the PCA was verified, while in the other 858 (85.8%) subjects, SCA branched from the BA separately. In 125 (12.4%) subjects, a common trunk of the SCA and the PCA was present unilaterally, and in 17 (1.7%) subjects bilaterally, which means that a total of 142 (14.2%) cases of a common trunk of the SCA and the PCA were present.

Table 5 shows the frequency of a common trunk of the SCA and the PCA in subjects with SCA duplication, and Figure 2 shows the frequency of the common trunk of the SCA and the PCA in subjects with one and those with two SCAs. Of the 223 duplicated SCAs, found in 198 subjects, a double SCA had a common trunk with the PCA in 39 (17.49%) cases, while in the group comprising the remaining 802 subjects (subjects with one SCA), a common trunk of the SCA and the PCA was found in 122 (13.96%) cases [Figure 2]. Figure 3 shows the forms of the common trunk of the SCA and the PCA.

Table 3: Dominance of one superior cerebellar artery in comparison to the other

	Dominant		
	Left SCA, *n* (%)	**Right SCA, *n* (%)**	**Total *n* (%)**
Male	3 (1.1)	2 (0.7)	5 (1.8)
Female	3 (0.6)	5 (1.0)	8 (1.6)
Total	6 (0.8)	7 (0.9)	13 (1.6)

SCA: Superior cerebellar artery

Table 4: Prevalence of a common trunk of the superior cerebellar and the posterior cerebral artery

	Right, *n* (%)	**Left, *n* (%)**	**Bilateral, *n* (%)**	**Total, *n* (%)**
Male	26 (6.65)	20 (5.32)	2 (0.8)	48 (12.77)
Female	35 (5.6)	44 (7.05)	15 (2.4)	94 (15.06)
Total	61 (6.1)	64 (6.4)	17 (1.7)	142 (14.2)

Table 5: Frequency of a common trunk of the superior cerebellar and the posterior cerebral artery in subjects with duplication of the superior cerebellar artery

	Right, *n* (%)	**Left, *n* (%)**	**Total, *n* (%)**
Male	12 (25.53)	7 (14.29)	19 (19.79)
Female	10 (14.29)	10 (16.67)	20 (15.75)
Total	22 (19.3)	17 (15.6)	39 (17.49)

Discussion

Internal diameter of the superior cerebellar artery

The mean external diameter of SCA in an autopsy study by Idowu *et al*. was 2.06 ± 0.34 mm.[9] Two anatomical studies showed the mean external diameter of the right and left SCA to be: 1.8 ± 0.5 mm and 1.6 ± 0.4 mm,[10] 1.45 mm and 1.46 mm.[1] In the study conducted by Habibi *et al*., the average external diameter of the right SCA was 1.63 ± 0.5 mm, and the external diameter of the left SCA was 1.66 ± 0.42 mm.[11] The average diameter of the SCA at the point of separation from the BA in the study by Aydin *et al*. was 3 mm.[12] In the literature published so far and available to us, we did not find any results presented of the average internal diameter of the SCA on MRA studies.

In this study, the average internal diameter of the SCA was 1.24 ± 0.2 mm, which is closest to the results of Songur *et al*.[13] There was no significant difference in diameter between the right and left SCA. On average, the left SCA was only 0.01 mm larger than the right SCA. The diameter of the SCA was 1.27 ± 0.21 mm in men and was significantly greater ($P < 0.0001$) compared to the diameter of the SCA in women (1.21 ± 0.19 mm).

Anatomical variations of the superior cerebellar artery

The SCA branches from the distal part of the BA. The BA bifurcation represents an important orientation point when visualizing the branching of the SCA. The most common anatomical variations of SCA are duplication, triplication, a common trunk of the SCA with the P1 segment of the PCA, hypoplasia, early branching of the SCA, and fenestration.[3] Duplication and early bifurcation of the SCA can cause trigeminal neuralgia if one of the branches of the SCA has a caudal flow.[4] The oculomotor nerve passes between the PCA and the SCA. Lateral deviation of the common trunk of the SCA and the P1 segment of the PCA can compress the proximal segment of the oculomotor nerve and lead to its paresis.[5] In addition, preoperative identification of anatomical variations of the SCA can prevent certain surgical complications.[7]

In our research, in 63.3% of cases, the right and left SCA were symmetrical, which is fewer that in the results of the study by Davidoiu *et al*., who presented bilateral symmetry in 70.7% of their subjects.[2] In this research, asymmetry of the right and left SCA was present in 15.4% of the subjects, and in only 1.6% of the subjects was one SCA dominant in comparison to the other, which is less than the result in the study by Songur *et al*. who presented the dominance of one SCA over the other in 10.9% of subjects.[13]

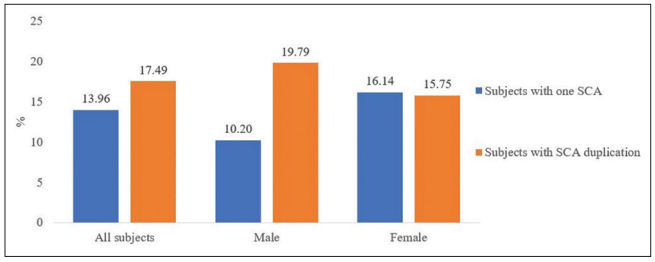

Figure 2: Frequency of a common trunk of the superior cerebellar artery (SCA) and the posterior cerebral artery in subjects with one, and subjects with two SCAs. SCA: Superior cerebellar artery

SCA hypoplasia in the present study was verified in only 0.2% of subjects, and no SCA aplasia was found in any subject. Uchino *et al*. could not identify SCA on 145 MR angiograms in 9 subjects.[14] In their angiographic study, Krzyżewski *et al*. reported 12 cases of SCA aplasia (3%), which they explained by the fact that hemodynamically inefficient arteries are not visible on angiographic studies, and that MRA is more suitable for detailed imaging.[1]

The prevalence of unilateral SCA duplication in the study by Songur *et al*. was 14.5% for the right and 12.7% for the left SCA.[13] Uchino *et al*. presented unilateral duplication of the SCA on the right in 4.4% of subjects and in 2.9% of subjects on the left.[14] The prevalence of unilateral duplication of the SCA in other studies was 20%,[15] 14%,[16] and 25% of subjects.[17] Bilateral duplication was verified in 8%,[18] 2%,[16] 2.2%,[14] 7.2%,[13] and 2.9%[19] of subjects. Triplication of the SCA was found in 2%,[16] 8%,[18] and 1.9%[10] of subjects. Pekcevik and Pekcevik reported SCA duplication in 60 (17.6%) cases, with right SCA duplication in 9.4% of cases and left SCA duplication in 8.2% of cases.[19]

In the present research, unilateral duplication of the SCA was verified in 17.3% of subjects (8.9% right and 8.4% left), which corresponds to the results of published studies and is closest to the results of Salamon and Huang[15] Bilateral duplication was verified in 2.5% of subjects, which corresponds to the results of other authors.[14,19] No significant difference in the frequency of SCA duplications was found between males and females, but bilateral duplication was more frequent in males ($P = 0.03$).

The prevalence of a common trunk of the SCA and the P1 segment of the SCA varies between studies. Hardy *et al*. presented this variation in 4%[16] and Caruso *et al*. in 1% of subjects.[20] In an autopsy study, Songur *et al*. presented the prevalence of a common trunk of the SCA and the P1 segment in 6.3% of cases on the right, 10% of cases on the left, and 1.8% of cases bilaterally.[13] In an MR angiographic study, Uchino *et al*. presented a common trunk of the SCA and the P1 segment in 0.7% of cases on the right, 2.9% on the left, and 0.7% on both sides, which

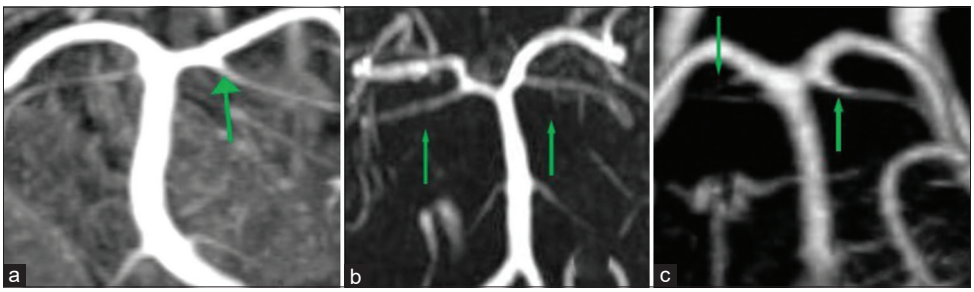

Figure 3: Common trunk of the superior cerebellar artery (SCA) and the posterior cerebral artery (PCA), highlighted by green arrows: (a) Left, (b) bilateral, and (c) duplication of the right SCA with a common trunk of the SCA and the PCA bilaterally

is significantly fewer than in the aforementioned autopsy studies.[14] In their angiographic study, Pekcevik and Pekcevik reported a SCA-PCA common trunk in 17 (4.9%) of their subjects, with a bilateral common trunk in 3 (0.9%) subjects.[19] Ogeng'o *et al*. reported a common SCA-PCA trunk in 10 (2.5%) cases[21] and Kalaiyarasi and Chitra in 5 (3.1%) cases.[10]

In the present research, a common trunk of the SCA and the P1 segment was verified in 14.2% of subjects. In 6.1% of subjects, a common trunk of the two arteries was present on the right, in 6.4% on the left, and in 6.1% on both sides. These results are closest to the results of the autopsy study by Songur *et al*.[13] In the present study, the prevalence of the common trunk of the SCA and the P1 segment was higher in subjects with duplication of the SCA (17.49%) compared to subjects who had one SCA (13.96%). A common trunk of the SCA and the PCA was more common in male subjects with a double SCA (19.79%) compared to male subjects with a single SCA, in which the common trunk of the SCA and the PCA was present in 10.2% of subjects. In the available literature, we did not find studies that dealt with the question of whether the prevalence of a common trunk and the P1 segment of the PCA is higher in people who have duplication of the SCA compared to people with a single SCA, or whether a duplicated SCA has a common trunk with the P1 segment more often than separate branching from the BA.

Fenestrations of SCA are extremely rare. Davidoiu *et al*. verified one case of SCA fenestration in their study performed on 205 subjects.[2] In our study, SCA fenestration was verified in 2 (0.2%) subjects.

Conclusion

The SCA exhibits a wide range of anatomical variations that are crucial for clinicians to understand to diagnose accurately and effectively treat different pathologies. These variations may have profound clinical implications, influencing surgical approaches, endovascular interventions, and overall patient management strategies. MRA offers noninvasive, high-resolution visualization of the SCA, making it a superior method for comprehensive assessment of SCA anatomy and possible variations.

Financial support and sponsorship

Nil.

Conflicts of interest

There are no conflicts of interest.

References

1. Krzyżewski RM, Stachura MK, Stachura AM, Rybus J, Tomaszewski KA, Klimek-Piotrowska W, *et al.* Variations and morphometric analysis of the proximal segment of the superior cerebellar artery. Neurol Neurochir Pol 2014;48:229-35.
2. Davidoiu AM, Lazăr M, Vrapciu AD, Rădoi PM, Toader C, Rusu MC. An update on the superior cerebellar artery origin type. Medicina (Kaunas) 2023;59:2164.
3. Malicki M, Szmyd BM, Bobeff EJ, Karuga FF, Piotrowski MM, Kościołek D, *et al.* The superior cerebellar artery: Variability and clinical significance. Biomedicines 2023;11:2009.
4. Maarbjerg S, Gozalov A, Olesen J, Bendtsen L. Trigeminal neuralgia – A prospective systematic study of clinical characteristics in 158 patients. Headache 2014;54:1574-82.
5. Belotti F, Zanin L, Fontanella MM, Panciani PP. The oculomotor neurovascular conflict: Literature review and proposal of management. Clin Neurol Neurosurg 2020;195:105920.
6. Chaudhry N, Srivastava A, Joshi L. Hemifacial spasm: The past, present and future. J Neurol Sci 2015;356:27-31.
7. Ikram A, Zafar A. Basilar artery infarct 2023. In: StatPearls. Treasure Island (FL): StatPearls Publishing; 2024.
8. Grasso G, Alafaci C, Passalacqua M, Tschabitscher M, Salpietro FM, Tomasello F. Landmarks for vertebral artery repositioning in bulbar compression syndrome: Anatomic and microsurgical nuances. Neurosurgery 2005;56:160-4.
9. Idowu OE, Malomo AO, Akang EU. Surgical anatomy of the vertebrobasilar territory and posterior circle of willis. West Afr J Med 2010;29:230-4.
10. Kalaiyarasi S, Chitra PS. A study of variations in the origin of superior cerebellar artery and the dimensions of its proximal segment. Int J Anat Res 2018;6:4849-53.
11. Habibi Z, Meybodi AT, Maleki F, Tabatabai S. Superior and anterior inferior cerebellar arteries and their relationship with cerebello-pontine angle cranial nerves revisited in the light of cranial cephalometric indexes: A cadaveric study. Turk Neurosurg 2011;21:504-15.
12. Aydın ME, Kaya AH, Kopuz C, Demir MT, Corumlu U, Dagcinar A. Bilateral origin of superior cerebellar arteries from the posterior cerebral arteries, and clues to its embryologic basis. Anat Cell Biol 2011;44:164-7.
13. Songur A, Gonul Y, Ozen OA, Kucuker H, Uzun I, Bas O, *et al.* Variations in the intracranial vertebrobasilar system. Surg Radiol Anat 2008;30:257-64.
14. Uchino A, Sawada A, Takase Y, Kudo S. Variations of the superior cerebellar artery: MR angiographic demonstration. Radiat Med 2003;21:235-8.
15. Salamon G, Huang YP. Radiologic Anatomy of the Brain. Berlin: Springer-Verlag; 1976. p. 305-6.
16. Hardy DG, Peace DA, Rhoton AL Jr. Microsurgical anatomy of the superior cerebellar artery. Neurosurgery 1980;6:10-28.
17. Dagcinar A, Kaya AH, Hilmi A, Aydin ME, Kopuz C, Senel A, *et al*. The superior cerebellar artery: Anatomic study with review. Neurosurg Q 2007;17:235-40.
18. Mani RL, Newton TH, Glickman MG. The superior cerebellar artery: An anatomic-roentgenographic correlation. Radiology 1968;91:1102-8.
19. Pekcevik Y, Pekcevik R. Variations of the cerebellar arteries at CT angiography. Surg Radiol Anat 2014;36:455-61.
20. Caruso G, Vincentelli F, Rabehanta P, Giudicelli G, Grisoli F. Anomalies of the P1 segment of the posterior cerebral artery: Early bifurcation or duplication, fenestration, common trunk with the superior cerebellar artery. Acta Neurochir (Wien) 1991;109:66-71.
21. Ogeng'o J, Elbusaidy H, Sinkeet S, Olabu B, Mwachaka P, Inyimili M. Variant origin of the superior cerebellar artery in a black Kenyan population. Eur J Anat 2015;19:287-90.

Original Article

The Localization and Incidence of Metoptic Canal and Warwick's Foramen in Adult Skulls from West Anatolia

Funda Aksu, Selım Karabekır[1], Nuket Gocmen-Karabekir

Departments of Anatomy and [1]Neurosurgery, Dokuz Eylul University School of Medicine, Izmir, Turkey

Abstract

Purpose: Metoptic canal (MC) is located between the superior orbital fissure and the optic canal. Warwick's foramen (WF) is viewed on the inner side of the orbit together with the foramen rotundum and superior orbital fissure. The aim of the present study was to determine the presence and incidence of MC and WF and to examine their morphometric characteristics in a sample of Turkish skulls from West Anatolia. **Materials and Methods:** A total of 153 dried human skulls and 11 dried skull bases from a West Anatolian Turkish population collected at the Anatomy Department of Dokuz Eylul University were examined. The presence and incidence of the MC and of WF were determined. The distance between reference points and the structures examined within the orbit was measured using a caliper. Student's *t*-test was used for comparisons between the right- and left-sided measurements. SPSS 22.0 software pack was used for statistical analysis. **Results:** MC was detected in 10 of the 153 dry human skulls: 4 (2.6%) on the right side, 5 (3.2%) on the left side, and 1 (0.06%) bilaterally. There were no statistically significant differences between right and left side measurements ($P > 0.05$). WF was observed in 2 (18.2%) of the 11 dry skulls, and both were on the left. **Conclusion:** The relationships between MC, WF, and other anatomical structures may be of clinical importance in surgical operations involving the orbit.

Keywords: *Foramen rotundum, metoptic canal, optic canal, orbit, superior orbital fissure, Warwick's foramen*

Introduction

The optic canal and superior orbital fissure represent the two main anatomical openings connecting the orbit to the cranial cavity. While anatomical variations of the optic canal are quite uncommon, those involving the superior orbital fissure are frequent and well-established. However, minor connections between these two main cavities are not present in all human orbits, and therefore, studies involving these are scarce as compared to major channels. An artery or vein can frequently pass through the small channels within the skull, posing the risk of serious bleeding during surgery.[9] A difference in the ossification patterns is thought to be responsible for the formation of MC, which has a keyhole-like appearance. MC is a channel ranging in length from 120 μm to 1.2 mm that passes through the optical strut[23] and it can be observed below the optic canal during the ossification process.[4,9,17,20] It usually closes within 2 months before birth or within the first few years of life.[17,20,26]

WF is an extremely rare anatomical structure with a reported incidence of < 1%, and not surprisingly, has been subject to very few publications. It is located between the superior orbital fissure and the foramen rotundum, connecting the orbit with the cranial cavity. Bertelli and Regoli described the Warwick foramen (WF) as a rare (0.74%) variation of the superior orbital fissure.[4]

WF has a crescentic or round shape, and the inferior ophthalmic vein (IOV) is thought to pass through it, although no clinical relevance has been reported so far.[4,5,15,17,28] Possibly, this vein connects the cavernous sinus and the pterygoid venous plexus.[15] Since the IOV may serve as a route for transmission of facial infections to the cavernous sinus, sound radiological and surgical knowledge on the location of WF may be useful for clinicians. De Lott *et al*. were the first investigators to report a patient with limited diffusion on magnetic resonance imaging (MRI) in both the superior orbital vein (SOV) and the IOV in a patient with cavernous sinus thrombosis (CST) due to masticator

How to cite this article: Aksu F, Karabekır S, Gocmen-Karabekir N. The localization and incidence of metoptic canal and Warwick's foramen in adult skulls from West Anatolia. J Anat Soc India 2025;74:46-51.

Article Info

Received: 12 February 2024
Revised: 01 January 2025
Accepted: 19 February 2025
Available online: 31 March 2025

Address for correspondence:
Dr. Funda Aksu,
Department of Anatomy, Dokuz Eylul University Medical Faculty, Inciralti, Izmir 35340, Turkey.
E-mail: funda.aksu@deu.edu.tr

Access this article online

Website: https://journals.lww.com/joai
DOI: 10.4103/jasi.jasi_22_24
Quick Response Code:

space abscess.[12] It was the first report of CST with MRI evidence of restricted diffusion, not only in a thrombosed SOV but also in a thrombosed IOV.[12] Lee *et al*., in their article on cavernous sinus syndrome, reminded the fact that both cavernous sinuses receive venous drainage from various structures in the face and eye and that the superior and IOVs flow anteriorly into the sinus.[22] CST is a life-threatening and rapidly progressing emergency that generally results from facial trauma and paranasal sinus infections attributed to *Staphylococcus aureus*.[7] Due to the involvement of critical anatomical structures, CST can be associated with significant mortality[13,25] or long-term complications such as hemiparesis and blindness.[7,25]

Despite the definitions of numerous well-established foramina and canals in the orbit, WF and metoptic canal (MC) are not commonly observed in anatomical samples and related studies are scarce.[4,6,9,10,14,17,19,25,27]

Detailed knowledge of the anatomy of WF and MC may be of clinical significance in certain neurosurgical procedures involving mass lesions, herniation due to increased intracranial pressure, orbital or skull base traumas, isolated fractures, or the fractures of the adjacent bone complex such as the superior orbital margin, zygoma, sphenoid, or temporal bones. In this regard, morphometric measurements of MC and WF and their distance to certain important anatomical reference points may provide valuable insights for neurosurgeons.

In this study, we aimed to determine the incidence of MC and WF in a sample of West Anatolian skulls along with morphometric measurements.

Materials and Methods

In this study, 153 human-dried skulls and 11 dried skull bases from West Anatolia stored at the Anatomy Department of Dokuz Eylul University were evaluated. Ethical approval was not obtained for this study as it did not require the participation of any live subjects instead only bony material was used. The age and sex of the skulls were unknown, and none of the bones had deformity from previous orbital surgery or trauma. After the identification of MC and WF, the incidence of these structures was determined [Figures 1 and 2]. Figures 3 and 4 show the measured distances from WF and MC, and the predefined anatomical landmarks, respectively. Measurements within the orbit were performed using a caliper (Mitutoyo, Japan). SPSS 22.0 (SPSS Inc., Chicago, IL, USA) software pack was used for statistical analysis. Student's *t*-test was used to determine the differences between measurements within the same side and between the right and left sides. $P < 0.05$ was considered statistically significant.

Metoptic canal and Warwick's foramen measurements

Following measurements related to MC were made: (i) the distance between frontozygomatic suture and metoptic

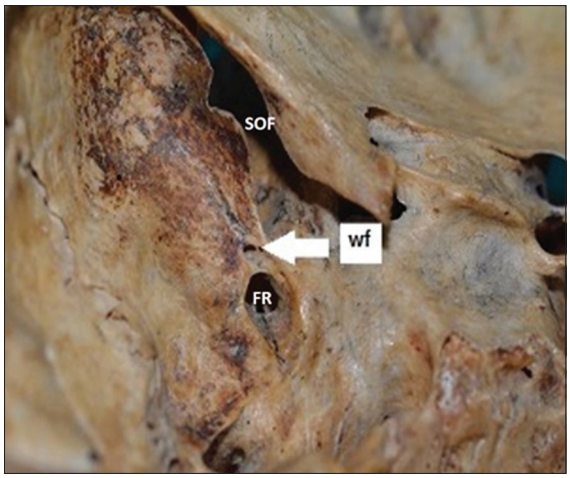

Figure 1: View from the inside of the skull base. WF: Warwick's Foramen, FR: Foramen rotundum, SOF: Superior orbital fissure

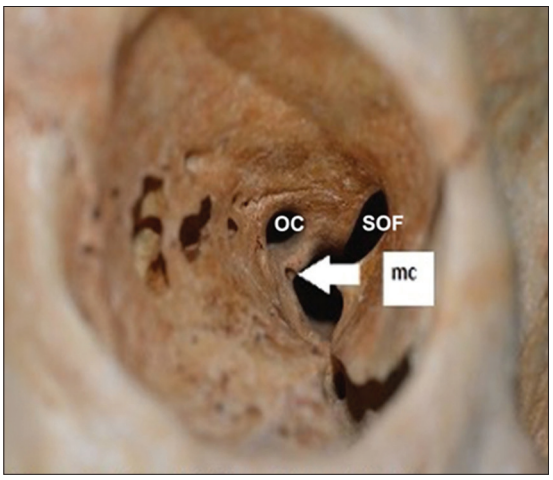

Figure 2: Front view of orbit. MC: Metoptic canal, OC: Optic canal, SOF: Superior orbital fissure

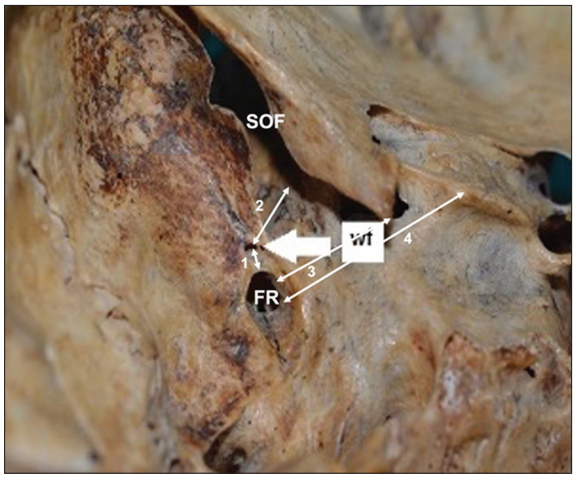

Figure 3: The measurements between the Warwick's foramen and defined anatomical points (1) Distance between Warwick's foramen and foramen rotundum (WFFR); (2) Distance between Warwick's foramen and supraorbital fissure (WFSO); (3) Distance between Warwick's foramen and processus clinoideus anterior; (4) Distance between Warwick's foramen and processus clinoideus medius. WF: Warwick's Foramen, FR: Foramen rotundum, SOF: Superior orbital fissure

canal (FZMC) and (ii) the distance between supraorbital notch or foramen and metoptic canal (SNMC). In addition, the distances between WF and the following structures were measured: foramen rotundum (WFFR), superior orbital fissure (WFSO), anterior clinoid process (WFACP), and medial clinoid process (WFMCP).

Results

Among 153 human skulls, MC was present on the right side in 4, on the left side in 5, and bilaterally in one [Table 1]. The mean FZMC length was 49.62 ± 4.30 mm on the right and 52.47 ± 3.05 mm on the left. The mean SNMC length on the right was 50.83 ± 4.38 mm and 54.02 ± 1.84 mm on the left [Table 2].

In 11 orbits, WF was never observed on the right and was present only on the left in two (18.2%) [Table 3]. The mean WFFR length on the right was 1.86 ± 0.25 mm, the mean WFSO length was 2.37 ± 0.42 mm, the mean WFACP was 14.78 ± 1.07 mm, and the mean WFMCP was 20.66 ± 1.29 mm [Table 4].

Discussion

The orbit harbors narrow channels through which arteries, veins, and nerves pass. These structures and channels are important for both clinical and anatomical studies. Among these, MC and WF have been relatively less studied and characterized. The aim of the current study was to provide data regarding the distances between these rare structures and other anatomical landmarks as well as the incidences of these structures, which could be especially useful for surgeons working in the field of orbital surgery. The majority of these channels are thought to close during the development of the orbit, but there is little information regarding their clinical significance in adult skulls. Furthermore, further studies may be warranted to determine whether age and gender affect the development of these channels. In addition,

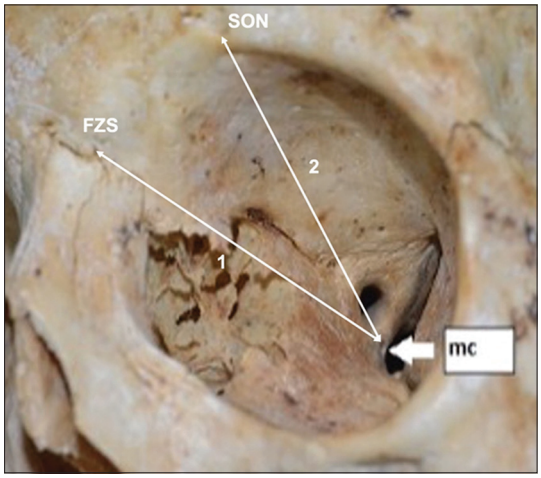

Figure 4: The measurements made between the metoptic canal and defined anatomical points (1) The distance between the frontozygomatic suture and the metoptic canal (FZMC); (2) The distance between the supraorbital notch or foramen and the metoptic canal (SNMC). SON: Supraorbital notch or foramen, FZS: Frontozygomatic suture, MC: Metoptic canal

Table 1: Number and percentage of metoptic canal's found on the right and left sides

	n (%)
MC right	
Presence	4 (2.6)
Absence	149 (97.4)
Total	153 (100.0)
MC left	
Presence	5 (3.2)
Absence	148 (96.8)
Total	153 (100.0)
MC bilaterally	
Presence	1 (0.06)

MC: Metoptic canal

Table 2: Mean distances between the metoptic canal and the reference points (mm)

MC	*n*	Minimum	Maximum	Median	Mean	SD	*P*
FZMC							
Right	5	44.98	53.96	50.98	49.62	4.30	0.414
Left	6	47.35	55.85	52.89	52.47	3.05	
SNMC							
Right	5	44.29	54.65	52.43	50.83	4.38	0.233
Left	6	50.83	55.90	54.56	54.02	1.84	

MC: Metoptic canal, FZMC: Frontozygomatic suture and metoptic canal, SNMC: Supraorbital notch or foramen and metoptic canal, SD: Standard deviation

Table 3: Number and percentage of Warwick's foramen's found on the right and left sides of the skull base

	n (%)
WF right	
Presence	0
Absence	11 (100.0)
Total	11 (100.0)
WF left	
Presence	2 (18.2)
Absence	9 (81.8)
Total	11 (100.0)

WF: Warwick's foramen

Table 4: Mean distances between the Warwick's foramen and the reference points (mm)

Left	*n*	Minimum	Maximum	Median	Mean	SD
WFFR	2	1.68	2.04	1.86	1.86	0.25
WFSO	2	2.07	2.66	2.37	2.37	0.42
WFACP	2	14.02	15.54	14.78	14.78	1.07
WFMCP	2	19.75	21.57	20.66	20.66	1.29

SD: Standard deviation, WFFR: Warwick's foramen and foramen rotundum, WFSO: Warwick's foramen superior orbital fissure, WFACP: WF and anterior clinoid process, WFMCP: WF and medial clinoid process

there is no information on possible pathologies of the nerve or vascular structures that pass through these channels between the anterior and posterior parts of the orbit, which may emerge in the presence or absence of these channels.

Metoptic canal incidence

Earlier, Macchi *et al*. reported that the MC is a somewhat overlooked anatomical entity found in 8.74% of orbits.[23] Chockalingam and Babu found MC only in 4 (7.8%) of the 32 dry human skulls; 3 were found on the right orbit and 1 was found on the left.[9] Hizay and Sindel found MC in 20 of the 92 dry human skulls, unilaterally. The authors observed MC in 11 (11.9%) skulls on the right and in 9 (9.7%) skulls on the left.[17] Regoli and Bertelli identified MC in 8% of the orbits they examined.[27] We identified the presence of MC in 10 of 153 (6.5%) dry human skulls: 4 (2.6%) of these were on the right, 5 (3.2%) were on the left, and 1 (0.06%) was bilateral. In some previous studies, bilateral canals were not found at all, or the majority of unilateral canals were localized on the right side. On the other hand, there was a more balanced distribution of MC in terms of the side in the present study. It remains to be seen whether these differences between published reports are related with ethnic origin or developmental factors. We also measured the distance between MC and frontozygomatic suture and the supraorbital notch to provide some information for surgical procedures involving this area.

Warwick's foramen incidence

The size and morphological characteristics of WF and adjacent structures play an important role in determining the most appropriate operative techniques to approach the skull base or for gender determination in forensic medicine. Preoperative assessment of the WF for determining the operative safe zone needs to include correlations between surgical and morphometric parameters. Furthermore, a detailed knowledge of the bony anatomy of this anatomical area may improve the general safety of the surgery.

Until now, WF has been studied only scarcely, research on its incidence has never been done, and little is known regarding the structures transmitted through it.[5,28] Furthermore, the morphology and size of this foramen appear to be highly variable. Based on a groove running backward into the cavernous sinus, Warwick hypothesized that it could convey an IOV.[28]

Chockalingam and Babu failed to observe any WF in 32 dry skulls studied.[9] Bertelli, in his study of 943 skulls, reported a WF incidence of 0.74%. In that study, WF was never bilateral, with 8 and 6 on the left and right orbits, respectively.[3] Furthermore, in another study, 0.6%–0.7% of the skulls examined by Regoli and Bertelli were found to have WF.[27]

WF incidence was higher (2.17%) than previous reports in the study by Araya *et al*., who examined dry skull specimens of Chilean origin. In that study, there was one case with right-sided WF, one with left-sided WF, and one with bilateral WF.[2] Hizay and Sindel, in their study of 92 skulls, found the frequency of WF to be 13.0%. All WFs were unilateral, with 7 (7.6%) on the right, and 5 (5.4%) on the left.[17] Similarly, in another previous study, WF was bilateral only in one case.[5] In our study, 11 human dry skull bases were examined for the presence of WF. Although the number of bone samples was small, we observed a unilateral left canal in 2 (18.2%). This may have been due to ethnic differences, developmental factors, or just coincidental.

Morphometric measurements

We also performed morphometric measurements in our study to provide data that can aid in surgical procedures. For this purpose, several anatomical reference points were used, including the frontozygomatic suture, supraorbital notch, foramen rotundum, superior orbital fissure, and anterior and medial clinoid processes. Groups were compared in terms of these measurements and no statistically significant difference was found ($P > 0.05$).

Metoptic canal measurements

The distances between MC and frontozygomatic suture reported in the study by Hizay and Sindel were 29.51 ± 11.20 mm and 27.98 ± 5.67 mm on the right and left sides, respectively.[17] The corresponding figures reported by Chockalingam and Babu were 5.1 and 6.5 cm.[9] In the present study, the measured distance was 49.62 ± 4.30 mm on the right and 52.47 ± 3.05 mm on the left side, similar to the results of Chockalingam and Babu, although they were slightly lower. These differences may reflect ethnic variations.

The distance between MC and supraorbital notch reported by Hizay and Sindel was 40.62 ± 8.87 mm on the right and 42.24 ± 12.77 mm on the left vs. 5.3 cm and 6 cm in another study by Chockalingam and Babu.[9,17] In the present study, this distance was 50.83 ± 4.38 and 54.02 ± 1.84 mm on the right and left sides, respectively, in general agreement with those of Chockalingam and Babu.

Warwick's foramen measurements

In Hizay and Sindel's study, the measured distance between WF and foramen rotundum was 7.27 ± 2.47 mm on the right and 6.18 ± 1.50 mm on the left side.[17] This distance was only measured on the left side in our study (1.86 ± 0.25 mm). In the abovementioned study, the distance between WF and the superior orbital fissure was 5.44 ± 1.85 mm on the right side and 5.96 ± 2.47 mm on the left side.[17] In our study, only a left-sided measurement was possible (2.37 ± 0.42 mm).

Surgical importance of the foramens

Serious ocular injury has been shown to occur, but there is conflict about the rate of occurrence and localization.[11] The middle fossa injuries can lead to serious cranial nerve injuries when they involve the foramina through which cranial nerves are transmitted.[16,21] Attention has already been drawn to the structural variations and differences and relative strength of the walls of the orbit and their relationship with the intracranial structures such as WF. Fractures of the posterior 1/3 of the orbit are uncommon. The posterior orbit contains a number of significant and sensitive structures, including the optic nerve, ophthalmic vessels, and ocular muscles as well as their motor nerves, which may pose significant challenges for the surgeon.[18] The most common surgical procedures used to treat orbital lesions involve the lateral wall approach, transethmoidal approach, transmaxillary approach from the orbital floor, and transcranial approach, in which the orbital roof is removed.[24] It has been previously reported that injury to arteries passing through the small foramen during orbital surgery prolongs the duration of surgical operations and puts structures passing through the superior orbital fissure at risk. During surgery, deep dissection of the lateral wall of the orbit can often lead to bleeding, which can be severe.[1,8] Postoperative complications in orbital surgery include visual disturbances, enophthalmos, facial asymmetry, and orbital dystopia. Some of these complications may result from severe ischemia.[23] It may also be important to assess the WF before surgical interventions for cranial tumors, herniation due to increased intracranial pressure, and trauma in the orbit or skull base. Furthermore, fractures of the region may occur in isolation or can be independently associated with fractures of the adjacent bone complex such as the superior orbital margin, the zygoma, the sphenoid, or temporal bones. Orbital fractures can be generally divided into four types: zygomatic complex fractures, isolated fractures of the orbital rim, isolated fractures of the orbital walls, and complex comminuted fractures. Fractures of the orbit should be approached with caution and proper management is essential to prevent esthetic and functional complications. The purpose of surgery is to identify and characterize blunt ocular and periocular injuries and to identify orbital cranial nerve lesions and lesions of neighborhood structures such as WF as well as other associated complications. A consensus-based classification of injuries involving this region may assist in developing surgical reconstruction strategies and may allow meaningful comparisons between surgical outcomes. Consultation with ophthalmic, neurosurgical, plastic, and maxillofacial surgeons can be of crucial importance for demonstrating anatomical location and accompanying lesions as well as for proper treatment and follow-up. Good knowledge of the size and morphological characteristics of WF and the adjacent structures is crucial for establishing the safest and most appropriate operative techniques in neurosurgery or for gender determinations in forensic medicine. During the preoperative evaluation of WF for the operative safe zone, the correlation between both surgical and morphometric parameters of WF needs to be taken into consideration. Detailed knowledge of the bony anatomy of this region is of great importance in terms of the safety of the surgical procedure.

In this study, the distances between some rarely observed anatomical structures and reference points within the orbit were analyzed. Despite limitations in the sample size and measurement techniques, we believe that the data generated may be of use for future studies. Awareness of the presence of orbital structures such as small channels will have clinical implications and shed light to further studies with more detailed hypotheses and robust contributions to science. Confirmation of the existence of these channels in other regions and ethnical groups requires the examination and analysis of skulls from other geographical regions. Morphological and morphometric characteristics of the MC and WF may be useful for orbital surgeons who are dealing with a variety of procedures such as tumor resection, decompression, or posttraumatic orbital or anterior skull base reconstruction. We believe that the data generated in this study may be valuable for researchers in the fields of anatomy, orbital surgery, and neurosurgery.

Author contribution

F Aksu: Project development, Data collection and management, Manuscript writing and editing. S Karabekir: Data analysis, Manuscript writing. N Karabekir: Manuscript writing and editing.

Ethical approval

This is a study conducted with the approval of our university's anatomy department. It was made on bones belonging to the university in the anatomy laboratory. Ethical Approval obtained from the Anatomy Department of Dokuz Eylul University Medical School is submitted as a file.

Availability of data and materials

Data and materials are available to the authors and can be used.

Financial support and sponsorship

Nil.

Conflicts of interest

There are no conflicts of interest.

References

1. Abed SF, Shams P, Shen S, Adds PJ, Uddin JM, Manisali M. A cadaveric study of the cranio-orbital foramen and its significance in orbital surgery. Plast Reconstr Surg 2012;129:307e-11e.
2. Araya C, Silva J, Soto M, Salcedo A, Donoso V, Arcos S. Cavernous orbital venous foramen: Warwick's foramen. Int J Morphol 2018;36:1480-4.

3. Bertelli E. Metoptic canal, duplication of the optic canal and Warwick's foramen in human orbits. Anat Sci Int 2014;89:34-45.
4. Bertelli E, Regoli M. Branching of the foramen rotundum. A rare variation of the sphenoid. Ital J Anat Embryol 2014;119:148-53.
5. Bisaria KK, Kumar N, Jaiswal AK, Sharma PK, Mittal M, Bisaria SD. An accessory foramen deep in the infraorbital fissure. J Anat 1996;189:461-2.
6. Calori L. On various osteological peculiarities of the base of the human skull. Mem R Acad 1891;2:287-304.
7. Cannon ML, Antonio BL, McCloskey JJ, Hines MH, Tobin JR, Shetty AK. Cavernous sinus thrombosis complicating sinusitis. Pediatr Crit Care Med 2004;5:86-8.
8. Celik S, Kazak Z, Ozer MA, Govsa F. Navigational area of the cranio-orbital foramen and its significance in orbital surgery. Surg Radiol Anat 2014;36:981-8.4.
9. Chockalingam S, Babu Y. Incidence and morphometric analysis of metoptic canal and Warwick's foramen in South Indian skulls. Biosci Biotechnol Res Commun 2020;13:192-5.
10. Choudhry R, Choudhry S, Anand C. Duplication of optic canals in human skulls. J Anat 1988;159:113-6.
11. Cook T. Ocular and periocular injuries from orbital fractures. J Am Coll Surg 2002;195:831-4.
12. De Lott LB, Trobe JD, Parmar H. Restricted diffusion of the superior and inferior ophthalmic veins in cavernous sinus thrombosis. J Neuroophthalmol 2013;33:268-70.
13. Desa V, Green R. Cavernous sinus thrombosis: Current therapy. J Oral Maxillofac Surg 2012;70:2085-91.
14. Diamond MK. Homologies of the meningeal-orbital arteries of humans: A reappraisal. J Anat 1991;178:223-41.
15. Engin Ö, Adriaensen GF, Hoefnagels FW, Saeed P. A systematic review of the surgical anatomy of the orbital apex. Surg Radiol Anat 2021;43:169-78.
16. Heine RD, Catone GA, Bavitz JB, Grenadier MR. Naso-orbital-ethmoid injury: Report of a case and review of the literature. Oral Surg Oral Med Oral Pathol 1990;69:542-9.
17. Hizay A, Sindel M. Metoptic canal and Warwick's foramen: Incidence and morphometric analysis by several reference points in the human orbit. Eurasian J Med 2019;51:1-4.
18. Karaki M, Kobayashi R, Mori N. Removal of an orbital apex hemangioma using an endoscopic transethmoidal approach: Technical note. Neurosurgery 2006;59:E159-60.
19. Keyes JE. Observation on four thousand optic foramina in human skulls of known origin. Arch Ophthalmol 1935;13:538-68.
20. Kier EL. Embryology of the normal optic canal and its anomalies. An anatomic and roentgenographic study. Invest Radiol 1966;1:346-62.
21. Kinnunen I, Aitasalo K. A review of 59 consecutive patients with lesions of the anterior cranial base operated on using the subcranial approach. J Craniomaxillofac Surg 2006;34:405-11.
22. Lee AG, Ghosh A, Bhat N, Bindiganavile SH. Cavernous Sinus Syndrome; 2022. Available from: https://eyewiki.aao.org/Cavernous_Sinus_Syndrome. [Last accessed on 2024 Feb 01].
23. Macchi V, Regoli M, Bracco S, Nicoletti C, Morra A, Porzionato A, *et al*. Clinical anatomy of the orbitomeningeal foramina: Variational anatomy of the canals connecting the orbit with the cranial cavity. Surg Radiol Anat 2016;38:165-77.
24. Martins C, Costa E Silva IE, Campero A, Yasuda A, Aguiar LR, Tatagiba M, *et al*. Microsurgical anatomy of the orbit: The rule of seven. Anat Res Int 2011;2011:468727.
25. Matthew TJ, Hussein A. Atypical cavernous sinus thrombosis: A diagnosis challenge and dilemma. Cureus 2018;10:e3685.
26. Radoievitch S, Jovanovic S. Relations of the optic canal of children to the posterior paranasal sinuses (contribution to the development of the sphenoid sinus). Acta Anat (Basel) 1960;41:172-83.
27. Regoli M, Bertelli E. The revised anatomy of the canals connecting the orbit with the cranial cavity. Orbit 2017;36:110-7.
28. Warwick R. A juvenile skull exhibiting duplication of the optic canals and subdivision of the superior orbital fissure. J Anat 1951;85:289-91.

Original Article

Evaluation of the Relationship between Morphological Measurements of the Knee and Anterior Cruciate Ligament Injuries along with Meniscus Injuries

Begüm Incedemır Ündey, Ayfer Metın Tellıoglu, Elif Aydın[1], Yasemin Durum Polat[2]

Departments of Anatomy, [1]Physical Medicine and Rehabilitation and [2]Radiology, Faculty of Medicine, Aydin Adnan Menderes University, Efeler, Aydin, Turkey

Abstract

Background: Ligamentum cruciatum anterius (LCA) and meniscus injuries are common pathologies, accounting for 40%–50% of all ligament-related knee injuries. **Aims and Objectives:** To evaluate anatomical measurements as potential risk factors for LCA and meniscus injuries by comparing MRI records of individuals with isolated LCA injuries, combined LCA and meniscus injuries, and a control group with normal knee findings. **Materials and Methods:**The study analyzed MRI records of 310 individuals: 200 diagnosed with LCA injury and 110 with normal knee findings. The participants were divided into two groups: isolated LCA injury and combined LCA and meniscus injury. Various anatomical measurements were compared between the study groups and the control group. **Results:** Significant differences were found in anatomical measurements. In both the isolated LCA injury and combined injury groups, condylus medialis width, condylus lateralis width, bicondylar width, eminentia intercondylaris width, tibia width, patellar length, ligamentum patellae length, patella facies articularis angle, and sulcus trochlearis angle were significantly higher. In contrast, fossa intercondylaris shape index, fossa intercondylaris index, tibial medial slope, sulcus trochlearis depth, trochlear facet asymmetry, sulcus trochlearis and tuberositas tibia distance, and patellar tilt were significantly lower in the injury groups. **Conclusion:** Specific anatomical measurements can serve as potential risk factors for LCA and meniscus injuries. These measurements could be incorporated into clinical practice for early identification of individuals at higher risk for these injuries.

Keywords: *Anterior cruciate ligament injuries, knee injuries, knee joint, magnetic resonance imaging, meniscus*

Introduction

The knee joint is the largest joint in the body. In addition to flexion–extension movement, it also allows rotational movements, albeit to a small extent. The ligamentum cruciatum anterius (anterior cruciate ligament [ACL]) extends from the inner surface of the condylus lateralis of the femur to the area intercondylaris, a structure belongs to the tibia. This ligament also runs diagonally from posterior lateral to anterior medial.[1]

Menisci, which are mostly composed of fibrous cartilage, serve to reduce the inconsistency between the articular surfaces in the knee joint. The meniscus medialis (MM) is more oval and C-shaped when viewed from above, whereas the slightly smaller meniscus lateralis (ML) is more rounded.[2]

ACL injuries are one of the most common injuries of the knee region, therefore, they are of high clinical and surgical importance. Although ACL injuries are mostly related to trauma, anatomical differences between individuals may make some individuals more vulnerable to ACL injuries. MM is more prone to injury because it is more strongly fixed and heterogeneous in shape. Lesions of MM, ACL, and collateral tibial ligament, called the unhappy triad, often appear together in different combinations.[2]

Anatomical studies investigating the relationship between ACL injuries and bone morphology have focused more on the intercondylar fossa (intercondylar notch), femoral condyles, and tibial plateau, and the link between narrow intercondylar fossa and ACL injury has been clearly demonstrated. In recent years, femoral trochlear dysplasia (TD) has been frequently investigated as a potential risk

How to cite this article: Ündey BI, Tellıoglu AM, Aydın E, Polat YD. Evaluation of the relationship between morphological measurements of the knee and anterior cruciate ligament injuries along with meniscus injuries. J Anat Soc India 2025;74:52-61.

Article Info

Received: 06 May 2024
Accepted: 18 November 2024
Available online: 31 March 2025

Address for correspondence:
Dr. Ayfer Metin Tellioglu, Department of Anatomy, Faculty of Medicine, Aydin Adnan Menderes University, Efeler, Aydin, Turkey.
E-mail: ayfer.tellioglu@adu.edu.tr

Access this article online

Website: https://journals.lww.com/joai
DOI: 10.4103/jasi.jasi_56_24
Quick Response Code:

factor for ACL injuries. TD is a condition in which the distal femur loses its normal concave shape and the patella cannot adapt to the convex articular surface. There are also studies reporting that TD causes an increase in ACL load.[3]

Studies in which tibial, femoral, and patellar variation and morphological changes are handled separately and associated with ACL injuries are available in the literature. However, there is no in-depth study in which all bone structures involved in the joint are considered holistically, and variations in different structures are associated with each other, ACL, and meniscus injuries. In our study, we aim to reveal the morphological measurements and variations in the bone structures involved in the knee joint in a comparative way in the group with ACL injury, the group with combined ACL and meniscus injury, and the control group.

Materials and Methods

Our study includes 200 patients who were referred to Aydın Adnan Menderes University Radiology Department for knee magnetic resonance imaging (MRI) between 1 June 2015 and 1 June 2021 and were diagnosed with ACL injuries according to MRI reports, and 110 patients reported as normal knee MRI (a total of 310 patients). The records were reviewed through our hospital PACS (Picture Archiving and Communication Systems) Sectra Workstation IDS7 Version 23.2.2.5087 2021. Before the study, the approval of the Non-Interventional Clinical Research Ethics Committee dated 17.09.2021 and numbered E-53043469-050.04.04.-76301 was obtained.

The subjects to be included in the study have completed bone development between the ages of 18–60 and have no congenital, traumatic (except ACL and meniscus injuries) or inflammatory knee diseases, no bone fractures, dislocation or space-occupying lesions in the bones or other tissues joining the knee joint, no signs of osteoarthritis, and no evidence of previous surgery in the knee region. In addition, images with problems such as the presence of artifacts in the regions where the measurement is planned were also excluded from the study.

The images were divided into two groups according to the presence or absence of companying meniscal injury. In addition, images interpreted as normal MRI of the knee, which will be included in the control group, were also taken from the archive.

The gender of the subjects, the age at the time of imaging, and type of the knee injury were recorded. Length measurements were recorded in millimeters, and angle measurements were recorded in degrees.

Radiological evaluation and measurements

In the evaluation of images, axial, coronal, and sagittal sections of MR images taken in the extension position were examined. T1 and T2 sequences were analyzed together to evaluate the ACL, menisci, and bony structures in and around the knee joint. All measurements were obtained with a radiologist with 12 years of experience.

Measurements used to evaluate patella morphology

Patellar length (PL) and patellar ligament length (PLL) were also measured on the longest axis of the patella in the sagittal section. The Insall–Salvati Index (ISI), which is the PLL/PL value, was also obtained.[4] Patellar width (PW) and Patellar facies articularis (facet) angle wiberg angle (WA) were measured in the axial section where the patella is widest[5] [Figure 1].

Measurements used to evaluate femur morphology

Measurements of medial condyle width (MCW), lateral condyle width (LCW), bicondylar width (BW), and intercondylar notch width (NW) were obtained in the coronal section. Intercondylar notch index (NI) is obtained by dividing NW by BW.[6] Intercondylar notch depth (ND) and intercondylar notch angle (NA) were measured as in the coronal section. Intercondylar notch shape index (NSI) was obtained by dividing NW by ND.[7] Sulcus trochlearis depth (STD) was measured in the axial section and trochlear facet asymmetry (TFA) was calculated[8,9] [Figure 2].

Intercondylar notch morphological classification (NMC): It was made by morphologically separating the intercondylaris fossa into three types. Type A: narrow fossa intercondylaris; Type U: wide fossa intercondylaris; wide and Type W: double apex fossa intercondylaris[10] [Figure 3].

Measurements used to evaluate tibia morphology

Tibia width (TW) and eminentia interconylaris width (EIW) were measured in the coronal section [Figure 4]. Eminentia intercondylaris width index (EWI) was calculated by dividing EIW by TW.[11] Medial tibial slope (MTS), lateral tibial slope (LTS), and medial tibial depth (MTD) were measured in the midsagittal section[6] [Figure 4].

Measurements used to evaluate patellofemoral concordance

Tibial tuberosity and trochlear groove (sulcus trochlearis) distance (TT-TG) are measured in the two axial sections and calculated.[5] Patellar tilt (PT), lateral patellofemoral

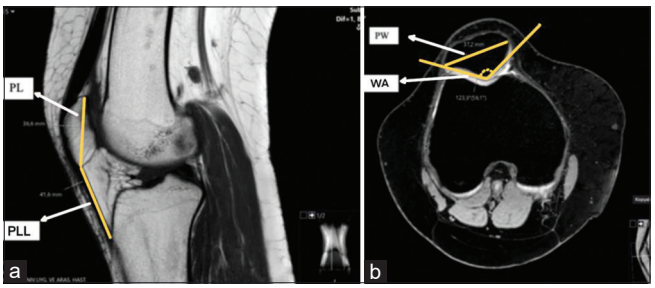

Figure 1: (a) Patellar length, patellar ligament length, and Insall–Salvati Index measurement in the sagittal section of the right knee. (b) Patellar width value and wiberg angle measurements of the patella in the axial section of the right knee. PL: Patellar length, PLL: Patellar ligament length, ISI: Insall–Salvati index, BW: Bicondylar width, WA: Wiberg angle

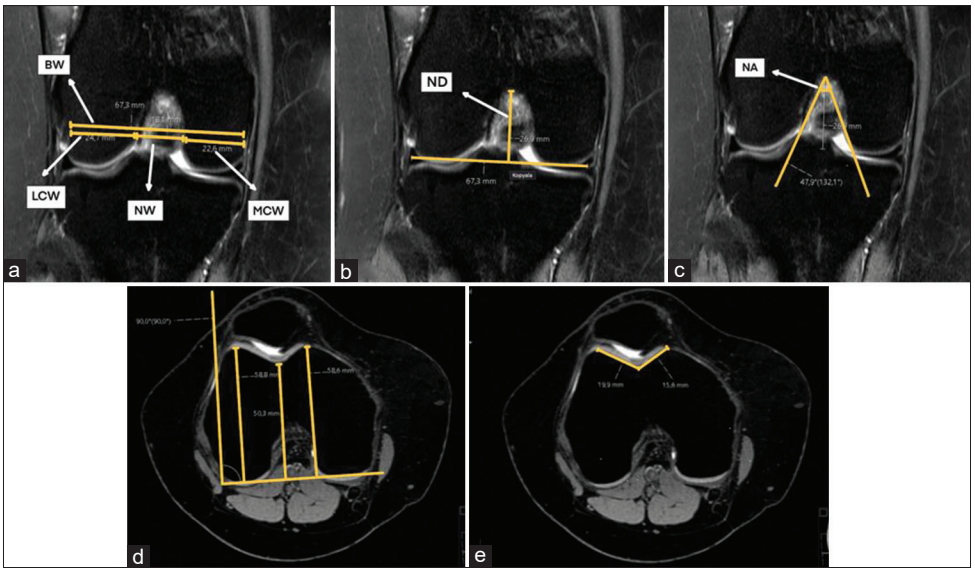

Figure 2: (a) Medial condyle width, lateral condyle width, bicondylar width, notch width measurements in the coronal section of the right knee, (b) notch depth in the coronal section of the right knee, (c) notch angle measurement in the coronal section of the right knee, (d) sulcus trochlearis depth measurement in the axial section of the right knee, (e) trochlear facet asymmetry measurement in the axial section of the right knee. MCW: Medial condyle width, LCW: Lateral condyle width, BW: Bicondylar width, NW: Intercondylar notch width, ND: Intercondylar notch depth, NA: Intercondylar notch angle, TFA: Trochlear facet asymmetry, STD: Sulcus trochlearis depth

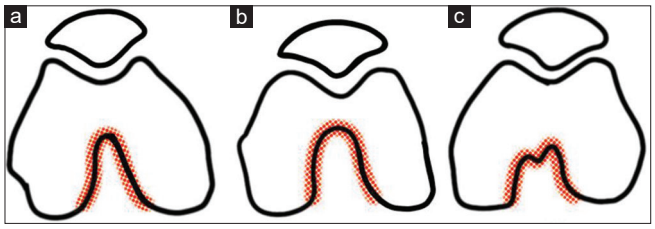

Figure 3: Notch morphological classification. A-type fossa intercondylaris (a) (right knee), U-type fossa intercondylaris (b) (left knee), W-type intercondylaris (c)

angle (LPFA), and sulcus trochlearis angle (STA) were measured in the axial section.[5] Congruence angle (CA) was measured as the angle between the line dividing the STA obtained in the axial section and the line extending from the deepest point of the sulcus trochlearis to the point of the articular surface of the patella that is closest to the femur[12] [Figure 5].

Statistical method

Research data were evaluated using Statistical Package for the Social Sciences 21.0 statistical program. The conformity of continuous variables to normal distribution was investigated using visual (histogram and probability graphs) and analytical methods (Kolmogorov–Smirnov/Shapiro–Wilk tests). For the descriptive statistics of the study, the mean and standard deviation in data with normal distribution, median, minimum, and maximum in data that do not fit normal distribution are shown. The Chi-square test was used to show whether there is a difference between categorical variables in the study. Student'd *t*-test or one-way ANOVA was used to compare continuous variables with parametric properties in independent groups, and Mann–Whitney U-test or Kruskal–Wallis analysis of variance was used to compare continuous variables with nonparametric properties in independent groups. Receiver operating characteristic (ROC) analysis was used to show whether a variable recorded by numerical measurement was diagnostic or exclusionary. For statistical significance, the *P* value was determined to be <0.05.

Results

A total of 310 cases were included in the study, 110 of which were in the control group and 200 in the study group (cases with ACL injury). Out of 200 cases in the study group, 78 with isolated ACL injury and 122 with ACL and meniscal injury were divided into two separate study groups.

When the demographic characteristics of the cases were examined, 58.18% of the cases in the control group were female, 41.82% were male, 46.15% of the cases in the isolated ACL injury group were female, 53.85% were male, combined ACL and meniscus injury. It was determined that 46.72% of the cases in the group were female and 53.28% were male. In addition, the median age of the cases was 31.00 (18.00–54.00) in the control group, 38.00 (18.00–57.00) in the isolated ACL injury group, and 40.00 (18.00–57.00) in the ACL and meniscus combined injury group found. When we examined the MRIs in our study, no statistically significant difference was found between the groups with fossa intercondylaris morphological classification.

In Table 1, the measurement values of the anatomical structures related to the knee joint were compared between the control group and isolated ACL injury groups.

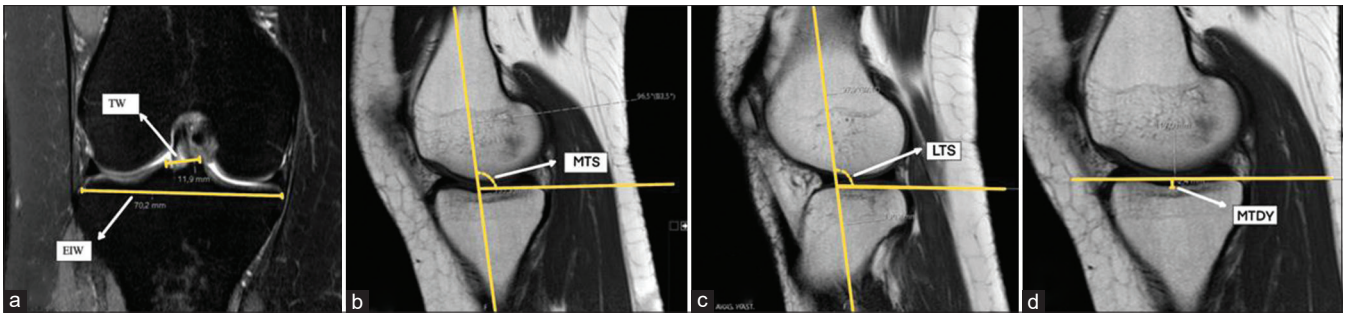

Figure 4: (a) Measurement of Eminentia intercondylaris width index in the coronal section of the right knee. (b) Measurement of the medial tibial slope in the sagittal section of the right knee. (c) Measurement of the lateral tibial slope in the sagittal section of the right knee. (d) Medial tibial depth in the right knee. EWI: Eminentia Intercondylaris width index, LTS: Lateral tibial slope, MTS: Medial tibial slope, MTD: Medial tibial depth

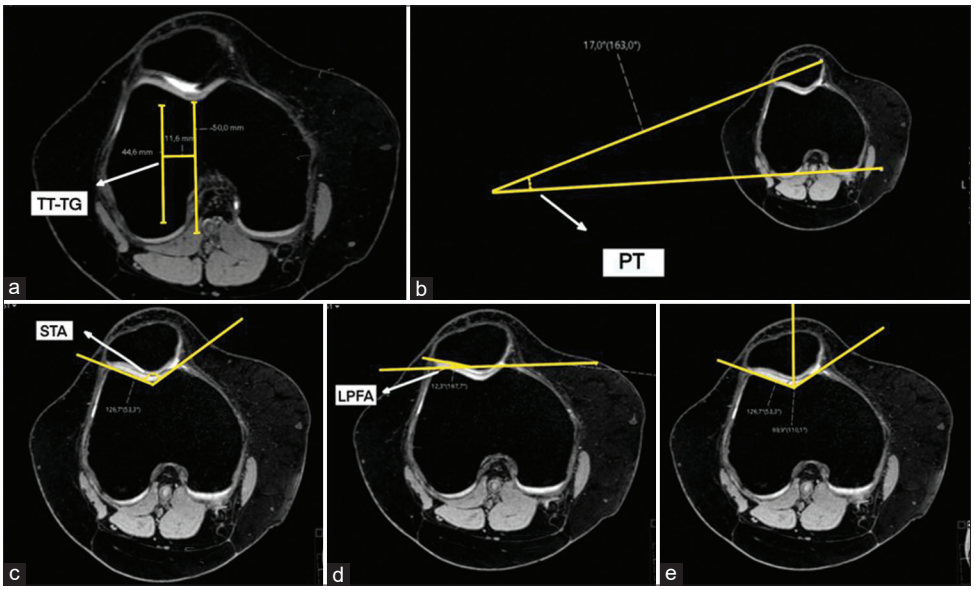

Figure 5: (a) Measurement of tibial tuberosity and trochlear groove in the axial section of the right knee. (b) Patellar tilt measurement in the axial section of the right knee. (c) Measurement of the sulcus trochlearis angle in the axial section of the right knee. (d) sulcus trochlearis angle measurement in the axial section of the right knee. (e) Congruence angle measurement in the axial section of the right knee. PT: Patellar tilt, TT-TG: Tibial tuberosity to trochlear groove distance, STA: Sulcus trochlearis angle, LPFA: Lateral patellofemoral angle, CA: Congruence angle

In Table 2, the measurement values of the anatomical structures related to the knee joint were compared between the control group and the ACL and meniscus combined injury groups.

When the measurement values of the anatomical structures related to the knee joint were evaluated by ROC analysis between the control and isolated ACL injury groups. Details are shown in Table 3.

When the measurement values of the anatomical structures related to the knee joint were evaluated by ROC analysis between the control and ACL and meniscus combined injury groups. Details can be seen in Table 4.

Discussion

There are many studies investigating predisposing factors for ACL and meniscal injuries. Some of the factors are morphological factors in knee anatomy. Many morphological characteristics of bone structure have been associated with increased ACL injuries such as intercondylar notch stenosis, low intercondylar NI, and tibia eminentia stenosis.[13,14]

The distal femur is an anatomical region that is frequently investigated to ACL injuries due to its role in load transfer in the knee joint. In the study conducted by Kızılgöz *et al*., while the CMW value measured in the coronal plane was found to be associated with ACL injuries, they did not find a statistically significant relationship between CLW and BW values.[6] Park *et al*. found CMW value to be associated with ACL injury.[15] In the light of the data in our study, we think that the high CMW value may play a role as a predisposing factor for all isolated ACL and accompanying meniscal injuries.

Many measurements such as NW, ND, NA, and NSI have been reported in the literature in close association with ACL injuries.[16-19] In a study, it was stated that the structure of the fossa intercondylaris (intercondylar notch) is the most

Table 1: Comparison of the measurement values of the anatomical structures of the knee joint between the control group and isolated anterior cruciate ligament injury groups

	Group		*P*
	Control group (*n*=110)	Isolated ACL injury group (*n*=78)	
MCW	24.03±2.25	25.82±2.88	0.000
LCW	25.50 (21.00–30.20)	26.20 (18.70–36.40)	0.013
BW	69.10 (59.30–84.30)	73.10 (59.50–87.30)	0.009
NW	18.87±2.89	18.56±3.24	0.494
ND	23.60±2.35	24.19±2.47	0.102
NA	57.05 (38.70–79.00)	56.70 (41.30–73.90)	0.330
NSI	0.80±0.12	0.77±0.11	0.037
NI	0.27±0.03	0.25±0.004	0.008
EIW	12.60 (8.20–21.40)	13.50 (9.10–18.40)	0.007
TW	71.00 (60.00–84.30)	74.75 (63.30–85.90)	0.014
EWI	0.18 (0.12–0.26)	0.18 (0.11–0.24)	0.168
PL	40.53±3.20	41.95±3.81	0.006
PLL	43.76±5.51	44.41±5.59	0.425
ISI	1.08±0.14	1.06±0.14	0.346
MTD	2.65±0.87	2.73±0.90	0.511
MTS	5.52±2.56	5.34±2.86	0.650
LTS	5.59±3.26	5.84±3.11	0.592
PW	41.10 (34.10–53.40)	42.80 (28.50–50.60)	0.060
Patella facies articularis angle (WA)	126.60 (104.30–139.50)	129.45 (112.10–150.40)	0.036
STA	131.45 (115.40–144.30)	133.55 (122.60–162.40)	0.011
STD	7.39±1.39	6.81±1.54	0.007
TFA	0.79 (0.54–0.99)	0.75 (0.049–1.01)	0.002
TT-TG	9.60 (1.20–24.50)	8.10 (−7.70–19.00)	0.023
PT	9.40 (1.80–34.90)	10.05 (1.80–28.20)	0.546
LPFA	9.92±4.54	11.02±4.94	0.117
CA	1.30 (−21.60–21.20)	−2.85 (−32.40–47.30)	0.711

CA: Congruence angle, LPFA: Lateral patellofemoral angle, PT: Patellar tilt, TT-TG: Tibial tuberosity to trochlear groove distance, TFA: Trochlear facet asymmetry, STD: Sulcus trochlearis depth, STA: Sulcus trochlearis angle, PW: Patella width, LTS: Lateral tibial slope, MTS: Medial tibial slope, MTD: Medial tibial depth, ISI: Insall–Salvati index, PLL: Patellar ligament length, PL: Patellar length, EWI: Eminentia Intercondylaris width index, TW: Tibia width, EIW: Eminentia intercondylaris width, NI: Intercondylar notch index, NSI: Intercondylar notch shape index, NA: Intercondylar notch angle, ND: Intercondylar notch depth, NW: Intercondylar notch width, BW: Bicondylar width, LCW: Lateral condyle width, MCW: Medial condyle width, ACL: Anterior cruciate ligament, WA: Wiberg angle

important anatomical factor related to ACL injuries.[16] Cha *et al*. combined arthroscopy and MRI in their study and showed that mucoid hypertrophy occurs due to compression of the ACL fibers during movement in people with narrow intercondylaris fossa, and therefore suggested that the narrow fossa plays a role as a predisposing factor in ACL injuries.[17] In addition, Li *et al*. classified the NI and NSI values as risk factors for MM and ML injuries.[19] In our study, no significant difference was found between the isolated ACL injury group and the control group in NW, ND, and NA measurements. However, NSI was found to be significantly lower in the isolated ACL injury group ($P < 0.05$). When groups were compared NW measurements were significantly lower in groups with ACL injury ($P < 0.05$). According to the ROC analysis results for these measurements, breakpoints were determined for NW, NI, and NSI measurements [Tables 3 and 4]. In the light of this information, while low NSI and NI values can be considered a predisposing factor for ACL injuries, we think that low NW values together with other factors may pose a risk for meniscal injuries. These results of the morphological features of the fossa intercondylaris obtained in our study support the literature.

The morphological classification of the fossa intercondylaris (NMC) was made by evaluating the shape of the fossa intercondylaris in three types. There are studies in the literature concluding that Type A fossa structure is a predisposing factor for ACL injury.[18] At the same time, there are also studies that do not find NMC differences statistically significant in terms of risk of ACL injury.[20] In our study, there was no statistically significant difference in FIMS rates between the groups. The fact that the NMC is a visual scale and not based on an objective and metric value may have caused this classification to have a lower correlation between scientific studies compared to measurements such as NW, NSI, and NI.

It has been reported that patellofemoral kinematics, contact area, contact pressure, and stability are significantly

Table 2: Comparison of the measurement values of the anatomical structures related to the knee joint between the control group and the anterior cruciate ligament and meniscus combined injury groups

	Group		*P*
	Control group (*n*=110)	ACL and meniscus combined injury group (*n*=122)	
MCW	23.65 (19.50–30.90)	25.80 (6.50–41.00)	0.000
LCW	25.72±2.35	27.02±3.52	0.001
BW	69.10 (59.30–84.30)	72.60 (59.70–89.90)	0.003
NW	18.87±2.89	18.02±3.30	0.038
ND	23.60±2.35	24.09±2.68	0.144
NA	57.14±7.65	55.51±8.25	0.121
NSI	0.80±0.12	0.75±0.12	0.001
NI	0.27 (0.19–0.35)	0.25 (0.13–0.36)	0.000
EIW	12.60 (8.20–21.40)	13.20 (9.10–19.10)	0.044
TW	71.00 (60.00–84.30)	73.80 (62.70–87.80)	0.003
EWI	0.18 (0.12–0.26)	0.18 (0.11–0.25)	0.384
PL	40.53±3.20	41.79±3.85	0.007
PLL	43.76±5.51	45.53±6.22	0.023
ISI	1.08±0.14	1.10±0.16	0.547
MTD	2.60 (0.70–5.40)	2.80 (0.80–22.00)	0.125
MTS	5.52±2.56	4.64±2.68	0.011
LTS	5.59±3.26	6.04±3.60	0.324
PW	41.10 (4.40–53.40)	43.05 (33.20–52.30)	0.005
WA	126.60 (104.30–139.50)	130.30 (106.60–157.40)	0.000
STA	131.45 (115.40–144.30)	134.05 (117.50–160.50)	0.001
STD	7.39±1.39	6.82±1.56	0.003
TFA	0.79 (0.54–0.99)	0.74 (0.39–1.72)	0.000
TT-TG	9.60 (1.20–24.50)	7.30 (−6.90–23.60)	0.000
PT	9.40 (1.80–34.90)	8.15 (1.20–24.40)	0.016
LPFA	9.92±4.54	10.71±5.14	0.216
CA	1.30 (−21.60–21.20)	1.95 (−31.40–38.70)	0.319

CA: Congruence angle, LPFA: Lateral patellofemoral angle, PT: Patellar tilt, TT-TG: Tibial tuberosity to trochlear groove distance, TFA: Trochlear facet asymmetry, STD: Sulcus trochlearis depth, STA: Sulcus trochlearis angle, PW: Patella width, LTS: Lateral tibial slope, MTS: Medial tibial slope, MTD: Medial tibial depth, ISI: Insall–Salvati index, PLL: Patellar ligament length, PL: Patellar length, EWI: Eminentia Intercondylaris width index, TW: Tibia width, EIW: Eminentia intercondylaris width, NI: Intercondylar notch index, NSI: Intercondylar notch shape index, NA: Intercondylar notch angle, ND: Intercondylar notch depth, NW: Intercondylar notch width, BW: Bicondylar width, LCW: Lateral condyle width, MCW: Medial condyle width, ACL: Anterior cruciate ligament, WA: Wiberg angle

affected by TD. Işıklar *et al*. suggested that the strength of the extensor mechanism in knees with TD may cause ACL injuries by causing a change in the normal position of the patella.[21] Some of the measurements used to define TD are: STA, STD, and TFA in sulcus trochlearis. In many studies, higher values of STA are determined to be an indicator for TD.[22] In our study, it was found to be 133.55° (min: 122.60°; max: 162.40) in the isolated ACL injury group and 134.05° (min: 117.50°; max: 160.50°) in the ACL and meniscus combined injury group. STA degrees were to be statistically significantly higher than the control group ($P < 0.05$).

Pfirrmann *et al*. reported that in cases with suspected TD, the specificity and sensitivity of STD measurement are also high, as is the case with STA measurement.[8] In our study, STD values were found to be statistically significantly lower in the isolated ACL injuries and ACL and meniscus combined injury group compared to the control group ($P = 0.007$, $P = 0.003$). In our study, the fact that the STD value was significantly lower in the groups with ACL injury compared to the control group, although it was not on the limit of trochlear hypoplasia and dysplasia in the groups with ACL injury, indicates the relationship between STD and ACL injuries.

The number of studies examining the relationship between TFA and ACL or meniscal injuries is very few. Kwak *et al*. found no statistically significant relationship between TFA and ACL injuries in their study.[3] In the study by Chen *et al*., the rate of TFA was found to be statistically significantly lower in the group with ACL injury.[23] In our study, we found the TFA value to be statistically significantly lower in the isolated ACL injuries group and in the ACL and meniscus combined injury group compared to the control group ($P = 0.002$, $P = 0.000$). Considering that lower values in TFA are associated with TD, the findings of our study support the close relationship between TD and ACL injuries. According to the results of the ROC analysis, since the area under the curve value was above 0.6 in both groups, TFA measurement with a cutoff value of 76% can be recommended to clinicians for ACL risk assessment as a qualified clinical assessment tool.

Increased tibial inclination (slope) values can be considered a predisposing factor in ACL injuries by causing an increase in anterior translation load during knee movements.[14] When we look at the literature, it can be seen that there are many studies that associate the increase in tibial medial inclination and tibial lateral inclination with ACL injuries.[14,24] When we examined all the data in our study, we saw that the MTS and LTS values were distributed in a wide range. There was no statistically significant difference in the MTS value in the isolated ACL injuries group compared to the control group. In the ACL and meniscus combined injury group, the MTS value was found to be significantly lower than in the control group ($P = 0.011$). There was no statistically significant difference between the groups in LTS value. While high MTS and LTS values cause a biomechanical problem that may cause pathological conditions by increasing anterior translation, there is no data that low values within the normal range cause a pathology in knee joint biomechanics.

In a study conducted on cadavers, it was reported that there was a correlation between the ACL volume and the EIW value, however, female individuals were more

Table 3: Evaluation of the measurement values of the anatomical structures related to the knee joint between the control group and isolated anterior cruciate ligament injury groups by receiver operating characteristic analysis

	AUC	AUC %95 CI		*P*	Cut point	Sensitivity	Specificity
		lower limit	Upper limit				
MCW	0.687	0.611	0.763	0.000	24.45	0.692	0.591
LCW	0.606	0.524	0.688	0.013	26.05	0.590	0.582
BW	0.612	0.530	0.694	0.009	70.10	0.641	0.545
NI	0.599	0.516	0.681	0.021	0.2618	0.577	0.573
EIW	0.615	0.532	0.698	0.007	13.05	0.564	0.627
TW	0.606	0.524	0.687	0.014	74.05	0.564	0.600
PL	0.604	0.521	0.687	0.015	41.45	0.526	0.627
WA	0.590	0.508	0.672	0.036	128.25	0.577	0.555
STA	0.609	0.528	0.691	0.011	132.25	0.551	0.573
STD	0.613	0.530	0.696	0.008	7.35	0.628	0.564
TFA	0.636	0.554	0.718	0.002	0.7605	0.603	0.618
TT-TG	0.597	0.514	0.681	0.023	8.70	0.590	0.582

AUC: Area under the curve, CI: Confidence interval, CA: Congruence angle, LPFA: Lateral patellofemoral angle, PT: Patellar tilt, TT-TG: Tibial tuberosity to trochlear groove distance, TFA: Trochlear facet asymmetry, STD: Sulcus trochlearis depth, STA: Sulcus trochlearis angle, PW: Patella width, LTS: Lateral tibial slope, MTS: Medial tibial slope, MTD: Medial tibial depth, ISI: Insall–Salvati index, PLL: Patellar ligament length, PL: Patellar length, EWI: Eminentia Intercondylaris width index, TW: Tibia width, EIW: Eminentia intercondylaris width, NI: Intercondylar notch index, NSI: Intercondylar notch shape index, NA: Intercondylar notch angle, ND: Intercondylar notch depth, NW: Intercondylar notch width, BW: Bicondylar width, LCW: Lateral condyle width, MCW: Medial condyle width, ACL: Anterior cruciate ligament, WA: Wiberg angle

Table 4: Evaluation of the measurement values of the anatomical structures related to the knee joint between the control and anterior cruciate ligament and meniscus combined injury groups by receiver operating characteristic analysis

	AUC	AUC %95 CI		*P*	Cut point	Sensitivity	Specificity
		Lower limit	Upper limit				
MCW	0.708	0.642	0.773	0.000	24.85	0.631	0.627
LCW	0.597	0.524	0.669	0.011	26.10	0.566	0.582
BW	0.612	0.540	0.684	0.003	70.70	0.607	0.573
NW	0.575	0.501	0.648	0.049	18.35	0.557	0.555
NSI	0.610	0.538	0.682	0.004	0.7730	0.549	0.545
NI	0.648	0.578	0.719	0.000	0.2584	0.623	0.618
EIW	0.577	0.503	0.650	0.044	12.65	0.590	0.555
TW	0.612	0.540	0.685	0.003	72.35	0.598	0.573
PL	0.596	0.523	0.669	0.012	40.95	0.549	0.545
PLL	0.575	0.502	0.649	0.047	43.95	0.582	0.564
MTS	0.598	0.526	0.671	0.010	4.95	0.566	0.564
PW	0.607	0.534	0.679	0.005	41.85	0.582	0.582
PFAA	0.657	0.588	0.727	0.000	129.75	0.590	0.609
STA	0.624	0.552	0.695	0.001	132.50	0.623	0.582
STD	0.609	0.536	0.681	0.004	7.15	0.590	0.582
TFA	0.638	0.567	0.710	0.000	1.315	0.607	0.618
TT-TG	0.678	0.609	0.747	0.000	8.15	0.648	0.636
PT	0.591	0.518	0.664	0.016	9.15	0.574	0.564

AUC: Area under the curve, CI: Confidence interval, CA: Congruence angle, LPFA: Lateral patellofemoral angle, PT: Patellar tilt, TT-TG: Tibial tuberosity to trochlear groove distance, TFA: Trochlear facet asymmetry, STD: Sulcus trochlearis depth, STA: Sulcus trochlearis angle, PW: Patella width, LTS: Lateral tibial slope, MTS: Medial tibial slope, MTD: Medial tibial depth, ISI: Insall–Salvati index, PLL: Patellar ligament length, PL: Patellar length, EWI: Eminentia Intercondylaris width index, TW: Tibia width, EIW: Eminentia intercondylaris width, NI: Intercondylar notch index, NSI: Intercondylar notch shape index, NA: Intercondylar notch angle, ND: Intercondylar notch depth, NW: Intercondylar notch width, BW: Bicondylar width, LCW: Lateral condyle width, MCW: Medial condyle width, ACL: Anterior cruciate ligament, WA: Wiberg angle

prone to ACL injuries due to low EIW and thus low ACL volume.[25] In our study, when the study groups were compared with the control group, it was observed that the EIW value was significantly higher in the groups with ACL

injury ($P < 0.05$). It was observed that the EWI value was not significantly different between the groups.

There are not many studies in the literature examining the width of the coronal tibial plateau as a risk factor. Mısır *et al*. in their study, they found the relationship between TW and ACL injuries statistically.[26] In our study, we found that the TW value for the isolated ACL injury group and the ACL and meniscus combined injury group was statistically significantly higher than the control group ($P = 0.014$, $P = 0.003$). We think that it is possible to evaluate it as a risk factor. To support our theory, larger studies examining the relationship between ACL injuries and TW value are required.

Misir *et al*. suggested that the high MTD value can be used to interpret the risk of ACL injury independently of other values.[26] In our study, we did not find a statistically significant difference in terms of MTD between groups.

There are studies in the literature that associate the size of the TT-TG distance with ACL injuries.[27,28] In our study, no significant difference was found in the TT-TG distances of the isolated ACL injuries group. However, when the ACL and meniscus combined injury group were compared with the control group, the TT-TG distance was found to be significantly lower in patients with ACL injuries for the whole group ($P = 0.000$). In the ROC analysis, the limit value was calculated as 8.15.

The patella plays a key role in load transmission in knee joint biomechanics. In the case of patella alta or patella baja can result in deterioration in knee biomechanics.[29] In our study, we used the ISI, which is reported to be the most reliable method to interpret patella location. When all MRIs in our study were examined, no statistically significant difference was observed in the ISI value when looking at the combinations between the groups with ACL injury and the control groups.

Although there are very few studies in the literature that associate PL, PLL, and PW values with ACL and meniscal injuries, Akgün *et al*. in their study, while they found the high ISI and PLL values to be statistically significant as a risk factor in ACL injuries, they reported that they could not find a statistically significant difference in the PL value.[30] Vasconcelos *et al*. stated in their study that the PL value was significantly lower in cases with ACL injury.[31] In our study, PL values in the isolated ACL injury group and ACL and meniscus combined injury group were statistically significantly higher than the control group ($P = 0.006$, $P = 0.007$). When the PLL values were examined in our study; In the ACL and meniscus combined injury group, it was found to be statistically significantly higher than the control group ($P = 0.023$). When the PW values in our study were examined, there was no significant difference between the isolated ACL injuries group and the control group; PW value was found to be statistically significantly higher in the ACL and meniscus combined injury group than in the control group ($P = 0.005$). The high PLL value only in the group accompanied by meniscus showed that this value can be associated with meniscus injuries.

Other parameters used to evaluate patellar instability can be listed as patellar facies articularis angle WA, PT, LPFA, and CA. Vasconcelos *et al*. reported that they found CA values to be statistically significantly higher in the group with ACL injury in their study on X-ray images.[31] There was no statistically significant difference between the groups in CA measurements in our study. In the study from Vasconcelos *et al*., the LPFA value was found to be statistically significantly lower in the group with ACL injury.[31] There was no statistically significant difference between the groups in LPFA measurements in our study. Again, in the study of Vasconcelos *et al*., PT was evaluated and it was found to be significantly lower in cases with ACL injury.[31] In our study, there was no statistically significant difference between the group with isolated ACL injury and the control group in the evaluation made over the measured PE values, while PT in the with ACL and meniscus combined injury group was found to be significantly lower than the control group ($P = 0.016$). In the light of this information, the low PT values in our study support the literature. Since the low PT value in groups accompanied by meniscal injury is a finding that has not been investigated before, it should be supported by larger studies.

Patellar facies articularis angle or WA is also a test used to evaluate patellar instability. WA measurement has not been previously investigated as a predisposing factor for ACL or meniscal injuries. In our study, WA with isolated ACL injury was found to be statistically significantly higher ($P = 0.036$). WA was also found to be significantly higher in the case group compared to the control group ($P = 0.000$). In the ROC analysis, the threshold value was found to be 128.25° for isolated ACL injuries ($P = 0.036$), whereas the threshold value was found to be 129.75° for combined ACL and meniscus injuries ($P = 0.000$). Because it provides patellofemoral harmony in terms of anatomical relationship, sulcus trochlearis and patellar facies articularis structures show key-lock harmony as the opposite faces of the joint. WA measurement is evaluated by many researchers in the literature in terms of ACL and meniscus injuries, and while its increase is associated with an increased risk of ACL injury; there is no data we found other than our current study regarding the relationship of WA value with ACL and meniscus injuries.

Conclusion

In our study, we planned to reveal the risk factors that can be associated with ACL and meniscus injury.

The limitations of our study; that it is retrospective, the body mass index and height information of the individuals

cannot be obtained, the dominant extremity of the individuals is unknown, the subclassification of meniscus injuries cannot be made, and the measurements are made by a single physician. Measured in our study; MCW, LCW, BW, EIW, TW, PL, PLL, WA, and STA values were found to be statistically significantly different in both isolated ACL injury and ACL and meniscus combined injury groups. Again evaluated in our study; NSI, NI, MTS, STD, TFA, TT-TG, and PT values were found to be statistically significantly different in both isolated ACL injury and ACL and meniscus combined injury groups.

Based on our findings, we think that it is possible that the high MTD value can be considered as a risk factor for ACL injuries. To support our hypothesis, larger studies examining the relationship between ACL injuries and MTD value are required. In order to explain more clearly the relationship between the incidence of ACL and meniscus combined injuries, which we showed in our study, and the increase in WA and the PLL, and the decrease in the TT-TG distance and the PT, in the coming years; Large-scale case–control and knee biomechanics studies are needed to examine the risk formation mechanism between ACL and meniscal injuries and these measurements.

We think that by examining these findings in daily clinical practice, individuals can be evaluated whether they are at risk for ACL and meniscus injuries.

Financial support and sponsorship

Nil.

Conflicts of interest

There are no conflicts of interest.

References

1. Arıncı K, Elhan A. Anatomi. 6th ed., Vol. 1. Güneş Tıp Kitabevleri; 2014.
2. Washke J, Tobias M. Böckers, Friedrich Paulsen. Sobotta Anatomi Konu Anlatımı. (Mustafa Fevzi Sargon, ed.). Amsterdam: Elsevier GmbH; 2016.
3. Kwak YH, Nam JH, Koh YG, Park BK, Hong KB, Kang KT. Femoral trochlear morphology is associated with anterior cruciate ligament injury in skeletally immature patients. Knee Surg Sports Traumatol Arthrosc 2020;28:3969-77.
4. Leiprecht J, Mauch F, Huth J, Ambros LP, Best R. Weight-bearing MRI with a knee flexion angle of 20°: A study on additional MRI investigation modalities to support a more accurate understanding of patellofemoral instability. BMC Musculoskelet Disord 2021;22:902.
5. Sebro R, Weintraub S. Knee morphometric and alignment measurements with MR imaging in young adults with central cartilage lesions of the patella and trochlea. Diagn Interv Imaging 2017;98:429-40.
6. Kızılgöz V, Sivrioğlu AK, Ulusoy GR, Aydın H, Karayol SS, Menderes U. Analysis of the risk factors for anterior cruciate ligament injury: An investigation of structural tendencies. Clin Imaging 2018;50:20-30.
7. Stein V, Li L, Guermazi A, Zhang Y, Kent Kwoh C, Eaton CB, *et al.* The relation of femoral notch stenosis to ACL tears in persons with knee osteoarthritis. Osteoarthritis Cartilage 2010;18:192-9.
8. Pfirrmann CW, Zanetti M, Romero J, Hodler J. Femoral trochlear dysplasia: MR findings. Radiology 2000;216:858-64.
9. Choi W, Lee SJ, Oh J, Baek H, Yang J, Shin J, *et al.* Magnetic resonance ımaging of patellofemoral morphometry reveals age and gender variations in the knees of children and adolescents. Diagnostics (Basel) 2021;11:1985.
10. Chen C, Ma Y, Geng B, Tan X, Zhang B, Jayswal CK, *et al.* Intercondylar notch stenosis of knee osteoarthritis and relationship between stenosis and osteoarthritis complicated with anterior cruciate ligament ınjury: A study in MRI. Medicine (Baltimore) 2016;95:e3439.
11. Uhorchak JM, Scoville CR, Williams GN, Arciero RA, St Pierre P, Taylor DC. Risk factors associated with noncontact injury of the anterior cruciate ligament: A prospective four-year evaluation of 859 West point cadets. Am J Sports Med 2003;31:831-42.
12. Dai Y, Yin H, Xu C, Zhang H, Guo A, Diao N. Association of patellofemoral morphology and alignment with the radiographic severity of patellofemoral osteoarthritis. J Orthop Surg Res 2021;16:548.
13. Rahnemai-Azar AA, Abebe ES, Johnson P, Labrum J, Fu FH, Irrgang JJ, *et al*. Increased lateral tibial slope predicts high-grade rotatory knee laxity pre-operatively in ACL reconstruction. Knee Surg Sports Traumatol Arthrosc 2017;25:1170-6.
14. Suprasanna K, Chamala T, Kumar A. Comparison of anatomical risk factors for noncontact anterior cruciate ligament injury using magnetic resonance imaging. J Clin Orthop Trauma 2019;10:143-8.
15. Park JS, Nam DC, Kim DH, Kim HK, Hwang SC. Measurement of knee morphometrics using MRI: A comparative study between ACL-ınjured and non-ınjured knees. Knee Surg Relat Res 2012;24:180-5.
16. Stijak L, Nikolić V, Blagojević Z, Radonjić V, Santrac-Stijak G, Stanković G, *et al*. Influence of morphometric intercondylar notch parameters in ACL ruptures. Acta Chir Iugosl 2006;53:79-83.
17. Cha JH, Lee SH, Shin MJ, Choi BK, Bin SI. Relationship between mucoid hypertrophy of the anterior cruciate ligament (ACL) and morphologic change of the intercondylar notch: MRI and arthroscopy correlation. Skeletal Radiol 2008;37:821-6.
18. Fahim SM, Dhawan T, Jagadeesh N, Ashwathnarayan YP. The relationship of anterior cruciate ligament injuries with MRI based calculation of femoral notch width, notch width index, notch shape – A randomized control study. J Clin Orthop Trauma 2021;17:5-10.
19. Li W, Liang J, Zeng F, Lin B, Liu C, Huang S, *et al*. Anatomic characteristics of the knee influence the risk of suffering an isolated meniscal injury and the risk factors differ between women and men. Knee Surg Sports Traumatol Arthrosc 2021;29:3751-62.
20. Ireland ML, Ballantyne BT, Little K, McClay IS. A radiographic analysis of the relationship between the size and shape of the intercondylar notch and anterior cruciate ligament injury. Knee Surg Sports Traumatol Arthrosc 2001;9:200-5.
21. Isıklar S, Ozdemir ST, Gokalp G. An association between femoral trochlear morphology and non-contact anterior cruciate ligament total rupture: A retrospective MRI study. Skeletal Radiol 2021;50:1441-54.
22. Duran S, Cavusoglu M, Kocadal O, Sakman B. Association between trochlear morphology and chondromalacia patella: An MRI study. Clin Imaging 2017;41:7-10.

23. Chen M, Qin L, Li M, Shen J. Correlation analysis between femoral trochlear dysplasia and anterior cruciate ligament injury based on CT measurement. Quant Imaging Med Surg 2020;10:847-52.
24. Imhoff FB, Comer B, Obopilwe E, Beitzel K, Arciero RA, Mehl JT. Effect of slope and varus correction high tibial osteotomy in the ACL-deficient and ACL-reconstructed knee on kinematics and ACL graft force: A biomechanical analysis. Am J Sports Med 2021;49:410-6.
25. Chandrashekar N, Slauterbeck J, Hashemi J. Sex-based differences in the anthropometric characteristics of the anterior cruciate ligament and its relation to intercondylar notch geometry: A cadaveric study. Am J Sports Med 2005;33:1492-8.
26. Misir A, Sayer G, Uzun E, Guney B, Guney A. Individual and combined anatomic risk factors for the development of an anterior cruciate ligament rupture in men: A multiple factor analysis case-control study. Am J Sports Med 2022;50:433-40.
27. Shen X, Xiao J, Yang Y, Liu T, Chen S, Gao Z, *et al*. Multivariable analysis of anatomic risk factors for anterior cruciate ligament injury in active individuals. Arch Orthop Trauma Surg 2019;139:1277-85.
28. Polat AE, Polat B, Gürpınar T, Sarı E, Çarkçı E, Erler K. Tibial tubercle-trochlear groove (TT-TG) distance is a reliable measurement of increased rotational laxity in the knee with an anterior cruciate ligament injury. Knee 2020;27:1601-7.
29. Biedert RM, Tscholl PM. Patella alta: A comprehensive review of current knowledge. Am J Orthop (Belle Mead NJ) 2017;46:290-300.
30. Akgün AS, Agirman M. Associations between anterior cruciate ligament ınjuries and patella alta and trochlear dysplasia in adults using magnetic resonance Imaging. J Knee Surg 2021;34:1220-6.
31. de Vasconcelos DP, de Paula Mozella A, de Sousa Filho PG, Oliveira GC, de Araújo Barros Cobra HA. Femoropatellar radiographic alterations in cases of anterior cruciate ligament failure. Rev Bras Ortop 2015;50:43-9.

Original Article

Analgesic Effect of Nabuprofen Combined with Ultrasound-guided Rectus Sheath Block on Patients Undergoing Gynecological Single-port Laparoscopic Surgery

Haiqin Lv, Xiaomin Feng, Xiufang Li[1]

Department of Nursing, Henan Vocational College of Nursing, [1]Department of Gynecology, Anyang Cancer Hospital, Anyang, China

Abstract

Objective: The article aims to explore the analgesic effect of nabuprofen combined with ultrasound-guided rectus sheath block (RSB) on patients undergoing gynecological single-port laparoscopic surgery. **Materials and Methods:** This study involved 60 patients hospitalized between August 2021 and September 2022, who underwent elective single-port abdominal surgery for benign gynecological tumors. They were divided into two groups: Group A received intravenous nalbuphine (0.1 mg/kg) 30 min presurgery, while Group B did not. Both the groups underwent ultrasound-guided RSB. Indicators measured included pain hypersensitivity, Numerical Rating Scale (NRS) and Visual Analog Score pain scores at various postoperative intervals, remifentanil dosage, analgesic side effects, and heart rate (HR) and mean arterial pressure (MAP) at multiple surgical stages. **Results:** The pain threshold measured 24 h postsurgery indicates that Group A has a significantly lower threshold than both the preoperative baseline and Group B ($P < 0.05$). In addition, the secondary hyperalgesia area around the incision is significantly larger in Group B compared to Group A ($P < 0.05$). At T1, NRS pain scores significantly differ between the two groups ($P < 0.05$), although both remain below 4, indicating mild-to-moderate pain. No significant difference in postoperative NRS scores is noted at 24 h ($P > 0.05$). MAP and HR comparisons show no significant differences ($P > 0.05$). Group A received lower intraoperative dosages of propofol and remifentanil ($P < 0.05$) and had shorter recovery times than Group C ($P < 0.05$). Group A also used the analgesic pump less frequently than Group B ($P < 0.05$), which had a higher incidence of postoperative adverse reactions ($P < 0.05$). **Conclusion:** Combining nalbuphine and ultrasound-guided rectus sheath nerve block can significantly improve patients' overall pain. Moreover, it can significantly improve their prognosis, reduce the incidence of adverse reactions, and have important clinical application value.

Keywords: *Analgesic effect, gynecological single-port laparoscopic surgery, nalbuphine, ultrasound-guided rectus sheath block*

Introduction

Single-port laparoscopic (SPL) is an advanced laparoscopic technique. This method involves inserting an SPL instrument into the abdominal cavity through a single incision on the patient's navel for surgery.[1] Compared with traditional porous laparoscopy, the surgical incision of SPL is usually located on the navel, and the surgical incision is larger.[2] The postoperative pain is not as good as imagined or even more severe. In addition to abdominal incision pain, laparoscopic surgery also causes damage to the peritoneum and diaphragm due to the injection of a large amount of carbon dioxide into the pneumoperitoneum, resulting in postoperative shoulder and lower back pain for patients.[3] Effectively controlling postoperative pain can reduce patient pain, reduce hospital stay and costs, improve patient satisfaction, and promote the rational allocation of medical resources. With the widespread application of domestic visualization technology in clinical practice, nerve block surgery has become an easy-to-master surgical method. Rectus sheath block (RSB) is an injection of local anesthetic into the rectus abdominis (RA) muscle and its posterior sheath, blocking the T6–T11 subcostal nerve, Somers *et al*. between them to achieve pain relief during abdominal surgery.[4] The abdomen has RA muscle on

How to cite this article: Lv H, Feng X, Li X. Analgesic effect of nabuprofen combined with ultrasound-guided rectus sheath block on patients undergoing gynecological single-port laparoscopic surgery. J Anat Soc India 2025;74:62-72.

Article Info

Received: 20 August 2024
Revised: 20 December 2024
Accepted: 02 January 2025
Available online: 31 March 2025

Address for correspondence:
Dr. Xiaomin Feng, Department of Nursing, Henan Vocational College of Nursing, Anyang 455000, China.
E-mail: vivian_fxm@163.com

Access this article online

Website: https://journals.lww.com/joai

DOI: 10.4103/jasi.jasi_127_24

Quick Response Code:

both sides, 4–5 cm below the navel, and is surrounded by the RA muscle's sheath.[5] The anterior layer is formed by the connection of the outer oblique and RA sheath edge aponeurosis, while the posterior layer is formed through fusing the transverse and oblique aponeurosis. In SPL surgery, RSB can effectively reduce the use of opioids during and after surgery while also preventing adverse reactions caused by excessive drug use.[6] In addition, RSB can effectively alleviate pain in the early stages of surgery, reduce drug absorption rate, and prolong pain relief time.[7] If postoperative pain relief can be done well, it can better promote the postoperative recovery of patients, allowing them to start exercising earlier and prevent the occurrence of diseases such as thrombosis, pulmonary infection, and pulmonary embolism.[8] Patient-controlled intrauterine analgesia (PCIA) is a commonly used analgesic method, often using opioid analgesics. It achieves the rapid and efficient analgesic effects in the short term and has a significant effect on improving postoperative pain in patients undergoing laparoscopic surgery. Recent studies have confirmed that opioid analgesics used in PCIA experience side effects including nausea and respiratory depression as the dosage increases, which poses great difficulties for surgical treatment of patients.[9] Therefore, finding a safe and efficient analgesic method to alleviate postoperative pain in laparoscopic surgery patients and improve postoperative rehabilitation is currently an urgent clinical problem to be solved. Nalbuphine is an opioid drug that can antagonize μ-opioid receptors and exert analgesic effects by activating κ-opioid receptors. Moreover, it can also antagonize μ-opioid receptors and reduce psychological side effects including nausea, vomiting, and skin itching. Moreover, its respiratory inhibitory effect is relatively small, and it has a "capping" effect.[10] Previous studies have confirmed that nalbuphine can alleviate adverse reactions such as skin itching caused by opioid drugs such as morphine and fentanyl and effectively prevent postoperative side effects.[11,12] This study combines preemptive analgesia with ultrasound-guided RA sheath nerve block and explores its clinical application value in gynecological SPL surgery.

Materials and Methods

Research objects

This study was a randomized controlled trial approved by the hospital ethics committee. This study selected 60 patients who were hospitalized from August 2021 to September 2022 and underwent elective single-port abdominal surgery for benign gynecological tumors. A computer-generated randomization table was used to divide the enrolled patients into Group A with 30 cases and Group B with 30 cases. Surgical anesthesiologists performed general anesthesia and ultrasound-guided RSB in the groups. After the surgery, the anesthesia nurse evaluated the surgical effect 24 h after operation in the postanesthesia care unit (PACU) and general ward and provided painkillers as instructed by the doctor. Because anesthesiologists themselves are the operators of surgery, they are fully aware of the patient's grouping situation. However, both the researchers and the patients themselves were double blind in terms of postoperative observation and evaluation of pain.

Group A: Age ranges from 39 to 67 years old, averaged (53.17 ± 5.35); body mass index (BMI) is 18.46–25.15 kg/m^2, averaged (21.91 ± 2.52). The surgical types include single-hole ovarian cyst removal, single-hole salpingectomy, uterine fibroid removal, total hysterectomy, and single-hole adnexectomy. Group B: Age ranges from 20 to 67 years old, averaged (33.98 ± 4.21); BMI is 18.39–25.09 kg/m^2, averaged (21.89 ± 2.54). The surgical types include single-hole ovarian cyst removal, single-hole salpingectomy, uterine fibroid removal, total hysterectomy, and single-hole adnexectomy.

The inclusion criteria for the research subjects are: (1) 18–65 years old; (2) the American Society of Anesthesiologists (ASA) is classified as Grades I–II; (3) BMI is 18–28 kg/m^2; (4) patients who choose to undergo single-hole ovarian cyst removal, laparoscopic uterine fibroid removal, single-hole salpingectomy, total hysterectomy, or single-hole adnexectomy; (5) no chronic pain-related diseases before surgery; and (6) no mental illness, peripheral nervous system disorders, or cognitive-communication disorders. The exclusion criteria are as follows: (1) having abnormal coagulation function or immune system diseases; (2) individuals with other important organ dysfunction; (3) individuals with infection or skin lesions at the puncture site, as well as scar constitution; (4) having a history of long-term use of analgesics; (5) refusing to participate; (6) previously used anticoagulants; (7) suspected of severe adhesion; (8) allergy to local anesthetics; (9) having serious neurological or mental illness; (10) pregnancy or breastfeeding; (11) changing to using traditional laparoscopic surgery; (12) transferring to open surgery; and (13) neural block failure.

Figure 1 shows the inclusion process of patients in this study.

Experimental methods

Main experimental instruments, equipment, and drugs

Figure 2 shows the main instruments and devices used in this study. The pain detection instrument – the von Frey system, developed by American Life Sciences, has replaced the currently used handheld ciliated mechanical stimulation needles (von Frey Hairs). It realizes the detection of pain threshold and pain sensitivity amplitude.[13] In addition, the system can also achieve automatic recording of mechanical pain thresholds, with simple operation, accurate numerical values, compact size, and easy portability. The electronic von Frey used in the early stage of this study

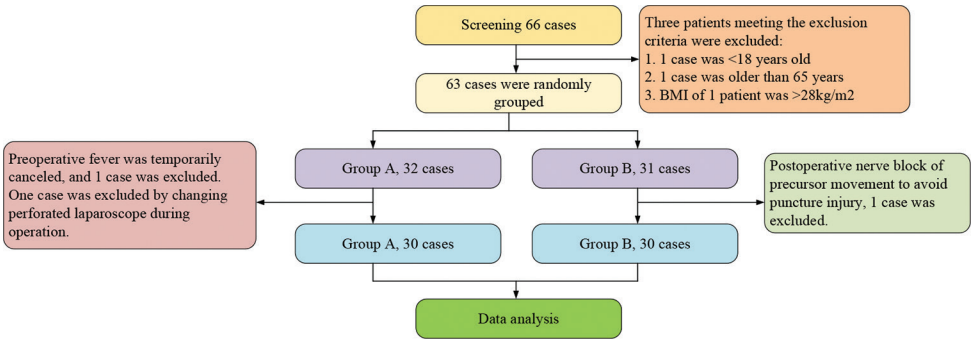

Figure 1: Patient inclusion process

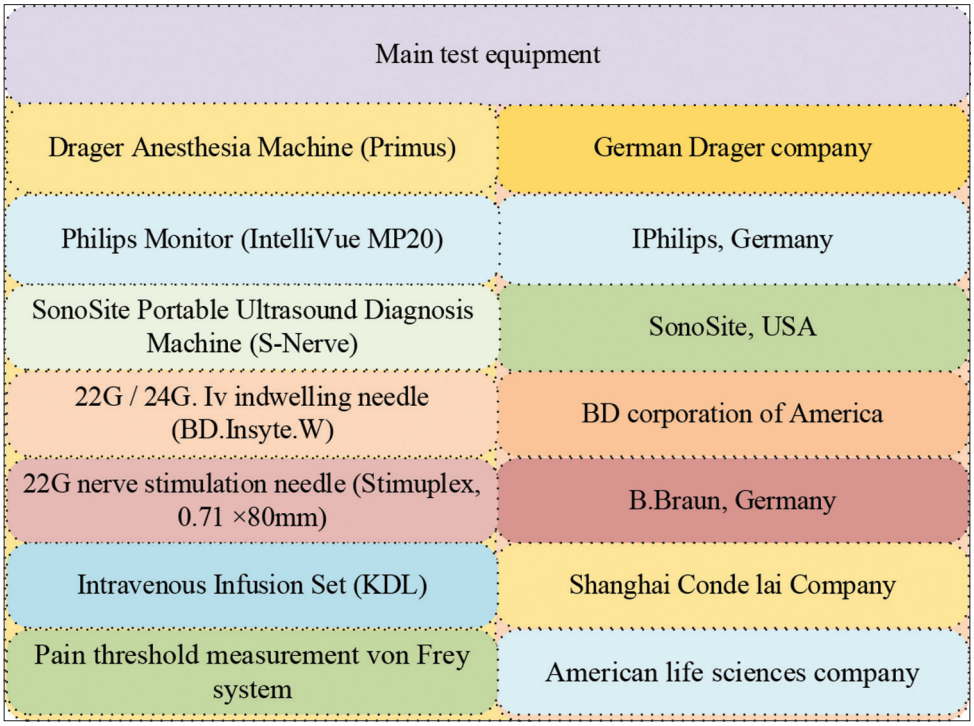

Figure 2: Main instruments and equipment

is a new quantitative method for quantifying mechanical pain thresholds. It has been clinically proven to be faster and more accurate than traditional von Frey Mechanical. mechanical thresholds based on ciliary mechanical stimulation.

Table 1 shows the drugs used in this study.

Analgesic methods for the two groups

Both the groups underwent ultrasound-guided RSB before awakening from anesthesia after postoperative skin suturing. Both the groups of patients underwent SPL anesthesia under local anesthesia and underwent skin suturing before postoperative recovery. After the patient's tracheal intubation was completed, patients were connected to an anesthesia machine for mechanical ventilation. Intravenous infusion of propofol 2.5–4.0 μg/ml, remifentanil 4.0–6.0 ng/ml, and atracurium cisbesylate was administered to stabilize blood pressure and heart rate (HR) within the normal range. Group A received intravenous injection of 0.1 mg/kg nalbuphine 30 min before surgery. Group B did not receive treatment with nalbuphine.

Specific anesthesia processes for the two groups

Anesthesiologists establish venous channels around the patient with informed consent before surgery. Patients were educated on pain scores, and the Numerical Rating Scale (NRS) pain assessment scale was introduced to help them make reasonable and accurate evaluations of their own pain levels.

During the surgery, the patient's electrocardiogram, noninvasive blood pressure, and pulse oxygen saturation were measured. General anesthesia was induced using propofol (2 mg/kg), benzenesulfonate cisatracurium (0.2 mg/kg), and sufentanil (0.2 μg/kg). After tracheal intubation under visual laryngoscope, anesthesia was maintained with sevoflurane.

Table 1: Main experimental drugs

Restoratives	Specification	Approval number	Manufacturer
Propofol injection	10 mL: 100 mg	H20150665	Beijing Fresenius Kabi Pharmaceutical Co., LTD
Flurbiprofen exate injection	5 mL: 50 mg	H20041508	Beijing Tide Pharmaceutical
Sufentanil citrate injection	1 mL: 50 μg	H20054171	Yichang Renfu Pharmaceutical
Remifentanil hydrochloride for injection	1 mg/piece	H20030197	Yichang Renfu Pharmaceutical
Cisatracurium benzosulfonate for injection	10 mg/piece	H20060869	Jiangsu Hengrui Pharmaceuticals Co., LTD
Oxycodone injection	1 mL: 10 mg	H20213987	Beijing Huasu Pharmaceutical Co., LTD
Ondansetron hydrochloride injection	4 mL: 8 mg	H10970064	Qilu Pharmaceutical Co., LTD
Atropine sulfate injection	1 mL: 0.5 mg	H12020382	Tianjin Jinyao Pharmaceutical Co., LTD
Neostigmine methosulfate injection	2 mL: 1 mg	H31022770	Shanghai Xinyi Jinzhu Pharmaceutical Co., LTD
Ropivacaine hydrochloride injection	10 mL: 75 mg	H20140764	AstraZeneca AB, Sweden
Nalbuphine	2 mL: 20 mg	H20130127	Yichang Renfu Pharmaceutical

The combination of sevoflurane (1.8%–2%) and remifentanil (0.1–0.2 μg/kg, adjusted with blood pressure) was administered intravenously to control systolic blood pressure within 20% of baseline. The respiratory parameters were adjusted, and the end-expiratory carbon dioxide concentration was kept between 35 and 45 mmHg. The sevoflurane inhalation bottle and remifentanil injection pump were closed after surgery. Conventional drugs such as neostigmine and atropine were used. The patient's breathing condition, tidal volume, muscle strength, and other conditions were observed. After awakening from general anesthesia, patients were transferred to PACU.

Whether they need emergency analgesia was assessed 0–24 h after surgery. In PACU, when NRS ≥4 and patients needed pain relief, 2–4 mg of oxycodone was given and reexamined until the patient no longer had needs, and the pain score was below 3. In the routine ward, the same method was used to evaluate the patient's pain. Both anesthesia nurses and ward supervisors can use the same method to assess. The need for analgesics was determined based on the Symptom Rating Scale and the patient's needs. When the NRS score was below 4, if necessary, patients were given analgesic drug flurbiprofen axetil 50 mg.

Specific process of ultrasound-guided rectus sheath block

Both the groups underwent ultrasound-guided RSB examination before awakening from anesthesia after postoperative skin suturing. The examination method was to scan along the horizontal direction of the navel with a high-frequency ultrasound probe. The subcutaneous layers were sequentially: anterior sheath of RA, posterior sheath of RA, and anterior sheath of transverse abdominis. The abdominal wall artery was identified using color Doppler mode. The anatomical structure of abdominal muscles is shown in Figure 3.

A plane puncture was performed around the navel, with the needle insertion point 1–2 cm away from the probe and a needle angle of 45°. Starting from the outside to the inside, starting from the outside of RA muscle, it passed through the skin, subcutaneous tissue, and RA muscle in sequence.[14] The puncture point was between the posterior sheath of RA muscle and its line.[8] Usually, drugs are injected on the outer side of RA muscle's posterior sheath. After injection of medication, the RA muscle separated from the posterior sheath of the rectus muscle. 0.375% ropivacaine can also be injected when RA muscle and its posterior sheath are separated.

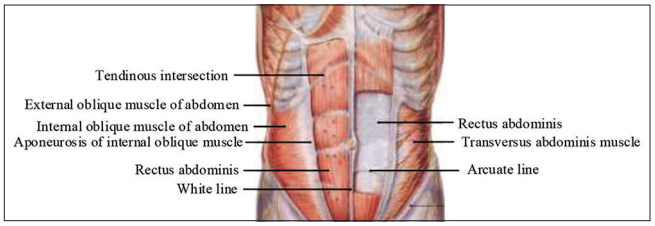

Figure 3: Anatomical structure of abdominal muscles

Testing method for pain hypersensitivity area

One week before surgery, anesthesiologists who were unaware of patient grouping followed up with patients to determine if they met the inclusion criteria. After fully informing the trial items and obtaining the consent of patients and their families, patients signed the informed consent form. A detailed explanation was given to these patients, detailing the steps for detecting mechanical skin pain thresholds. First, it is important to explain the precautions to patients to help them relax and avoid feelings of tension and fear. It should make patients aware of the importance of pain thresholds, so that they can correctly determine the pain threshold.[15] The patient was instructed to take a supine position after surgery, loosen the upper garment and pants, and fully expose the skin of the forearm and forearm during the operation. During the experiment, a pain gauge applied pressure to the navel and right forearm ulnar near the cubital fossa, and patients' response was closely observed.[16] Once the patient feels pain, they will record the value of the pain meter, which is the patient's pain threshold. Three consecutive measurements are conducted at each position to obtain

three stable values. The average value is calculated and recorded.

The area of pain hypersensitivity is tested in the following way: starting from the navel, there are four directions, passing through this center horizontally and vertically. This study uses a force measuring instrument 309 as a reference, from 5 cm from the circle center to the navel point in four directions.[17,18] If the patient does not feel pain, the operator needs to continue moving 0.5 cm toward the center of the navel. The above operations are repeated in the experiment, and the distance from this point to the midpoint of the navel is recorded when the patient reports pain. Such measurements are conducted in all four directions, and the average of these four measurements is obtained, represented by L. The area of pain hypersensitivity defined for this study is 4 L^2 (2 L × 2 L).

Evaluation indicators

The pain scores at 0, 1, 2, 6, 12, and 24 h after operation are observed, as well as the proportion of total pain relief agent dosage and recovery force within 24 h. Intraoperative examinations are performed by the surgical anesthesiologists. The evaluation after surgery is completed by anesthesia nurses who do not know the allocation plan. The postoperative pain score is evaluated using the NRS. Zero stands for "no pain," and 10 means "most severe pain." Patients are allowed to make their own choices and select one number to represent the intensity of pain they are experiencing at that time. A score of 1–3 is relatively mild and can be tolerated, indicating patients' sleep will not be disturbed, and their daily life can also proceed normally. A score of 4–6 stands for that the patient's pain is unbearable and can cause some disturbance to their sleep. At this time, painkillers should be used for pain relief. A score of 7–10 is a very serious pain, indicating that the pain is severe, and it is difficult to relieve sleep, requiring the use of painkillers.[19] Postoperatively, the dosage of remifentanil, the side effects of analgesics, the time of first exhaust, the time of first ambulation, the length of hospital stay, and expenses are recorded. Analgesics' side effects include dizziness, sedation, respiratory depression, nausea, and vomiting. Meanwhile, this study evaluates complications related to RSB, including intestinal perforation, abdominal hematoma, and systemic toxic reactions to local anesthetics.

In postoperative pain assessment, the Visual Analog Score (VAS) was used to score the patient's pain sensation at rest and during coughing at 2, 6, 12, and 24 h postoperatively on a scale of 0–10. Zero stands for no pain, while 10 stands for unbearable severe pain. The HR and mean arterial pressure (MAP) of the patient are evaluated before skin cutting (t1), during skin cutting (t2), after laparoscopic lens fixation (t3), at the end of the surgery (t4), and when transferring to PACU (t5).

Processing and analysis of the experimental data

The statistical software used is SPSS 25.0 (IBM, Armonk, New York, USA). The Shapiro–Wilk test is used to test the normality of quantitative data. Quantitative data that conform to a normal distribution are represented as mean ± standard deviation, and two independent sample *t*-tests are used for intergroup comparison. Nonnormally distributed quantitative data are represented by median and interquartile intervals, and rank sum tests are used for intergroup comparison. Count data are expressed in frequency and compared between the groups using Chi-square test or Fisher's exact probability method. Two sets of repeated measurement data are compared between the groups using two-factor repeated measurement analysis of variance, and the intergroup effects are calculated. $P < 0.05$ indicates statistical significance.

Results

General information

From Table 2, the general information of the two groups had no significant difference, including age, BMI, ASA grading, and education. The comparison of preoperative and intraoperative time between these two groups showed $P > 0.05$.

Comparison of mechanical pain thresholds before surgery and pain sensitive area around the incision site 24 h after surgery

In Figure 4a, the comparison of basic mechanical pain thresholds on the medial forearm and around the incision of the two groups before surgery showed $P > 0.05$. However, the pain threshold measured 24 h after surgery showed that Group A was significantly lower than the preoperative baseline value and Group B ($P < 0.05$). In Figure 4b, Group B had a higher mechanical pain threshold on the inner forearm and around the incision 24 h after surgery than Group A ($P < 0.05$). In Figure 4c, for the comparison of the area of secondary hyperalgesia that occurred around the incision 2 h after surgery, Group B had a significantly larger

Table 2: General data of these two groups

Comparison item	A (*n*=30)	B (*n*=30)
Age (years), $\bar{x}\pm s$	53.17±5.35	33.98±4.21
BMI (kg/m^2), $\bar{x}\pm s$	21.91±2.52	21.89±2.54
ASA classification (%)		
Class I	65.49	69.99
Class II	34.51	30.01
Educational level (%)		
Primary school and below	10.29	16.69
Secondary school	48.29	56.69
University or above	41.42	26.7
Entry time (min), $\bar{x}\pm s$	148.12±44.47	162.89±43.48
Operation duration (min), $\bar{x}\pm s$	101.19±41.29	117.31±40.11

BMI: Body mass index, ASA: American Society of Anesthesiologists

area ($P < 0.05$). Moreover, the area of pain hypersensitivity 24 h after surgery was also larger ($P < 0.05$).

Comparison of postoperative pain scores between the two groups

From Table 3, Groups A and B had only a significant difference in NRS pain scores at T1 after surgery ($P < 0.05$). However, both the groups were below 4 points and only had mild-or-moderate pain. The postoperative NRS pain score at 24 h compared to Group B showed $P > 0.05$.

From Figure 5, around the incision after surgery, Groups A and B showed $P < 0.05$ in the duration of pain, while others showed $P > 0.05$.

Comparison of intraoperative and postoperative vital signs

From Table 4, the comparison of MAP and HR between these two groups at various time points during and after operation showed $P > 0.05$.

Table 3: Comparison of pain scores 24 h after surgery (score, $\bar{x}\pm s$)

Time	Pain score		*P*
	A (*n*=30)	B (*n*=30)	
T_1 (0 h)	2.07±0.88	2.71±0.94	0.012
T_2 (1 h)	1.89±0.65	2.05±0.81	0.066
T_3 (2 h)	1.75±1.01	1.62±0.62	0.051
T_4 (6 h)	1.45±0.66	1.56±0.71	0.071
T_5 (12 h)	1.66±1.31	1.64±1.01	0.055
T_6 (24 h)	1.11±0.51	1.34±0.44	0.063

Comparison of postoperative pain levels at different time points

Table 5 shows the overall analysis results. The comparison of VAS score time, intergroup, and interaction between these two groups during rest and cough showed $P < 0.05$. Group A had lower VAS scores at rest and during coughing at 2, 6, 12, and 24 h after surgery than Group B ($P < 0.05$). The VAS scores at rest and cough at 6, 12, and 24 h after surgery in both the groups were lower than those at 2 h after operation in the same group ($P < 0.05$). Both the groups had lower VAS scores at rest and cough at 12 and 24 h after operation than those at 6 h after operation in the same group ($P < 0.05$). Both the groups had lower VAS scores at rest and cough 24 h after operation compared to the same group at 12 h after surgery ($P < 0.05$).

Comparison of intraoperative anesthetic and analgesic dosage between the two groups

In Figure 6, Group A had lower intraoperative dosage of propofol and remifentanil than Group B ($P < 0.05$).

Comparison of postoperative spontaneous breathing recovering time, recovering time, extubating time, and number of self-control times of analgesic pumps within 24 h between the two groups

In Table 6, Group A had shorter postoperative spontaneous breathing recovery time, awakening time, and extubation time compared to Group B. It had fewer self-control times with the analgesic pump within 24 h compared to Group B ($P < 0.05$).

Table 4: Comparison of vital signs between the two groups (score, $\bar{x}\pm s$)

Time	MAP			HR		
	A (*n*=30)	B (*n*=30)	*P*	A (*n*=30)	B (*n*=30)	*P*
t1	71.79±3.79	72.39±3.88	0.051	98.19±4.06	97.48±3.88	0.081
t2	72.99±3.88	75.89±4.99	0.067	107.29±4.77	109.78±4.58	0.123
t3	73.28±3.88	73.07±4.06	0.054	110.39±3.19	107.99±4.29	0.111
t4	72.69±5.11	74.09±5.49	0.055	103.78±3.77	104.39±4.29	0.053
t5	71.78±4.51	72.19±3.79	0.074	95.19±4.59	96.06±4.69	0.178

HR: Heart rate, MAP: Mean arterial pressure

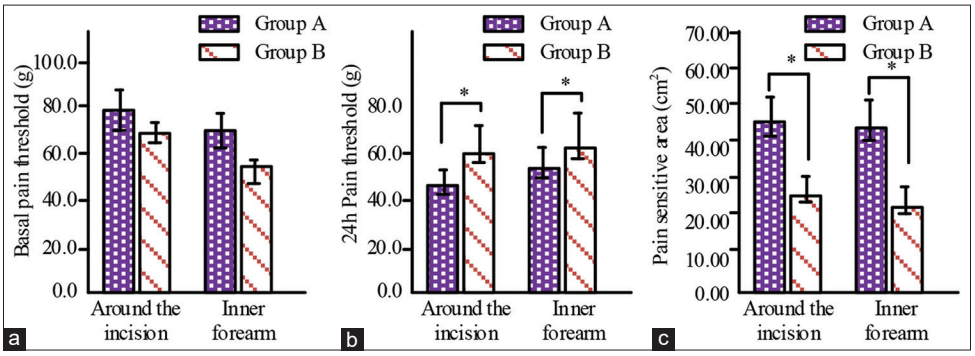

Figure 4: Comparison of the mechanical pain area before surgery and the pain sensitive area around the incision 24 h after surgery. (a) Comparison of preoperative baseline pain thresholds. (b) Comparison of 24 h postoperative pain thresholds. (c) Comparison of sensitive area 24 h after surgery

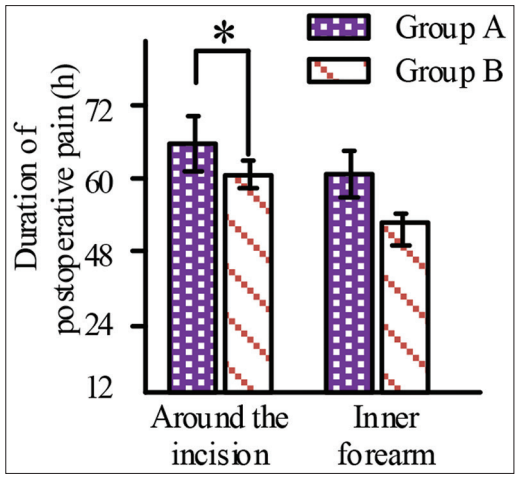

Figure 5: Comparison of postoperative pain duration

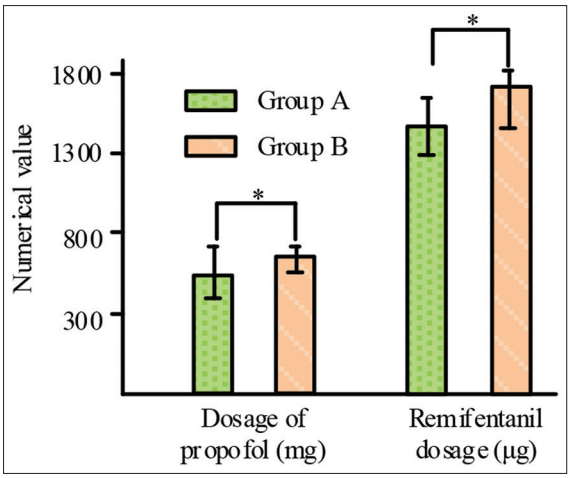

Figure 6: Comparison of intraoperative anesthetic and analgesic drug dosage between the two groups

Table 5: Comparison of postoperative pain at different time points (score, $\bar{x}\pm s$)

Group	VAS score at rest	VAS score during coughing
Group A (n=30)		
2 h postoperatively	2.30±0.47[d]	4.13±0.87[d]
6 h postoperatively	2.15±0.39[a,d]	3.67±0.75[a,d]
12 h postoperatively	2.04±0.41[a,b,d]	3.31±0.49[a,b,d]
24 h postoperatively	1.83±0.35[a,b,c,d]	2.93±0.51[a,b,c,d]
Group B (n=30)		
2 h postoperatively	3.15±0.55	5.78±0.95
6 h postoperatively	2.71±0.51[a]	4.59±0.79[a]
12 h postoperatively	2.59±0.39[a,b]	4.21±0.63[a,b]
24 h postoperatively	2.45±0.35[a,b,c]	3.71±0.55[a,b,c]
F_{time}, P_{time}	35.179, 0.023	28.159, 0.013
$F_{interclass}$, $P_{interclass}$	26.681, 0.021	30.249, 0.021
$F_{interaction}$, $P_{interaction}$	40.249, 0.012	20.123, 0.016

Compared with 2 h after surgery in this group, [a]P<0.05; Compared with 6 h after surgery in this group, [b]P<0.05; Compared with 12 h after surgery in this group, [c]P<0.05; Compared with the same period in Group B, [d]P<0.05. VAS: Visual Analog Score

Comparison of satisfaction with the cut esthetic appearance of the two groups

In Table 7, the umbilical intradermal suture method has the advantage that the incision is easily covered by skin wrinkles. Its esthetic comparison showed $P > 0.05$. After a 3-month follow-up, there were no incisional hernias or infections.

Incidence of adverse reactions in the two groups

In Table 8, 13 patients experienced postoperative nausea and vomiting. Six patients experienced postoperative drowsiness and dizziness. Eleven patients experienced postoperative chills. No occurrence of skin itching was observed. Group B had significantly higher incidence of postoperative nausea and vomiting than Group A ($P < 0.05$). Comparing with Group A, the incidence of postoperative chills in Group B was significantly increased ($P < 0.05$). In addition, neither group experienced any other complications of nerve block such as abdominal puncture or local anesthesia poisoning.

Index correlation analysis

Figure 7 shows the correlation between patient spontaneous breathing recovering time, awakening time, extubating time, number of analgesia pump self-control times, MAP, HR, and BMI, and there was no direct correlation.

Figure 8 shows the correlation between patient spontaneous breathing recovering time, awakening time, extubating time, number of analgesia pump self-control times, MAP, HR, NRS, and VAS. The number of self-controlled analgesia pumps, MAP, and HR all showed a positive correlation with NRS ($r = 0.641$, $P = 0.02$; $r = 0.641$, $P = 0.02$; and $r = 0.608$, $P = 0.04$) and a positive correlation with VAS ($r = 0.598$, $P = 0.03$; $r = 0.596$, $P = 0.02$; and $r = 0.635$, $P = 0.04$). However, the other three indicators have no direct correlation with NRS and VAS.

Discussion

Pain is known as the "fifth vital sign," which is a complex emotional experience and a major challenge in medical work.[20,21] The postoperative pain not only causes subjective pain in patients but may also have an impact on multiple systems such as cardiovascular, cerebrovascular, respiratory, and digestive systems.[22,23] A large clinical study in the United States shows that most patients experience moderate-to-severe pain after surgery.[24] In recent years, the effectiveness of various analgesic therapies has not been ideal, and improving pain management is still an important issue faced by clinical doctors.[25] Therefore, for the understanding and treatment of pain, scientific research and clinical practice need to be promoted simultaneously to provide patients with better pain management plans. SPL surgery is a minimally invasive surgical method that involves inserting instruments into the abdominal cavity through a single-needle insertion point, leaving only a small

scar after the surgery.[26] Although this surgery has been widely used in clinical practice due to its advantages of rapid recovery and scarless appearance, the surgical incision is larger and the pain is also greater.[27] Postoperative pain mainly originates from surgical wound pain, intraoperative inhalation pulling on the diaphragm and peritoneum, as well as abdominal pain caused by the uterus, ovaries, and other factors. At present, there is no specific gold standard for pain relief in SPL surgery. The main methods include intravenous analgesia, transverse abdominal nerve block, incision local anesthesia, and RSB. Multimodal pain relief typically involves two or more methods to achieve optimal analgesic effects. With the widespread application of domestic visualization technology, ultrasound-guided nerve blockade surgery, especially RSB surgery, has become a safe and reliable analgesic method. RSB can effectively block the ventral branch of the 7–12 intercostal nerve, relieving pain from the median incision. RSB is mainly used to relieve physical pain, but it cannot alleviate visceral pain. Multimodal anesthesia combined with intraperitoneal injection of anesthesia has been proven to significantly reduce pain scores within 24 h after surgery and alleviate

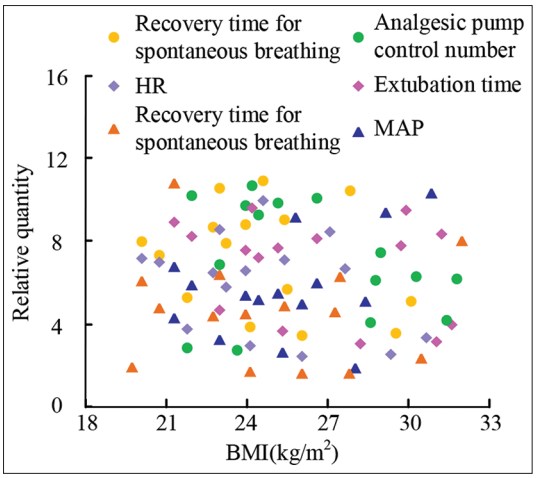

Figure 7: Correlation degree of patients' spontaneous breathing recovering time, wake time, extubating time, number of analgesic pump self-control, mean arterial pressure, heart rate, and body mass index

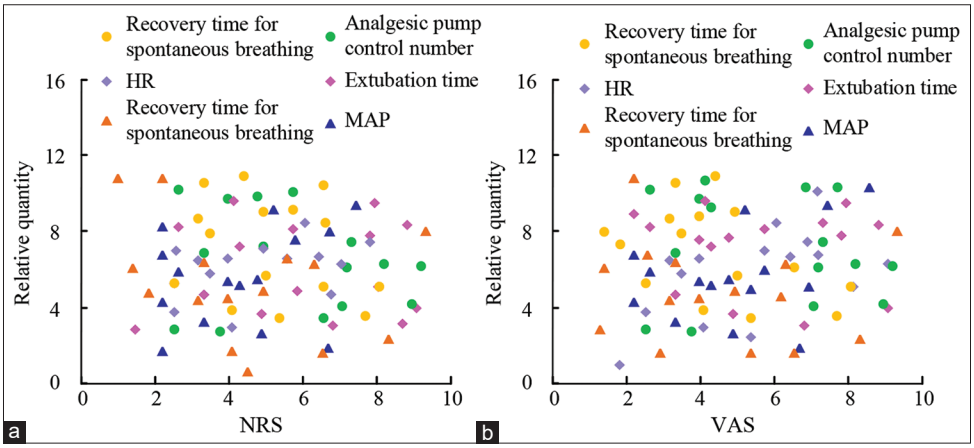

Figure 8: Correlation degree of patients' spontaneous respiration recovering time, wake time, extubating time, number of analgesic pump self-control, mean arterial pressure, heart rate, Numerical Rating Scale, and Visual Analog Score. (a) NRS. (b) VAS

Table 6: Comparison results of postoperative recovering time of spontaneous respiration, recovering time, extubating time, and the number of self-controlled analgesic pump in 24 h between the two groups ($\bar{x}\pm s$)

Group	Recovering time for spontaneous respiration (min)	Recovering time (min)	Extubating time (min)	Number of analgesic pump control within 24 h (times)
Group A (n=30)	4.81±0.77	3.49±0.71	5.91±0.69	15.29±3.99
Group B (n=30)	5.71±0.91	4.16±0.69	7.23±0.79	35.58±6.18
t	6.576	5.139	9.410	27.399
P	0.012	0.023	0.025	0.011

Table 7: Comparison results of esthetic satisfaction with knife edge between the two groups

Group	Very satisfied (percentage of cases)	Satisfactory (percentage of cases)	General satisfaction (percentage of cases)	Less satisfied (percentage of cases)	Very dissatisfied (percentage of cases)	Satisfaction (%)
Group A (n=30)	15 (50.00)	7 (23.33)	6 (20.00)	2 (6.67)	0	93.33
Group B (n=30)	13 (43.33)	8 (26.67)	6 (20.00)	3 (10.00)	1 (3.33)	90.00
χ^2	/	/	/	/	/	9.211
P	/	/	/	/	/	0.051

Table 8: Comparison of the incidence of postoperative adverse reactions (%)

Group	Shiver, *n* (%)	Nausea and vomiting, *n* (%)	Lethargy and dizziness, *n* (%)	Pruritus
A (*n*=30)	3 (10.00)	4 (13.33)	2 (6.67)	0
B (*n*=30)	8 (26.67)	9 (30.00)	4 (13.33)	0
χ^2	9.867	8.21	0.821	/
P	0.021	0.043	0.056	/

adverse reactions such as patient pain and respiratory forgetting.[28]

At present, opioid drugs are still the main means of clinical treatment for acute and chronic pain. However, recent studies have found that opioid drugs can also cause opioid-induced hyperalgesia (OIH). OIH refers to the decrease in pain threshold and high sensitivity to common pain in patients after exposure to such drugs. Toscano *et al*. confirmed that 0.2–0.3 mg/kg of nalbuphine could alleviate the postoperative analgesic effect of remifentanil and had a certain improvement effect on symptoms such as nausea, vomiting, and chills after general anesthesia with remifentanil.[29] In this study, the time for administering the first analgesic dose after surgery was significantly shorter in Group A than in Group B, indicating a statistically significant difference. This means that Group A patients experience a high degree of pain hypersensitivity shortly after surgery, and their pain sensitivity is significantly higher than that of Group B. This may be due to the nervous system response caused by pain stimulation, making it more sensitive to pain. Within 24 h after surgery, the pain threshold in the medial forearm and surgical incision area of Group B patients was significantly higher than Group A ($P < 0.05$). This discovery indicates that infusion of remifentanil leads to significant pain hypersensitivity effects. This may be due to the impact of remifentanil on the nervous system, which enhances the patient's perception of pain. Meanwhile, the combination of nalbuphine and ultrasound-guided RSB can have a synergistic effect, further reducing the postoperative pain hypersensitivity compared to using ultrasound-guided RSB alone. This may be due to the simultaneous action of nabuprofen and ultrasound-guided RSB on the nervous system, which can more effectively block the transmission of pain signals, thereby reducing the degree of postoperative pain hypersensitivity. This result indicates that the combination of nalbuphine and ultrasound-guided RSB can effectively reduce postoperative pain sensitivity, increase patient pain threshold, and reduce the occurrence of postoperative pain. This study found that patients using naborphanine combined with ultrasound-guided RSB had a significantly reduced area of secondary hyperalgesia caused by remifentanil after surgery compared to Group B. This indicates that this combination therapy regimen can effectively reduce the range of pain impact and alleviate the patient's pain perception. Compared with Group B, patients who used naborphanine combined with ultrasound-guided RSB also showed a significant reduction in postoperative sufentanil use. This means that the patient's dependence on additional analgesics is reduced during postoperative recovery, which is beneficial for their recovery. In addition, compared with Group B, the area of secondary hyperalgesia induced by remifentanil in Group A after surgery was significantly reduced, which was statistically significant. This means that in Group A, the range of pain perception caused by remifentanil is more limited, which helps to alleviate postoperative pain in patients. The above experiments indicate that nalbuphine can alleviate remifentanil-induced hyperalgesia, and ultrasound-guided RSB by nalbuphine may have a synergistic effect on remifentanil-induced hyperalgesia.

Overall, the time, intergroup, and interaction effects of VAS scoring indicators had significant differences at rest and during coughing. Group A had lower VAS score at rest than Group B at 2, 6, 12, and 24 h after operation ($P < 0.05$). The VAS scores at rest at 6, 12, and 24 h after surgery were lower than the controlling groups, and these VAS scores significantly decreased during coughing ($P < 0.05$). These scores at rest and cough at 12 and 24 h after operation in both the groups were lower than those at 6 h after surgery in this group ($P < 0.05$). Both the groups had lower VAS scores at rest and cough 24 h after operation compared to the group at 12 h after surgery ($P < 0.05$). In this study, Group A had lower intraoperative propofol and remifentanil usage and shorter postoperative spontaneous breathing recovering time, awakening time, and extubating time. Its overall incidence of adverse reactions was lower than that of Group B. These findings confirm that the analgesic regimen of nabuprofen combined with ultrasound-guided RSB not only reduces postoperative pain in patients but also reduces the dosage and adverse reactions of opioid analgesics.

Therefore, the combination of nalbuphine and ultrasound-guided RA sheath nerve block can significantly improve the overall pain of patients. Moreover, this can significantly improve the prognosis of patients, reduce the incidence of adverse reactions, and has important clinical application value. However, the limitation of this study is that the sample size is small, which may affect the results accuracy. In the future, more large-scale and diverse studies are needed to verify the effectiveness of this treatment plan.

Availability of data and materials

The datasets used and/or analyzed during the current study available from the corresponding author on reasonable request.

Ethics approval and consent to participate

Informed consent was obtained from all individual participants included in the study. Study approval statement: This study protocol was reviewed and approved by

Affiliated Henan Vocational College of Nursing. Consent to participate statement: Informed consent was obtained from participants (or their parent/legal guardian/next of kin) to participate in the study.

Financial support and sponsorship

Nil.

Conflicts of interest

There are no conflicts of interest.

References

1. Yu P, Zhang J, Wang J. Nalbuphine for spinal anesthesia: A systematic review and meta-analysis. Pain Pract 2022;22:91-106.
2. Liu X, Hu J, Hu X, Li R, Li Y, Wong G, *et al.* Preemptive intravenous nalbuphine for the treatment of post-operative visceral pain: A multicenter, double-blind, placebo-controlled, randomized clinical trial. Pain Ther 2021;10:1155-69.
3. Weisshaar E, Szepietowski JC, Bernhard JD, Hait H, Legat FJ, Nattkemper L, *et al.* Efficacy and safety of oral nalbuphine extended release in prurigo nodularis: Results of a phase 2 randomized controlled trial with an open-label extension phase. J Eur Acad Dermatol Venereol 2022;36:453-61.
4. Somers LN, Jackson DH, Dugger KM, Burco JD. A mixture of nalbuphine, azaperone, and medetomidine for immobilizing ringtails (*Bassariscus astutus*). J Wildl Dis 2023;59:610-5.
5. Schoppmann S, Spiess D, Müller D, Burch A, Zimmermann R, Simões-Wüst AP. Nalbuphine: A candidate for treatment of women overwhelmed with sudden, intense labor pain? J Matern Fetal Neonatal Med 2022;35:6112-4.
6. Leister N, Trieschmann U, Yücetepe S, Ulrichs C, Muenke N, Wendt S, *et al.* Nalbuphine as analgesic in preschool children undergoing ophthalmic surgery and the occurrence of emergence delirium. Br J Ophthalmol 2023;107:1522-5.
7. Nair A, Dudhedia U, Rangaiah M, Panchawagh S. Efficacy of intravenous nalbuphine for managing post-anaesthesia shivering: A systematic review and meta-analysis of randomised controlled trials with trial sequential analysis. Indian J Anaesth 2023;67:853-65.
8. Ienello L, Kennedy M, Wendt-Hornickle E, Baldo C, Moshnikova V, Guedes A. Ultrasound-guided rectus sheath block injections in miniature swine cadavers: Technique description and distribution of two injectate volumes. Vet Anaesth Analg 2022;49:210-8.
9. He K, Ji W, Zhao H, Wei Y, Yang S, Wen Q. Pharmacokinetic comparison of nalbuphine with single injection and patient-controlled analgesia mimic method in healthy Chinese volunteers. J Clin Pharm Ther 2021;46:1166-72.
10. Lee JH, Cho SH, Eoh KJ, Lee JY, Nam EJ, Kim S, *et al.* Effect of bupivacaine versus lidocaine local anesthesia on postoperative pain reduction in single-port access laparoscopic adnexal surgery using propensity score matching. Obstet Gynecol Sci 2020;63:363-9.
11. Seo JW, Lee IO, Kim JC, Chung JE. The role of port site local anesthetic injection in laparoendoscopic single site surgery: A prospective randomized study. Obstet Gynecol Sci 2020;63:387-94.
12. Ramy MS, Fatma AA. Ultrasound-guided oblique subcostal transversus abdominis plane block versus erector spinae plane block as pre-emptive analgesia for open umbilical hernia repair: A comparative, randomized, double-blinded clinical trial. Int J Surg 2022;41:934-9.
13. Shim JW, Jung S, Moon HW, Lee JY, Park J, Lee HM, *et al.* Rectus sheath block for acute pain management after robot-assisted prostatectomy. Asian J Surg 2022;45:1843-8.
14. Ferreira TH, Schroeder CA, St James M, Hershberger-Braker KL. Description of an ultrasound-guided rectus sheath block injection technique and the spread of dye in calf cadavers. Vet Anaesth Analg 2022;49:203-9.
15. Yamamoto T, Seino Y, Matsuda K, Imai H, Bamba K, Sugimoto A, *et al.* Preoperative implementation of transverse thoracic muscle plane block and rectus sheath block combination for pediatric cardiac surgery. J Cardiothorac Vasc Anesth 2020;34:3367-72.
16. Tan S, Chen W, Liu Y, Wei L. Combination of ultrasound-guided serratus anterior plane block and rectus sheath block provide analgesia for open hepatectomy: A report on 3 cases. Am J Med Case Rep 2022;10:68-71.
17. Esmende SM, Solomito MJ, Eisler J, Finkel KJ, Kainkaryam PP, Maffeo-Mitchell CL. Utility of the transversus abdominis plane and rectus sheath blocks in patients undergoing anterior lumbar interbody fusions. Spine J 2022;22:1660-5.
18. Onishi E, Saito K, Kumagai M, Oba R, Murakami T, Sugino S, *et al.* Evaluation of contrast-enhanced ultrasonography with Sonazoid(®) in visualization of local anesthetic distribution in rectus sheath block: A prospective, clinical study. J Anesth 2022;36:405-12.
19. Liu X, Gao J, Wang J, You J, Chu J, Jin Z. Esthetics effect and the modified placement of robotic-assisted single-site laparoscopic gynecologic surgery by common robotic instruments and LAGIS single-site port. J Invest Surg 2022;35:434-9.
20. Zhang Y, Zhu Y. Comparison of conventional versus single port laparoscopy for surgical treatment of gynecological diseases: A pilot study. Wideochir Inne Tech Maloinwazyjne 2022;17:252-60.
21. Wong JM, Moore KJ, Carey ET. Investigation of the association between surgeon sex and laparoscopic device ergonomic strain in gynecologic surgery. J Minim Invasive Gynecol 2022;29:984-91.
22. Wong JM, Moore KJ, Lewis P, Reid M, Saul K, Carey ET. Ergonomic assessment of surgeon characteristics and laparoscopic device strain in gynecologic surgery. J Minim Invasive Gynecol 2022;29:1357-63.
23. Vanderbecq Q, Gregory J, Dana J, Burgio M D, Garzelli L, Raynaud L, *et al*. Improving pain control during transarterial chemoembolization for hepatocellular carcinoma performed under local anesthesia with multimodal analgesia. Diagn Interv Imag 2023;104:123-132.
24. Bhatia U, Mona P, Shyni A, Shah C. Ultrasound guided bilateral rectus sheath block for post operative analgesia in patients undergoing umbilical surgeries under GA, A comparative study between bupivacaine, levobupivacaine and ropivacaine. Anaesthesia 2020;7:32-8.
25. Copperthwaite A, Sahebally SM, Raza ZM, Devane L, McCawley N, Kearney D, *et al*. A meta-analysis of laparoscopic versus ultrasound-guided transversus abdominis plane block in laparoscopic colorectal surgery. Ir J Med Sci 2023;192:795-803.
26. Shi X, Chen S, Yang Y, Liu L, Huang L. Laparoscopic surgeries for uterine fibroids and ovarian cysts reduce ovarian reserve via age- and surgical type-manner. Gynecol Endocrinol 2022;38:1068-72.
27. Dornelas RS, Lima DA. Correlation filters in machine learning algorithms to select de-mographic and individual features for autism spectrum disorder diagnosis. JDSIS 2023;3:7-9.
28. Zanolli NC, Fuller ME, Krishnamoorthy V, Ohnuma T,

Raghunathan K, Habib AS. Opioid-sparing multimodal analgesia use after cesarean delivery under general anesthesia: A retrospective cohort study in 729 US Hospitals. Anesth Analg 2023;1372:256-66.

29. Toscano A, Capuano P, Attisani M, Rinaldi M, Brazzi L. Transversus thoracic plane block and rectus sheath block for left ventricular assist device implantation via full median sternotomy: A case report. J Card Surg 2022;37:2115-9.

Case Report

Variations in Coronary Arteries: A Rare Case Report

Anjali Singal, Anju Choudhary, Priti Chaudhary

Department of Anatomy, All India Institute of Medical Sciences, Bathinda, Punjab, India

Abstract

Cardiomegaly with variations in coronary arteries has rarely been reported. We report a case of an enlarged heart noticed during routine dissection. The weight of the heart was 600 g; the length, breadth, and thickness of the heart were 15.1, 10.4, and 7.7 cm respectively. The ventricular walls and interventricular walls were thicker than normal. There was a separate ostium for the right conus branch in Valsalva's right sinus along with a short main trunk of the left coronary artery (LCA); 2 mm and trifurcation of the LCA. It is important to report such cases, as an enlarged heart poses a risk for heart complications, and the use of advanced image diagnostic and interventional techniques is required, which demand in-depth knowledge of the typical and atypical coronary anatomy.

Keywords: *Cardiomegaly, conus branch, coronary artery, separate ostium, trifurcation*

Introduction

Cardiomegaly represents an enlargement of the heart either due to myocardial hypertrophy, chamber dilatation, or both.[1] The large size of the heart on visual judgment, the increased transverse and vertical diameter, and the weight of the heart are indicative of cardiomegaly.[2] Diagnosis is chiefly through a chest X-ray, a cardiothoracic ratio (CTR) of more than 0.5 suggests cardiomegaly.[3] It is considered a frequent cause of sudden cardiac death in adults.[4] Different processes may result in the development of cardiac hypertrophy, some may be physiological responses, and others develop due to some pathologic etiology.[5] Cardiomegaly is well reported in the literature; however, cardiomegaly with variations in coronary arteries has rarely been, as per the best literature search. In the present cadaveric case, an enlarged heart with more than normal weight, size, and ventricular wall thickness along with variations of coronary arteries has been stated. The information about the coronary artery variations in an enlarged heart will be of use to cardiologists.

Case Report

During the routine dissection of a 69-year-old male cadaver, when the anterior thoracic wall was dissected, the large size of the heart was noticed. The cause of death was reported as cardiac arrest and congestive heart failure and the records revealed that he was hypertensive. After opening the pericardial cavity, great vessels were cut and the heart was removed. It was washed thoroughly and squeezed properly to remove blood. The different parameters were measured using Digital Vernier Caliper (Milotoya, Japan, 0.02 mm), measuring tape. The heart was thoroughly examined and photographed. The coronary vessels were dissected and variations were noticed.

The following observations were made [Figure 1a and b]:

a. Weight of heart-600 g
b. CTR [Figure 1b] a = 4 cm, b = 8 cm, c = 19 cm; CTR (a + b/c) =0.63
c. Length of heart - 15.1 cm
d. Thickness of heart - 7.7 cm
e. Breadth/transverse size of heart - 10.4 cm
f. Length of ventricle from posterior aspect/longitudinal size - 8.9 cm
g. Right ventricle-wall thickness - 0.97 cm
h. Left ventricle-wall thickness - 1.9 cm
i. Interventricular wall thickness - 1.8 cm.

Variations in coronary arteries [Figure 1c and d]:

a. Separate ostium for the right conus branch that originated directly from Valsalva's right sinus along with the right coronary artery

How to cite this article: Singal A, Choudhary A, Chaudhary P. Variations in coronary arteries: A rare case report. J Anat Soc India 2025;74:73-5.

Article Info

Received: 14 May 2024
Accepted: 11 August 2024
Available online: 20 September 2024

Address for correspondence:
Dr. Anjali Singal, Department of Anatomy, All India Institute of Medical Sciences, Bathinda - 151 001, Punjab, India.
E-mail: anjali_singal@rediffmail.com

Access this article online

Website: https://journals.lww.com/joai
DOI: 10.4103/jasi.jasi_35_24
Quick Response Code:

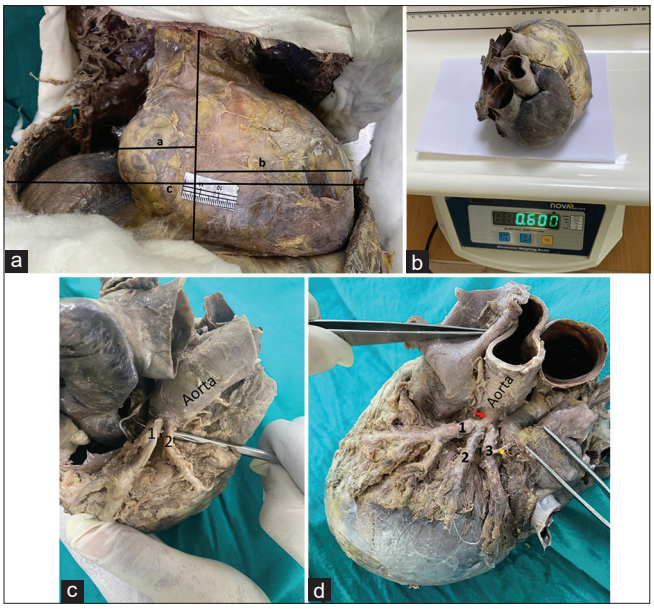

Figure 1: (a) Heart *in situ* showing measurement of different parameters for cardiothoracic ratio a + b/c (0.63). a: horizontal line from most convex point on the right side of the midline; b: horizontal line from a most convex point on the left side of the midline; c: maximum width of thorax, (b) weight of the heart in grams (600) using an electronic weighing machine, (c) two separate branches that originated directly from Valsalva's right sinus of aorta (1) Right coronary artery; (2) The right conus branch, (d) trifurcation of left coronary artery into (1) Left anterior descending; (2) Ramus intermedius; (3) Circumflex branch, and the short main trunk of left coronary artery with a length of 2 mm (red arrow)

b. Trifurcation of the left coronary artery (LCA) into left anterior descending, ramus intermedius, and circumflex branch
c. Short main trunk of LCA with a length of 2 mm.

Discussion

Cardiomegaly is defined as an increase in heart size because of ventricular hypertrophy or chamber dilation such that the ratio of heart diameter to maximum thorax diameter, measured transversely, is more than 0.5.[6,7] Although neither cardiomegaly nor the other variations like trifurcation of the LCA, short left coronary segment, and separate ostium for the right conus branch in the anterior aortic sinus are occasional conditions, it have rarely been reported together. It is important to report such cases, as an enlarged heart increases the risk for heart complications and the use of advanced image diagnostic and interventional techniques is required, which demand in-depth knowledge of the anatomy of the normal coronary and its variations.

The weight of the heart and the CTR represent an important piece of information for cardiomegaly.[6,8,9] A reference range of 233–383 g for the adult male human heart has been proposed[10] and a recent study suggested that "If it is not possible to find the predicted values, 500 g in adults male may be considered as a reasonable cut-off".[2] Hence, as the weight of the heart in the present case is 600 g [Figure 1b], it is clearly an enlarged heart.

The normal values for CTR, range between 0.42 and 0.50, and a value >0.50 is considered abnormal and may direct cardiomegaly.[11] In the present case, the CTR [0.63; Figure 1a] was more than the reported normal value. The length and width of the heart are useful parameters to judge the cardiac size. The average length and width of the heart have been reported as 12 cm and 8.5 cm and 11.41 ± 2.15 and 8.21 ± 4.38 cm, respectively, in previous reports.[12,13] In the present case, the length, breadth, and thickness of the heart were more than the defined mean values. As per the literature, the left ventricular wall thickness, right ventricular wall thickness, and ventricular septal thickness, if more than 14, 5, and 15 mm, respectively, are considered abnormal.[6] In the current case, the walls were abnormally thicker.

In the present case, there was a separate ostium for the conus branch along with the right coronary artery, so it originated directly from the right sinus of Valsalva and the trifurcation of the LCA into the left anterior descending, ramus intermedius, and circumflex branch was also observed [Figure 1d]. The incidence of trifurcation of LCA has been reported to vary from 6.7% to 55% in different cadaveric and clinical studies.[14-16] Previous studies reported the incidence of extra openings in the right aortic sinus for conus artery in 36% of the population; 34.8% of males and 27.8% of females.[13,17] Although these two variations are supposed to fall within the limit of normality,[18] considered to pose no threat, and do not demand any diagnostic workup, however, the prehand information of such variations especially in the cases with cardiomegaly may be important to interventional cardiologist and radiologists in the diagnosis and to avoid vascular trauma during therapeutic procedures.[19] The average length of the LCA trunk has been reported as 10 mm and the trunks with lengths of <5 mm and >15 mm are classified as short and long common trunks.[20] In the present case, the length of the main trunk was 2 mm and is of concern as in such cases, there may be failures of adequate coronary perfusion. While performing aortic valve surgery, myocardial perfusion depends on the placement of one or more cannulas in the coronary arteries. In cases with a short LCA trunk, the catheter may be inserted into one of the terminal branches, thus producing an ischemic area, which can lead to arrhythmia, myocardial ischemia, or both. The smaller length has also been considered a risk factor for developing coronary atherosclerosis.[16]

Conclusion

The prehand knowledge of such cases is important as occasionally, normal variants, such as multiple ostia, short LCA, and trifurcation of the LCA may confuse the interpretation of the images and may pose difficulty during procedures, such as angiography, angioplasty, and coronary artery bypass grafting in cases with cardiomegaly. Further studies may be planned to study the variations in

coronary arteries in cardiomegaly and to find if there is any association between them.

Acknowledgments

The authors are thankful to the cadaver whose viscera were used in the study. May his soul rest in peace.

Financial support and sponsorship

Nil.

Conflicts of interest

There are no conflicts of interest.

References

1. Akosa AB, Armah H. Cardiomegaly in Ghana: An autopsy study. Ghana Med J 2005;39:122-7.
2. Basso C, Michaud K, d'Amati G, Banner J, Lucena J, Cunningham K, *et al.* Cardiac hypertrophy at autopsy. Virchows Arch 2021;479:79-94.
3. Mensah YB, Mensah K, Asiamah S, Gbadamosi H, Idun EA, Brakohiapa W, *et al.* Establishing the cardiothoracic ratio using chest radiographs in an indigenous Ghanaian population: A simple tool for cardiomegaly screening. Ghana Med J 2015;49:159-64.
4. Tavora F, Zhang Y, Zhang M, Li L, Ripple M, Fowler D, *et al.* Cardiomegaly is a common arrhythmogenic substrate in adult sudden cardiac deaths, and is associated with obesity. Pathology 2012;44:187-91.
5. Rivera JP, Sugrañes M, Antonetti A, Arrieta A, Lopez AR, Sandoval J. Extreme cardiac hypertrophy in a male cadaver in our human anatomy class-a case report. Int J Anat Appl Physiol 2018;4:91-4.
6. Truszkiewicz K, Poręba R, Gać P. Radiological cardiothoracic ratio in evidence-based medicine. J Clin Med 2021;10:2016.
7. Ungerleider HE, Gubner R. Evaluation of heart size measurements. Am Heart J 1942;24:494-510.
8. Cunningham KS, Spears DA, Care M. Evaluation of cardiac hypertrophy in the setting of sudden cardiac death. Forensic Sci Res 2019;4:223-40.
9. Vanhaebost J, Faouzi M, Mangin P, Michaud K. New reference tables and user-friendly Internet application for predicted heart weights. Int J Legal Med 2014;128:615-20.
10. Molina DK, DiMaio VJ. Normal organ weights in men: Part I-the heart. Am J Forensic Med Pathol 2012;33:362-7.
11. Kearney MT, Fox KA, Lee AJ, Prescott RJ, Shah AM, Batin PD, *et al.* Predicting death due to progressive heart failure in patients with mild-to-moderate chronic heart failure. J Am Coll Cardiol 2002;40:1801-8.
12. Mohammadi S, Hedjazi A, Sajjadian M, Ghoroubi N, Mohammadi M, Erfani S. Study of the normal heart size in Northwest part of Iranian population: A cadaveric study. J Cardiovasc Thorac Res 2016;8:119-25.
13. Standring S, Ellis H, Healy JC, Johnson D, Williams A, Collins P. Heart and great vessels. In: Gray's Anatomy –The Anatomical Basis of Clinical Practice. 39th ed. London: Churchill Livingstone; 2005. p. 1008-17.
14. Bosco GA. Diagnóstico Anátomo-Topográfico De La Obstrucción Arterial Coronaria. Buenos Aires: Artes Gráficas Modernas; 1935. p. 27-30.
15. Hosapatna M, D'Souza AS, Prasanna LC, Bhojaraja VS, Sumalatha S. Anatomical variations in the left coronary artery and its branches. Singapore Med J 2013;54:49-52.
16. Kumar A, Ajmani ML, Klinkhachorn PS. Morphological variation and dimensions of left coronary artery: A cadaveric study. MOJ Anat Physiol 2018;5:266-70.
17. Sahni D, Jit I. Origin and size of the coronary arteries in the North-West Indians. Indian Heart J 1989;41:221-8.
18. Angelini P. Coronary artery anomalies: An entity in search of an identity. Circulation 2007;115:1296-305.
19. Kastellanos S, Aznaouridis K, Vlachopoulos C, Tsiamis E, Oikonomou E, Tousoulis D. Overview of coronary artery variants, aberrations and anomalies. World J Cardiol 2018;10:127-40.
20. Bhele AV, Ughade HM, Shaikh S, Joge US. A study of course, branches and variations of the coronary arteries in the human cadaveric heart. Int J Contemp Med Res 2017;4:1533-7.

Case Report

A Case Report on Hepatopancreatic Anomaly in Adult Cadaver: A Histomorphological Study

Jeneeta Baa, Mamata Sar, Srikanta Kumar Mishra

Department of Anatomy, Veer Surendra Sai Institute of Medical Sciences and Research, Burla, Odisha, India

Abstract

The pancreas is a soft, lobulated, and mixed gland. As the liver and pancreas develop together from the hepatopancreatic bud, it is common that congenital anomalies of liver and pancreas exist together. This study was done during routine practical dissection where a band of the tissue was found extending from the head of the pancreas to the root of the mesentery. On histological examination, the tissue was confirmed to be the pancreas. It is seen that the hepatic bud grows at the expense of the ventral pancreas. In the present study, we found an atrophied left lobe of the liver and an abnormally rare and large uncinate process of the pancreas.

Keywords: *Accessory lobe, hepatopancreatic bud, pancreas, uncinate process*

Introduction

The pancreas is a soft and lobulated gland, which measures about 12–15 cm extending from the duodenum to the spleen in the lesser sac of the peritoneum. It is divided into the head with its uncinate process, neck, body, and tail. Congenital anomalies of the pancreas are not uncommon and manifest in many ways ranging from abdominal pain to pancreatitis. Although they are incidentally detected, they are sometimes surgically corrected, so surgeons must be familiar about their anatomical knowledge and occurrence.

Case Report

This histomorphological study was conducted on a band of tissue, which was found in the infracolic compartment, in a 65-year-old male cadaver. This unidentified tissue was long, ribbon like, approximately 12 cm long and 3 cm wide extending from the head of the pancreas on the right to the posterior abdominal wall on the left side of the midline [Figure 1]. Proximally, it was continuous with the head of the pancreas and distally it blended with the root of the mesentery near the duodenojejunal junction. The superior mesenteric vessels were related anterior to the said structure. To confirm the nature of the tissue, we did a histological study. A few samples of the tissue were processed and embedded in paraffin wax by the routine method. Sections were cut at 4–6 μm thickness, stained in hematoxylin and eosin, and studied under microscope in different magnifications.

Results

The band of the tissue that was obtained from the cadaver was found to be a pancreatic tissue on H and E staining [Figure 2]. Serous acini were seen with their duct system. Plenty of pancreatic islets was also seen scattered between the acini.

As the liver and pancreas develop together from the hepatopancreatic bud, we searched for any abnormality in the development of the liver. In our study, the left lobe was hypoplastic, from the apex of which a long fibrous band extended toward the left up to the diaphragm (fibrous appendix of the liver) [Figure 3]. The porta hepatis was situated more closer to the posterior surface than to the inferior surface and was so narrow that it led to the crowding of the structures passing through it. This posterior shift of the porta hepatis resulted in decreased size of the caudate lobe and a reciprocal increase in the size of the quadrate lobe. The caudate lobe was rudimentary in size, whereas the quadrate lobe was large and irregular with a tongue-like accessory lobe projecting

How to cite this article: Baa J, Sar M, Mishra SK. A case report on hepatopancreatic anomaly in adult cadaver: A histomorphological study. J Anat Soc India 2025;74:76-8.

Article Info

Received: 20 May 2021
Revised: 07 February 2022
Accepted: 14 May 2023
Available online: 31 March 2025

Address for correspondence:
Dr. Jeneeta Baa, Department of Anatomy, Veer Surendra Sai Institute of Medical Sciences and Research, Burla, Odisha, India. E-mail: drjeneetabaa@gmail.com

Access this article online

Website: https://journals.lww.com/joai

DOI: 10.4103/jasi.jasi_93_21

Quick Response Code:

from its lower part. There was obliteration of the fissure for ligamentum teres hepatis because a mass of liver tissue (pons hepatis) bridged the fissure. As a result of which the lesser omentum was attached to the entire inferior surface at the site of the quadrate lobe [Figure 4]. The free margin of lesser omentum could not be traced and so we failed to locate the epiploic foramen. An abnormal band of peritoneum extended from the fundus of the gallbladder to the transverse colon (cystocolic ligament), due to which the gallbladder was horizontally placed in its fossa [Figure 5].

Discussion

At about the 4th week of gestation, the pancreas first appears as two diverticula arising from the junction of the foregut and midgut. The pancreatic tissue develops under the influence of pancreas and duodenal homeobox gene 1. The two buds of pancreatic tissue are expanded by the activation and deactivation of Sonic Hedgehog signaling. The ventral bud of endodermal tissue is formed in the ventral mesentery and the larger cluster of endoderm forms the dorsal pancreatic bud within the dorsal mesentery. The dorsal bud elongates rapidly to form the tail, body, and part of the head of the pancreas. The ventral bud is initially a paired structure, the left portion of which atrophies and the right portion grows and is pulled posteriorly as the duodenum rotates.[1] Around the 6th week of gestation, the persistent part of ventral primordium fuses with the dorsal pancreatic bud to form the remainder of the head and uncinate process of the pancreas.[2]

The parenchyma develops from branching of endodermal pancreatic buds into the surrounding mesoderm. Because of their different surrounding tissues, different signals induce

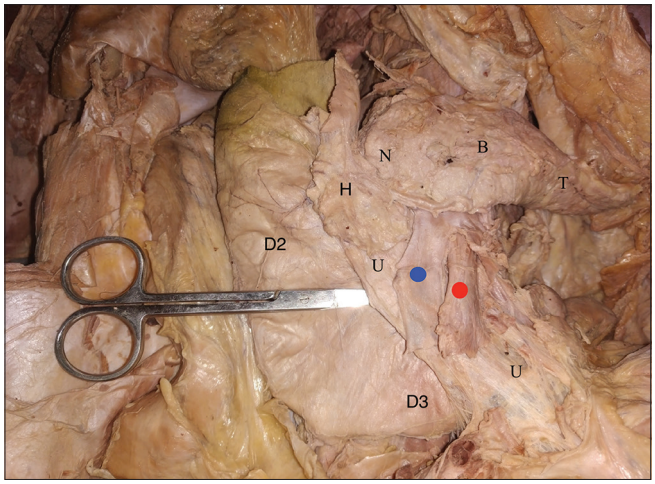

Figure 1: Pancreas with an unusually long uncinate process in the C-shape curvature of the duodenum. D2: Second part of duodenum, D3: Third part of duodenum, U: Uncinate process, H: Head of pancreas, N: Neck of pancreas, B: Body of pancreas, T: Tail of pancreas, ●: superior mesenteric vein, ●: superior mesenteric artery

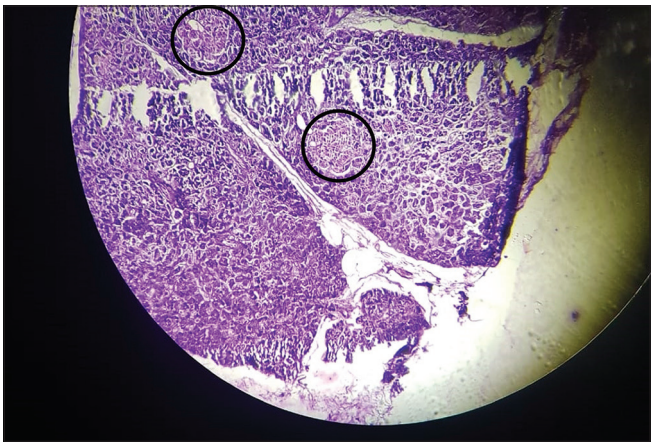

Figure 2: The pancreatic tissue on ×4 resolution and H and E staining showing serous acini in lobules with plenty of islets of Langerhans (black circle) scattered between the acini

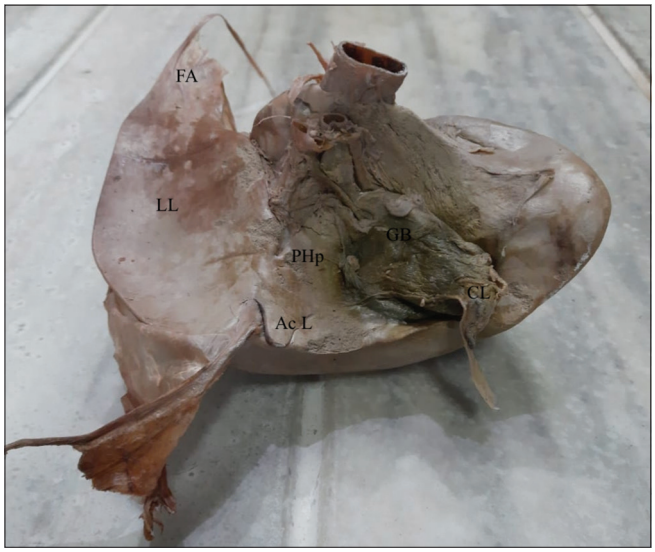

Figure 3: Picture showing both anatomical lobes of the liver. LL: Atrophied Left Lobe of the liver, FA: Fibrose Appendix of the liver, Ac L: Accessory Lobe, PHp: Pons Hepatis, GB: Gallbladder

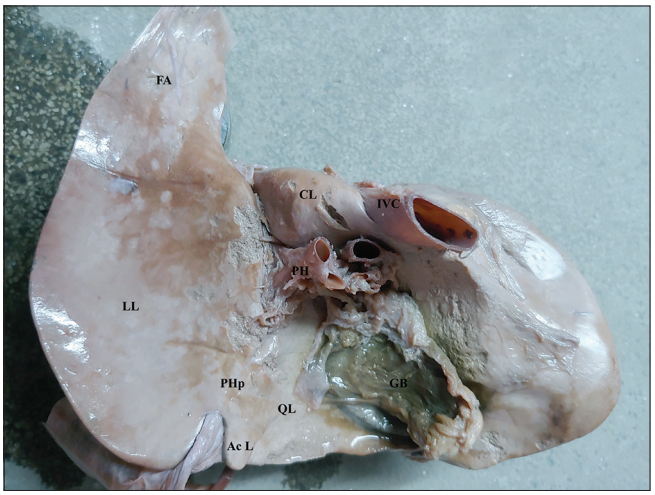

Figure 4: Reduced posterior surface with rudimentary caudate lobe and large inferior surface with an enlarged quadrate lobe along with posterior shifting of porta hepatis. FA: Fibrose Appendix of the liver, LL: Atrophied Left Lobe of the liver, CL: Caudate Lobe, FA: Fibrose Appendix of the liver, Ac L: Accessory Lobe, PH: Porta Hepatis, PHp: Pons hepatis, GB: Gallbladder, IVC: Inferior vena cava, QL: Quadrate lobe

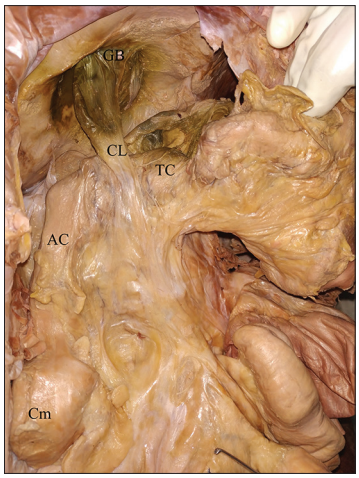

Figure 5: Liver and Gallbladder *in situ*. GB: Gallbladder, CL: Cystocolic ligament, Cm: Caecum, AC: Ascending colon, TC: Transverse colon

dorsal and ventral pancreatic buds. The dorsal pancreatic endoderm lies in close proximity to the dorsal aorta, the endothelium of which provides inductive signals to the dorsal endoderm, inducing the formation of a pancreatic bud expressing Pdx1 and Ptf1a.[3] Signals from lateral plate mesoderm (retinoic acid) and notochord (fibroblast growth factors [FGF] 2 and activin) are required for dorsal bud induction. In contrast, FGF signaling from cardiac mesoderm inhibits ventral pancreatic bud specifications.[4] Thereafter, the morphogenesis of the two buds is different. Unlike the dorsal pancreas, the ventral pancreas is not dependent on inducers from the endothelium.

The ventral pancreatic bud develops in close connection with the liver, the later receives instructive signaling from the cardiac mesoderm.[5] The function of Pdx1 and Ptf1a together with Hnf1b is essential for the formation of the ventral pancreas.[6] It is seen that the hepatic bud grows at the expense of the ventral pancreas.[7,8] In the present study, we found a hypoplastic left lobe of the liver and an abnormally large uncinate process of the pancreas. In intrauterine life, the fetal portal vein joins the umbilical vein in a smooth right-hand curve, maintained after birth, with a sharp angle between the portal trunk and its left branch; the left vascular lobe may, therefore, be at a circulatory disadvantage and unable to keep pace in growth with the right lobe. At the left end of the adult left lobe, a fibrous band (fibrous appendix of the liver) may appear as an atrophied remnant of a more extensive part of the left lobe as children.[9] Accessory pancreatic tissue may be scattered in the wall of an organ, and hence recognizable only on microscopic examination, or may form masses of appreciable size as reported by Reitmann which was 2 cm long and 1 cm or broader.[10] In our case, the tissue was much longer and such a large case in the literature where an unusual and extensive uncinate process was reported by Gandhi *et al*.[11] We concluded it to be an enlarged uncinate process owing to its relation with the superior mesenteric vessels which crossed anterior to it, unlike the findings of Nayak *et al*., where the uncinate process encircled the superior mesenteric vessels.[12] There is a lack of documentation of such congenital pancreatic anomaly and despite the advanced diagnostic techniques, such anomalies of the pancreas still remain unnoticed. The cause of a pancreatic hypertrophy can be either congenital or acquired. After staining, the tissue was confirmed to be a normal pancreas tissue. Such rare congenital conditions must be borne in mind during surgery on hepatopancreatic-biliary tree.

Conclusion

Congenital abnormality in the hepatopancreatic bud can manifest in various forms. This study may help the surgeons to be aware of such anomalies to avoid any accidents.

Financial support and sponsorship

Nil.

Conflicts of interest

There are no conflicts of interest.

References

1. Lewis FT. The bi-lobed form of the ventral pancreas in mammals. Am J Anat 1911;12:389-400.
2. Moore KL, Persaud TV. The Developing Human: Clinically Oriented Embryology. 8th ed. Philadelphia: Saunders; 2008. p. 264-5.
3. Lammert E, Cleaver O, Melton D. Induction of pancreatic differentiation by signals from blood vessels. Science 2001;294:564-7.
4. Kumar M, Jordan N, Melton D, Grapin-Botton A. Signals from lateral plate mesoderm instruct endoderm toward a pancreatic fate. Dev Biol 2003;259:109-22.
5. Yoshitomi H, Zaret KS. Endothelial cell interactions initiate dorsal pancreas development by selectively inducing the transcription factor Ptf1a. Development 2004;131:807-17.
6. Haumaitre C, Barbacci E, Jenny M, Ott MO, Gradwohl G, Cereghini S. Lack of TCF2/vHNF1 in mice leads to pancreas agenesis. Proc Natl Acad Sci U S A 2005;102:1490-5.
7. Gualdi R, Bossard P, Zheng M, Hamada Y, Coleman JR, Zaret KS. Hepatic specification of the gut endoderm *in vitro*: Cell signaling and transcriptional control. Genes Dev 1996;10:1670-82.
8. Jung J, Zheng M, Goldfarb M, Zaret KS. Initiation of mammalian liver development from endoderm by fibroblast growth factors. Science 1999;284:1998-2003.
9. Standring S. Gray's Anatomy. 38th ed. London, United Kingdom: Churchill Livingstone; 2008. p. 1803.
10. Reitmann K. Zwei Falle von accessorischem Pankreas. Anat Anz 1903;23:155.
11. Gandhi S, Sharma M, Pakhiddey R, Thakur A, Mehta V, Suri RK, *et al.* Unduly extensive uncinate process of pancreas in conjunction with pancreatico-duodenal fold. Anat Cell Biol 2015;48:81-3.
12. Nayak SB, Kumar N, Padur AA, Sirasanagandla SR, Shetty SD. Histomorphological study of unusual and extensive uncinate process of Pancreas encircling the superior mesenteric artery and its clinical importance. JOP 2016;17:281-3.

JASI

Revolutionizing Anatomy Education with the "Anatomy 3D Atlas" Tool: A New Era of Interactive Learning

Sir,

Teaching human anatomy is the foundation of medical education. However, it is one of the most challenging subjects for students to understand. Traditional methods of faculty members, including cadaver dissection and two-dimensional (2D) textbook graphics, are effective but lack anatomical structure complexity and spatial relationship. Integrating the "Anatomy 3D Atlas" tool into anatomy education has become increasingly important, representing a significant advancement in teaching and learning human anatomy. Anatomy 3D Atlas is an innovative platform that utilizes high-resolution 3D models to provide students with an interactive and immersive learning experience. Compared to static 2D images, the 3D models in this platform help students to understand and explore anatomical structures from every section and offer a more comprehensive understanding of the spatial relationships within the human body structure. This helps students who struggle with visualizing the 3D aspects of anatomy.[1]

The "Anatomy 3D Atlas" platform covers all major human body systems, including the skeletal, muscular, cardiovascular, nervous, and digestive systems. Each model is accurately detailed and able to rotate and separate individual structures. This level of detail and interactivity is unmatched by traditional learning resources. Students can separate the skull bones to study their intricate relationships away from muscle sections to understand their origins, insertions, and functions. Such features greatly enhance the learning process, enabling students to engage with the material in a way that promotes deeper retention.[2] "Anatomy 3D Atlas" has interactive labels and quizzes that allow students to test their knowledge in real time. These features can improve learning process and it provides immediate feedback which is helpful to identify weak areas of students. The platform's quizzes are designed to challenge students at various difficulty levels, from basic identification of structures to more advanced questions that require an understanding of their clinical relevance.[3]

Accessibility is another key advantage of Anatomy 3D Atlas. The platform is available on desktops, tablets, and smartphones, making it convenient for students to study whenever and wherever they choose. This flexibility is particularly important in the educational environment, where students often balance rigorous academic schedules with other responsibilities. Accessing high-quality anatomy resources on the go ensures that learning can continue outside the classroom.[1] Furthermore, the "Anatomy 3D Atlas" is continually updated to reflect the latest advances in anatomical knowledge. This ensures that students learn the most current and accurate information available. As the medical field evolves, the platform's commitment to staying up-to-date ensures that future healthcare professionals are well prepared for the challenges they will face in their careers.[4]

In conclusion, the "Anatomy 3D Atlas" represents a transformative tool for teaching human anatomy. Its high-resolution 3D models, interactive features, and accessibility make it an invaluable resource for medical students and faculty members. Integrating this innovative platform into medical education can improve the quality of anatomy education and prepare students for the complexities of clinical practice.

Financial support and sponsorship

Nil.

Conflicts of interest

There are no conflicts of interest.

Ankit K. Badge, Happy Bhuva[1], Nandkishor J. Bankar, Obaid Noman[2,3]

Departments of Microbiology, [1]Anatomy, [2]Pathology, and [3]Microbiology, Datta Meghe Medical College, Datta Meghe Institute of Higher Education and Research (DU), Nagpur, Maharashtra, India

Address for correspondence: *Dr. Nandkishor J. Bankar, Prof and Head, Department of Microbiology, Datta Meghe Medical College, Datta Meghe Institute of Higher Education and Research (DU), Nagpur - 441 110, Maharashtra, India.*
E-mail: drbankarnj28@gmail.com

References

1. Park S, Kim Y, Park S, Shin JA. The impacts of three-dimensional anatomical atlas on learning anatomy. Anat Cell Biol 2019;52:76-81.
2. Chaker R, Gallot M, Binay M, Hoyek N. User experience of a 3D interactive human anatomy learning tool. Educ Technol Soc 2021;24:136-50.
3. Bogomolova K, Sam AH, Misky AT, Gupte CM, Strutton PH, Hurkxkens TJ, *et al.* Development of a virtual three-dimensional assessment scenario for anatomical education. Anat Sci Educ 2021;14:385-93.

4. Demir BT, Eşme S, Patat D, Bilecenoğlu B. The effect of mobile applied anatomy learning on students' academic success, cognitive loads, and attitudes. Med Sci Educ 2023;33:1-8.

Article Info

Received: 16 August 2024
Revised: 07 January 2025
Accepted: 15 February 2025
Available online: 31 March 2025

Access this article online	
Quick Response Code:	**Website:** https://journals.lww.com/joai
	DOI: 10.4103/jasi.jasi_124_24

How to cite this article: Badge AK, Bhuva H, Bankar NJ, Noman O. Revolutionizing anatomy education with the "Anatomy 3D Atlas" tool: A new era of interactive learning. J Anat Soc India 2025;74:79-80.

The Editorial Process

A manuscript will be reviewed for possible publication with the understanding that it is being submitted to Journal of the Anatomical Society of India alone at that point in time and has not been published anywhere, simultaneously submitted, or already accepted for publication elsewhere. The journal expects that authors would authorize one of them to correspond with the Journal for all matters related to the manuscript. All manuscripts received are duly acknowledged. On submission, editors review all submitted manuscripts initially for suitability for formal review. Manuscripts with insufficient originality, serious scientific or technical flaws, or lack of a significant message are rejected before proceeding for formal peer-review. Manuscripts that are unlikely to be of interest to the Journal of the Anatomical Society of India readers are also liable to be rejected at this stage itself.

Manuscripts that are found suitable for publication in Journal of the Anatomical Society of India are sent to two or more expert reviewers. During submission, the contributor is requested to provide names of two or three qualified reviewers who have had experience in the subject of the submitted manuscript, but this is not mandatory. The reviewers should not be affiliated with the same institutes as the contributor/s. However, the selection of these reviewers is at the sole discretion of the editor. The journal follows a double-blind review process, wherein the reviewers and authors are unaware of each other's identity. Every manuscript is also assigned to a member of the editorial team, who based on the comments from the reviewers takes a final decision on the manuscript. The comments and suggestions (acceptance/ rejection/ amendments in manuscript) received from reviewers are conveyed to the corresponding author. If required, the author is requested to provide a point by point response to reviewers' comments and submit a revised version of the manuscript. This process is repeated till reviewers and editors are satisfied with the manuscript.

Manuscripts accepted for publication are copy edited for grammar, punctuation, print style, and format. Page proofs are sent to the corresponding author. The corresponding author is expected to return the corrected proofs within three days. It may not be possible to incorporate corrections received after that period. The whole process of submission of the manuscript to final decision and sending and receiving proofs is completed online. To achieve faster and greater dissemination of knowledge and information, the journal publishes articles online as 'Ahead of Print' immediately on acceptance.

Clinical trial registry

Journal of the Anatomical Society of India favors registration of clinical trials and is a signatory to the Statement on publishing clinical trials in Indian biomedical journals. Journal of the Anatomical Society of India would publish clinical trials that have been registered with a clinical trial registry that allows free online access to public. Registration in the following trial registers is acceptable: http://www.ctri.in/; http://www.actr.org.au/; http://www.clinicaltrials.gov/; http://isrctn.org/; http://www.trialregister.nl/trialreg/index.asp; and http://www.umin.ac.jp/ctr. This is applicable to clinical trials that have begun enrollment of subjects in or after June 2008. Clinical trials that have commenced enrollment of subjects prior to June 2008 would be considered for publication in Journal of the Anatomical Society of India only if they have been registered retrospectively with clinical trial registry that allows unhindered online access to public without charging any fees.

Authorship Criteria

Authorship credit should be based only on substantial contributions to each of the three components mentioned below:

1. Concept and design of study or acquisition of data or analysis and interpretation of data;
2. Drafting the article or revising it critically for important intellectual content; and
3. Final approval of the version to be published.

Participation solely in the acquisition of funding or the collection of data does not justify authorship. General supervision of the research group is not sufficient for authorship. Each contributor should have participated sufficiently in the work to take public responsibility for appropriate portions of the content of the manuscript. The order of naming the contributors should be based on the relative contribution of the contributor towards the study and writing the manuscript. Once submitted the order cannot be changed without written consent of all the contributors. The journal prescribes a maximum number of authors for manuscripts depending upon the type of manuscript, its scope and number of institutions involved (vide infra). The authors should provide a justification, if the number of authors exceeds these limits.

Contribution Details

Contributors should provide a description of contributions made by each of them towards the manuscript. Description should be divided in following categories, as applicable: concept, design, definition of intellectual content, literature search, clinical studies, experimental studies, data acquisition, data analysis, statistical analysis, manuscript preparation, manuscript editing and manuscript review. Authors' contributions will be printed along with the article. One or more author should take responsibility for the integrity of the work as a whole from inception to published article and should be designated as 'guarantor'.

Conflicts of Interest/ Competing Interests

All authors of must disclose any and all conflicts of interest they may have with publication of the manuscript or an institution or product that is mentioned in the manuscript and/or is important to the outcome of the study presented. Authors should also disclose conflict of interest with products that compete with those mentioned in their manuscript.

Submission of Manuscripts

All manuscripts must be submitted on-line through the website https://review.jow.medknow.com/jasi. First time users will have to register at this site. Registration is free but mandatory. Registered authors can keep track of their articles after logging into the site using their user name and password.

- If you experience any problems, please contact the editorial office by e-mail at editor@jasi.org.in

The submitted manuscripts that are not as per the "Instructions to Authors" would be returned to the authors for technical correction, before they undergo editorial/ peer-review. Generally, the manuscript should be submitted in the form of two separate files:

[1] Title Page/First Page File/covering letter:

This file should provide

1. The type of manuscript (original article, case report, review article, Letter to editor, Images, etc.) title of the manuscript, running title, names of all authors/ contributors (with their highest academic degrees, designation and affiliations) and name(s) of department(s) and/ or institution(s) to which the work should be credited, . All information which can reveal your identity should be here. Use text/rtf/doc files. Do not zip the files.
2. The total number of pages, total number of photographs and word counts separately for abstract and for the text (excluding the references, tables and abstract), word counts for introduction + discussion in case of an original article;
3. Source(s) of support in the form of grants, equipment, drugs, or all of these;
4. Acknowledgement, if any. One or more statements should specify 1) contributions that need acknowledging but do not justify authorship, such as general support by a departmental chair; 2) acknowledgments of technical help; and 3) acknowledgments of financial and material support, which should specify the nature of the support. This should be included in the title page of the manuscript and not in the main article file.
5. If the manuscript was presented as part at a meeting, the organization, place, and exact date on which it was read. A full statement to the editor about all submissions and previous reports that might be regarded as redundant publication of the same or very similar work. Any such work should be referred to specifically, and referenced in the new paper. Copies of such material should be included with the submitted paper, to help the editor decide how to handle the matter.
6. Registration number in case of a clinical trial and where it is registered (name of the registry and its URL)
7. Conflicts of Interest of each author/ contributor. A statement of financial or other relationships that might lead to a conflict of interest, if that information is not included in the manuscript itself or in an authors' form
8. Criteria for inclusion in the authors'/ contributors' list
9. A statement that the manuscript has been read and approved by all the authors, that the requirements for authorship as stated earlier in this document have been met, and that each author believes that the manuscript represents honest work, if that information is not provided in another form (see below); and
10. The name, address, e-mail, and telephone number of the corresponding author, who is responsible for communicating with the other authors about revisions and final approval of the proofs, if that information is not included on the manuscript itself.

[2] Blinded Article file: The main text of the article, beginning from Abstract till References (including tables) should be in this file. The file must not contain any mention of the authors' names or initials or the institution at which the study was done or acknowledgements. Page headers/ running title can include the title but not the authors' names. Manuscripts not in compliance with the Journal's blinding policy will be returned to the corresponding author. Use rtf/doc files. Do not zip the files. **Limit the file size to 1 MB.** Do not incorporate images in the file. If file size is large, graphs can be submitted as images separately without incorporating them in the article file to reduce the size of the file. The pages should be numbered consecutively, beginning with the first page of the blinded article file.

[3] Images: Submit good quality color images. **Each image should be less than 2 MB in size.** Size of the image can be reduced by decreasing the actual height and width of the images (keep up to 1600 x 1200 pixels or 5-6 inches). Images can be submitted as jpeg files. Do not zip the files. Legends for the figures/images should be included at the end of the article file.

[4] The contributors' / copyright transfer form (template provided below) has to be submitted in original with the signatures of all the contributors within two weeks of submission via courier, fax or email as a scanned image. Print ready hard copies of the images (one set) or digital images should be sent to the journal office at the time of submitting revised manuscript. High resolution images (up to 5 MB each) can be sent by email.

Contributors' form / copyright transfer form can be submitted online from the authors' area on https://review.jow.medknow.com/jasi.

Preparation of Manuscripts

Manuscripts must be prepared in accordance with "Uniform requirements for Manuscripts submitted to Biomedical Journals" developed by the International Committee of Medical Journal Editors (October 2008). The uniform requirements and specific requirement of Journal of the Anatomical Society of India are summarized below. Before submitting a manuscript, contributors are requested to check for the latest instructions available. Instructions are also available from the website of the journal (www.jasi.org.in) and from the manuscript submission site https://review.jow.medknow.com/jasi.

Journal of the Anatomical Society of India accepts manuscripts written in American English.

Copies of any permission(s)

It is the responsibility of authors/ contributors to obtain permissions for reproducing any copyrighted material. A copy of the permission obtained must accompany the manuscript. Copies of any and all published articles or other manuscripts in preparation or submitted elsewhere that are related to the manuscript must also accompany the manuscript.

Types of Manuscripts

Original articles:

These include randomized controlled trials, intervention studies, studies of screening and diagnostic test, outcome studies, cost effectiveness analyses, case-control series, and surveys with high response rate. The text of original articles amounting to up to 3000 words (excluding Abstract, references and Tables) should be divided into sections with the headings Abstract, Key-words, Introduction, Material and Methods, Results, Discussion and Conclusion, References, Tables and Figure legends.

An abstract should be in a structured format under following heads: **Introduction, Material and Methods, Results,** and **Discussion and Conclusion.**

Introduction: State the purpose and summarize the rationale for the study or observation.

Material and Methods: It should include and describe the following aspects:

Ethics: When reporting studies on human beings, indicate whether the procedures followed were in accordance with the ethical standards of the responsible committee on human experimentation (institutional or regional) and with the Helsinki Declaration of 1975, as revised in 2000 (available at http://www.wma.net/e/policy/17-c_e.html). For prospective studies involving human participants, authors are expected to mention about approval of (regional/ national/ institutional or independent Ethics Committee or Review Board, obtaining informed consent from adult research participants and obtaining assent for children aged over 7 years participating in the trial. The age beyond which assent would be required could vary as per regional and/ or national guidelines. Ensure confidentiality of subjects by desisting from mentioning participants' names, initials or hospital numbers, especially in illustrative material. When reporting experiments on animals, indicate whether the institution's or a national research council's guide for, or any national law on the care and use of laboratory animals was followed. Evidence for approval by a local Ethics Committee (for both human as well as animal studies) must be supplied by the authors on demand. Animal experimental procedures should be as humane as possible and the details of anesthetics and analgesics used should be clearly stated. The ethical standards of experiments must be in accordance with the guidelines provided by the CPCSEA and World Medical Association Declaration of Helsinki on Ethical Principles for Medical Research Involving Humans for studies involving experimental animals and human beings, respectively). The journal will not consider any paper which is ethically unacceptable. A statement on ethics committee permission and ethical practices must be included in all research articles under the 'Materials and Methods' section.

Study design:

Selection and Description of Participants: Describe your selection of the observational or experimental participants (patients or laboratory animals, including controls) clearly, including eligibility and exclusion criteria and a description of the source population. *Technical information*: Identify the methods, apparatus (give the manufacturer›s name and address in parentheses), and procedures in sufficient detail to allow other workers to reproduce the results. Give references to established methods, including statistical methods (see below); provide references and brief descriptions for methods that have been published but are not well known; describe new or substantially modified methods, give reasons for using them, and evaluate their limitations. Identify precisely all drugs and chemicals used, including generic name(s), dose(s), and route(s) of administration.

Reports of randomized clinical trials should present information on all major study elements, including the protocol, assignment of interventions (methods of randomization, concealment of allocation to treatment groups), and the method of masking (blinding), based on the CONSORT Statement (http://www.consort-statement.org).

Reporting Guidelines for Specific Study Designs

Initiative	Type of Study	Source
CONSORT	Randomized controlled trials	http://www.consort-statement.org
STARD	Studies of diagnostic accuracy	http://www.consort-statement.org/stardstatement.htm
QUOROM	Systematic reviews and meta-analyses	http://www.consort- statement.org/Initiatives/MOOSE/moose.pdf statement.org/Initiatives/MOOSE/moose.pdf
STROBE	Observational studies in epidemiology	http://www.strobe-statement.org
MOOSE	Meta-analyses of observational studies in epidemiology	http://www.consort- statement.org/Initiatives/MOOSE/moose.pdf

Statistics: Whenever possible quantify findings and present them with appropriate indicators of measurement error or uncertainty (such as confidence intervals). Authors should report losses to observation (such as, dropouts from a clinical trial). When data are summarized in the Results section, specify the statistical methods used to analyze them. Avoid non-technical uses of technical terms in statistics, such as 'random' (which implies a randomizing device), 'normal', 'significant', 'correlations', and 'sample'. Define statistical terms, abbreviations, and most symbols. Specify the computer software used. Use upper italics (*P* 0.048). For all *P* values include the exact value and not less than 0.05 or 0.001. Mean differences in continuous variables, proportions in categorical variables and relative risks including odds ratios and hazard ratios should be accompanied by their confidence intervals.

Results: Present your results in a logical sequence in the text, tables, and illustrations, giving the main or most important findings first. Do not repeat in the text all the data in the tables or illustrations; emphasize or summarize only important observations. Extra- or supplementary materials and technical detail can be placed in an appendix where it will be accessible but will not interrupt the flow of the text; alternatively, it can be published only in the electronic version of the journal.

When data are summarized in the Results section, give numeric results not only as derivatives (for example, percentages) but also as the absolute numbers from which the derivatives were calculated, and specify the statistical methods used to analyze them. Restrict tables and figures to those needed to explain the argument of the paper and to assess its support. Use graphs as an alternative to tables with many entries; do not duplicate data in graphs and tables. Where scientifically appropriate, analyses of the data by variables such as age and sex should be included.

Discussion: Include summary of *key findings* (primary outcome measures, secondary outcome measures, results as they relate to a prior hypothesis); *Strengths and limitations* of the study (study question, study design, data collection, analysis and interpretation); *Interpretation and implications* in the context of the totality of evidence (is there a systematic review to refer to, if not, could one be reasonably done here and now?, what this study adds to the available evidence, effects on patient care and health policy, possible mechanisms); *Controversies* raised by this study; and *Future research directions* (for this particular research collaboration, underlying mechanisms, clinical research).

Do not repeat in detail data or other material given in the Introduction or the Results section. In particular, contributors should avoid making statements on economic benefits and costs unless their manuscript includes economic data and analyses. Avoid claiming priority and alluding to work that has not been completed. New hypotheses may be stated if needed, however they should be clearly labeled as such. About 30 references can be included. These articles generally should not have more than six authors.

Review Articles:

These are comprehensive review articles on topics related to various fields of Anatomy. The entire manuscript should not exceed 7000 words with no more than 50 references and two authors. Following types of articles can be submitted under this category:

- Newer techniques of dissection and histology
- New methodology in Medical Education
- Review of a current concept

Please note that generally review articles are by invitation only. But unsolicited review articles will be considered for publication on merit basis.

Case reports:

New, interesting and rare cases can be reported. They should be unique, describing a great diagnostic or therapeutic challenge and providing a learning point for the readers. Cases with clinical significance or implications will be given priority. These communications could be of up to 1000 words (excluding Abstract and references) and should have the following headings: Abstract (unstructured), Key-words, Introduction, Case report, Discussion and Conclusion, Reference, Tables and Legends in that order.

The manuscript could be of up to 1000 words (excluding references and abstract) and could be supported with up to 10 references. Case Reports could be authored by up to four authors.

Letter to the Editor:

These should be short and decisive observations. They should preferably be related to articles previously published in the Journal or views expressed in the journal. They should not be preliminary observations that need a later

paper for validation. The letter could have up to 500 words and 5 references. It could be generally authored by not more than four authors.

Book Review: This consists of a critical appraisal of selected books on Anatomy. Potential authors or publishers may submit books, as well as a list of suggested reviewers, to the editorial office. The author/publisher has to pay INR 10,000 per book review.

Other:

Editorial, Guest Editorial, Commentary and Opinion are solicited by the editorial board.

References

References should be *numbered* consecutively in the order in which they are first mentioned in the text (not in alphabetic order). Identify references *in text*, tables, and legends by Arabic numerals in superscript with square bracket after the punctuation *marks. References cited only* in tables or figure legends should be numbered in accordance with the sequence established by the first identification in the text of the particular table or figure. Use the style of the examples below, which are based on the formats used by the NLM *in Index Medicus*. The titles of journals *should be abbreviated* according to the style used in Index Medicus. Use complete name of the journal for non-indexed journals. Avoid using abstracts as references. Information from manuscripts submitted but not accepted should be cited in the text as "unpublished observations" with written permission from the source. Avoid citing a "personal communication" unless it provides essential information not available from a public source, in which case the name of the person and date of communication should be cited in parentheses in the text. The commonly cited types of references are shown here, for other types of references such as newspaper items please refer to ICMJE Guidelines (http://www.icmje.org or http://www.nlm.nih.gov/bsd/uniform_requirements.html).

Articles in Journals

1. Standard journal article (for up to six authors): Parija S C, Ravinder PT, Shariff M. Detection of hydatid antigen in the fluid samples from hydatid cysts by co-agglutination. Trans. R.Soc. Trop. Med. Hyg.1996; 90:255–256.
2. Standard journal article (for more than six authors): List the first six contributors followed by *et al*.

Roddy P, Goiri J, Flevaud L, Palma PP, Morote S, Lima N. *et al*., Field Evaluation of a Rapid Immunochromatographic Assay for Detection of Trypanosoma cruzi Infection by Use of Whole Blood. J. Clin. Microbiol. 2008; 46: 2022-2027.

3. Volume with supplement: Otranto D, Capelli G, Genchi C: Changing distribution patterns of canine vector borne diseases in Italy: leishmaniosis vs. dirofilariosis. Parasites & Vectors 2009; Suppl 1:S2.

Books and Other Monographs

1. Personal author(s): Parija SC. Textbook of Medical Parasitology. 3rd ed. All India Publishers and Distributors. 2008.
2. Editor(s), compiler(s) as author: Garcia LS, Filarial Nematodes In: Garcia LS (editor) Diagnostic Medical Parasitology ASM press Washington DC 2007: pp 319-356.
3. Chapter in a book: Nesheim M C. Ascariasis and human nutrition. In Ascariasis and its prevention and control, D. W. T. Crompton, M. C. Nesbemi, and Z. S. Pawlowski (eds.). Taylor and Francis,London, U.K.1989, pp. 87–100.

Electronic Sources as reference

Journal article on the Internet: Parija SC, Khairnar K. Detection of excretory *Entamoeba histolytica* DNA in the urine, and detection of *E. histolytica* DNA and lectin antigen in the liver abscess pus for the diagnosis of amoebic liver abscess. *BMC Microbiology* 2007, **7**:41. doi:10.1186/1471-2180-7-41. http://www.biomedcentral.com/1471-2180/7/41

Tables

- Tables should be self-explanatory and should not duplicate textual material.
- Tables with more than 10 columns and 25 rows are not acceptable.
- Number tables, in Arabic numerals, consecutively in the order of their first citation in the text and supply a brief title for each.
- Place explanatory matter in footnotes, not in the heading.
- Explain in footnotes all non-standard abbreviations that are used in each table.
- Obtain permission for all fully borrowed, adapted, and modified tables and provide a credit line in the footnote.
- For footnotes use the following symbols, in this sequence: *, †, ‡, §, ‖,¶ , **, ††, ‡‡
- Tables with their legends should be provided at the end of the text after the references. The tables along with their number should be cited at the relevant place in the text

Illustrations (Figures)

- Upload the images in JPEG format. The file size should be within 1024 kb in size while uploading.
- Figures should be numbered consecutively according to the order in which they have been first cited in the text.
- Labels, numbers, and symbols should be clear and of uniform size. The lettering for figures should be large enough to be legible after reduction to fit the width of a printed column.
- Symbols, arrows, or letters used in photomicrographs

should contrast with the background and should be marked neatly with transfer type or by tissue overlay and not by pen.
- Titles and detailed explanations belong in the legends for illustrations not on the illustrations themselves.
- When graphs, scatter-grams or histograms are submitted the numerical data on which they are based should also be supplied.
- The photographs and figures should be trimmed to remove all the unwanted areas.
- If photographs of individuals are used, their pictures must be accompanied by written permission to use the photograph.
- If a figure has been published elsewhere, acknowledge the original source and submit written permission from the copyright holder to reproduce the material. A credit line should appear in the legend for such figures.
- Legends for illustrations: Type or print out legends (maximum 40 words, excluding the credit line) for illustrations using double spacing, with Arabic numerals corresponding to the illustrations. When symbols, arrows, numbers, or letters are used to identify parts of the illustrations, identify and explain each one in the legend. Explain the internal scale (magnification) and identify the method of staining in photomicrographs.
- Final figures for print production: Send sharp, glossy, un-mounted, color photographic prints, with height of 4 inches and width of 6 inches at the time of submitting the revised manuscript. Print outs of digital photographs are not acceptable. If digital images are the only source of images, ensure that the image has minimum resolution of 300 dpi or 1800 x 1600 pixels in TIFF format. Send the images on a CD. Each figure should have a label pasted (avoid use of liquid gum for pasting) on its back indicating the number of the figure, the running title, top of the figure and the legends of the figure. Do not write the contributor/s' name/s. Do not write on the back of figures, scratch, or mark them by using paper clips.
- The Journal reserves the right to crop, rotate, reduce, or enlarge the photographs to an acceptable size.

Protection of Patients' Rights to Privacy

Identifying information should not be published in written descriptions, photographs, sonograms, CT scans, etc., and pedigrees unless the information is essential for scientific purposes and the patient (or parent or guardian, wherever applicable) gives informed consent for publication. Authors should remove patients' names from figures unless they have obtained informed consent from the patients. The journal abides by ICMJE guidelines:

1. Authors, not the journals nor the publisher, need to obtain the patient consent form before the publication and have the form properly archived. The consent forms are not to be uploaded with the cover letter or sent through email to editorial or publisher offices.
2. If the manuscript contains patient images that preclude anonymity, or a description that has obvious indication to the identity of the patient, a statement about obtaining informed patient consent should be indicated in the manuscript.

Sending a revised manuscript

The revised version of the manuscript should be submitted online in a manner similar to that used for submission of the manuscript for the first time. However, there is no need to submit the "First Page" or "Covering Letter" file while submitting a revised version. When submitting a revised manuscript, contributors are requested to include, the 'referees' remarks along with point to point clarification at the beginning in the revised file itself. In addition, they are expected to mark the changes as underlined or colored text in the article.

Reprints and proofs

Journal provides no free printed reprints. Authors can purchase reprints, payment for which should be done at the time of submitting the proofs.

Publication schedule

The journal publishes articles on its website immediately on acceptance and follows a 'continuous publication' schedule. Articles are compiled in issues for 'print on demand' quarterly.

Copyrights

Checklist

Covering letter

- Signed by all contributors
- Previous publication / presentations mentioned
- Source of funding mentioned
- Conflicts of interest disclosed

Authors

- Last name and given name provided along with Middle name initials (where applicable)
- Author for correspondence, with e-mail address provided
- Number of contributors restricted as per the instructions
- Identity not revealed in paper except title page (e.g. name of the institute in Methods, citing previous study as 'our study', names on figure labels, name of institute in photographs, etc.)

Presentation and format

- Double spacing
- Margins 2.5 cm from all four sides
- Page numbers included at bottom
- Title page contains all the desired information
- Running title provided (not more than 50 characters)
- Abstract page contains the full title of the manuscript
- Abstract provided (structured abstract of 250 words for original articles, unstructured abstracts of about 150 words for all other manuscripts excluding letters to the Editor)
- Key words provided (three or more)
- Introduction of 75-100 words
- Headings in title case (not ALL CAPITALS)
- The references cited in the text should be after punctuation marks, in superscript with square bracket.
- References according to the journal's instructions, punctuation marks checked
- Send the article file without 'Track Changes'

Language and grammar

- Uniformly American English
- Write the full term for each abbreviation at its first use in the title, abstract, keywords and text separately unless it is a standard unit of measure. Numerals from 1 to 10 spelt out
- Numerals at the beginning of the sentence spelt out
- Check the manuscript for spelling, grammar and punctuation errors
- If a brand name is cited, supply the manufacturer's name and address (city and state/country).
- Species names should be in italics

Tables and figures

- No repetition of data in tables and graphs and in text
- Actual numbers from which graphs drawn, provided
- Figures necessary and of good quality (colour)
- Table and figure numbers in Arabic letters (not Roman)
- Labels pasted on back of the photographs (no names written)
- Figure legends provided (not more than 40 words)
- Patients' privacy maintained (if not permission taken)
- Credit note for borrowed figures/tables provided
- Write the full term for each abbreviation used in the table as a footnote

Journal of
The Anatomical Society of India

Salient Features:

- Publishes research articles related to all aspects of Anatomy and Allied medical/surgical sciences.
- Pre-Publication Peer Review and Post-Publication Peer Review
- Online Manuscript Submission System
- Selection of articles on the basis of MRS system
- Eminent academicians across the globe as the Editorial board members
- Electronic Table of Contents alerts
- Available in both online and print form.

The journal is registered with the following abstracting partners:
Baidu Scholar, CNKI (China National Knowledge Infrastructure), EBSCO Publishing's Electronic Databases, Ex Libris – Primo Central, Google Scholar, Hinari, Infotrieve, Netherlands ISSN center, ProQuest, TdNet, Wanfang Data

The journal is indexed with, or included in, the following:
SCOPUS, Science Citation Index Expanded, IndMed, MedInd, Scimago Journal Ranking, Emerging Sources Citation Index.

Impact Factor® as reported in the 2022 Journal Citation Reports® (Clarivate Analytics, 2023): 0.4

Editorial Office:
Dr. Vishram Singh, Editor-in-Chief, JASI
B5/3 Hahnemann Enclave, Plot No. 40, Sector 6,
Dwarka Phase – 2, New Delhi - 110 075, India.
Email: editorjasi@gmail.com
(O) | Website: www.asiindia.in

The journal is owned and run by The Anatomical Society of India